

POLITECNICO DI TORINO

Master's Program in Mechanical Engineering

**Numerical-experimental comparison
of the Levit paddle shift dynamic behaviour**



Advisors:

Prof. Elvio Bonisoli
Dr. Domenico Lisitano

Candidate

Caterina Sacco

December 2021

Acknowledgments

First of all, I would like to thank Prof. Elvio Bonisoli for his availability during all the project and for his support with significant comments about my work. I also thank Dr. Domenico Lisitano for his precious observations and the time spent for the experimental tests.

A warm thanks to Christian and Luigi who supervised me during my internship at Valeo. Their help has been of great importance for the success of this work. Thanks also to Barbara and all the Laboratory Team members for their support and friendship.

Thanks to my university colleagues for their friendship and collaboration during my studies.

Sincere thanks to my friends Beatrice, Davide, Fabrizio, Francesco, Lorenzo e Matteo. Their closeness and support are always very important to me.

A special thanks to Emanuele for his kindness and patience. Even if a little annoying, he motivates me to do my best.

Thanks to all my family for their constant support, encouragements and love. In particular, thanks to my mum and my sister for being with me all the time.

Thanks also to all the people who helped me and wished for me all success.

Index

Index.....	5
Abstract	7
Introduction.....	9
1. Levit device.....	11
1.1 Numerical model.....	15
2. Sweep test	22
2.1 Experiment description	22
2.2 Reference system and excitation.....	25
2.3 Numerical setup model	32
2.3.1 Accelerometers on Lupos.....	33
2.3.2 Results of model with accelerometers	36
2.3.3 Ema-Fea coupling	37
2.4 Overview on Testlab post-processing.....	39
2.5 Sweep experimental analysis	52
2.5.1 Transmissibility.....	52
2.5.2 Natural frequencies	63
2.5.3 Transmissibility and natural frequencies	64
2.5.4 Transmissibility synthesis	70
2.6 Sweep experimental MAC	73
2.7 Conclusions on first experiment	84
3. Roving hammer test	85
3.1 Experiment description	85
3.2 Frequency response function	86
3.3 Natural frequencies	89
3.4 Frequency response function and natural frequencies	91
3.5 Parametric analysis	94
3.5.1 Accelerometer mass	95
3.5.2 Steering bar stiffness	97
3.5.3 Magnets stiffness.....	101
3.5.4 Hinges stiffness	105
3.5.5 Density and Young modulus modification	109
3.5.6 Pin constraints modification.....	117
3.5.7 Pads asymmetry	122
3.6 Hammer experimental MAC.....	126
3.7 Conclusions on second experiment.....	130
4. Comparison between sweep and impact tests	132
5. Actuation and release test	140
5.1 Setup.....	140
5.2 Experiment description	143
5.3 Results of pad DOWN	146
5.4 Results of pad UP.....	156
5.5 Results comparison	163
5.6 Conclusions on third experiment	166
Conclusions.....	167
Appendix.....	169
Example of Matlab code for transmissibility graphs	169
Matlab code: Phi_correction.m	171
Example of Matlab code for parametric analysis.....	172

Matlab code for update 10174
Reference177

Abstract

This project addresses the vibration transmissibility of the leverage system of the paddle shift device at the steering wheel. The device under study is called Levit and is generally composed by a main body and by two pads which are the main subject of the analysis. The leverage system activation is influenced by the presence of magnets located on the main case which introduce some non-linearities. The main goal of this work is to develop and to tune a linearised dynamics analysis on the paddle shift with experimental tests.

The behaviour of the device is experimentally tested in Valeo laboratory, then the data are post processed with Siemens LMS Test.Lab17 and Matlab software. The experimental results are compared with the ones provided through the numerical model. This last one is already created and will be improved with this work. The numerical model and the relative data are elaborated in Lupos, a parametric FEM code developed in Matlab.

Two different experiments are conducted on the Levit in order to detect its natural frequencies and to identify the corresponding mode shapes. These two analyses consist in a sine sweep vibration and a roving hammer test. Furthermore, another experiment is carried out, focusing on the actuation and release of the pads to analyse more in details the reaction to excitation as in vehicle arrangement.

The sweep vibration test is applied along all the three axes of orientation of the Levit. For each axis three different displacements (0.005, 0.010 and 0.012 mm) are set to evaluate the natural frequencies in several excitation conditions. It is worth noting that the results from y axis at 0.005 mm are the more interesting. Moreover, it is chosen to refer to y axis since it has the same direction of the steering column, thus it becomes the most excited axis when the device is correctly assembled on the vehicle.

The second experiment conducted to study the linearized dynamic behaviour involves the usage of an impact hammer. The Levit pads have been hammered few times in perpendicular way with respect to the paddle surface. The smaller amount of data recovered from this experiment allows it to be easier used in the numerical model. Then, few parametric analyses are set in order to develop and improve the numerical model. In fact, the purpose is to bring numerical results closer to the experimental ones modifying one model parameter at time. Thanks to these updating actions, very good results are achieved in terms of natural frequencies and similitude of mode shapes between experimental and numerical fields.

The last experiment has the objective to simulate the Levit behaviour in the vehicle layout. It consists in many repetitive actuations and releases of one pad at time; both pads are tested. Excellent repetition of results is observed, due to the instrumentation used and the setting of automatic cycle. From the observed performance it is visible that during the release phase there are oscillations on both pads, the one which is excited and the other one that receives its dynamics. This is also influenced by the nonlinear behaviour proper of the magnets inside the device, which will be investigated in a future work.

Keyword: paddle shift device, transmissibility analysis, real modal analysis, sine sweep vibration test, roving hammer test, parametric analysis, model updating.

Introduction

This thesis is the final work for the Mechanical Engineering master's degree. The study proposed in this document is developed in partnership with Valeo S.p.A. within an internship in the context of the Politecnico di Torino's project "Tesi in azienda".

Valeo is a French global automotive supplier with a wide range of products to automakers and the aftermarket. The internship is developed in the site of Santena which focuses its production on internal switch controller.

The project is developed in collaboration with the R&D division of Valeo laboratory. It is focused on the study and improvement of an existing gearbox system placed at steering wheel: the Levit shown in Figure 1.

This device is a paddle shift leverage system composed by a main body and two paddles, whose analysis is the main subject of the study.

In Figure 2 the numerical modelling of the device created in SolidWorks is presented.



Figure 1 – Picture of the physical Levit device.

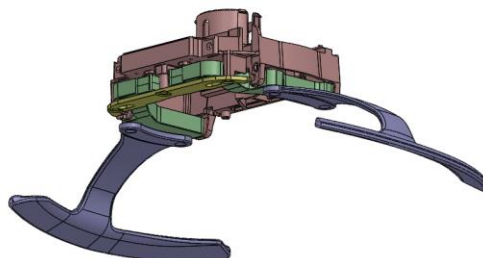


Figure 2 – CAD Levit model on SolidWorks.

The Levit is a type of paddle shift principally used in automatic/manual transmission system, which gets the input manually and shifts the gears electronically. In this scenario the two pads of Levit are considered, the right one is used to do the upshift, while the left is used to downshift.

This paddle shift has two magnets on the arms, just close to the bracket, which influence the behaviour of actuation and release of the pads. Previous studies have been conducted on the dynamic transmissibility of this device. These results are resumed in the report: “Technical evaluation through numerical time and/or modal approaches on LEVIT devices”. Moreover, some solutions were proposed with structural modification aiming to reduce the energy path between the two pads. One of the goals of this analysis is to find another possible solution for decoupling the pads.

Another important objective of this study is to characterize experimentally the transmissibility and to use experimental data to improve the numerical model developed in previous works. Two experimental tests are carried out in this project to study the natural frequencies and mode shapes of the device. Then, a third experiment is proposed to simulate the behaviour of Levit during actuation and release of pads.

Two different models are considered: a CAD model created in SolidWorks and a similar model built in Lupos. The development of model in Lupos is based on the CAD, nevertheless it is subjected to simplification of geometry due to the different software used. The technique used consists in a discretization in regular cubes of the device geometry and brings to the ‘Minecraft’ reduced model. The final results of this simplification is shown in Figure 3 and represents our starting point for the numerical model.

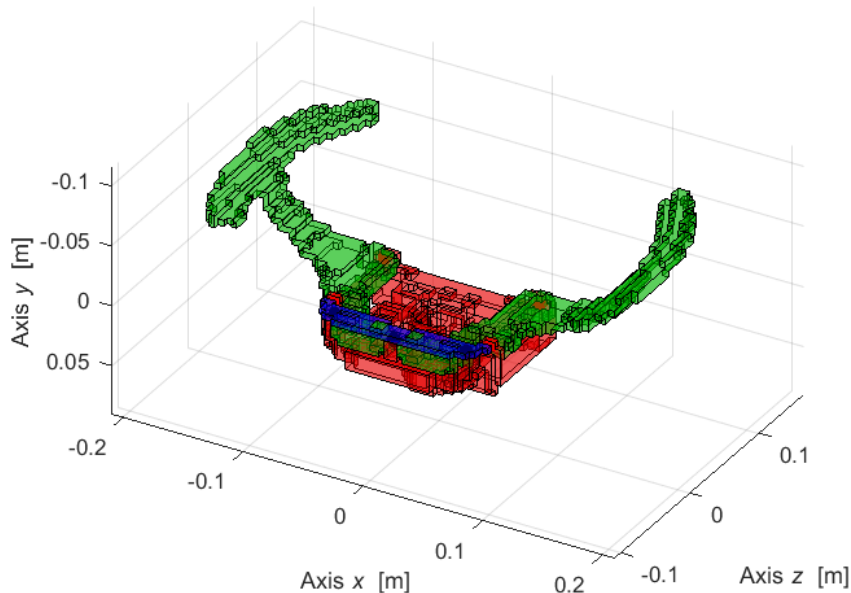


Figure 3 – Numerical Levit model on Lupos.

1. Levit device

The device under study is a paddle shift at the steering wheel. It is presented in Figure 1.1, while in Figure 1.2 there is the CAD Levit model on SolidWorks.



Figure 1.1 – Picture of the physical Levit device.

In Figure 1.2 the numerical modelling of the device created in SolidWorks is presented

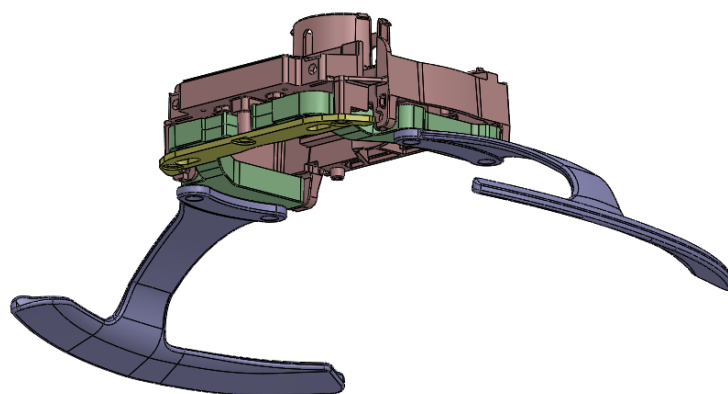
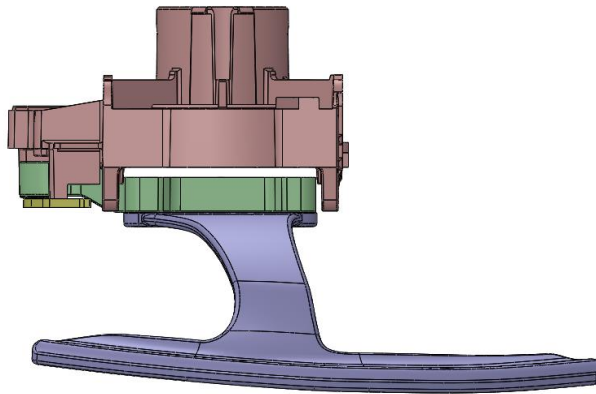
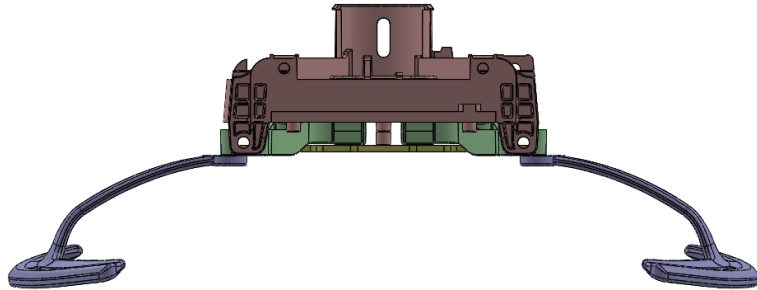


Figure 1.2 – CAD Levit model on SolidWorks.

Figure 1.3 shows the Levit from three different plane, xy , yz , zx . While Figure 1.4 shows the Levit model on different views.



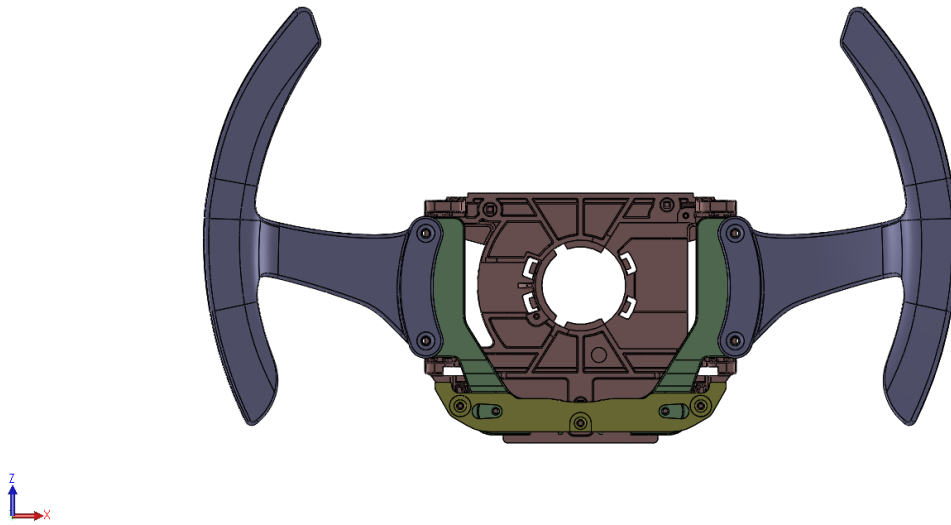


Figure 1.3 – Levit model on SolidWorks from three different planes.

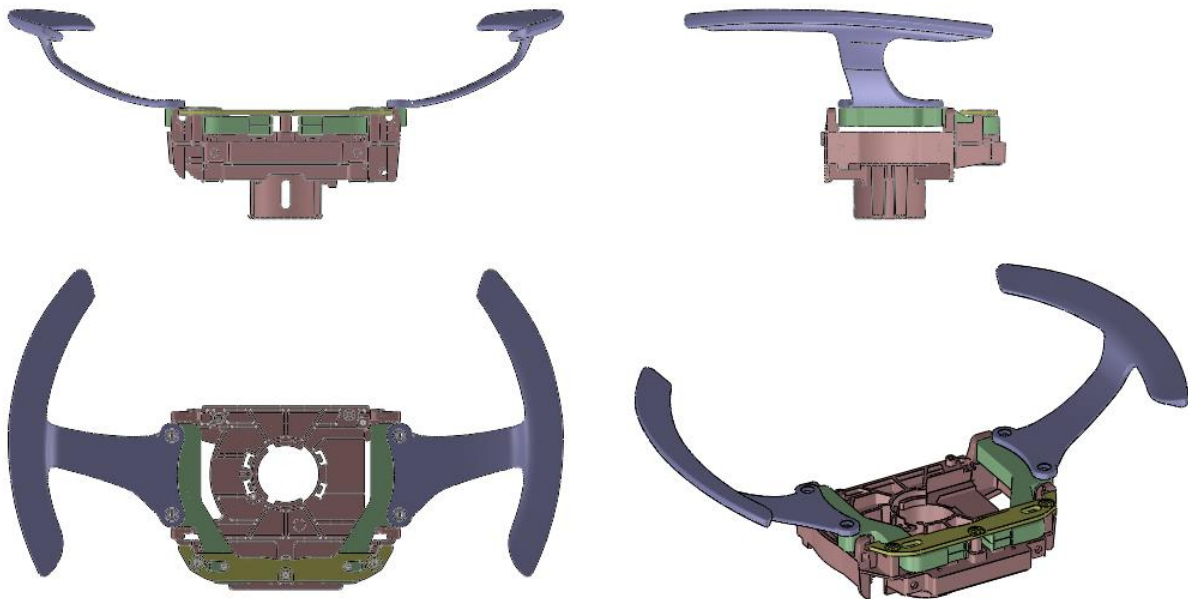


Figure 1.4 – Levit model on SW from different views.

In Figure 1.5 the main elements of the Levit are highlighted using numeration from 1 to 4. In Figure 1.6 the exploded view of model on SolidWorks is reported. In particular it is composed by:

1. Case: it is the main body of the Levit, through its centre hole the device connected to the steering column. On SolidWorks it is shown in red colour.
2. Arms: there are two arms, one for each side, left and right. They connect the pads to the main case, there are two cavities to place the magnets. Green coloured in SolidWorks.
3. Pads: they are two, positioned on arms and allow to shift the vehicle gear up and down. On SolidWorks they have blue coloration.

4. Bracket: it is positioned over the two arms to fix them to the main case. In CAD model is yellow coloured.



Figure 1.5 – Element’s numeration of Levit device.

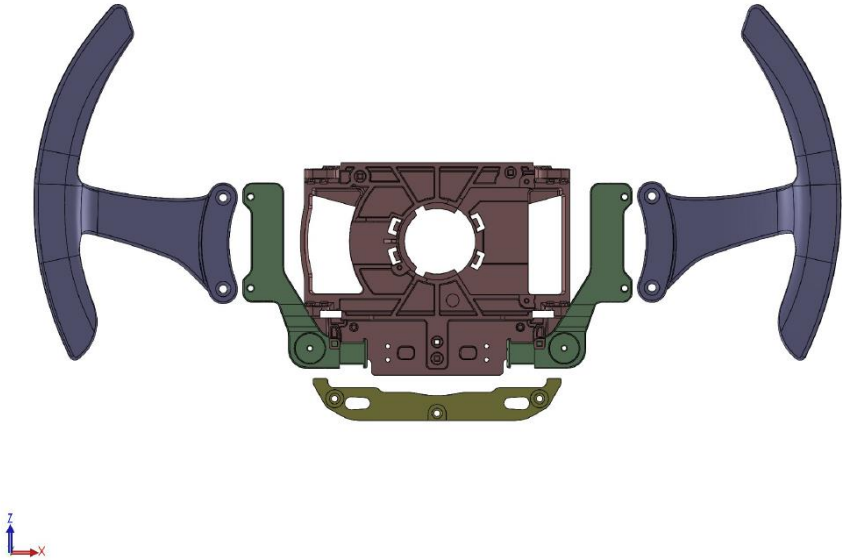


Figure 1.6 – Explosion view of SolidWorks Levit model.

The pads, in blue, are connected to the green arm elements. Each arm has a cavity for placements of magnets which are responsible for the main non linearity aspects. The motion of the arms is limited upward and downward by the bracket through two tips by each side. The metallic bracket is fixed to the case with screws while the arms are connected to it through pins.

1.1 Numerical model

Figure 1.1.1 shows the numerical model on Lupos. In this image it is possible to see the "Minecraft" simplification described above.

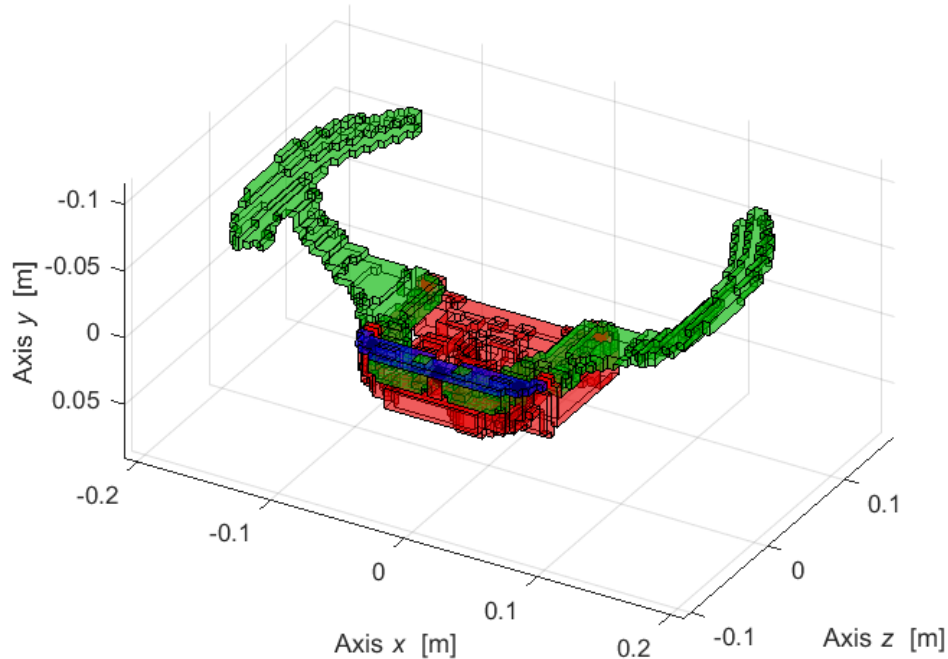


Figure 1.1.1 – Numerical Levit model on Lupos.

In order to describe more in details the model, the main parts are singularly analysed in the following points:

- Node elements

The nodes elements are the Geos, they possess 6 DOFs corresponding to the physical generalised displacements in the global coordinate system (GCS).

In the Figure 1.1.2 the nodes of the device are shown. From the Matlab interface we know that the model is composed by 7519 nodes

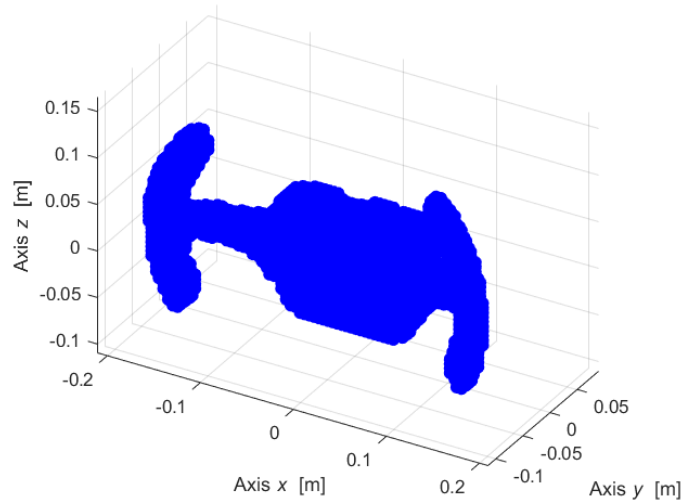


Figure 1.1.2 – Representation of all nodes.

- Boundary conditions

BCs are the boundary conditions of the model. In this case there are 6 BCs, one for each DOFs in GCS. They are all positioned in one point, at the base of the steering column. Since the Levit device is constrained by the steering wheel axis and position.

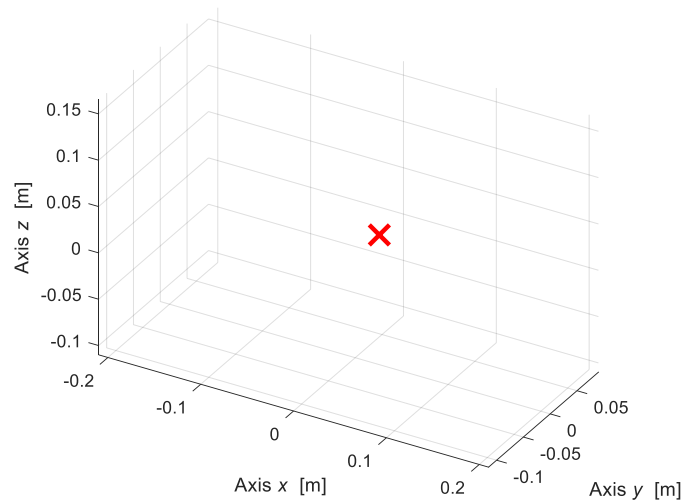


Figure 1.1.3 - Boundary conditions application point.

- Rigid joints

There are 6 rigid joints, which are the element of connection between two different parts of the device. In these points, the nodes must be unified adding a rigid joint. In the Figure 1.1.4 are shown the connection between the red body (case) and the blue part (bracket) through the rigid joints.

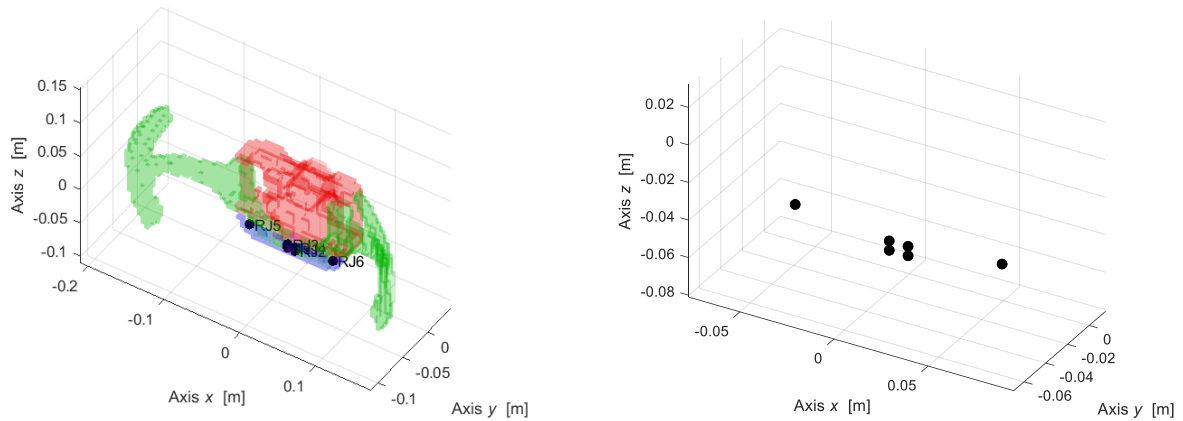


Figure 1.1.4 – Rigid joints on device (left), rigid joints (right).

- RBE

The rigid body is composed by 12 elements in the model device, they are another type of constraint, like RJs but less effective since they allow displacement along z axis. The RBE are the junction elements, positioned between the green elements (pads) and the red body.

In Figure 1.1.5 the RBE are represented by four red point, each one group three other point (one for each translational DOF).

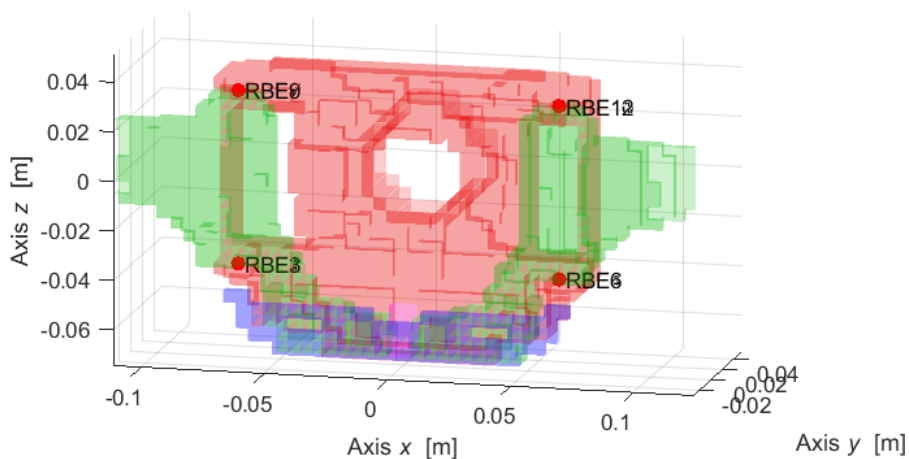


Figure 1.1.5 – RBE.

- Elastic elements

In this analysis, 722 elastic elements Els are considered, placed near the boundary condition, all around the hole of the case coloured in red. The elastic elements give the possibility to introduce in the model the stiffness between the steering column and the device under analysis.

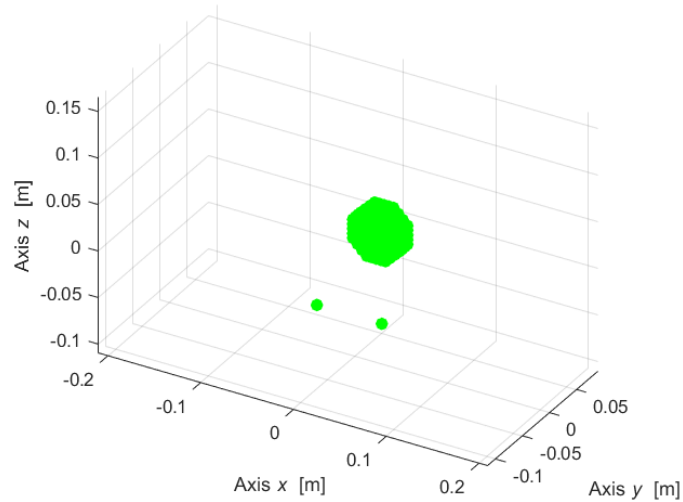


Figure 1.1.6 – Elastic elements.

- Damping elements

The damping elements Dmp have the same configuration of elastic elements. They introduce in the model the dissipative effect. The number of damping element (726) is comparable with the elastic ones

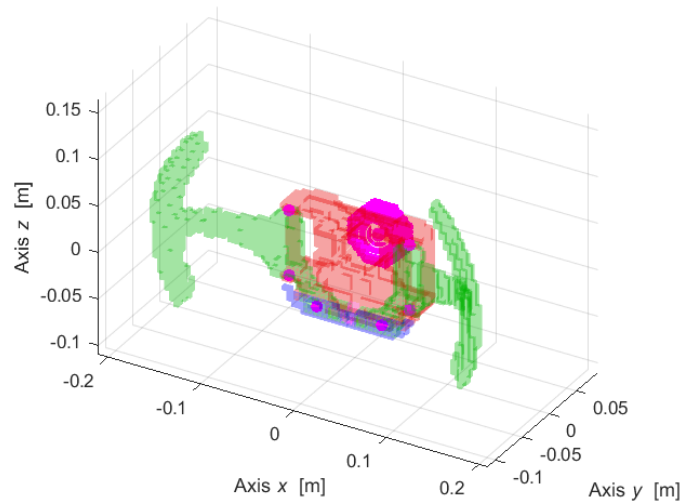


Figure 1.1.7 – Damping elements.

- Hexahedral elements

To model the shape of the model the hexa solid elements are used. These elements represent the link between eight nodes. The *Hex* and *Hex contours* options allow to represent the discretise model and give evidence of the device deformation during simulation. The hexa elements are used to visualize the deformation of Levit and study the energy exchange between one pad and another.

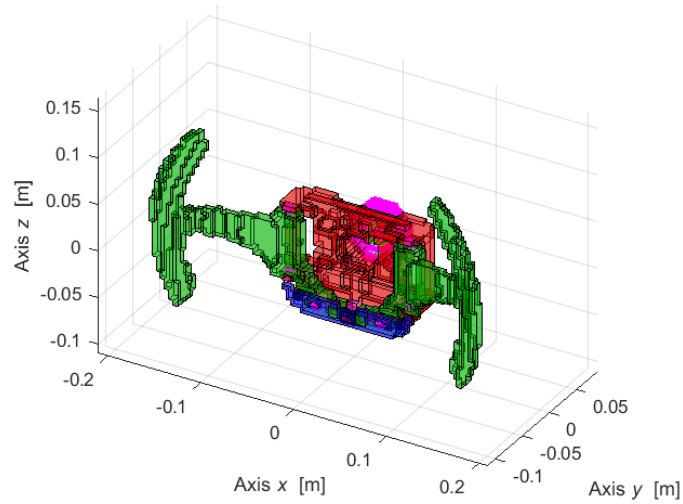


Figure 1.1.8 – Hex elements.

- Complete model

The complete model with all analysed element is presented in Figure 1.1.9.

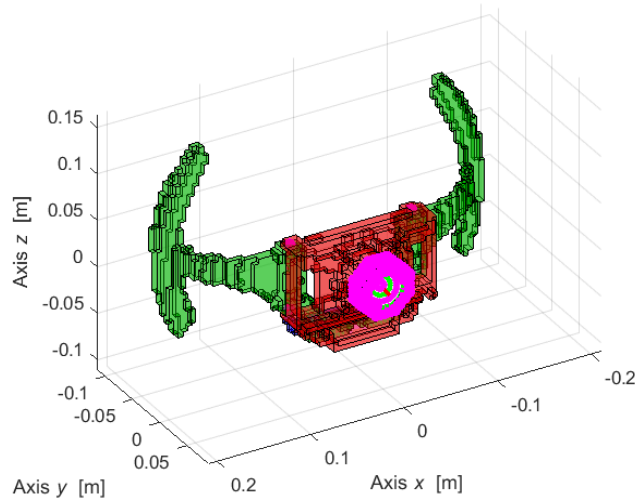
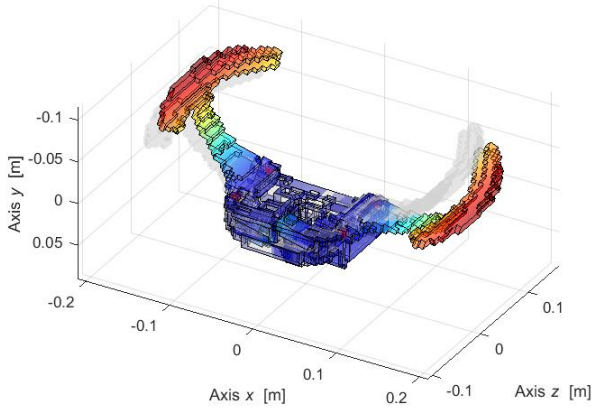


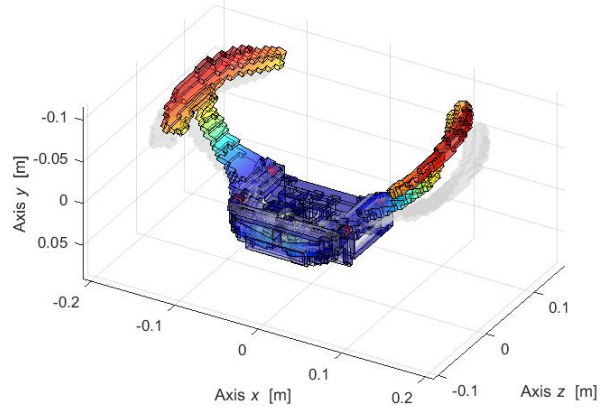
Figure 1.1.9 – Complete model.

After that, the principal numerical results are presented in Figure 1.1.10. Those data are the starting point of the study and come from real modal analysis.

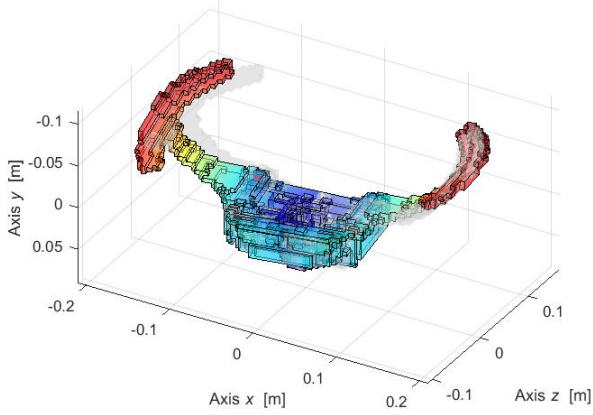
Mode 1 - 62.48 Hz



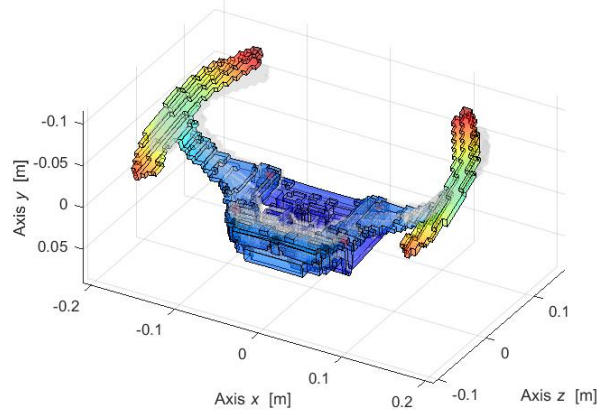
Mode 2 - 67.18 Hz



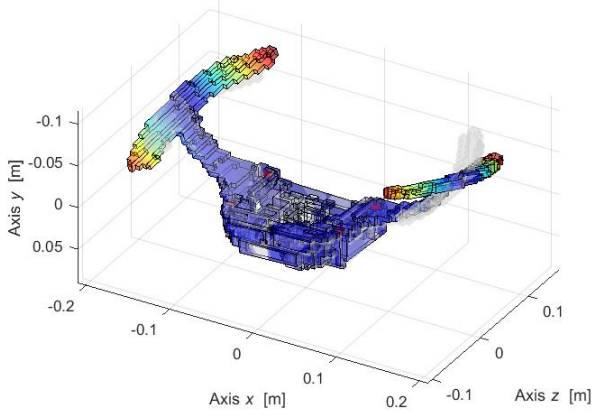
Mode 3 - 146.7 Hz



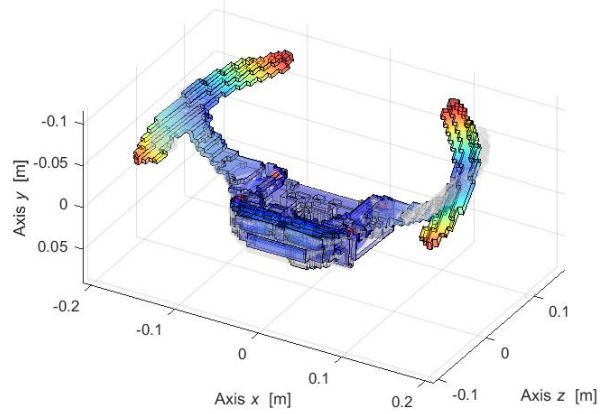
Mode 4 - 162.5 Hz



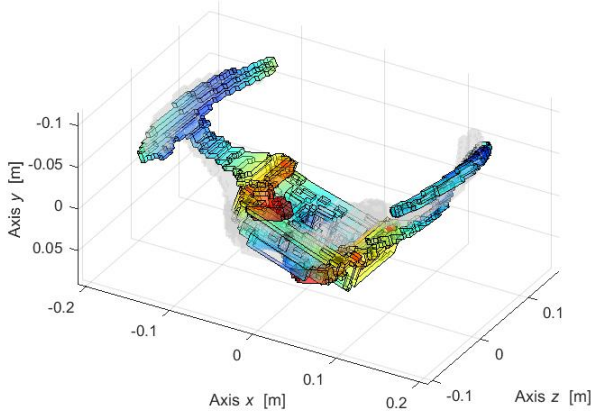
Mode 5 - 214.1 Hz



Mode 6 - 260.4 Hz



Mode 7 - 268.6 Hz



Mode 8 - 425.2 Hz

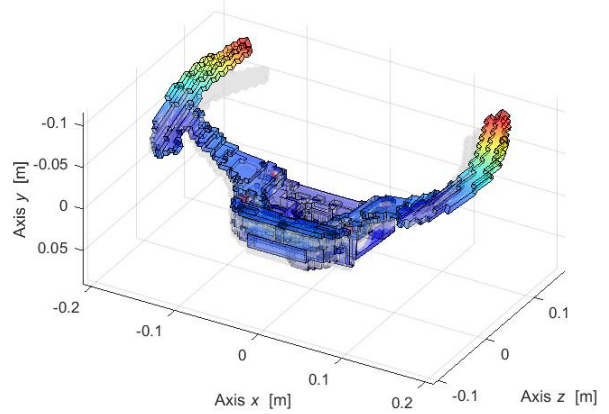


Figure 1.1.10 – First eight mode shapes of reference model.

The description part of Table 1.1.1 refers to the numerical model reference system.

Table 1.1.1 – Natural frequency and description of mode shapes of reference model.

Mode	Frequency [Hz]	Description
1	62.48	Coupled pads out of phase
2	67.18	Coupled pads in phase
3	146.7	Torsional out of phase
4	162.5	Torsional in phase
5	214.1	Bending of pads out of phase on yz plane
6	260.4	Bending of pads in phase on yz plane
7	268.6	Bending of pads out of phase on xy plane
8	425.2	Bending of pads in phase on xy plane

The real modal analysis is based on the reduced formulation of dynamics matrix problem:

$$\mathbf{M}\ddot{\mathbf{x}} + \mathbf{K}\mathbf{x} = \mathbf{f}(t)$$

where \mathbf{x} and $\ddot{\mathbf{x}}$ are the generalised displacements and acceleration. \mathbf{M} is the mass matrix (real symmetric, positive definite), \mathbf{K} is the stiffness matrix (real, symmetric, positive semidefinite) and \mathbf{f} is the generalised force vector.

Applying the Modal Analysis approach and the modal superposition method, it is possible to solve the eigenvalues problem and consequently find the natural frequencies and eigenvectors.

Usually, the eigenvalues are identified by ω_r^2 , the square root of these values correspond to the natural frequencies in [rad/s]. Through the formulation $\omega_r = 2\pi f_r$ it is possible to compute the values in [Hz]. Moreover, for every eigenvalue ω_r^2 there is real eigenvector Φ_r , which is called mode shapes. The collection of the real eigenvectors in the matrix φ or Φ is called modal matrix.

2. Sweep test

The first experimental test on Levit device is a sine sweep test and it is conducted at Valeo laboratory in 2021-05-26. In this chapter it is described as the experiment has been conducted and the main results achieved during this test.

The Levit is positioned on a shaker and a sweep test is done. Through accelerometer we have feedback on the displacements and movements of the device under test. We use TestLab.17 software to conduct both the experimental part and the data post processing. Moreover, these results are compared with the numerical model in order to develop and improve this one. The numerical model is developed within Lupos.

The aim of the test regards the correct setting of model. Thanks to a shaker it is possible to excitate the device and study the values for the natural frequencies. This experiment is useful to start the characterization of the model.

2.1 Experiment description

The Levit is positioned on a shaker and a sweep test is done. Thanks to accelerometers, we have feedback on the displacements and movements of the device under test. The Testlab 1.7 software is used to conduct both the experimental and the post processing parts.

Then, these results are compared with the numerical model in order to develop it and improve its performance. The numerical model is developed in MATLAB with the help of Lupos and is presented in the next paragraphs.

Figure 2.1.1 presents the experimental setup.

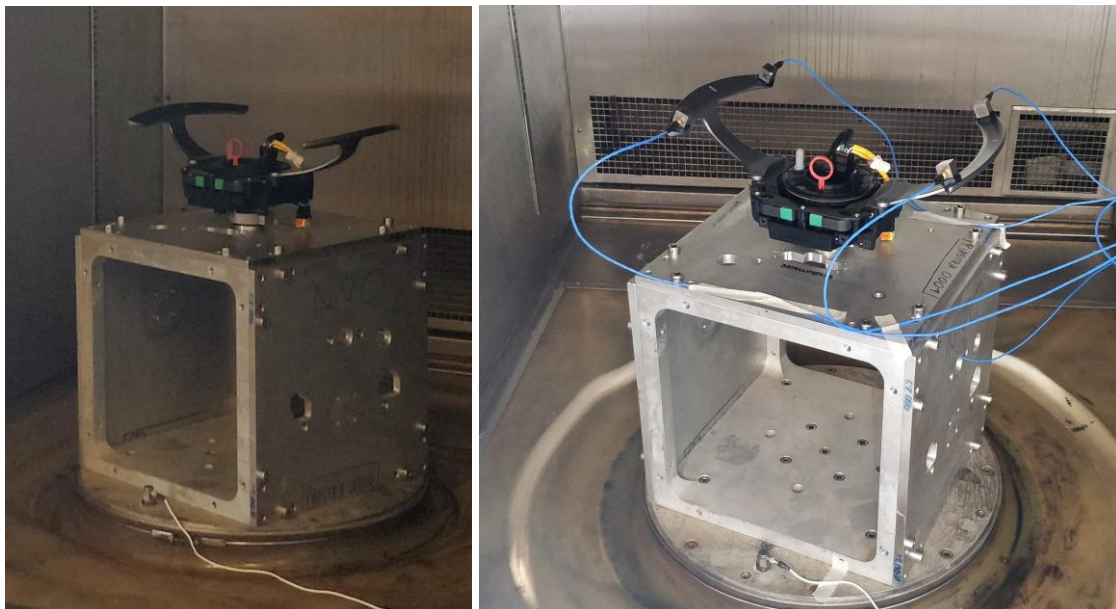


Figure 2.1.1 – Levit on the shaker (left), Levit on the shaker with accelerometers (right).

The analysis is based on a sweep vibration. A linear sweep is set from frequency of 10 Hz to 300 Hz with a rate of 0.2 Hz/s. The test is performed three time one for each axis of excitation x , y , and z .

For the test a shaker (Shaker LSD model 810 440) and an amplifier provided by Valeo are used. The acquisition and elaboration of data are performed by a Siemens Scada Mobile and then by the software TestLab17.

Table 2.1.1 resumes the test parameters, while Table 2.1.2 reports the data of the shaker used.

Table 2.1.1 – Independent and dependent linear sweep test parameters of acquisition.

Quantity	Symbol	Relationship	Value	Units
Total acquisition time	T	$T = (f_2 - f_1) \frac{1}{\Delta f / T}$	1450	s
Starting frequency	f_1		10	Hz
Final frequency	f_2		300	Hz
Rate linear sweep	$\Delta f / T$		0.2	Hz/s
Sample frequency	f_s		16384	Hz
Total samples	N	$N = f_s T$	622592	-
Bandwidth (max frequency)	f_b	$f_b = \frac{f_s}{2}$	8192	Hz

Table 2.1.2 – Parameters of the shaker used for acquisition.

Shaker		Model 810-440		
Amplifier		DPA 20K	DPA 15-20K	DPA 10-20K
Sine Force	kN	17.8	13.3	8.9
	(lbf)	4000	3000	2000
Random Force	kN	17.8	15.8	10.2
	(lbf)	4000	3400	2300
Velocity	m/s	1.5	1.5	1.5
	(in/s)	59	59	59
Acceleration	Sine g pk.	60	55.9	37.3
	Random g rms	50	50	33
Dynamic load capability				
Acceleration Sine 2g	kg	350	350	350
	(lb)	770	770	770
Acceleration Sine 6.33g (NAVMAT 9492)	kg	262	191	119
	(lb)	578	420	262
Acceleration Sine 15g	kg	96.6	66.4	36.1
	(lb)	213	146	79.6

Figure 2.1.2 shows the Levit positioned on the shaker. Firstly, the device is locked on the aluminium plate through a circular extrusion, which allow to fix the Levit in the same configuration as on the car, simulating the connection to the steering wheel. Then, the plate + Levit are fixed on the aluminium cube. Two other plates are added on the lateral face of the cube to guarantee rigidity to the structure. In order to test all axes of excitation the plates can be moved and re-fix through screws.



Figure 2.1.2 – Device with cube positioned on the shaker.

For the analysis 6 accelerometers are used, four of those are triaxial and are positioned on the extremities of the pads. Those accelerometers are necessary to measure both bending and torsional behaviour. The other two are monoaxial, the 5th is the control accelerometer placed on the shaker (white wire in Figure 2.1.2), while the 6th (real controller) is positioned as close as possible at the case of Levit, near the steering column. A detailed view of numbered accelerometers will be done for each axis configuration in next paragraphs.

Table 2.1.3 resumes the accelerometers coordinates with the Levit (numerical) reference system.

Table 2.1.3 – Coordinates of accelerometers respect to Levit reference system.

Coordinates of accelerometers on Levit			
Accelerometer number	<i>x</i>	<i>y</i>	<i>z</i>
1	+0.131	-0.083	+0.117
2	+0.150	-0.076	-0.054
3	-0.131	-0.083	+0.117
4	-0.150	-0.076	-0.054
5	0.000	+0.310	0.000
6	0.000	0.000	0.000

In Figure 2.1.3 is represented one of the four triaxial accelerometers. It is composed by a cube in titanium, which is the proper accelerometer, and by a black base in aluminium alloy. The stud is necessary to connect the accelerometer to the system elaboration input/output.



Figure 2.1.3 – Triaxial accelerometer PCB 356A15 assembly of accelerometer + base 080A12 + stud 081B05.

The device has been tested under all three axes in static condition and without any load, just to see which is the behaviour of the body and to have experimental evidence of the natural frequencies. So, the test is done on axis x , y , z imposing different displacements: 0.005, 0.010 and 0.012 mm. The amplitude of the tests is kept small due to technical problem with the simulation and with the acquisition system that was not able to record higher amplitude values. In Table 2.1.4 are resumed the test and the relative displacement imposed.

Table 2.1.4 – Details of tests.

Axis under test	Displacements [mm]
x	0.005
	0.010
	0.012
y	0.005
	0.010
	0.012
z	0.005
	0.010
	0.012

2.2 Reference system and excitation

For the experimental test is used a reference system that is different from the numerical one. In the description of this test, it is possible to see two different reference system. The one corresponding to the sweep experiment is called TestLab reference system, the other used for Lupos is named numerical reference system.

The numerical approach has the numerical reference system shown in Figure 2.2.1 in SolidWorks model.

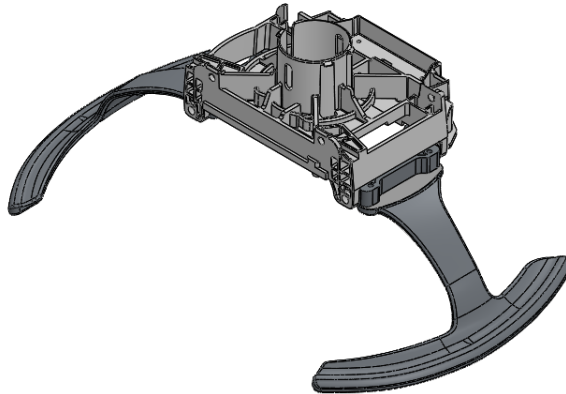


Figure 2.2.1 – Numerical reference system in SW.

In Figure 2.2.2 is shown the numerical system applied to the experimental setup.

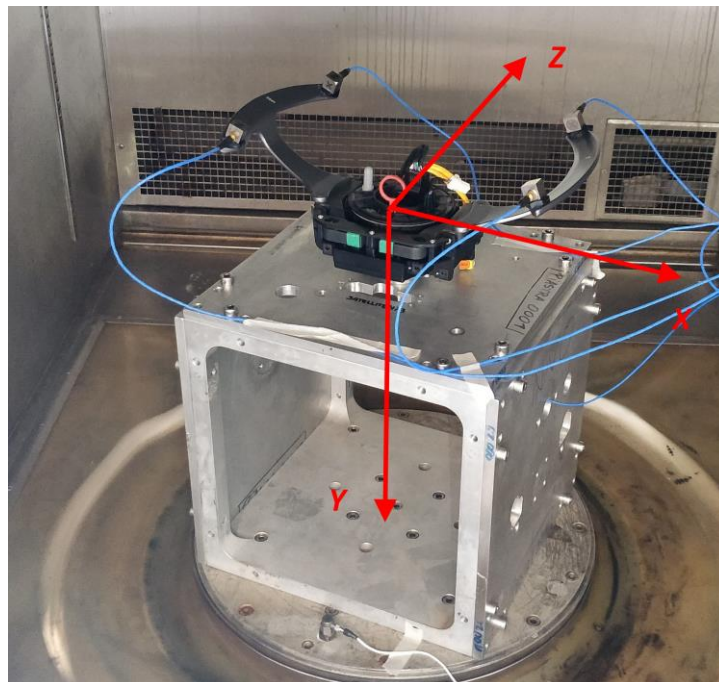


Figure 2.2.2 – Numerical reference system in experimental setup.

During the first experiment on 2021-05-26 it was used another reference system. For the post processing in Matlab, especially in the MAC analysis, the numerical reference system is considered, the one in Figure 2.2.2 in order to have good comparison of the data.

Instead, in Figure 2.2.3 is shown the experimental reference system used, the same reference system is used for the post processing of TR in TestLab.

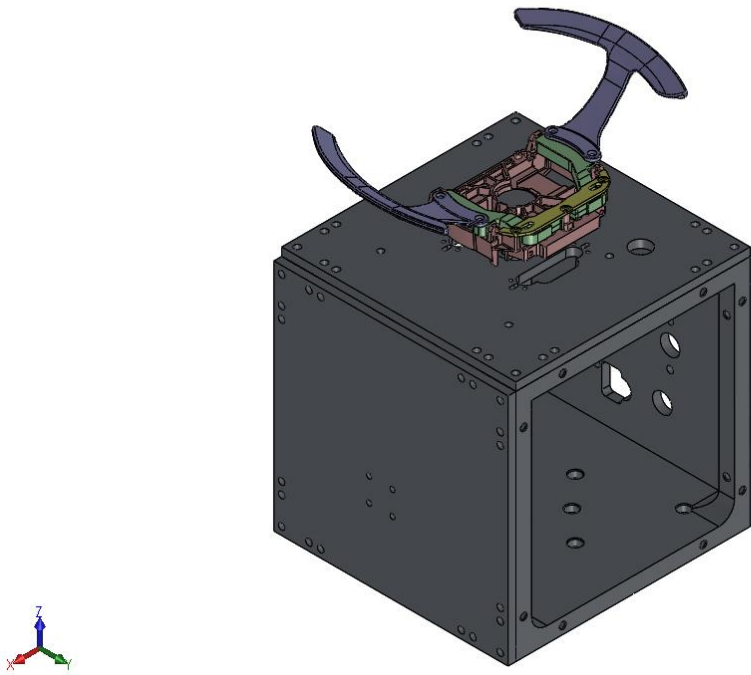


Figure 2.2.3 – Experimental reference system in SW.

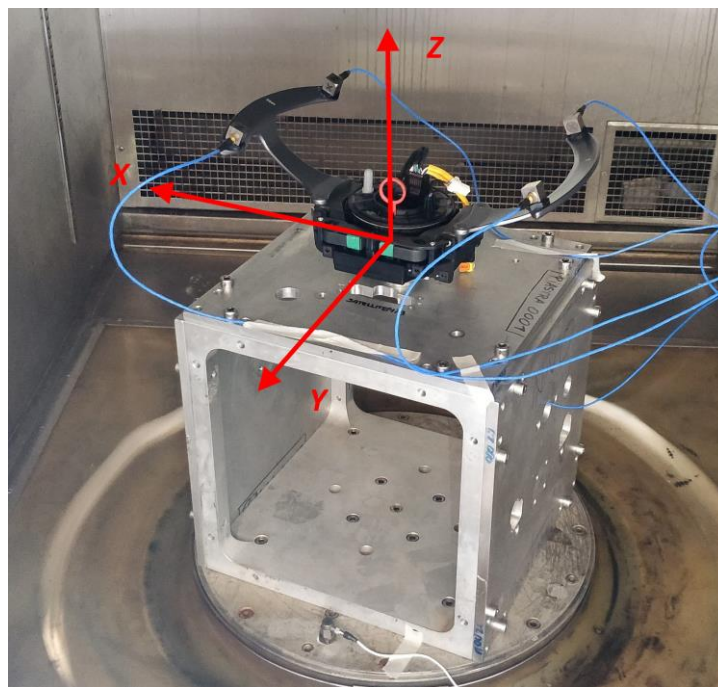


Figure 2.2.4 – Experimental reference system in experimental setup.

It is worth noticing that the name of axis excitation is not equal to the one used in numerical model. The reference system used was different. The x-axis in TestLab is the only one which coincides with the x-axis on the Levit coordinate system. On the contrary the y and z axis are switched in these two reference systems. The y-axis in TestLab corresponds to the z-axis on Levit reference system, while the z-axis in TestLab corresponds to y-axis on the device numerical reference system.

In Table 2.2.1 those reference systems are resumed.

Table 2.2.1 – Comparison of reference systems.

	Reference systems		
Levit under experimental test			
Vertical axis TestLab reference system	y	z	x
Vertical axis numerical Levit reference system	$-z$	$-y$	$-x$

Figure 2.2.5 represents the numerical and experimental reference system.

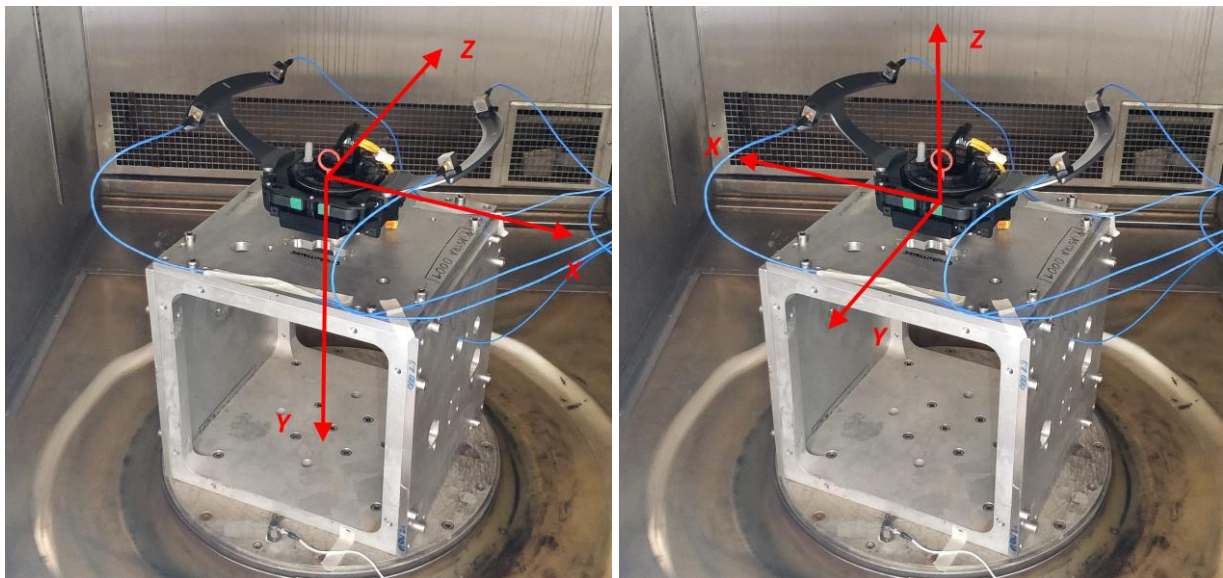


Figure 2.2.5 – Numerical reference system (left), experimental reference system (right).

In Table 2.2.2 are resumed the exchange needed to pass from the experimental to numerical reference system.

Table 2.2.2 – Reference system exchange.

From Experimental to Numerical reference system
$x \rightarrow -x$
$y \rightarrow -z$

$$z \rightarrow -y$$

The change $y \rightarrow -z$ gives the most important and useful data. We concentrate the main part of analysis on y axis of numerical reference frame, since it is the axis coincident to the steering wheel. Once clarified the reference system correlation, it is possible to proceed with the data analysis with the TestLab reference frame.

Moreover, in the next paragraphs the excitation axis is exposed and are added some observation useful for the analysis of experiments. The following paragraphs are named according to TestLab experimental reference system.

Excitation on x axis

According to TestLab experimental reference system are named these paragraphs. The device is tested for excitation on x axis as in Figure 2.2.6.

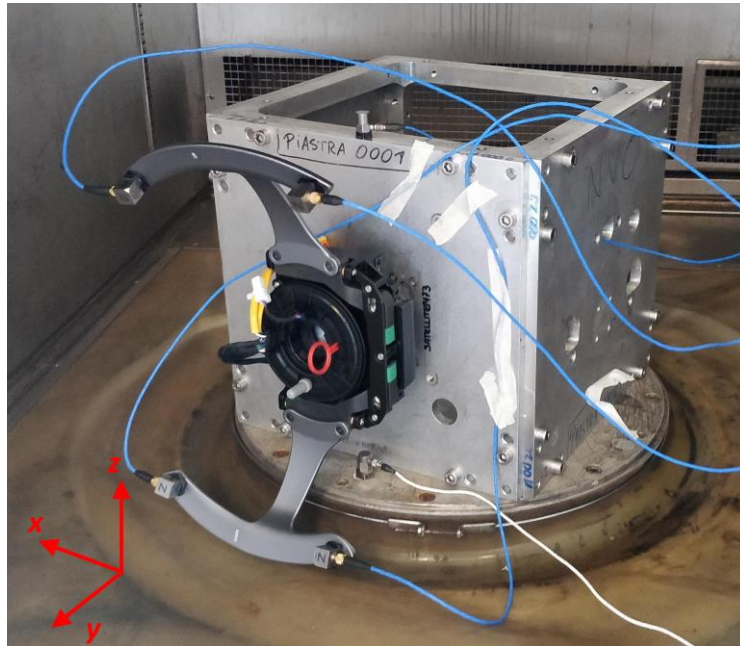


Figure 2.2.6 - Device positioned for excitation on x axis.

In Figure 2.2.7 are shown the numbered accelerometer and their position. The main difference concerns the position of the 6th accelerometer, which has been fixed on the cube. The position is not so close to the steering lock position due to difficulties to find a proper flat surface. Otherwise, it is possible to see that the position of the other five accelerometers is unchanged.

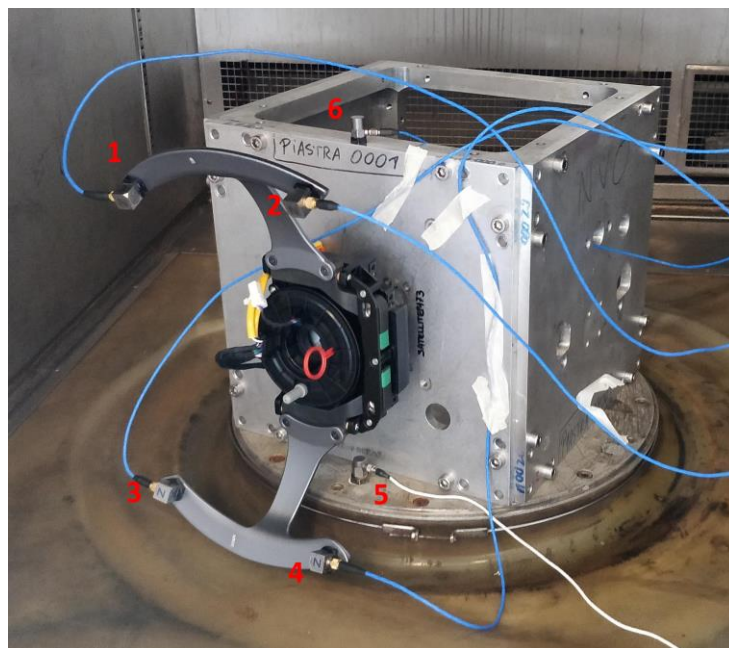


Figure 2.2.7 – Numeration of accelerometers.

Excitation on y axis

The device is positioned as in Figure 2.2.8 in order to test excitation on y axis.



Figure 2.2.8 – Device positioned for excitation along y axis.

In Figure 2.2.9 it is possible to see the accelerometers and the relative numbers. The first and second ones are on the right pad (up), the third and fourth accelerometer are on the left pad (down). The 5th is on the shaker and the sixth is placed on the plate just above the device.



Figure 2.2.9 – Numeration of accelerometers.

Excitation on z axis

The Levit device is positioned on the shaker as in Figure 2.2.10 to test the excitation on z axis.

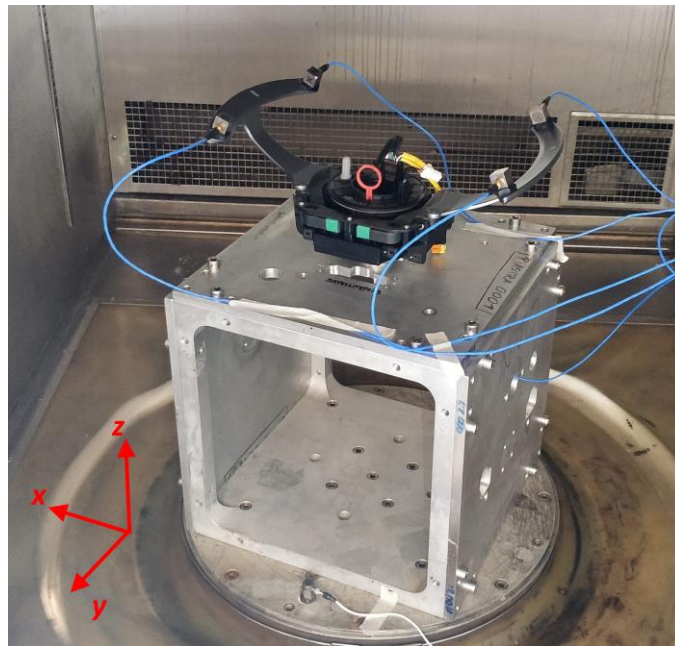


Figure 2.2.10 – Device positioned for excitation on z axis.

In Figure 2.2.11 the accelerometers and their number are shown. Their position on the device is the same of the previous cases, except for the 6th, which is moved on the plate below the device.



Figure 2.2.11 – Accelerometer number 1÷5 (left) and accelerometer number 6 (right).

2.3 Numerical setup model

The same experimental configuration (Levit+accelerometers) done at Valeo is reproduced on Lupos in order to have a numerical match and ensure the reliability of experimental results.

Thus, four accelerometers are added on the device, two per each side (right/left). The configuration of accelerometers wants to respect the symmetry of the device as much as possible, so one lumped mass is positioned at each extremity of the pads.

In Figure 2.3.1 it is possible to see the model of the device with configuration used for experimental tests.

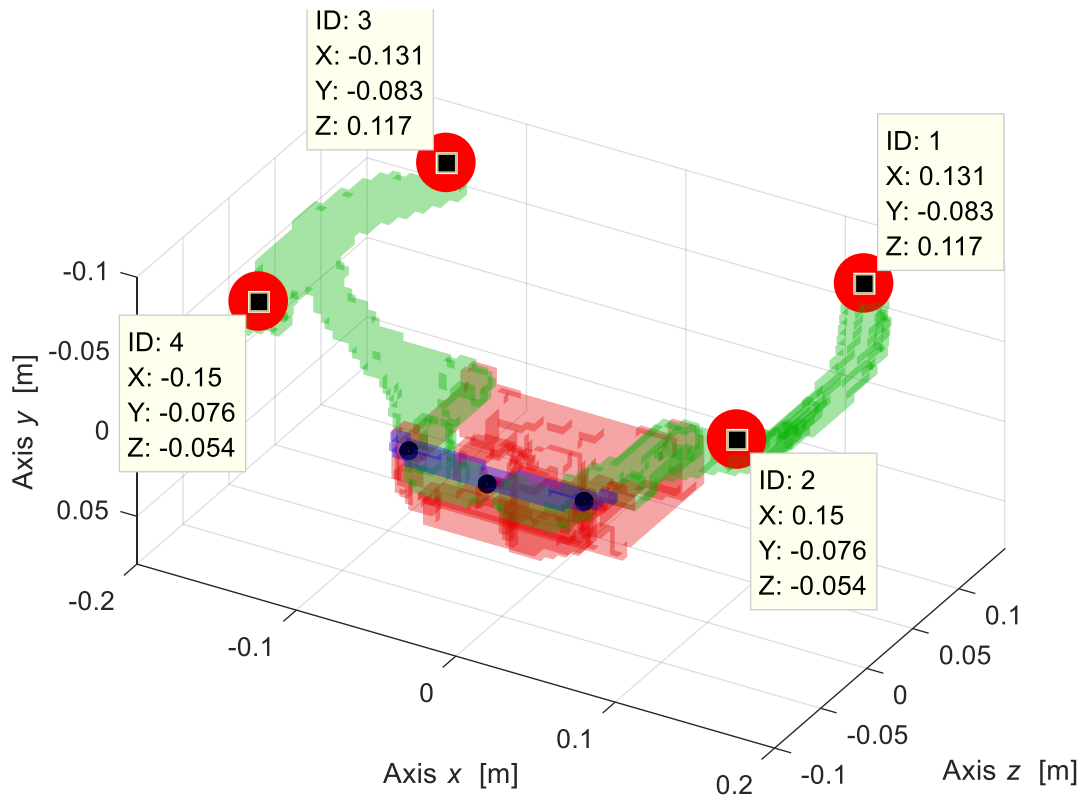


Figure 2.3.1 – Levit model with four accelerometers.

All accelerometers are triaxial, each one has different sensitivity. They are used to measure the accelerations in the space of each point where they are connected.

In Table 2.3.1 the main characteristics of the accelerometers are resumed.

Table 2.3.1 – Characteristics of accelerometers.

Property	Value
Equivalent cubic edge [m]	$14 \cdot 10^{-3}$
Mass [kg]	$14.2 \cdot 10^{-3}$
Model inertial tensor [I_{xx}, I_{yy}, I_{zz}] [kg m^2]	$[463.86, 463.86, 463.86] \cdot 10^{-9}$

2.3.1 Accelerometers on Lupos

In order to fix the accelerometers on Lupos the correct element must be chosen. The accelerometer can be assimilated to 1D element with a lumped mass, this can be the easiest and the most effective way to proceed modelling the accelerometers.

First of all, it is necessary to give to Lupos the coordinates of the accelerometers on the device, these coordinates are resumed in Table 2.3.1.1.

Table 2.3.1.1 – Coordinates of accelerometers.

Node	x	y	z
1	+0.1310	-0.0830	+0.1170
2	+0.1500	-0.0760	-0.0540
3	-0.1310	-0.0830	+0.1170
4	-0.1500	-0.0760	-0.0540

The mass representative of each accelerometer is connected to the device through four rigid joints. The lumped mass on Lupos is the element Mss with the required information:

Model.Mss = matrix of lumped masses [NodeId m Jxx Jyy Jzz Jxy Jxz Jyz] (M x 8)

In our model the configuration (M x 8) is used. All nodes are identified, the masses are all equals and through a model on SolidWorks the equivalent moment of inertia are calculated taking into account the accelerometer and its relative base.

Considering only the accelerometer cube we can have spherical ellipsoid for the moments of inertia, adding the base we lose the spherical properties. Since the spherical properties allow to not consider the Euler angles, we want to maintain these properties, which give advantage in the calculation.

Thus, it is created a proportion between the moments of inertia of the only cube configuration (mass $9.5 \cdot 10^{-3}$ kg) and the model with the accelerometer + base with a mass of $14.2 \cdot 10^{-3}$ kg.

The inertial tensor of the cube only is $[I_{xx}, I_{yy}, I_{zz}] = [310.33, 310.33, 310.33] \cdot 10^{-9}$ [kg m²], which become $[463.86, 463.86, 463.86] \cdot 10^{-9}$ [kg m²] after calculation.

In Table 2.3.1.2 are reported the moment of inertia for each accelerometer/node.

Table 2.3.1.2 – Moment of inertia.

Node	I _{xx} [kg·m ²]	I _{yy} [kg·m ²]	I _{zz} [kg·m ²]
1	$463.86 \cdot 10^{-9}$	$463.86 \cdot 10^{-9}$	$463.86 \cdot 10^{-9}$
2	$463.86 \cdot 10^{-9}$	$463.86 \cdot 10^{-9}$	$463.86 \cdot 10^{-9}$
3	$463.86 \cdot 10^{-9}$	$463.86 \cdot 10^{-9}$	$463.86 \cdot 10^{-9}$
4	$463.86 \cdot 10^{-9}$	$463.86 \cdot 10^{-9}$	$463.86 \cdot 10^{-9}$

The lumped masses are drawn on Lupos graphic interface by red points.

Similarly, the rigid joints elements RJs (black rod in Figure 1.1.4) are:

Model.RJs = matrix with rigid joints [NodeId1 NodeId2] (J x 2)

Having the accelerometers points, it is time to create the rigid joints, selecting firstly the master node (the only one belongs the accelerometers) and then the slave node, which is part of the node of the pad. These lasts nodes are placed on the device, to fix completely the accelerometers node are taken four nodes on the pad surface.

Figure 2.3.1.1 shows the position and details of node IDs for the RJs elements for all four accelerometers. In Table 2.3.1.3 are reported the number of node necessary to build the rigid joints.

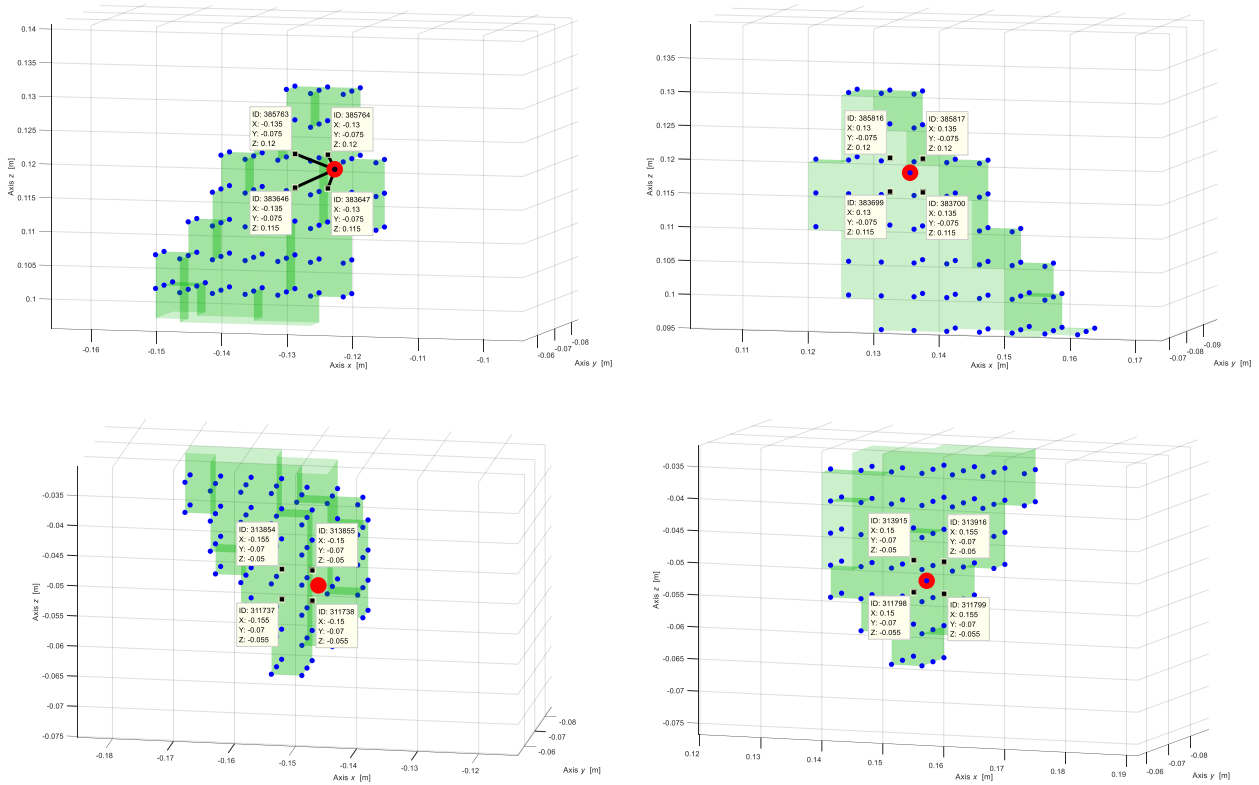


Figure 2.3.1.1 – Details of the four accelerometers positions and element used.

Table 2.3.1.3 – Nodes for rigid joints.

Node on accelerometer	Node on pads
1	383699
	383700
	385816
	385817
2	311798
	311799
	313915
	313916
3	383646
	383647
	385763
	385764
4	311737
	311738
	313854
	313855

2.3.2 Results of model with accelerometers

The goal of this analysis is to obtain a numerical model comparable with the experimental data, hence it is conducted a real modal analysis. The results of the real modal analysis are resumed for the first 6 modes in Figure 2.3.2.1.

Table 2.3.2.1 provides the frequency and description of each mode.

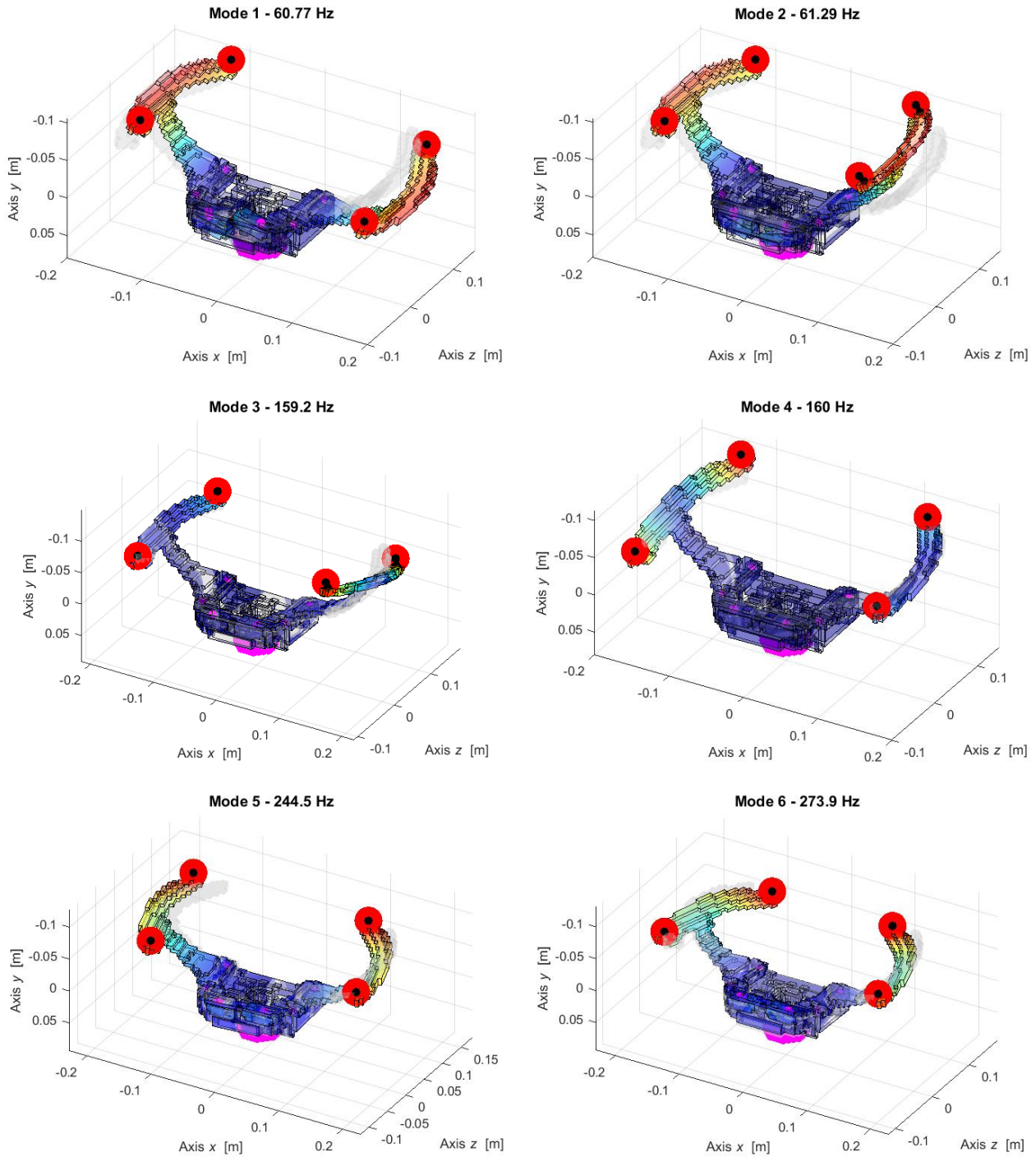


Figure 2.3.2.1 – Numerical real modal analysis of the first 6 mode shapes of the experimental test rig.

Table 2.3.2.1 – Natural frequencies and descriptions.

Mode	Frequency [Hz]	Description
1	60.77	Coupled pads out of phase
2	61.29	Coupled pads in phase
3	159.2	Torsional out of phase
4	160.1	Torsional in phase
5	244.5	Bending of pads out of phase on xz plane
6	273.9	Bending of pads in phase on xz plane

Observing the simulation of mode 3-4, about the torsional behaviour, it is evident that one pads have bigger motion than the other one.

2.3.3 Ema-Fea coupling

Since the reference systems are different using the EmaFeaCoupling code in Matlab, it is possible to have a double check on the correctness of information about the accelerometer position.

To set the script the nodes from experimental test and the ones used in Lupos have to be declared. Nodes Ema are the experimental nodes from TestLab, while in Nodes Fea are presented the nodes used on numerical model of the device.

Experimental nodes are taken after the use of MATLAB script Phi_corrections.m (Appendix) in which all coordinates coming from post processing on TestLab data are adapted to correct numerical reference system.

For numerical nodes are used data from the Lupos model implementation, where the accelerometers were added.

Table 2.3.3.1 – Nodes from experimental results.

Nodes EMA/FEA	x	y	z
1	0.131	-0.083	0.117
2	0.150	-0.076	-0.054
3	-0.131	-0.083	0.117
4	-0.150	-0.076	-0.054
5	0.000	0.310	0.000
6	0.000	0.000	0.000

In Table 2.3.3.2 is shown the equivalence distance between the nodes imposed in TestLab during the experiment and the nodes used to build the model on Lupos and their distance.

Table 2.3.3.2 – Correspondence between experimental and numerical nodes.

Nodes Ema	Nodes Fea	Distance[mm]
1	1	0.00
2	2	0.00

3	3	0.00
4	4	0.00
5	5	0.00
6	6	0.00

Because the distance is zero, that means the node are overlapped and so they are the same.

2.4 Overview on Testlab post-processing

All data are acquired by a Simcenter Scadas Mobile and through TestLab software. The data post processing is carried out in Testlab as well. The tests are done on three axis x , y , z changing the amplitude and imposing a displacement from 0.005 to 0.012 mm.

The first part of post processing includes the analysis of the FRF of different test. In Figure 2.4.1 is shown an example of the main page Navigator where all data are displayed.

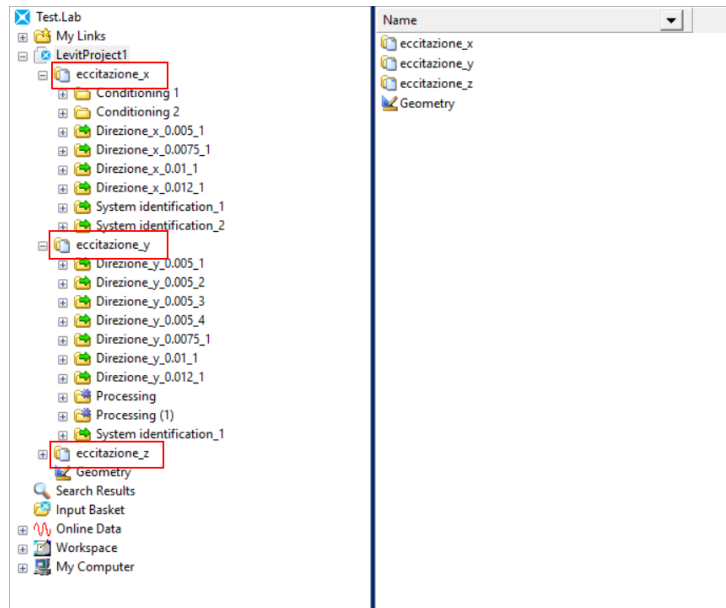


Figure 2.4.1 – Navigator page with all test done.

It is possible to open just one excitation at time and see only one test. For example, opening “Direzione_x_0.005_1” means that the x -axis is under excitation, the displacements imposed is 0.005 mm and that this is the first attempt.

The nomenclature of different accelerometers used in TestLab is resumed in Table 2.4.1.

Table 2.4.1 – Nomenclature of accelerometers.

TestLab	Single accelerometer on Levit
1:1	1
1:2	2
1:3	3
1:4	4
1:5	5
1:6	6

Acceleration profile

In order to control the acceleration, a quadratic profile is imposed as is shown in Figure 2.4.2. This profile is checked on the 6th accelerometer, from the data of TestLab.

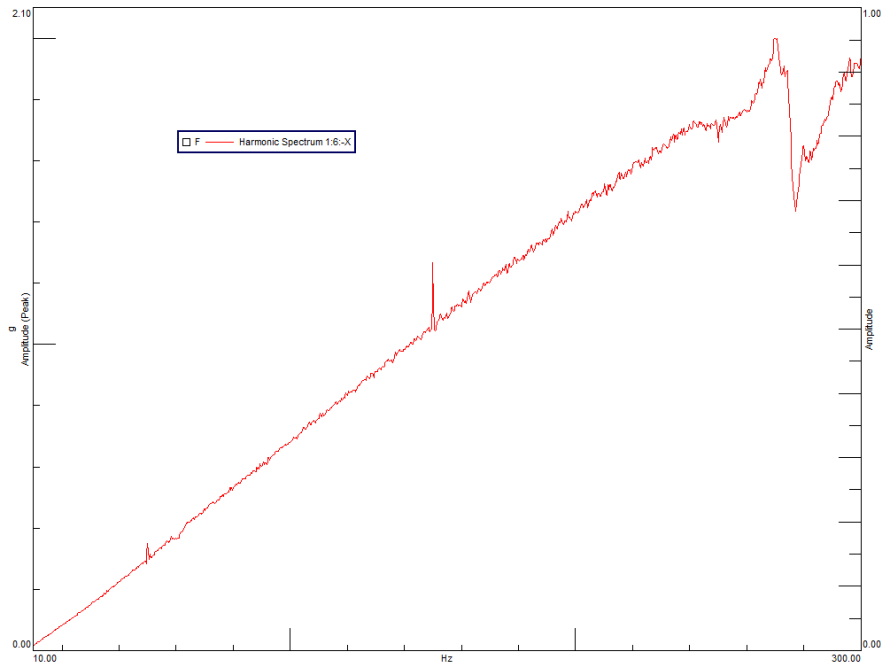


Figure 2.4.2 – Quadratic profile of acceleration.

The quadratic shape is not well visible due to the little magnitude of amplitude tested. Putting together different amplitude, the change of the profile with the amplitude becomes more visible. As the imposed displacements increase, it grows also the shape of acceleration curve, even if it remains a quadratic profile. In Figure 2.4.3 the green curve corresponds to displacements of 0.005 mm, it grows up passing by 0.075, 0.010 mm, until cyan curve which represent the displacements of 0.012 mm.

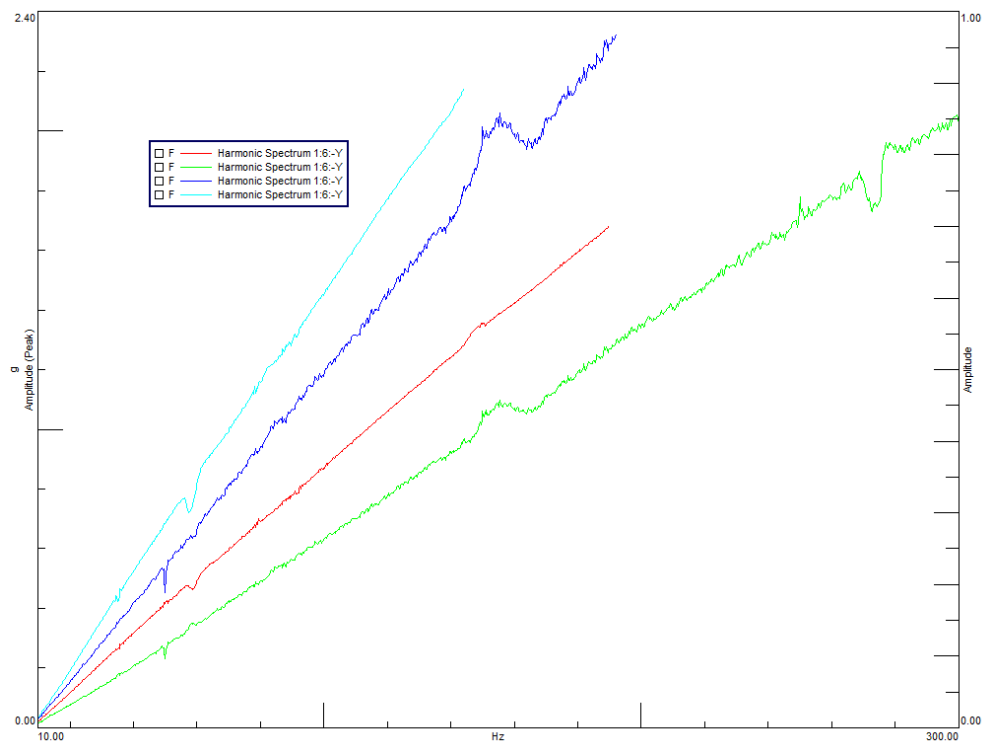


Figure 2.4.3 – Quadratic profile at different amplitude in y direction.

FRF analysis

The first useful results are the FRF frequency response function, for each direction test and for each amplitude there are FRF data.

It is defined as a ratio between the constant displacement imposed and the acceleration. Keep attention because in the analysed case it is better to define the transmissibility, which is a transfer function defined as acceleration on acceleration.

TestLab calls as default this ratio FRF without considering the quantity under analysis. In chapter 2.5 about post-processing on Matlab this distinction will be re-proposed.

Figure 2.4.4 shows the FRF present in the navigator of TestLab for one single direction/amplitude.

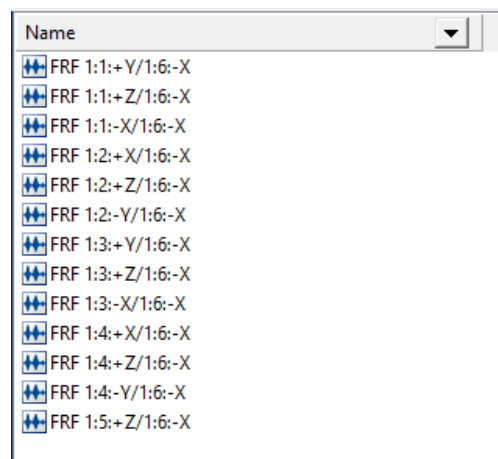


Figure 2.4.4 – Example of FRF in x direction.

It is important to notice that there are 6 accelerometers. And for each of them the three coordinates x , y , z are made explicit. The numbers five and six give the same information, the fifth measures and represents the motion of the shaker, while the information given by the sixth is used as comparing data. These measurements will be compared with those given by other accelerometers from one to five.

The information stored in the last line of Figure 2.4.4 represents the relation between fifth and sixth accelerometer, which are put into graph in Figure 2.4.5.

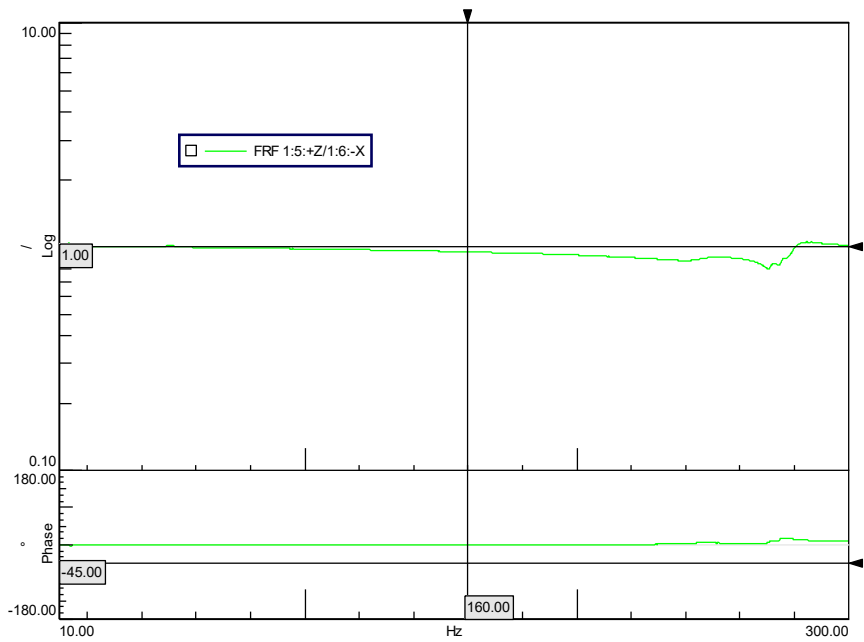


Figure 2.4.5 – Ex. FRF 1:5:+Z/1:6:-X in x direction.

Figure 2.4.5 shows in logarithmic scale the ratio between the the 5th and the 6th accelerometer. This ratio should be equal to one; from the graph it is possible to see that until 160 Hz this ratio is equal or very close to one, while at higher frequencies the ratio becomes smaller than one, which means the plate (6th) has higher displacement than the shaker (5th).

At frequencies higher than 200 Hz the motion of the plate becomes more relevant, influencing all data of test. In fact, during the experimental phase we have trouble in excitation of the device with big amplitude, the maximum amplitude tested was 0.012 mm. Over this value the test automatically stopped.

It is interesting to discuss the graph in Figure 2.4.6, where are represented the FRF curve of the first accelerometer for different amplituted. The red curve has an imposed displacements of 0.005 mm while the pink curve has a displacement of 0.012 mm. The frequency is limited in range [66.23:91.98] Hz to see better the behaviour of the curves. When the displacement increases there is a motion of the curves on the left-down.

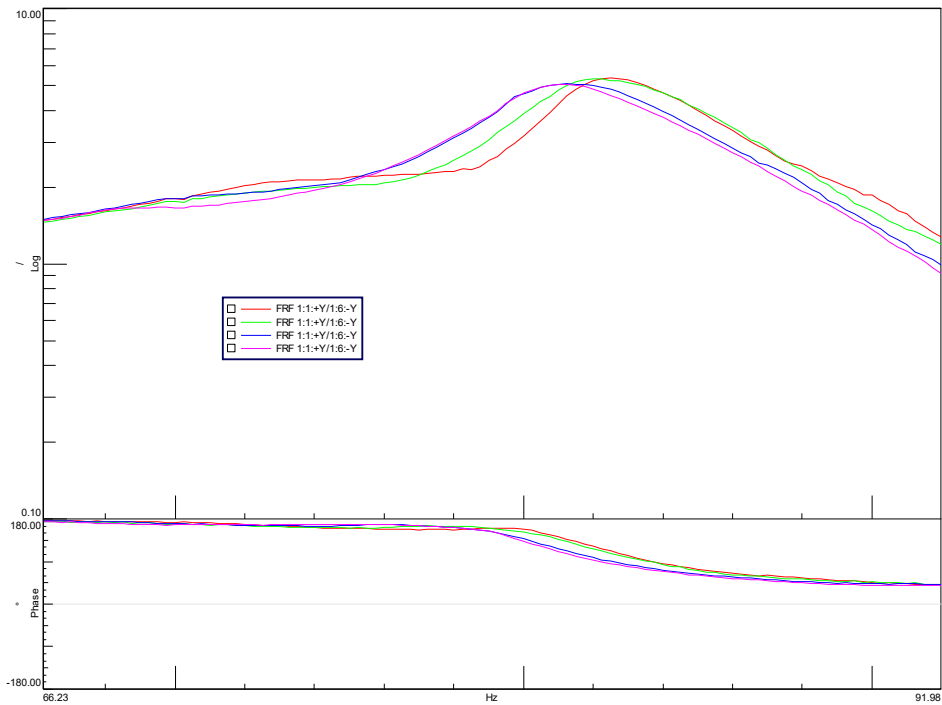


Figure 2.4.6 – FRF of the accelerometer n.º1 excited on y axis

That behaviour is more evident in Figure 2.4.7 near the peaks. Blue line stops at 200 Hz due to excitation problem at higher amplitude.

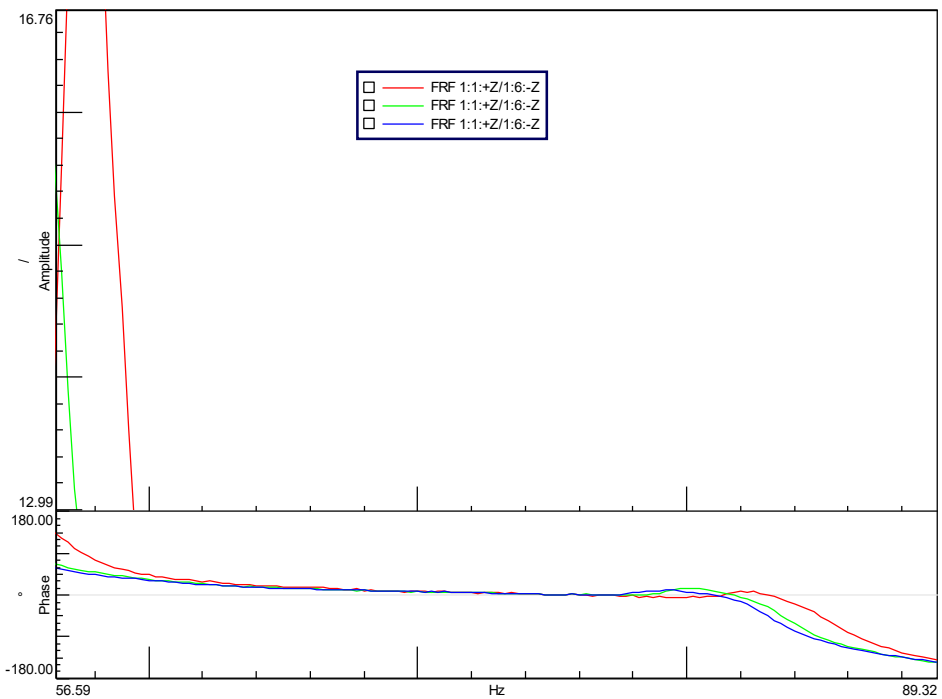


Figure 2.4.7 – FRF of the accelerometer n.º1 excited on z axis

Channel setup

It is useful to clarify how many channels give information about the device under test. It is important to notice that each triaxial accelerometers have three channels, corresponding to the axis x , y , z . The reference system used is the TestLab/experimental ones.

From Table 2.4.1 we can see 16 input, number 7 and 15 are not used for the measure, so they are not reported. Input 16 correspond to accelerometer number 6, which is the reference control for the experiment, while the other input simply measure accelerations. In Table 2.4.1 are resumed also the sensitivity for each axis of the accelerometers.

Table 2.4.1 – Channel setup for accelerometers.

Channel Id	Reference	Channel usage	Point	Direction	Accelerometer Sensitivity
Input1	False	Measure	1:1	+Y	96.1 mV/g
Input2	False	Measure	1:1	-X	97.3 mV/g
Input3	False	Measure	1:1	+Z	99.3 mV/g
Input4	False	Measure	1:2	-Y	101.6 mV/g
Input5	False	Measure	1:2	+X	104 mV/g
Input6	False	Measure	1:2	+Z	99.5 mV/g
Input8	False	Measure	1:3	+Y	102.5 mV/g
Input9	False	Measure	1:3	-X	97.5 mV/g
Input10	False	Measure	1:3	+Z	98.6 mV/g
Input11	False	Measure	1:4	-Y	102 mV/g
Input12	False	Measure	1:4	+X	102.1 mV/g
Input13	False	Measure	1:4	+Z	102.3 mV/g
Input14	False	Measure	1:5	+Z	9.83 mV/(m/s ²)
Input16	True	Control	1:6	-X	100.1 mV/g

The input given by the scadas is ± 10 V, then using an amplifier it is possible to reach higher or lower values.

Identification method

Once all data are collected, the post processing identification begins. To do one single identification it is needed to replace in the input basket one set of data, for example 'Direzione_x_0.005_1' as shown in Figure 2.4.8.

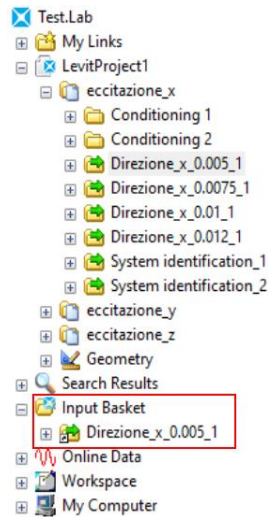


Figure 2.4.8 – Selected data in input basket (red box).

Then, it is necessary to go to the PolyMAX section on TestLab, where the mode shapes will be detected. Once all data relative to all axis of accelerometers have been selected, it is possible going to stabilization section. Here, stable points (S) in Figure 2.4.9 have to be searched and selected. The letter S means stable, it should be selected the first S in the column with a big number of other stable point on the upper levels. In Figure 2.4.9 cyan lines indicate the frequency that correspond to selected stable points. The relative frequencies are reported in Table 2.4.2.

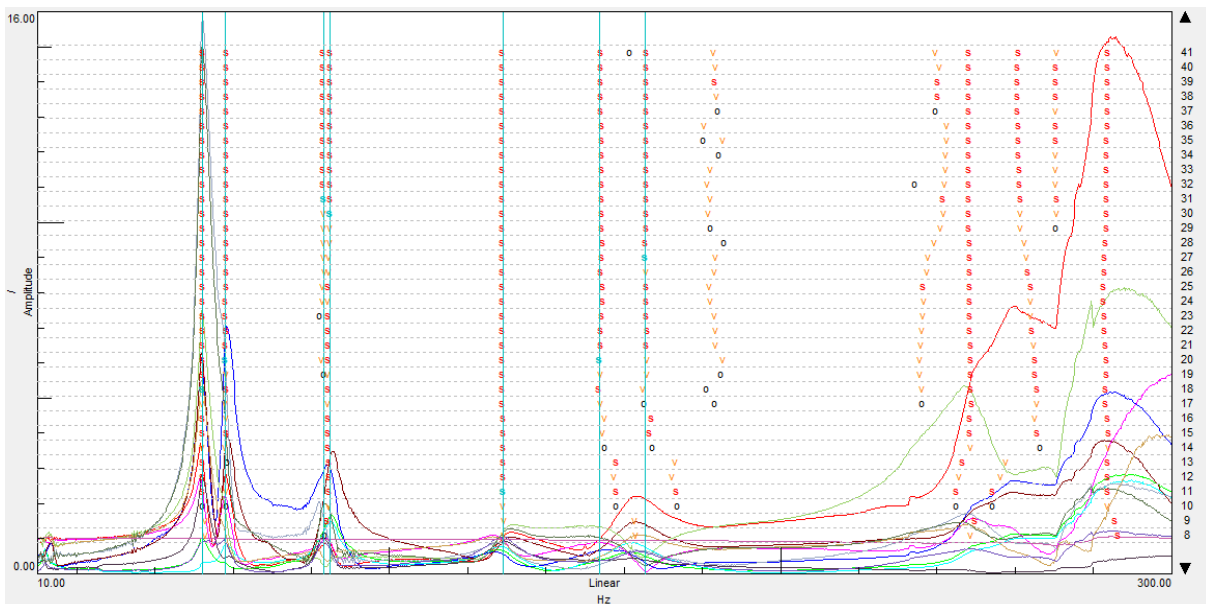


Figure 2.4.9 – Stabilization part of direction x at 0.005 mm.

Table 2.4.2 – Mode shapes for excitation on x axis at 0.005 mm.

Mode shape	Frequency [Hz]	Description
1	52.19	Coupled pads out of phase
2	58.13	Coupled pads in phase
3	83.06	Torsional out of phase
4	84.76	Torsional in phase
5	129.05	Testlab mode shapes
6	153.85	Bending of pads out of phase
7	165.59	Bending of pads in phase

Since there are differences between the numerical and the experimental model, it is not possible identify and give a description to all mode shapes. In particular, in this paragraph is not mandatory clarify all modes, it is better to give an accurate description in a second part of the analysis.

The mode shape number 5 has not an easy correspondence with the mode shaped on Lupos model, probably it depends on the motion of the assembly, cube + plates + Levit. The corresponding frequency at around 128 Hz is present in others identification in TestLab but not from data of Lupos simulation.

Sometimes the research of stable points could be difficult, such as for the stabilization part of x axis at 0.010 mm. As shows Figure 2.4.10 there are some peaks, but they are not easily identifiable.

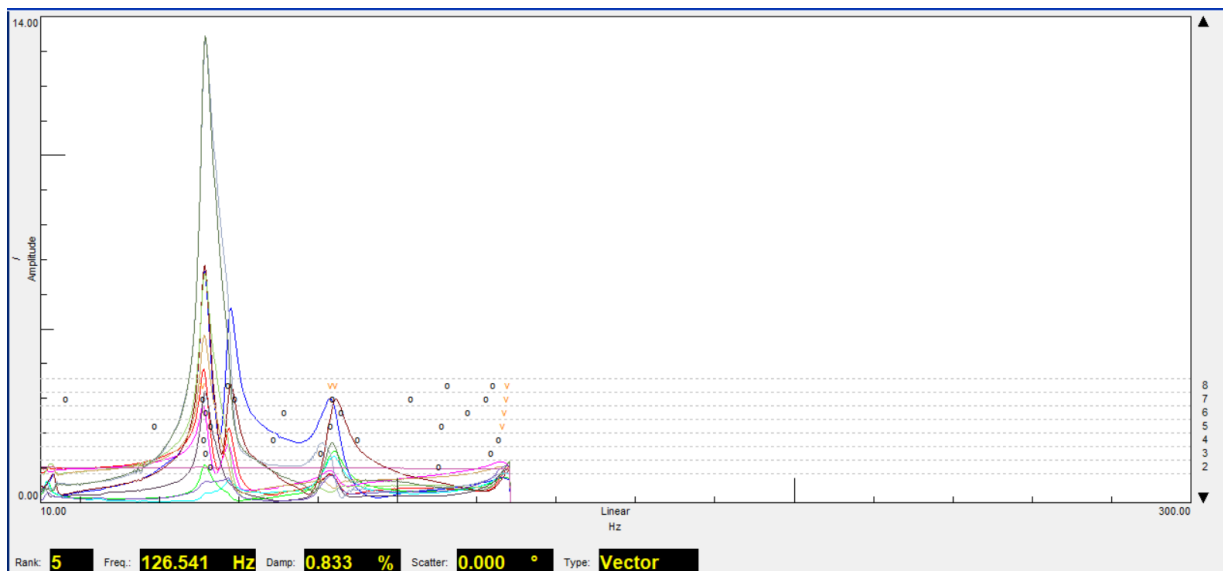


Figure 2.4.10 – Stabilization for x axis at 0.010 mm.

The next step consists in visualizing the shapes and check if they are feasible, then identify the modes and give them a description according to the results of Lupos simulation.

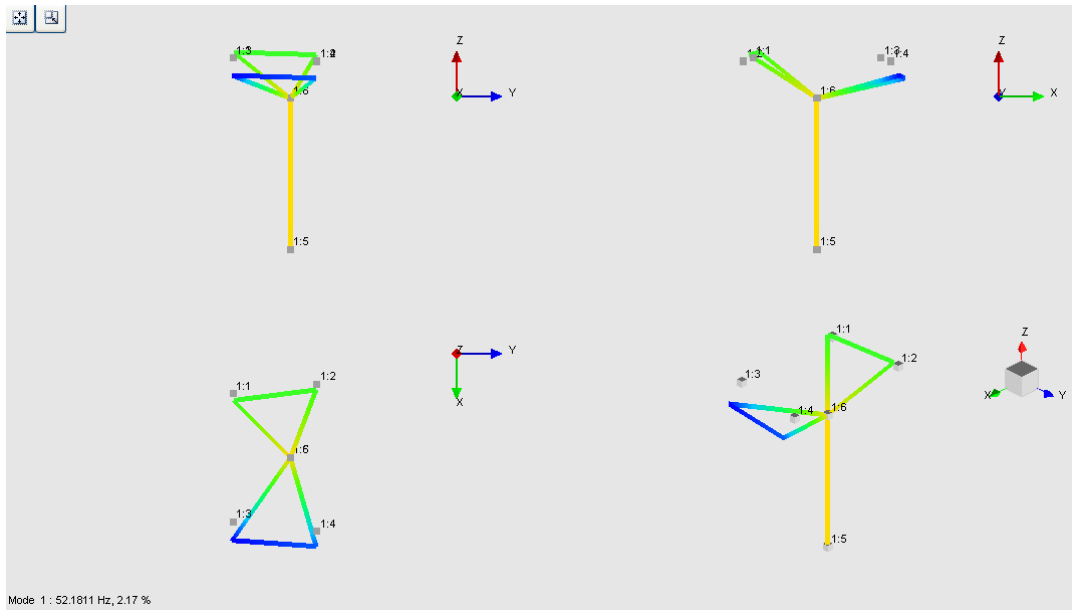


Figure 2.4.11 – Representation of mode 1, x excitation at 0.005 mm.

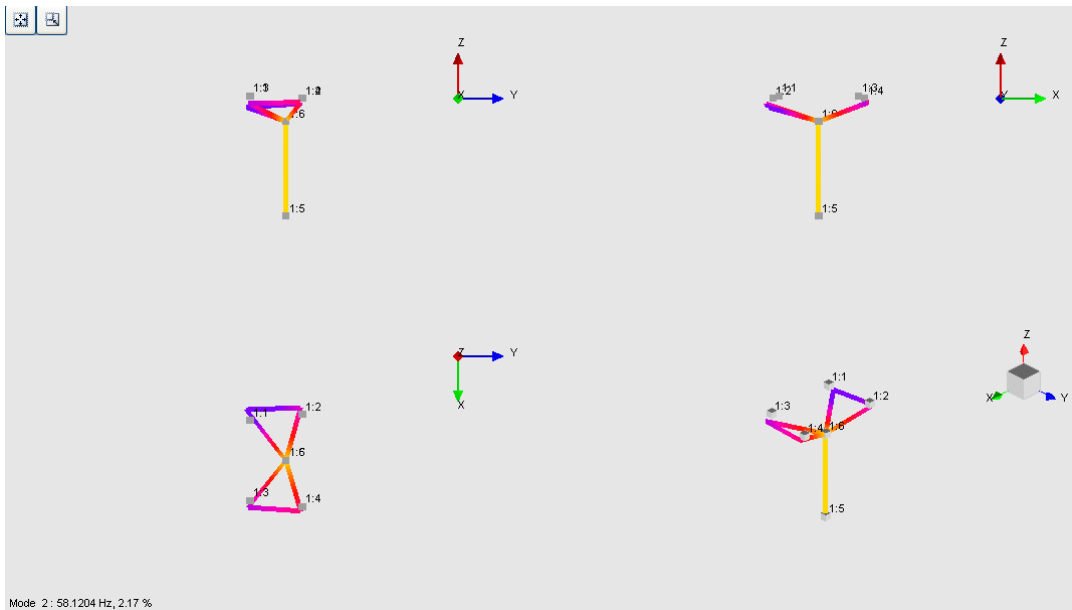


Figure 2.4.12 – Representation of mode 2, x excitation at 0.005 mm.

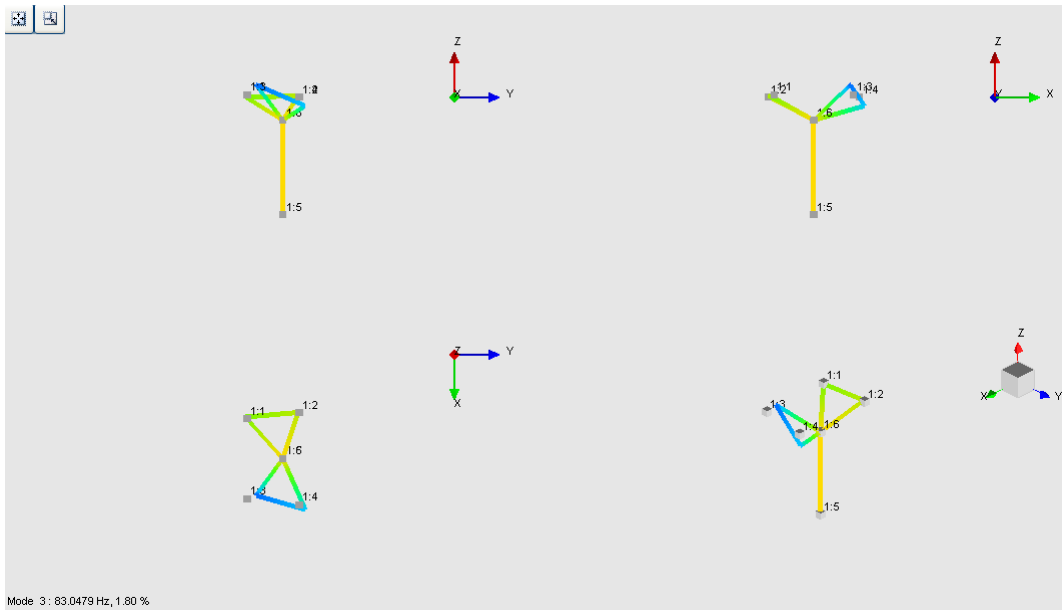


Figure 2.4.13 – Representation of mode 3, x excitation at 0.005 mm.

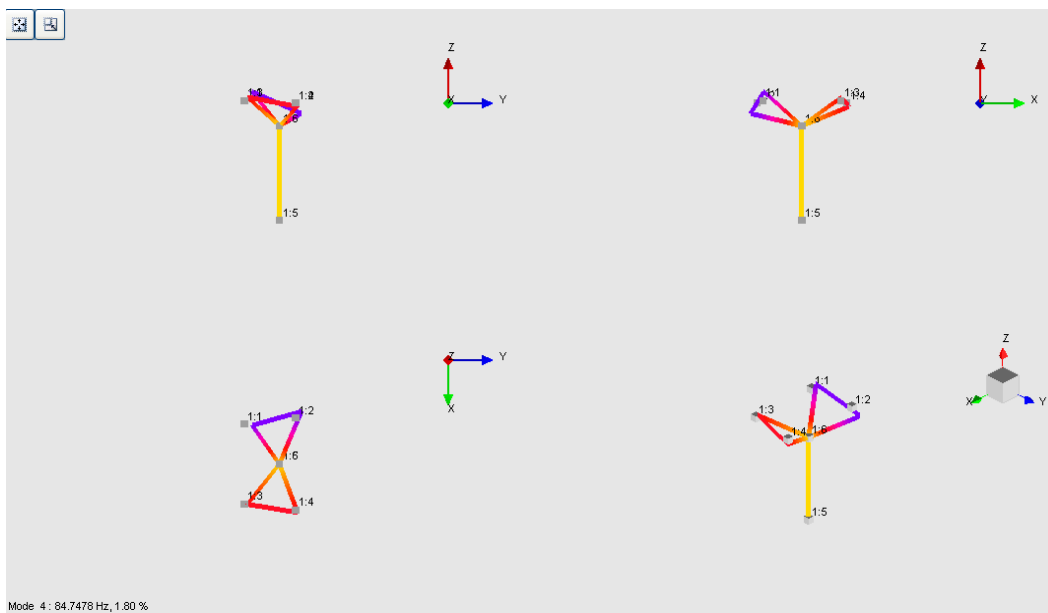


Figure 2.4.14 – Representation of mode 4, x excitation at 0.005 mm.

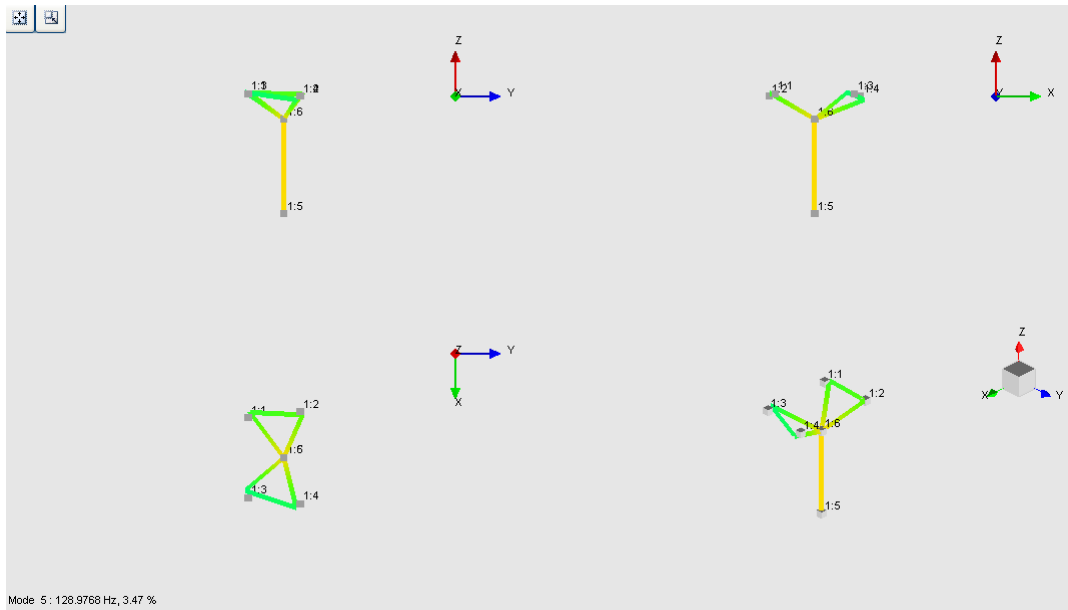


Figure 2.4.15 – Representation of mode 5, x excitation at 0.005 mm.

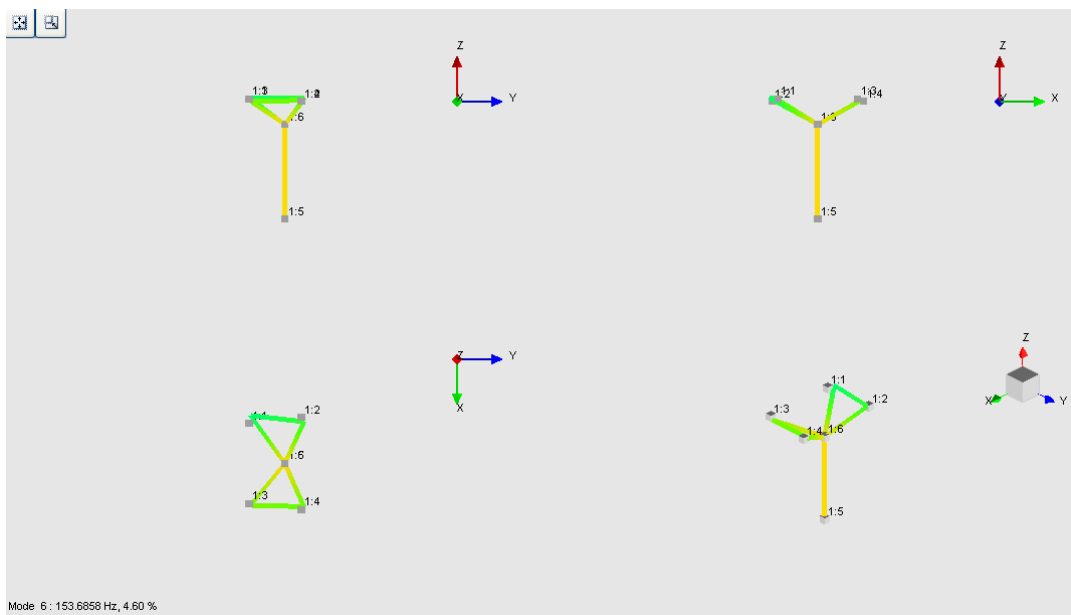


Figure 2.4.16 – Representation of mode 6, x excitation at 0.005 mm.

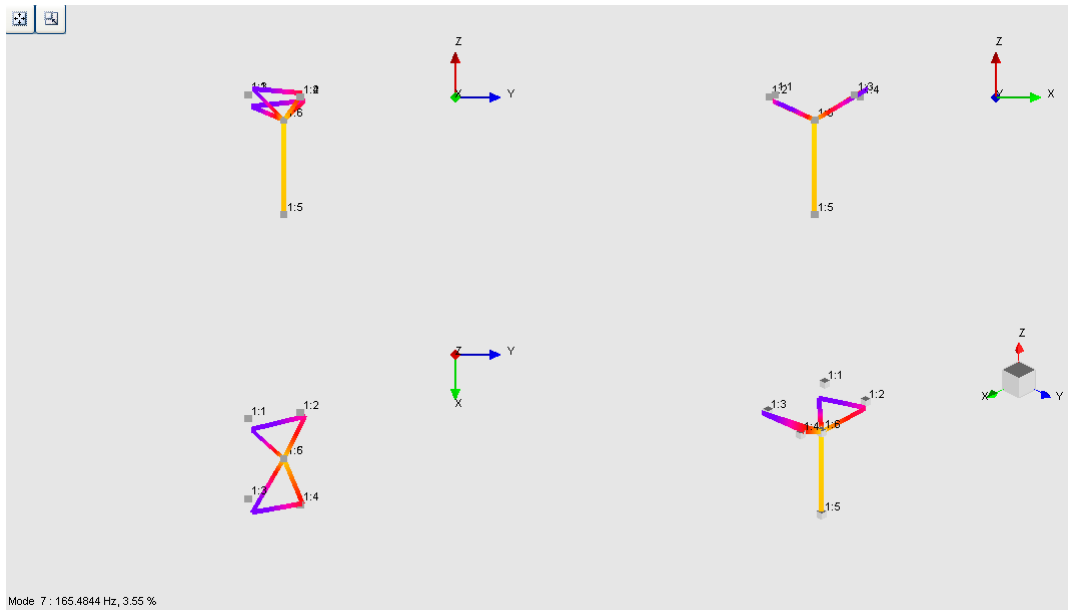


Figure 2.4.17 – Representation of mode 7, x excitation at 0.005 mm.

Modal validation

Once the frequencies are selected and the mode shapes identified, they have to be validated. In fact, it is necessary to see if the frequency chosen are correct.

In this part, it is calculated the Auto – MAC, an index which allows to understand if one mode shape is similar to another one. This technique is useful when comparing two different data excitations at different amplitude, to verify the similarities between modes.

In Figure 2.4.18 an example of Auto – MAC in table and in matrix form. The red squares indicate the diagonal where the similarities are at 100%. If in one square is present the index at 0%, it means that there is no relation between mode shapes.

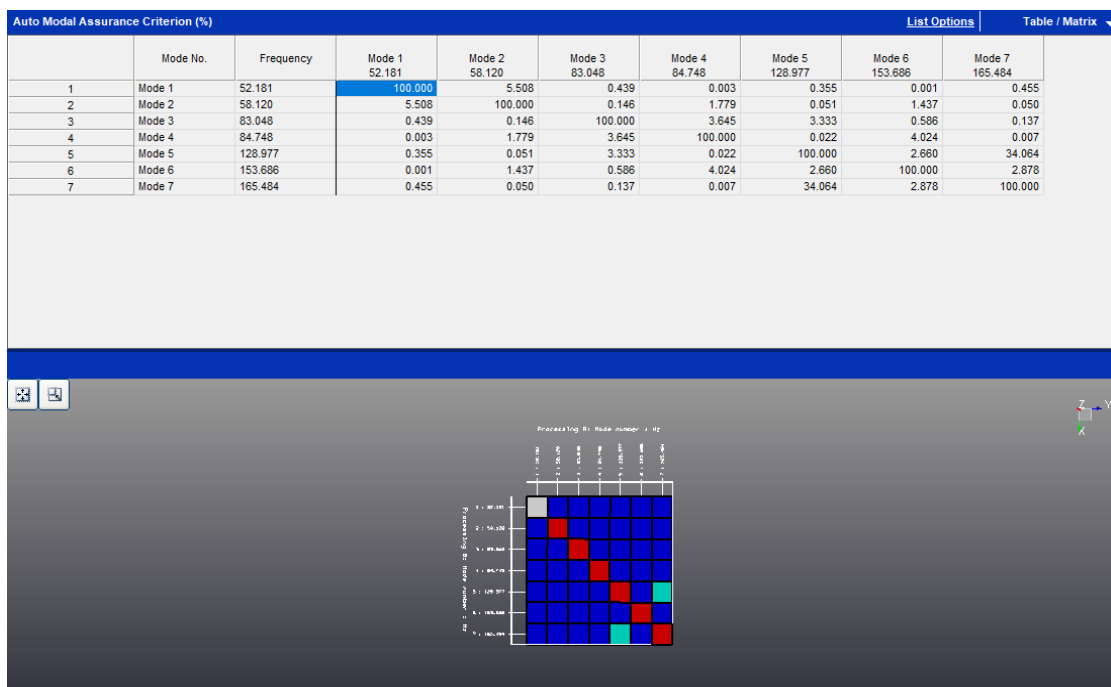


Figure 2.4.18 – Example of Auto – MAC with x excitation at 0.005 mm.

2.5 Sweep experimental analysis

The identifications on TestLab are done for all axes at three different imposed displacements 0.005, 0.010, 0.012 mm. Then, the result files are exported in MATLAB in order to manipulate and visualize all data better.

During identification some problems come out, especially for x axis, probably due to the position of the device testing x axis. Similar problems showed up for the identification of y axis at 0.012 mm probably due to the higher amplitude.

In Table 2.5.1 are resumed the data which are imported in Matlab and elaborated. Moreover, though TestLab is possible to analyse more axis at the same time, also this configuration is considered.

Table 2.5.1 – Identification done for each displacement on each axis.

Axis under test	Displacements [mm]
x	0.005
	0.010
	0.012
y	0.005
	0.010
	0.012
z	0.005
	0.010
	0.012
yz	0.005
	0.010
	0.012
xyz	0.005
	0.010
	0.012

2.5.1 Transmissibility

From Testlab the FRF are exported though universal file and used as 'file.dat' in Matlab. Since the imported data are calculated as acceleration on acceleration [g/g], the transfer function is defined as transmissibility. The acceleration considered are the ones from each single accelerometer on the data from the controller accelerometer (number 6). In this way it is possible to have a good representation of transmissibility TR.

In the Matlab code, the function UnwrapThres_deg is used to have clear result on the phase reducing the dense wave-like trend. The function is imposed with a threshold of 15° and a percentage correction of 100%. This way when the phase shows a change of value higher than 15° this data is corrected.

The axis notation of title refers to TestLab reference system.

Just to remind, Table 2.5.1.1 reports the reference system exchange.

Table 2.5.1.1 – Reference system exchange.

From Experimental to Numerical reference system
$x \rightarrow -x$
$y \rightarrow -z$
$z \rightarrow -y$

Transmissibility of x axis

In the following figure is represented the transmissibility (TR) when x axis is excited. For all the graphs the peaks have similar range of frequency, 50, 80, 130, 170 Hz, then at higher frequency the motion of plate influences the trend of curves.

In Figure 2.5.1.2, in the bottom graph, the green line is close to 1 for the range of frequency under analysis. Recalling that the position of the fifth and sixth accelerometer measure same data, it seems that the Levit and its plate move together, but the sixth accelerometer is placed quite far from the steering hole respect to the excitation axis.

The curves on excitation and response on x axis have similar trend at low frequency, in the other graph curves have not similar behaviour.

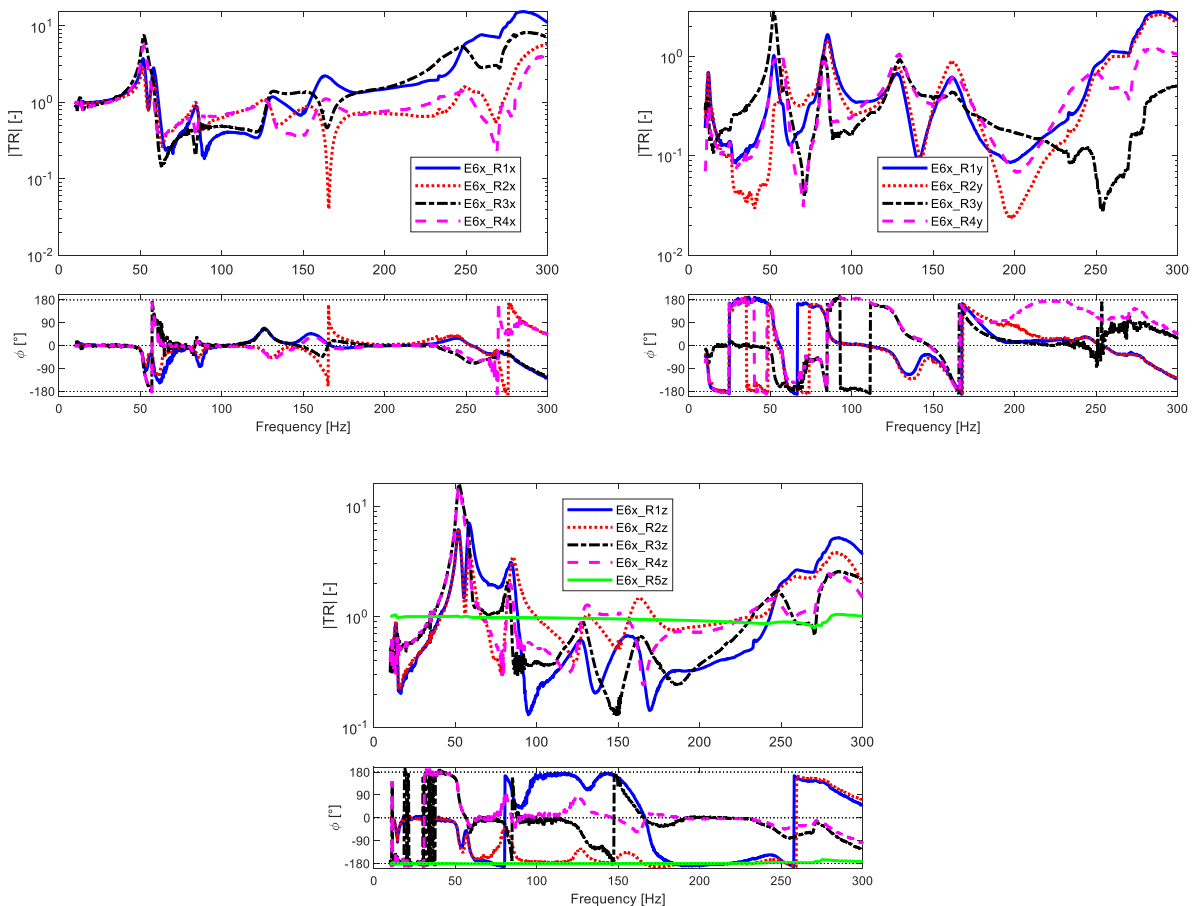


Figure 2.5.1.2 - TR at 0.005 mm x (top left), y (top right), z (bottom).

The curves of each single graph of Figure 2.5.1.3 have different trend from one direction to another. It is useful notice that for the TR at 0.010 and 0.012 mm the range of frequency under analysis decrease, from 0÷300 Hz to 0÷160 Hz, due to the higher values of displacements which produced an

interruption in the tests before the final target of 300 Hz. The graph with excitation and response on the same axis are more interesting than others.

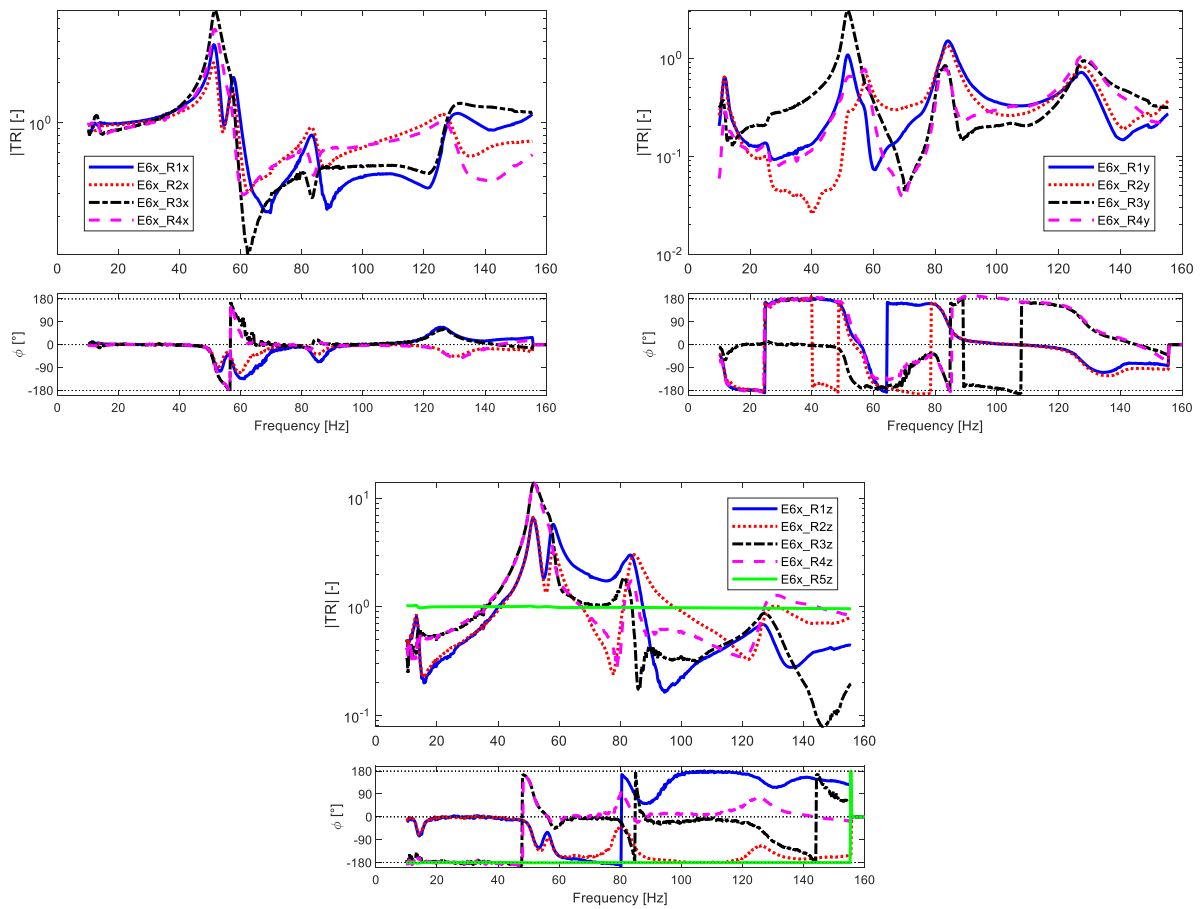


Figure 2.5.1.3 - TR at 0.010 mm x (top left), y (top right), z (bottom).

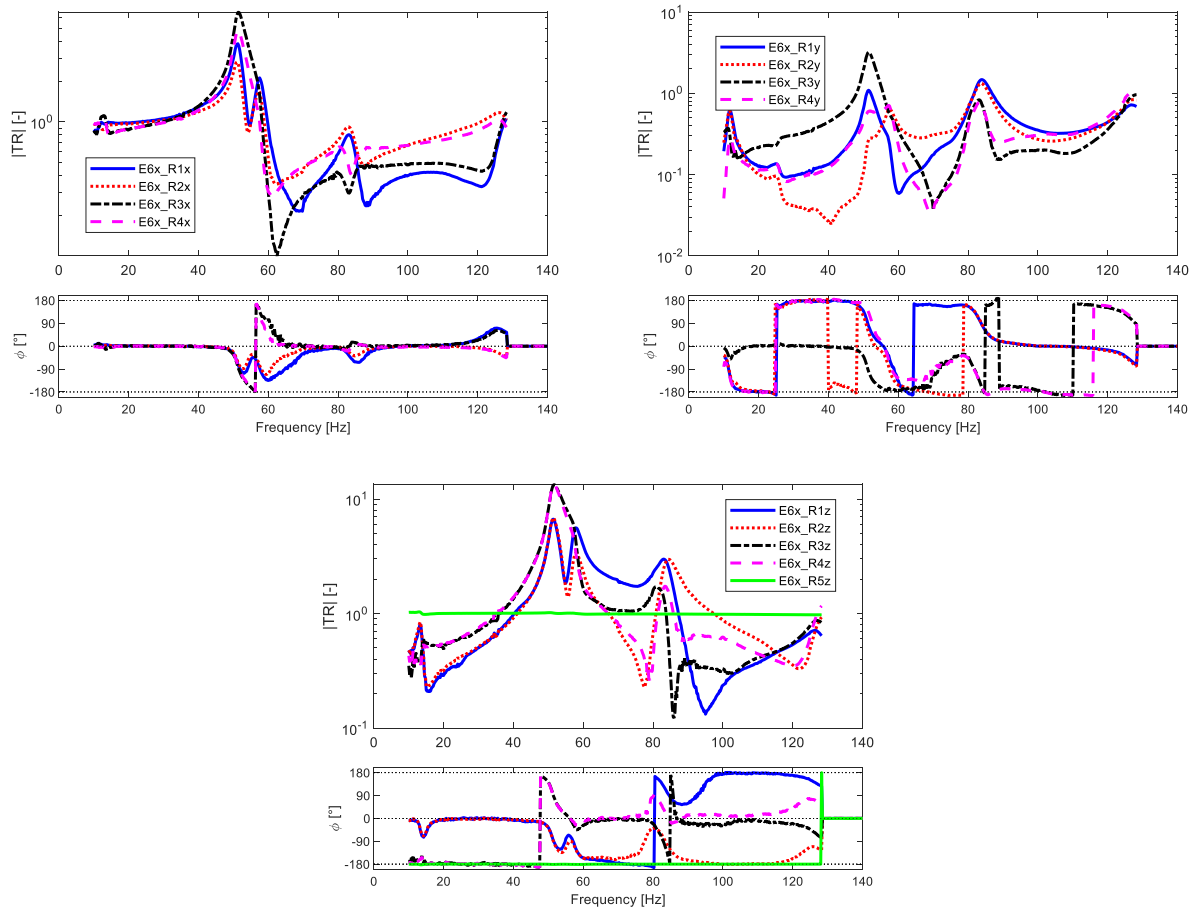


Figure 2.5.1.4 - TR at 0.012 mm x (top left), y (top right), z (bottom).

Transmissibility of y axis

Only the tests on y axis at 0.005 mm proceeds until the target of 300 Hz while the test with 0.010 mm reaches the maximum frequency of 190 Hz, the test at 0.012 mm stops at 140 Hz. Analogous consideration can be done also in this case, the most interesting graphs have excitation and response on y axis.

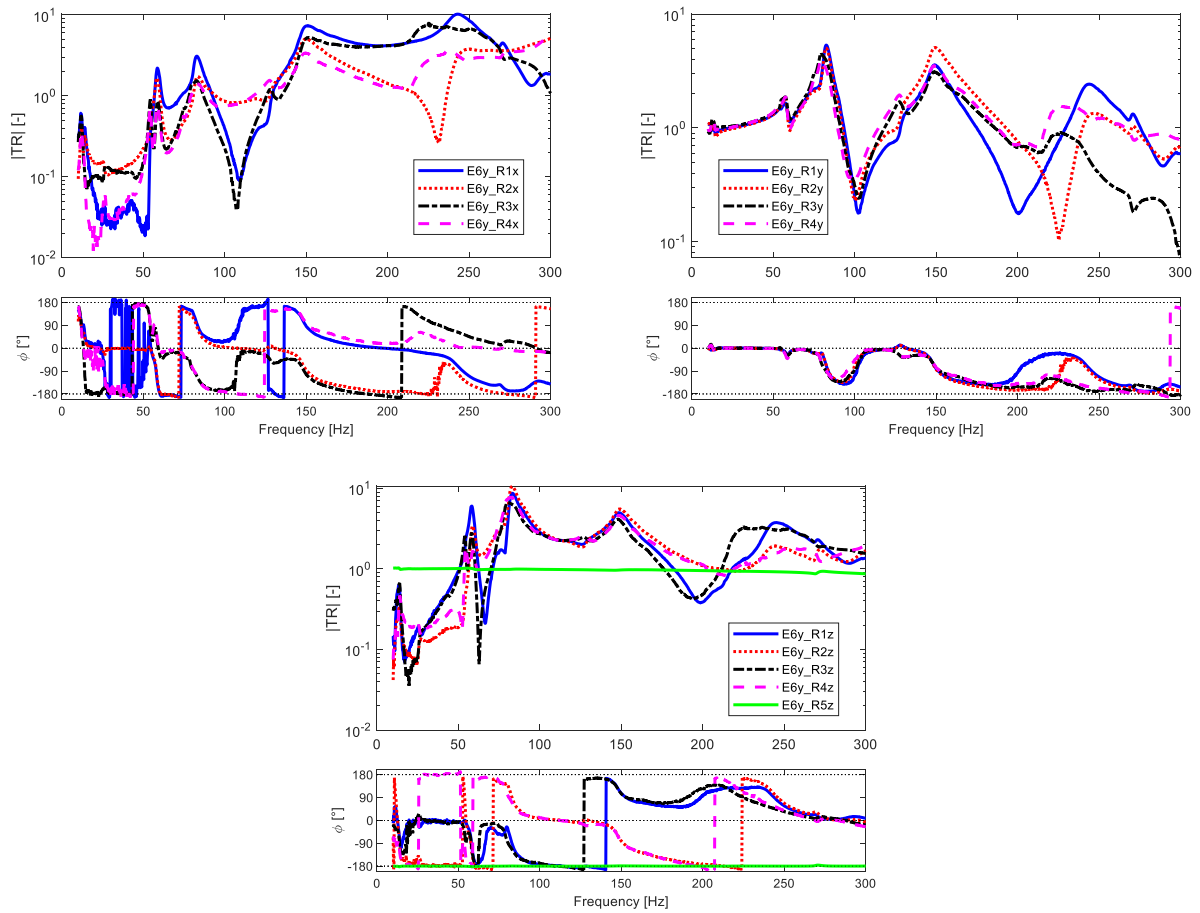


Figure 2.5.1.5 - TR at 0.005 mm x (top left), y (top right), z (bottom).

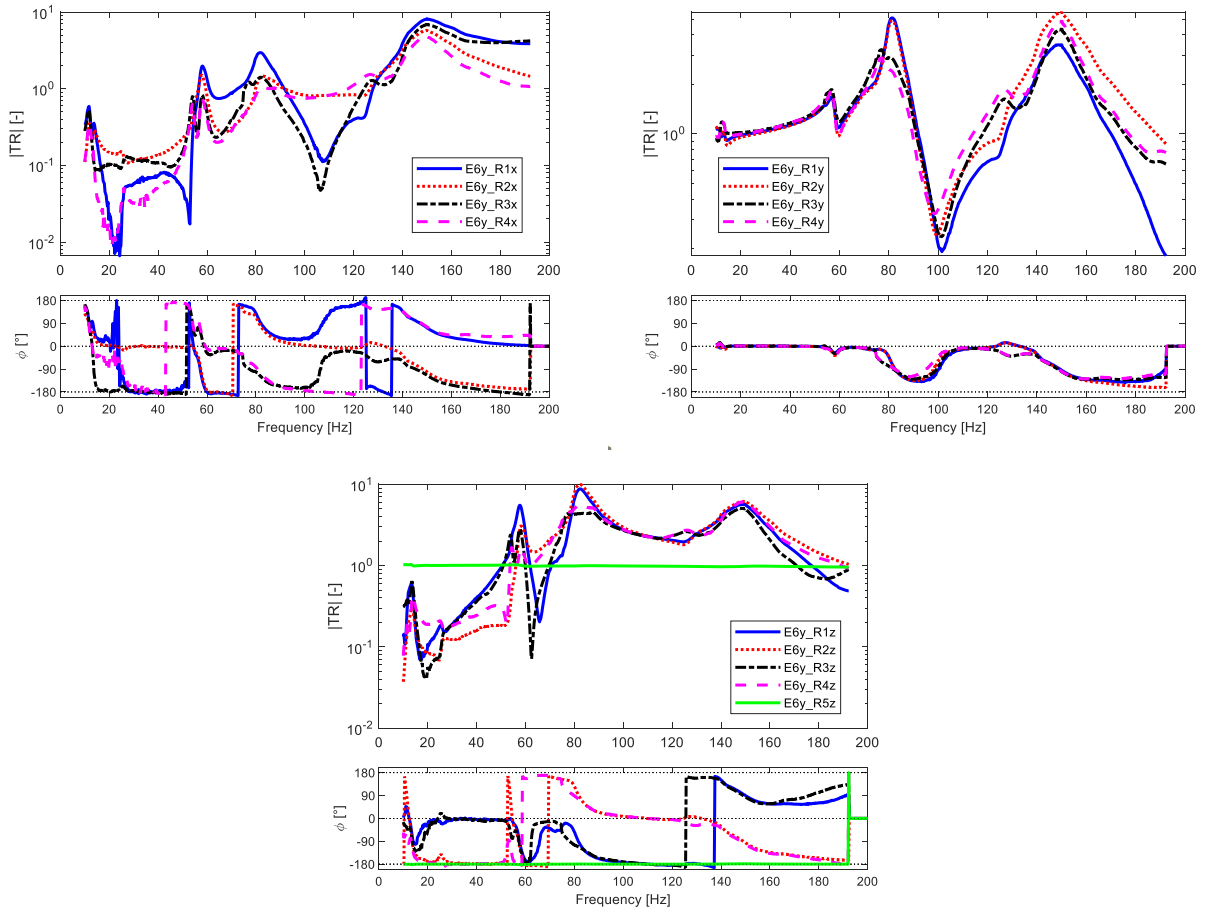


Figure 2.5.1.6 - TR at 0.010 mm x (top left), y (top right), z (bottom).

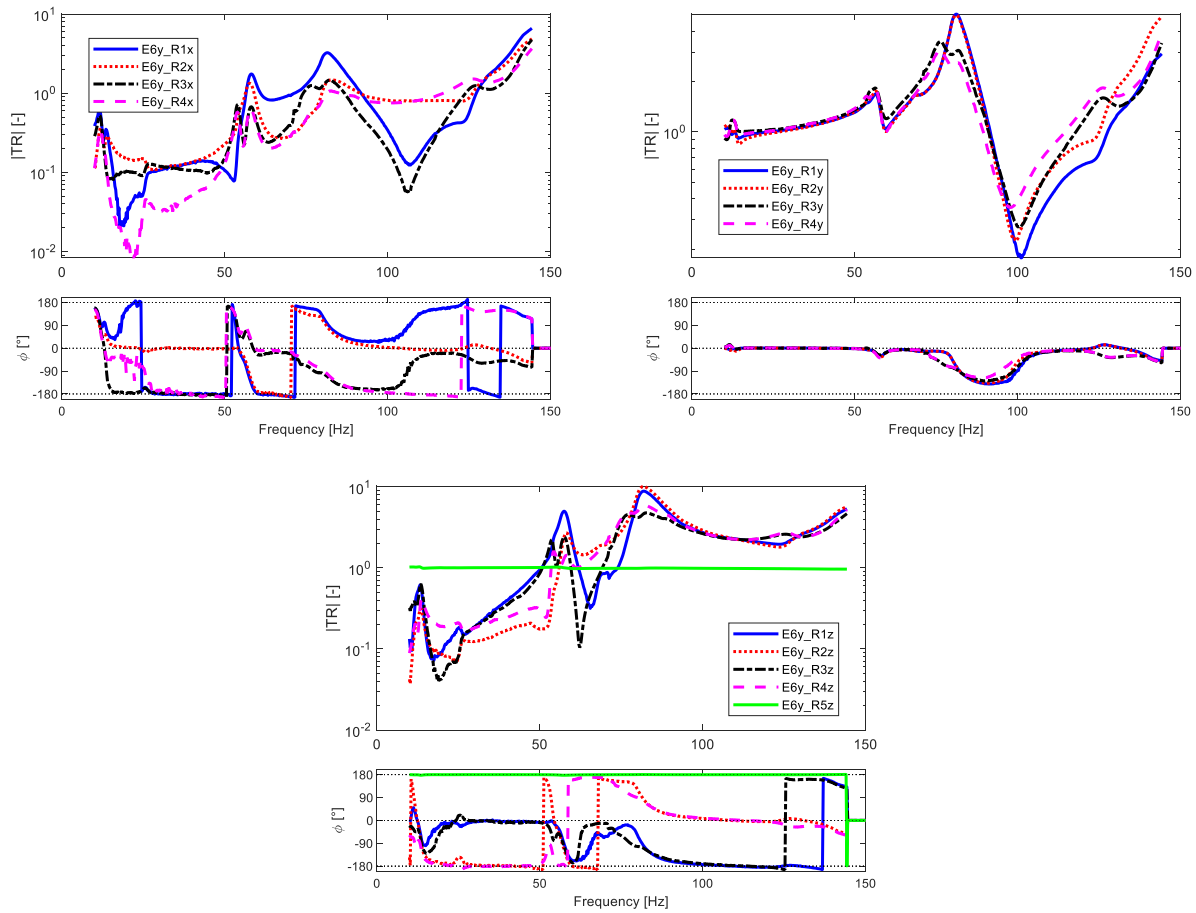


Figure 2.5.1.7 - TR at 0.012 mm x (top left), y (top right), z (bottom).

Increasing the amplitude of displacement from 0.005 to 0.012 mm, the results in phase increasing its variability. A good representation of the phase is present when the excitation and the TR of the accelerometer axis under analysis are the same. In this paragraph of y excitation, the clearest and the most representative phase lines are on y coordinates for each displacement, in Figure 2.5.1.7, upper right. The phase graph in other directions have more disturbances.

Transmissibility of z axis

In Figure 2.5.1.8 is represented the TR of 0.005 mm for the z axis of the four accelerometers 1÷4. There are four curves, the measure is about excitation on z direction and response on x direction. At 10 Hz there are some initial peaks due to the start of the sweep excitation, then at around 53÷58 Hz there are double peaks, and again at 80 Hz where the TR amplitude quickly decreases and increases. At 170 Hz the x component of accelerometers starts having different trend. These differences increase at higher frequency, due to the influence of the behaviour of the plate on which the Levit is placed.

In the graph of phase, it is visible that blue and red curve follow same path as well as the black and magenta line. Amplitude the difference between the response to excitation is more similar on all accelerometers.

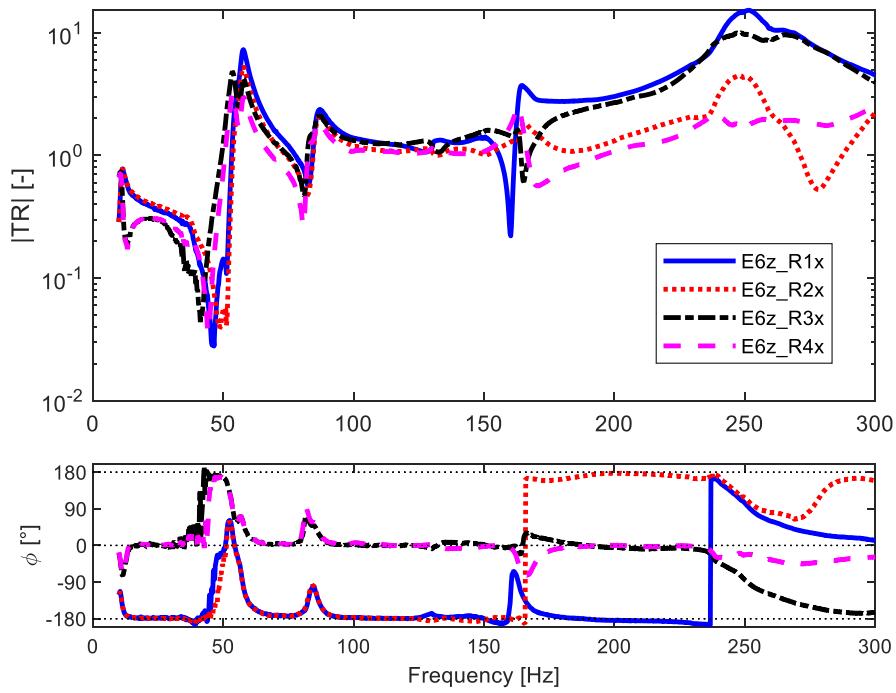


Figure 2.5.1.8 – TR of 0.005 mm for only x axis.

Similar consideration on frequency peaks can be done for Figure 2.5.1.9 where is reported TR at 0.005 mm with response on y axis of all accelerometers. Here blue and black lines follow similar path as well as red and magenta line, until 120 Hz, where the trend is wave-like, and then assumes similar behaviour at higher frequency, when the motion of the plate became dominant.

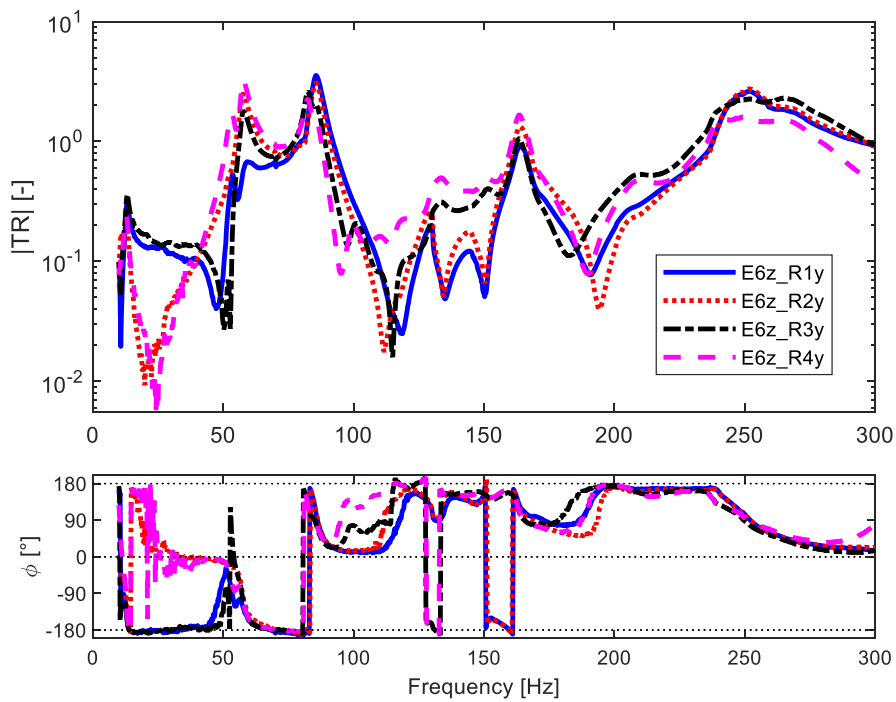


Figure 2.5.1.9 – TR of 0.005 mm for only y axis.

In Figure 2.5.1.10 are represented the transmissibility TR on z axis of the accelerometers, including the number five. The excitation and the response measured are both on z direction. The behaviour of the green curve is not very interesting with respect to the others, it just represents the displacements of the fifth accelerometer with respect to the sixth (controller). The black and blue curves have similar behaviour at lower frequency, as the red and pink, but all curves have peaks at same frequency. From 100 Hz to 150 Hz the trends of curves change one respect to another, but they reach a peak around 170 Hz.

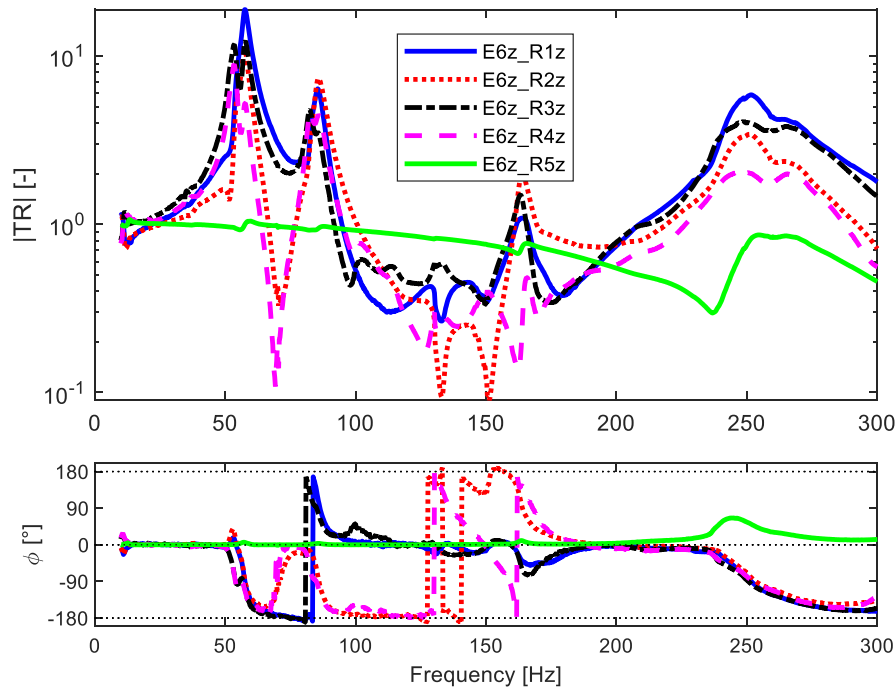


Figure 2.5.1.10 – TR of 0.005 mm for only z axis.

In Figure 2.5.1.11 are shown the TR of x, y, z at 0.010 mm. The frequencies of peaks have values similar to the TR at 0.005 mm. The general trend of curves is similar for blue and black lines as well as for the red and magenta lines.

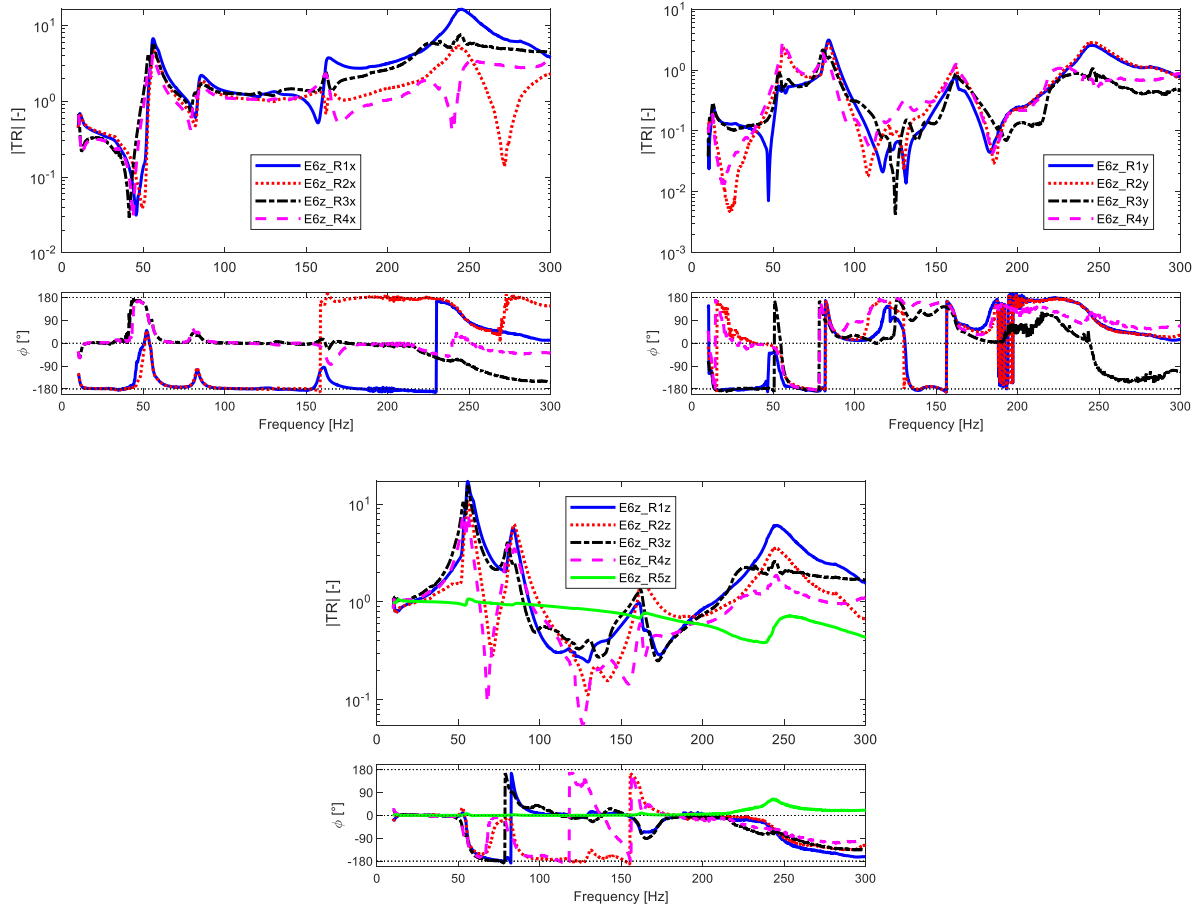


Figure 2.5.1.11– TR at 0.010 mm x (top left), y (top right), z (bottom).

Figure 2.5.1.12 shows the TR of x , y , z at 0.012 mm.

The peaks are at frequency similar to the amplitude of 0.010 mm, as the general trend of curves.

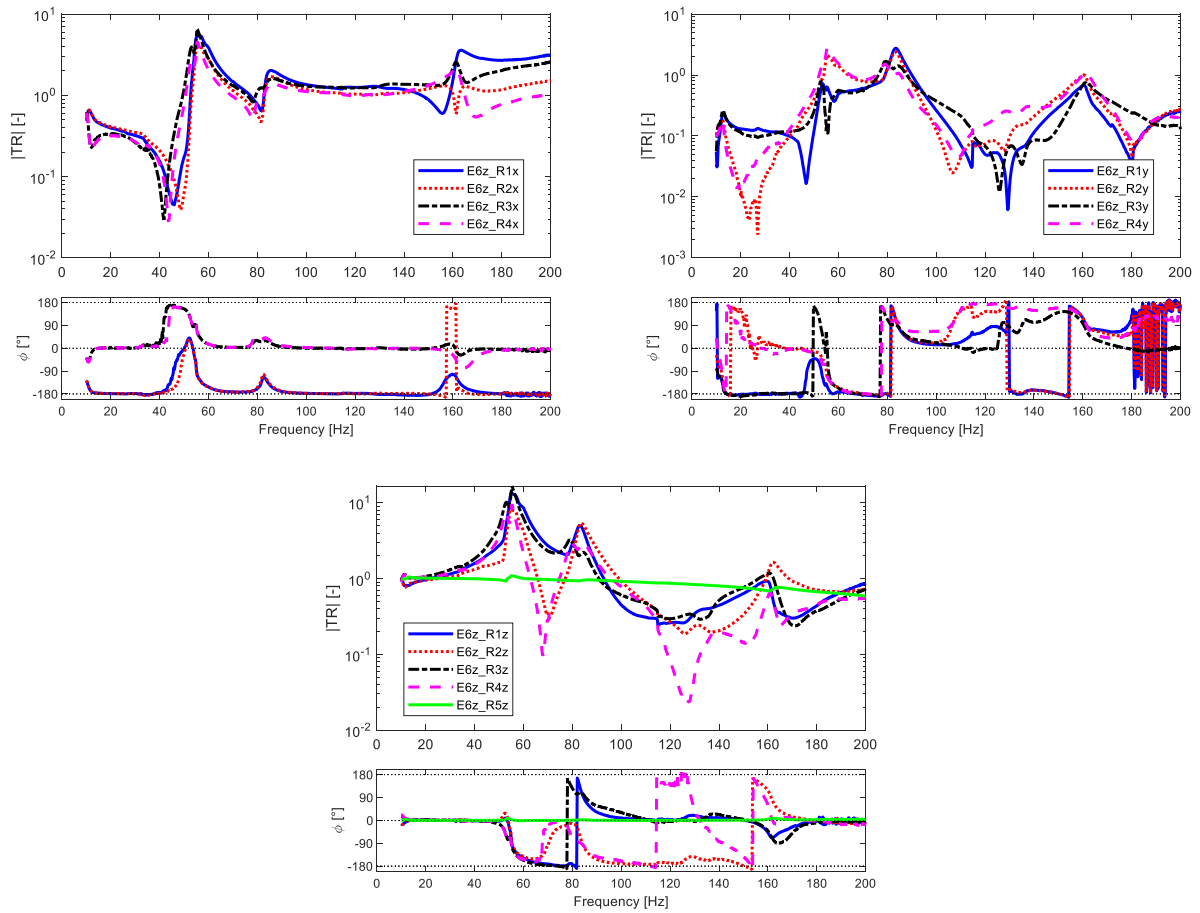


Figure 2.5.1.12 - TR at 0.012 mm x (top left), y (top right), z (bottom).

2.5.2 Natural frequencies

In following tables are resumed all frequencies found from the identification on TestLab. The range of frequency is similar for the majority of results. It can be notice that increasing the input displacement the highest natural frequency found decrease in magnitude.

Also, the identification on x axis was more difficult than the others. Probably because the accelerometer of control (6th) was not placed in best position and the orientation of the device under test could negatively influence the results.

Remember that the more important axis to control is the z axis, on the experimental reference system (which corresponds to $-y$ in the numerical ones).

Table 2.5.2.1 – Frequency of TestLab identification at 0.005 mm.

Frequency in [Hz] at displacement 0.005 mm					
Mode shape	x	y	z	yz	xyz
1	52.19	54.13	53.25	53.40	52.54
2	58.13	58.10	57.97	58.01	58.24
3	83.06	80.10	82.64	82.74	82.64
4	84.76	83.45	85.95	86.17	84.86
5	129.05	128.43	163.97	128.65	129.20
6	153.85	148.71	238.72	164.02	-
7	165.59	239.85	251.18	248.21	-
8	-	-	262.40	251.48	-

Table 2.5.2.2 – Frequency of TestLab identification at 0.010 mm.

Frequency in [Hz] at displacement 0.010 mm					
Mode shape	x	y	z	yz	xyz
1	51.76	53.94	52.87	53.22	52.54
2	57.85	57.60	55.59	55.68	58.24
3	83.92	80.94	80.95	80.93	82.64
4	128.78	83.55	84.95	84.37	84.86
5	-	127.37	162.66	148.57	129.20
6	-	140.51	246.44	162.54	-
7	-	148.42	-	-	-

Table 2.5.2.3 – Frequency of TestLab identification at 0.012 mm.

Frequency in [Hz] at displacement 0.012 mm					
Mode shape	x	y	z	yz	xyz
1	51.66	51.61	52.88	53.16	51.61
2	83.37	83.77	55.21	54.96	83.77
3	-	-	79.13	80.64	-
4	-	-	84.31	8382	-
5	-	-	161.58	125.90	-
6	-	-	-	143.16	-
7	-	-	-	161.67	-

2.5.3 Transmissibility and natural frequencies

In this paragraph are evidenced the transmissibility graphs and their natural frequencies when the excitation and response are on the same axis, it is also reported the table with frequency for each axis, in particular it is analysed the displacements of 0.005 mm. Moreover, at z axis is added a figure showing the frequencies and their mode shapes.

Even in this paragraph is kept the experimental reference system, so the main important axis to analyse is the z axis which correspond to the y axis on numerical reference system.

- **x axis**

Figure 2.5.3.1 shows the transmissibility between the excitation of the sixth accelerometer and the response of the paddles on x axis through the accelerometers 1÷4. Moreover, the natural frequencies are evidenced with vertical line on graph, in order to clearly identify the peaks.

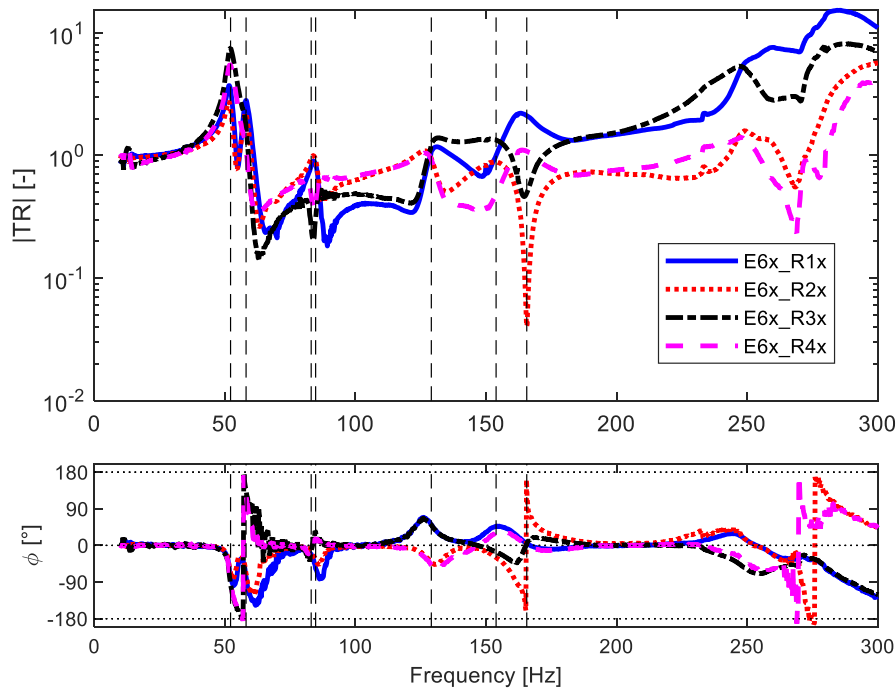


Figure 2.5.3.1 – Excitation of 6th accelerometer on x axis and response of four accelerometer on x axis at 0.005 mm.

Table 2.5.3.1 – Frequency of TestLab identification at 0.005 mm.

Excitation on x axis at displacement 0.005 mm	
Mode shape	Frequency [Hz]
1	52.19
2	58.13
3	83.06
4	84.76
5	129.05
6	153.85

7	165.59
---	--------

- **y axis**

Figure 2.5.3.2 shows excitation on y axis, the vertical line evidence the natural frequency identified during the post processing on TestLab, they are in correspondence of the peaks of the transmissibility. The magnitude of transmissibility on y is lower respect to the others direction, this behaviour is predictable thinking about how the Levit is positioned on the vehicle, on y axis the excitations are lower impactful respect to other axes.

Table 2.5.3.2 resumed natural frequency from experimental test.

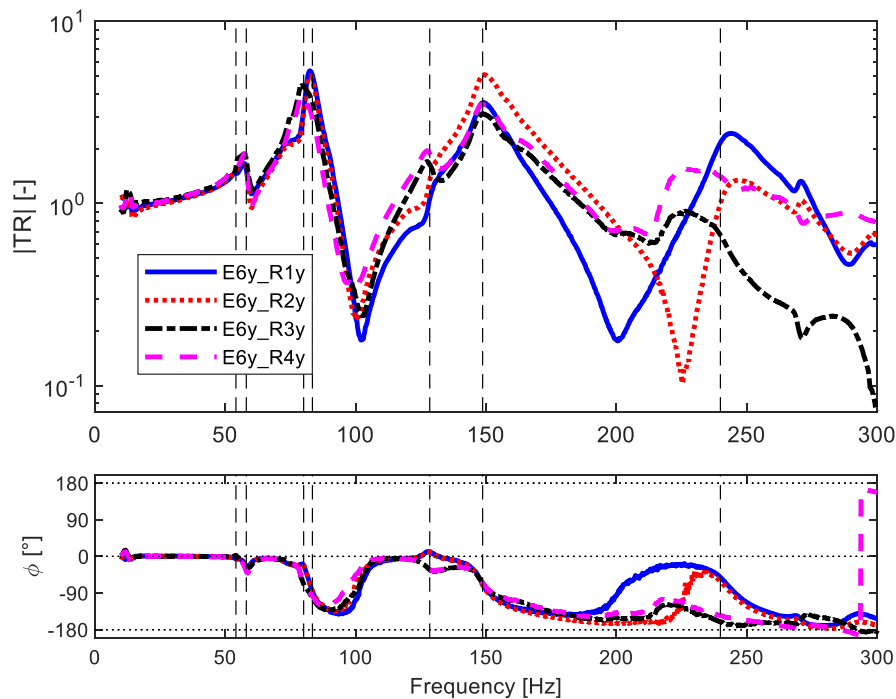


Figure 2.5.3.2 – Excitation of 6th accelerometer on y axis and response of four accelerometer on y axis at 0.005 mm.

Table 2.5.3.2 – Frequency of TestLab identification at 0.005 mm.

Excitation on y axis at displacement 0.005 mm	
Mode shape	Frequency [Hz]
1	54.13
2	58.10
3	80.10
4	83.45
5	128.43
6	148.71
7	239.85

- **z axis**

Figure 2.5.3.3 shows the transmissibility between excitation of one accelerometer and the response of the accelerometers 1÷4.

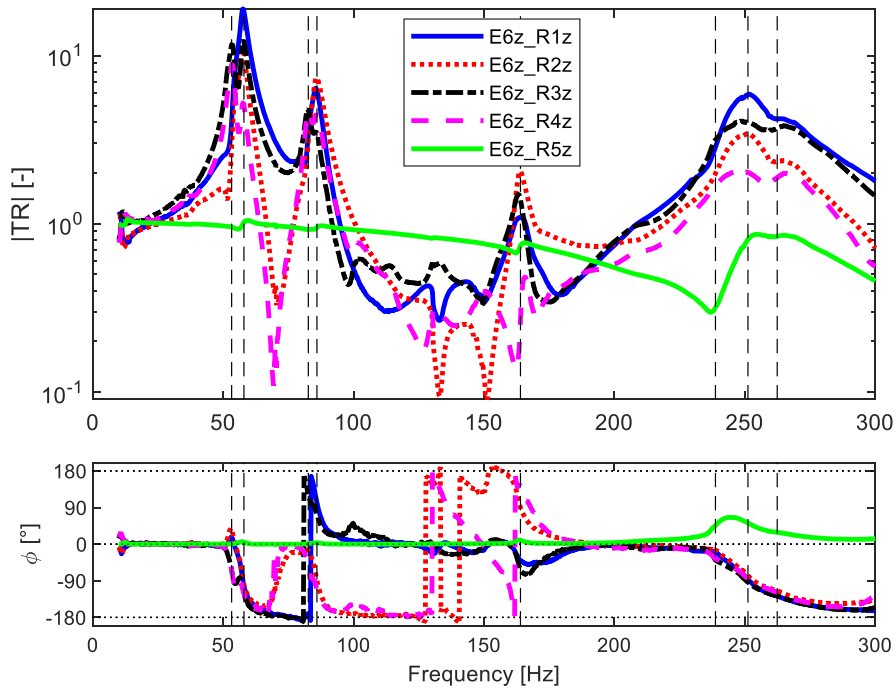


Figure 2.5.3.3 – Excitation of 6th accelerometer on z axis and response of four accelerometer on z axis at 0.005 mm.

Table 2.5.3.3 – Frequency of TestLab identification at 0.005 mm.

Excitation on z axis at displacement 0.005 mm	
Mode shape	Frequency [Hz]
1	53.25
2	57.97
3	82.64
4	85.95
5	163.97
6	238.72
7	251.18
8	262.40

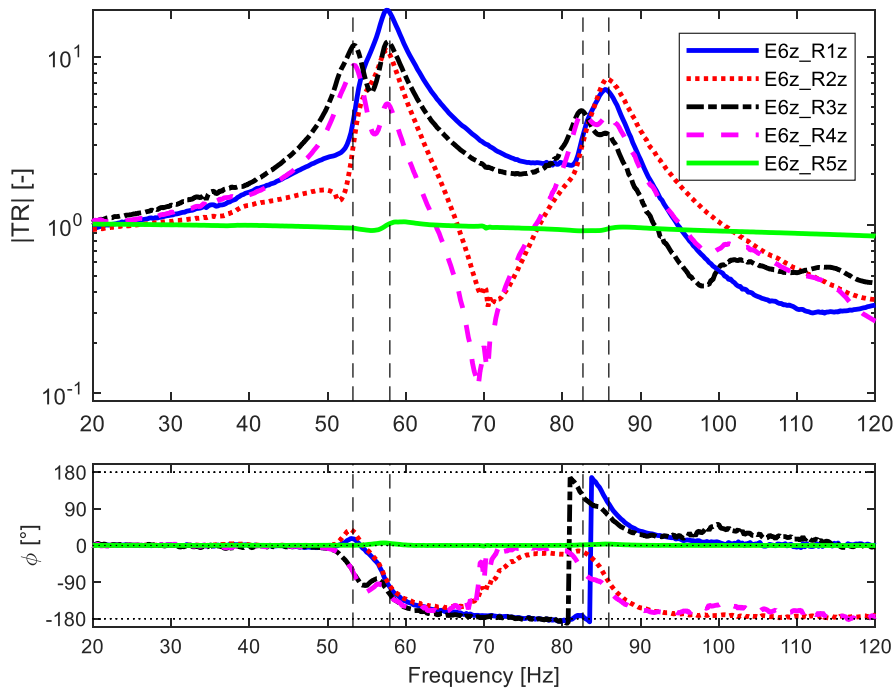


Figure 2.5.3.4 – Details of the firsts four natural frequency of excitation and response of accelerometers on z axis at 0.005 mm.

Figure 2.5.3.5 shows the height of frequency columns at different displacement on the excitation of z axis. The legend on graph already clarified the columns colour, but it is worth noticing that the blue line has slight bigger frequency respect to others from mode 1 to 5, in sixth mode the red frequency is lower than blue column. For the last two modes is not possible having a good comparison, the data are available just for one displacement.

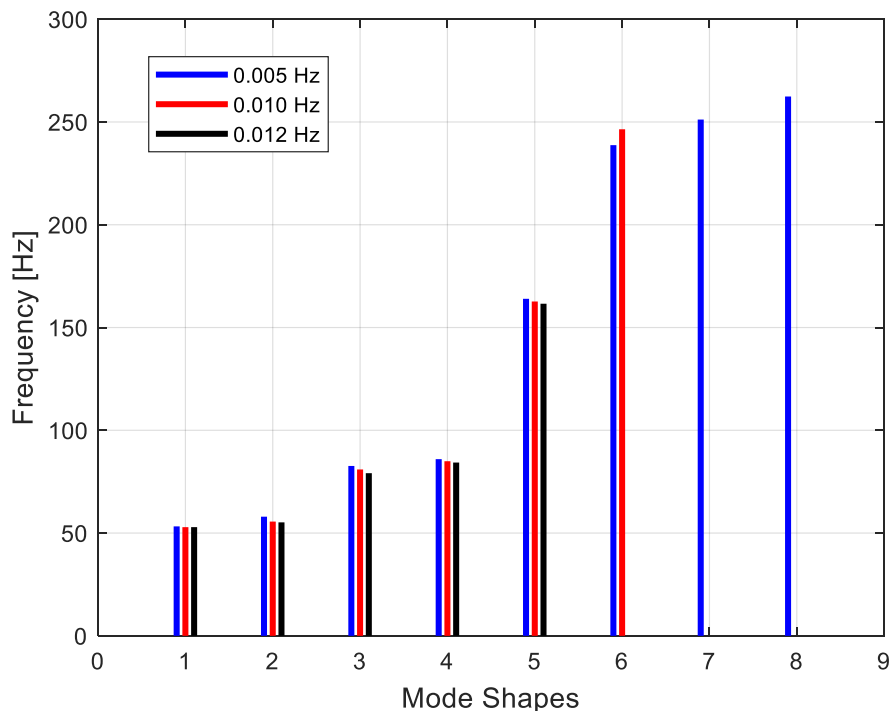


Figure 2.5.3.5– Representation of frequency at displacements 0.005, 0.010, 0.012 mm and their mode on z axis.

In Figure 2.5.3.6 is shown the transmissibility between the excitation from sixth accelerometer and the response of the others along z axis, the dot black vertical lines evidence the natural frequency, these values are reported also in Table 2.5.3.4. The data reported are referring to a displacements of 0.010 mm.

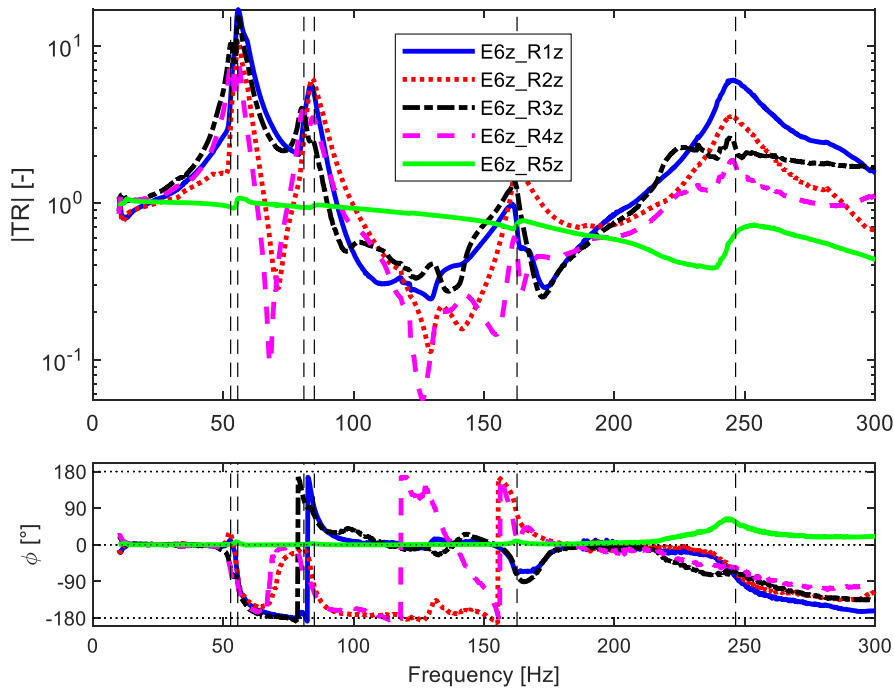


Figure 2.5.3.6 – Excitation 6 on z axis and response of four accelerometer on z axis at 0.010 mm.

Table 2.5.3.4 – Frequency of TestLab identification at 0.010 mm.

Excitation on z axis at displacement 0.010 mm	
Mode shape	Frequency [Hz]
1	52.87
2	55.59
3	80.95
4	84.95
5	162.66
6	246.44

- yz axes

Figure 2.5.3.7 reports the histogram of frequency-mode shapes for the three displacements tested. The frequencies at lower value are quite similar for all three cases, from five mode on the differences increase between one and another. The red column in mode number five has bigger values respect to others, while in previous excitation the blue lines are higher. Mode 7 and 8 present low number of data, they are less useful for the comparison.

From histogram it is possible to see that modes at frequency above 100 Hz could have misaligned one another. In example mode n.º7 has column with different heights, 248.21 Hz at 0.005 mm while at 0.012 mm the value is 161.67 Hz, these types of coupling influence the MAC correlation analysis in next paragraph.

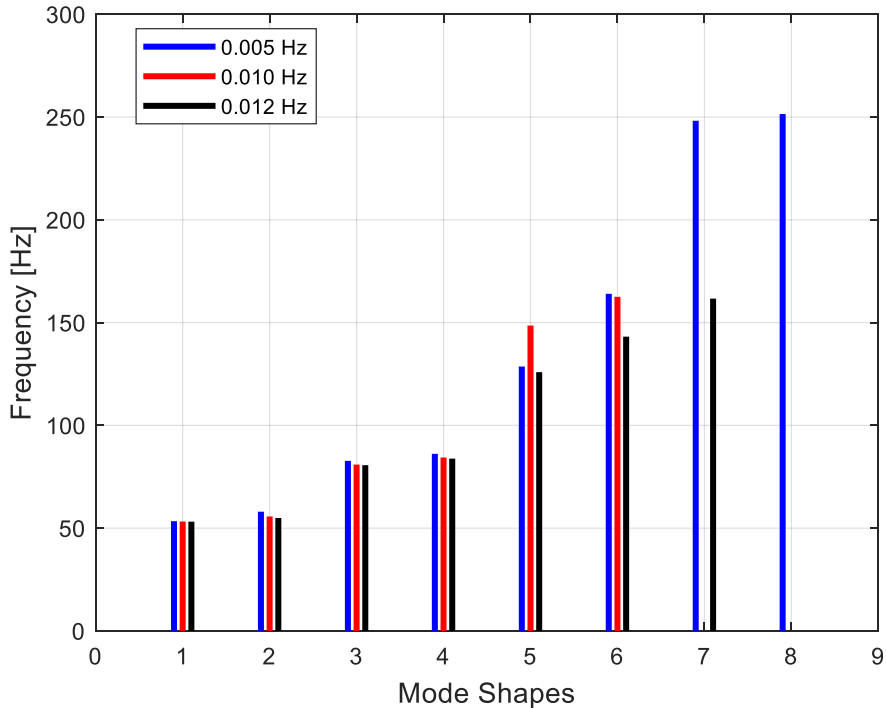


Figure 2.5.3.7 – Representation of frequency at displacements 0.005, 0.010, 0.012 mm and their mode on yz axes.

- **xyz axes**

Figure 2.5.3.8 illustrates the combination of experimental data on all three axes. The maximum frequency obtained is 150 Hz with excitation imposed of 0.010 mm. Mode 3 black column is higher than the frequency in the same mode, probably this value should be better compared with sixth mode, while the other frequencies are consistent with their mode.

From figure it is possible to see that the frequencies of firsts four mode are similar for blue and red columns.

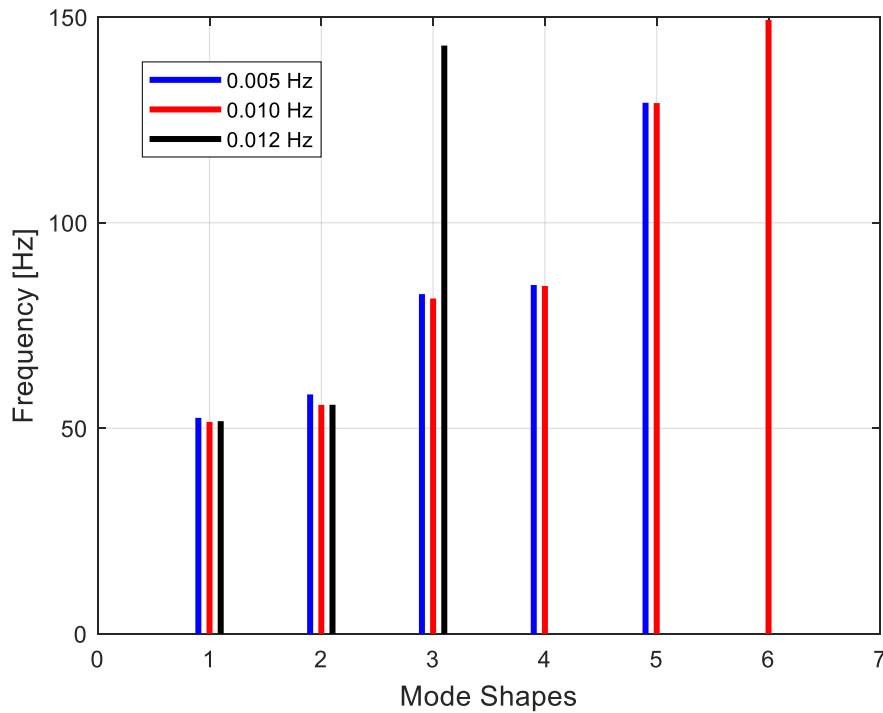


Figure 2.5.3.8 – Representation of frequency at displacements 0.005, 0.010, 0.012 mm and their mode on *xyz* axes.

2.5.4 Transmissibility synthesis

On TestLab there is the possibility to make a synthesis of the experimental results. This option creates a connection between the TR experimental data and the manual identification done with PolyMAX part. The peaks will be more centred on the natural frequency identified, also the phase is modified by synthesis option and with `UnwrapThres_deg.m` code.

The results presented refers to TestLab reference system.

Figure 2.5.4.1 presents the synthesized transmissibility done on TestLab.

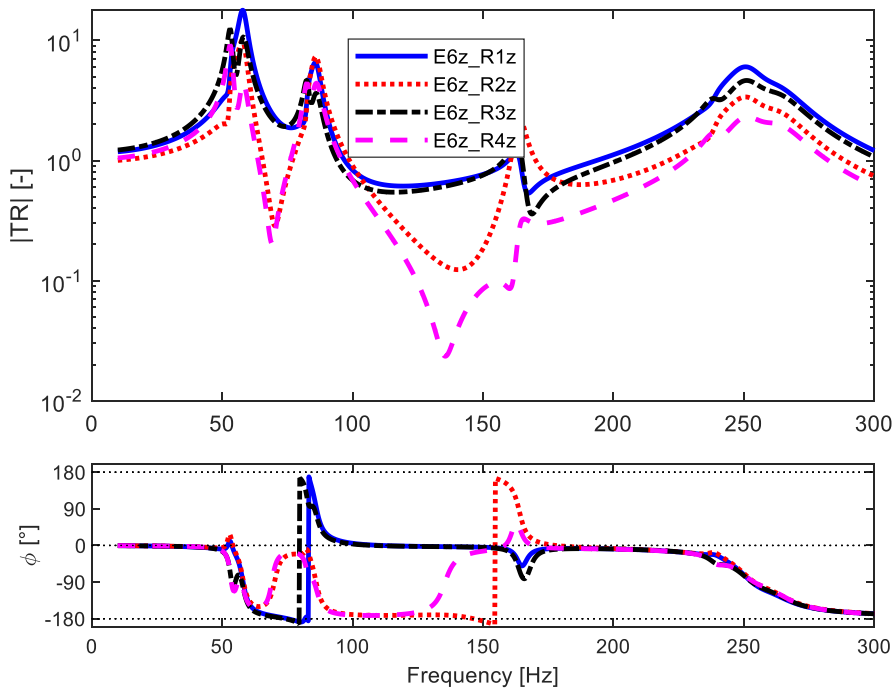


Figure 2.5.4.1– TR synthesized of z axis at 0.005 mm.

Figure 2.5.4.2 shows again the transmissibility from synthesis on the left, and the exact experimental data on the right. Both graphs have vertical line for evidence the experimental natural frequencies. Note that the curves in correspondence of vertical line have the same shape, while in the middle space the trend can change. For example, between 50 Hz and 90 Hz the shapes have little difference, or at 100÷150 Hz where the differences are more evident. This because on the left graph the behaviour is approximated based on values of natural frequencies, while on the right image is reported the real reaction of the accelerometers. Since the intermediate trend between vertical line are ‘built’ for synthesized, the phase became clearer in those images than in the real experimental graphs. Consider that the two graph have the same scale.

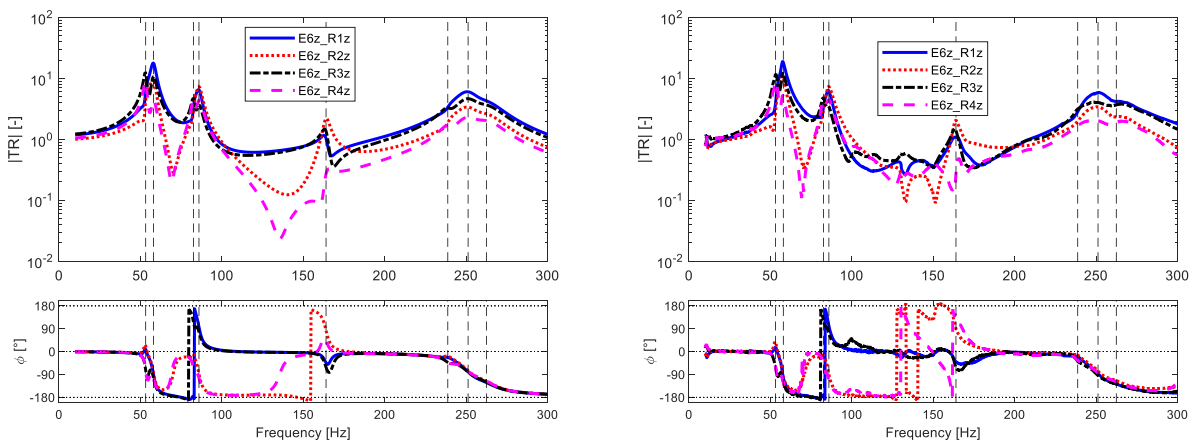


Figure 2.5.4.2 – TR synthesized (left) and TR experimental (right) of z axis at 0.005 mm.

Figure 2.5.4.3 reports the synthesized data with displacements of 0.010 mm.

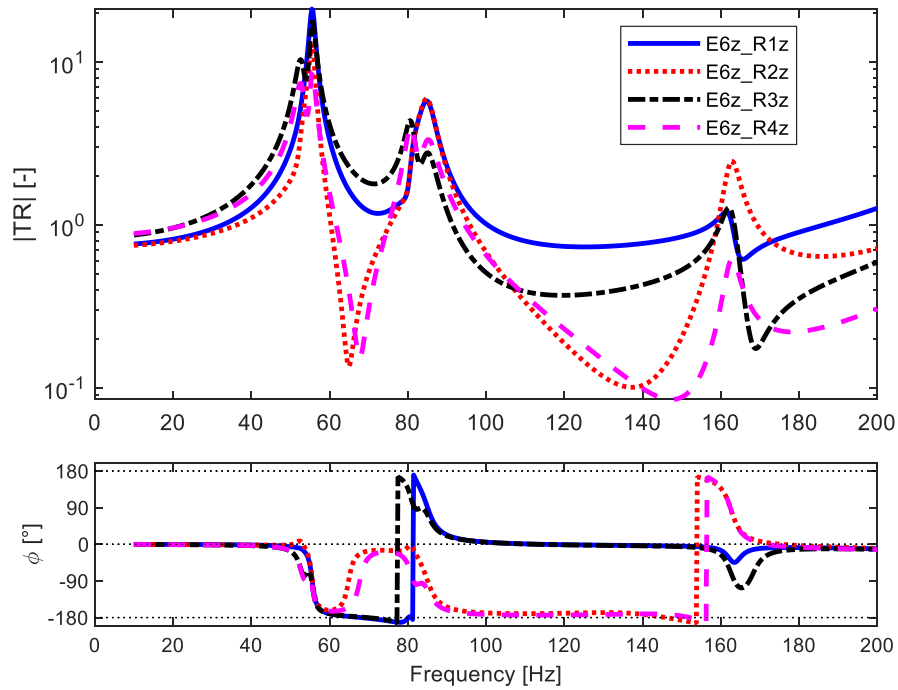


Figure 2.5.4.3 – TR synthesized of z axis at 0.010 mm.

Considering Figure 2.5.4.4 can be done comments similar to the ones of the previous graphs.

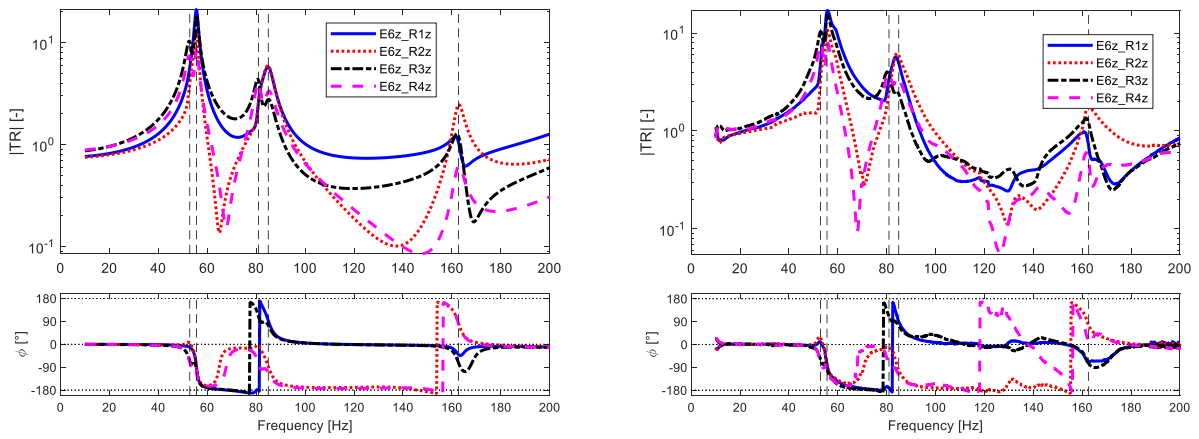


Figure 2.5.4.4 – TR synthesized (left) and TR experimental (right) at of z axis at 0.010 mm.

2.6 Sweep experimental MAC

The Modal Assurance Criterion (MAC index) is used to give an estimation of how similar two real eigenvectors are. In fact, it is important to give evidence of the correlation and similarities between the experimental and the numerical results of the Levit. Then, MAC correlation helps to maintain the connection between mode shapes and their frequencies.

The function of MAC is defined from the correlation of two real eigenvectors Φ_j and Φ_k :

$$MAC_{j,k} = \frac{[\Phi_j^T \Phi_k]^2}{[\Phi_j^T \Phi_j][\Phi_k^T \Phi_k]}$$

In our study is used MACW, a variation which allows to check the orthogonality of the real eigenvectors.

In the following part the MAC analysis and comparison of the experimental with the numerical results is presented. For EMA data are used the experimental result, while with FEA are represented the analytical/numerical data.

To have first evaluation of the MAC matrix, it is useful to see how much the matrix is close to the identity one; the black line in graph should represent the diagonal of the matrix. Each numerical results should be related with its respective experimental value and independent from the others.

The experimental data has been manipulated on MATLAB changing the coordinates according to scheme of reference system in Table 2.2.1. To have a correct comparison of data with MAC construction. Using Table 2.2.2 we change all sign of axis and switch y and z axis. We need to change the coordinates in order to compare in correct way with the same reference system the experimental and the numerical data.

Next paragraph titles refer to numerical reference system.

MAC on x axis

In Figure 2.6.1 is represented the MAC with imposed displacement 0.005 mm. The correlation of first and second mode is at 80% between experimental and numerical results for all the following graphs, while the correlation for third and fourth mode is lower, around 50-60%.

These last two modes are not perfectly on the main diagonal, so the correlation decrease respect to the previous two.

Few data are available for the comparison analysis in Figure 2.6.2 and Figure 2.6.3. The resultant MAC is good only for the firsts three modes with excitation at 0.010 mm, then with 0.012 mm the first and third mode have high correlation, but the data from experimental test are in small quantity.

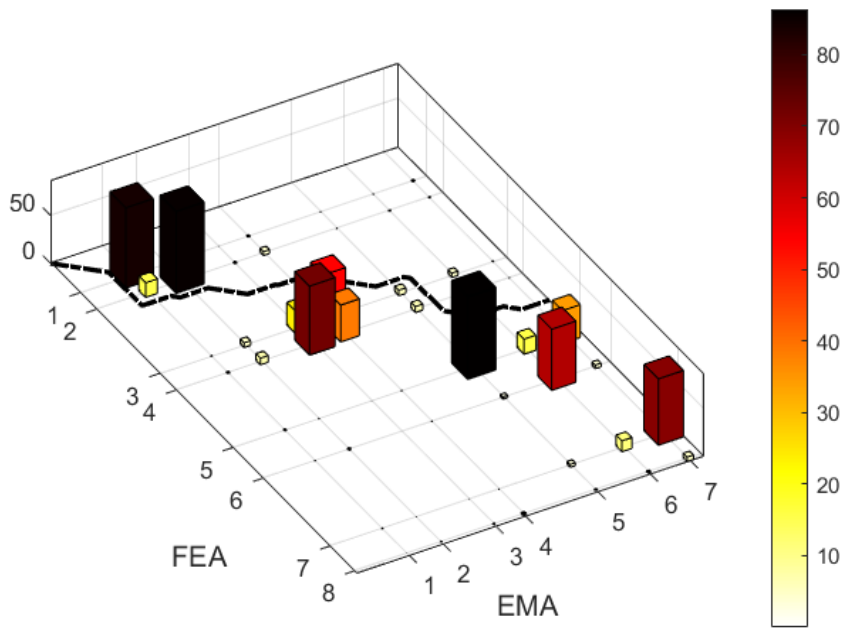


Figure 2.6.1 – MAC of x axis at 0.005 mm with frequency.

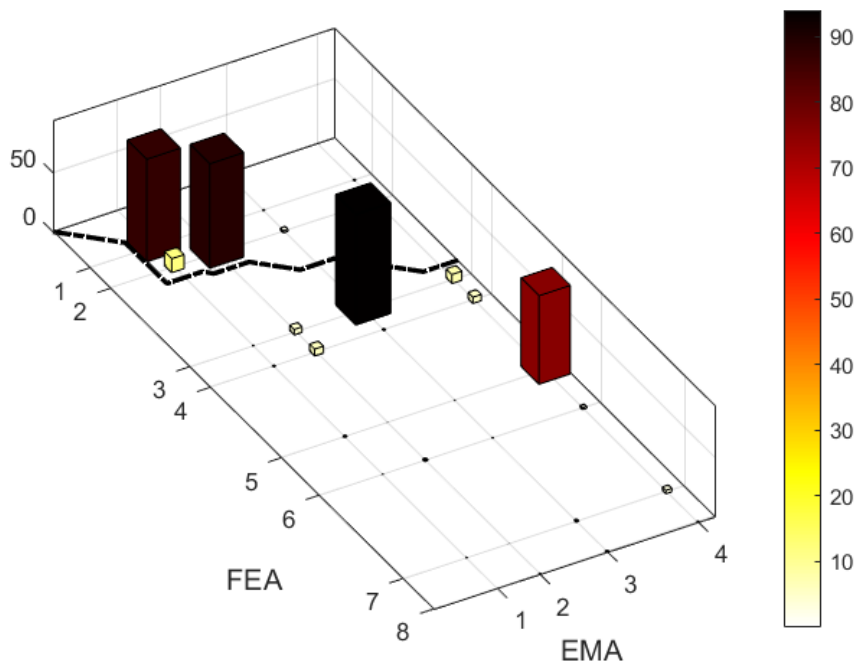


Figure 2.6.2 – MAC of x axis at 0.010 mm with frequency.

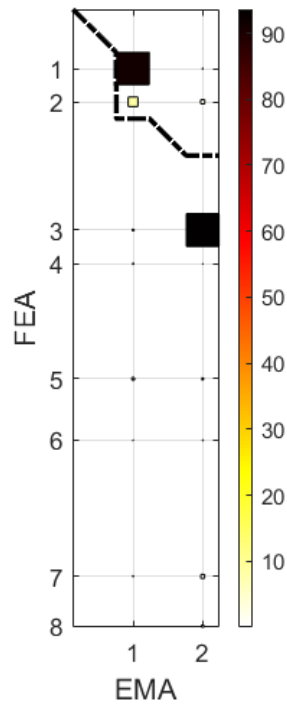


Figure 2.6.3 – MAC of *x* axis at 0.012 mm with mode shapes.

MAC on *y* axis

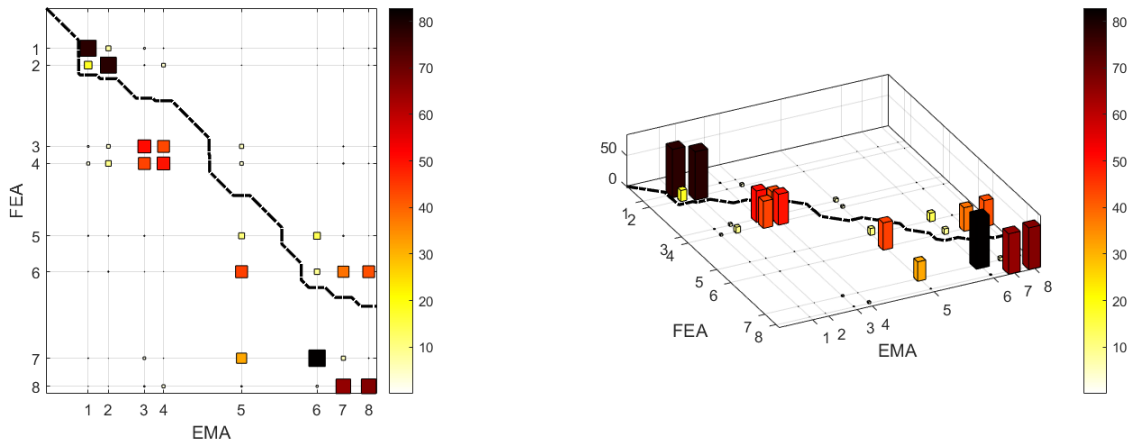


Figure 2.6.4 – MAC of *y* axis at 0.005 mm, top view (left) 3D view (right).

Table 2.6.1 – MAC correlation of *y* axis at 0.005 mm.

Mode FEA-EMA	Correlation [%]
1-1	77.94
2-2	78.17
3-3	50.61
4-4	49.75
3-4	43.31
4-3	43.73

5-5	10.93
6-6	8.98
6-5	44.02

In Figure 2.6.4 is shown the MAC correlation of y axis at 0.005 mm. It is visible a correlation of 80% at low frequency, at first and second mode, these values decrease when the frequency increase. Another acceptable value of correlation is found at the third and fourth mode of FEA with a correlation of 50%.

Table 2.6.1 resumes correlation values from Figure 2.6.4. These values are valid even for others graph or to have general idea of correlation numbers.

For both Figure 2.6.5 and Figure 2.6.6 the better correlation is at 80% on the second mode shapes, also the first mode shape has an acceptable correlation of 70%.

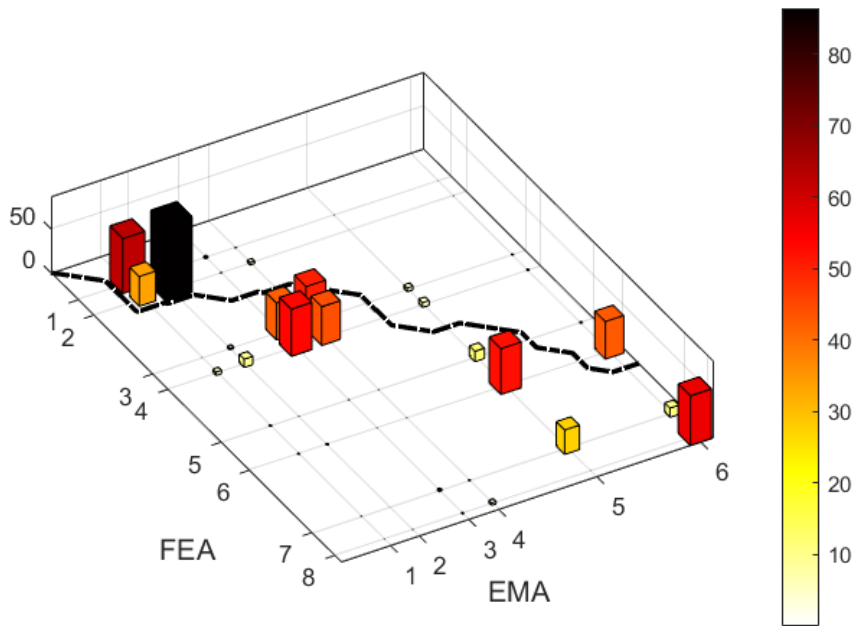


Figure 2.6.5 – MAC of y axis at 0.010 mm with mode shapes.

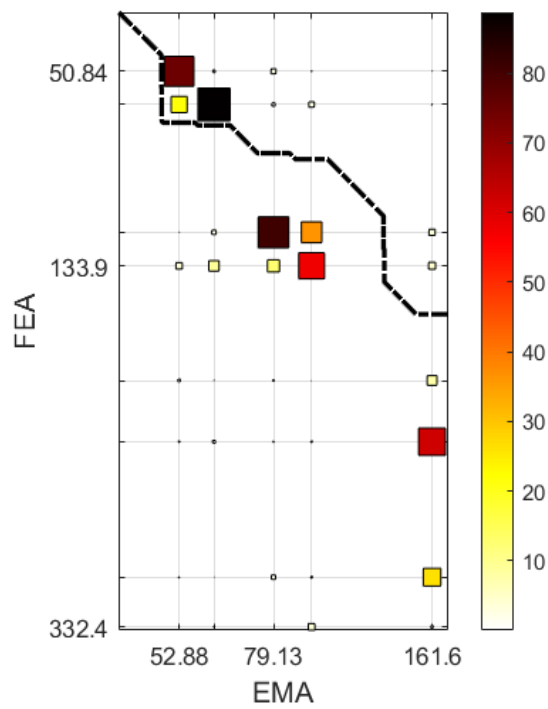


Figure 2.6.6 – MAC of y axis at 0.012 mm with indication of frequency.

MAC on z axis

Good values of correlation are present in the following graph, especially for the first two mode the correlation is around 70-80%. Other correlations are out of main diagonal for third, fourth mode shapes.

In Figure 2.6.7 the sixth mode has a value of 80% of MAC.

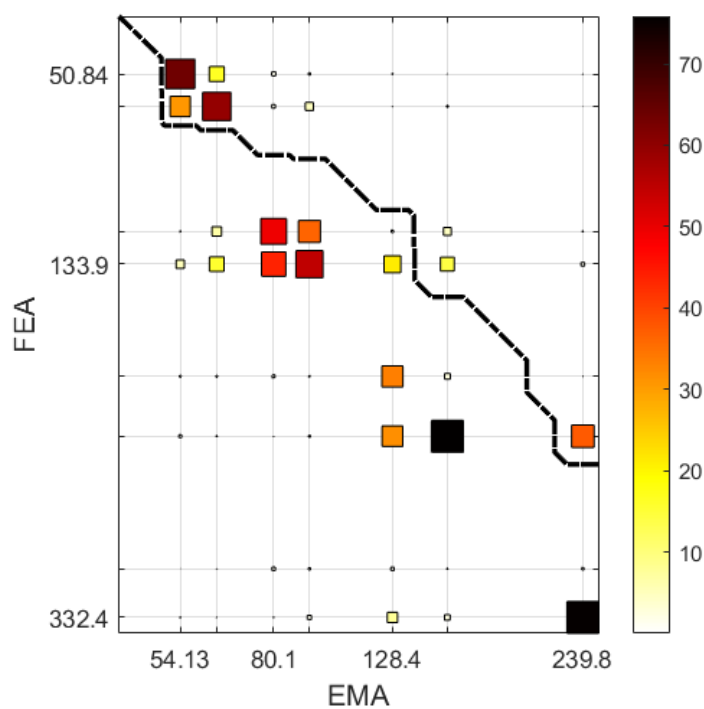


Figure 2.6.7 – MAC of z axis at 0.005 mm with mode shapes.

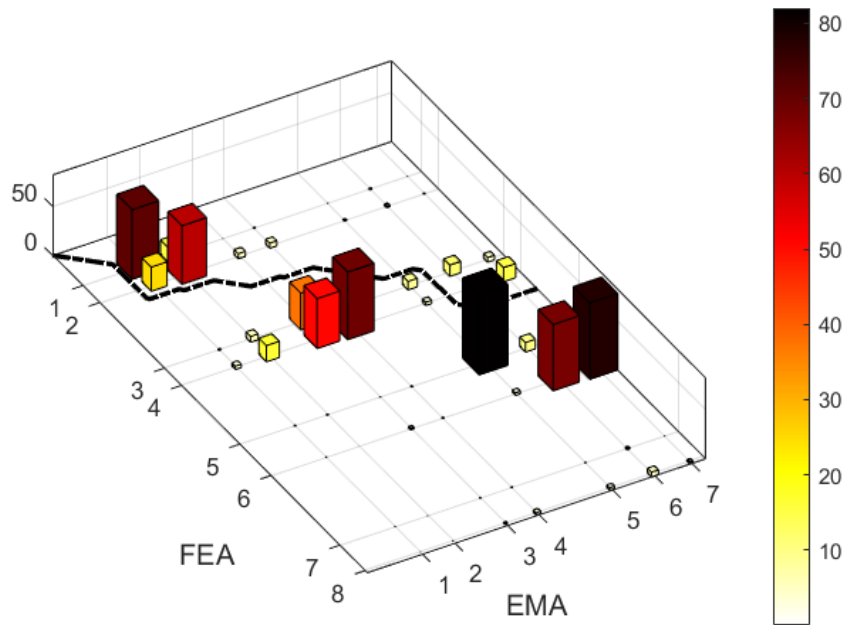


Figure 2.6.8 – MAC of z axis at 0.010 mm with mode shapes.

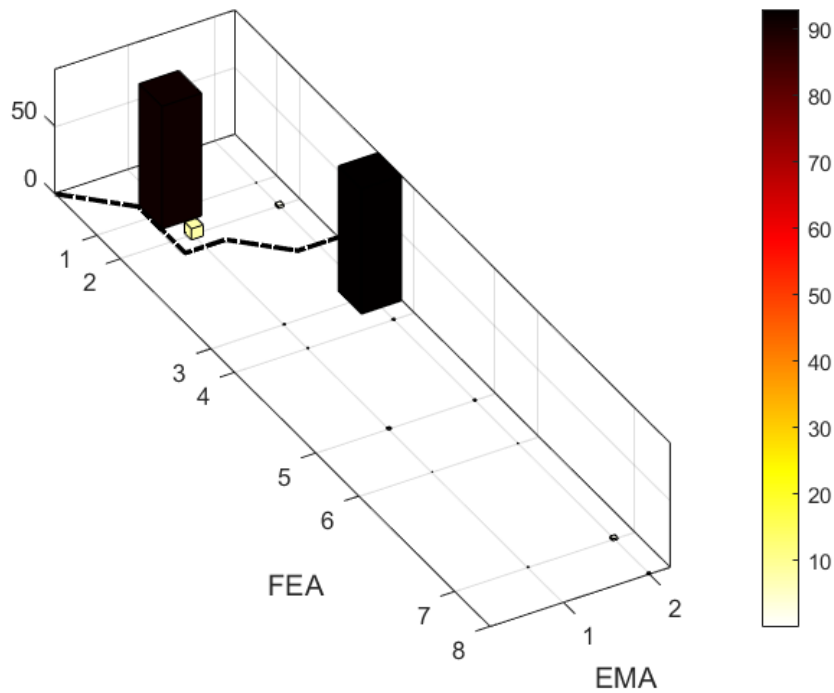


Figure 2.6.9 – MAC of z axis at 0.012 mm with frequency.

MAC on yz axes

The correlation using yz should be the best result from experimental point of view, also in this case the maximum correlation on diagonal is at 80% on the first/second mode shapes. From graphs it seems that another high correlation (55-65%) between eigenvector there is between FEA and EMA n°3-4 mode shapes.

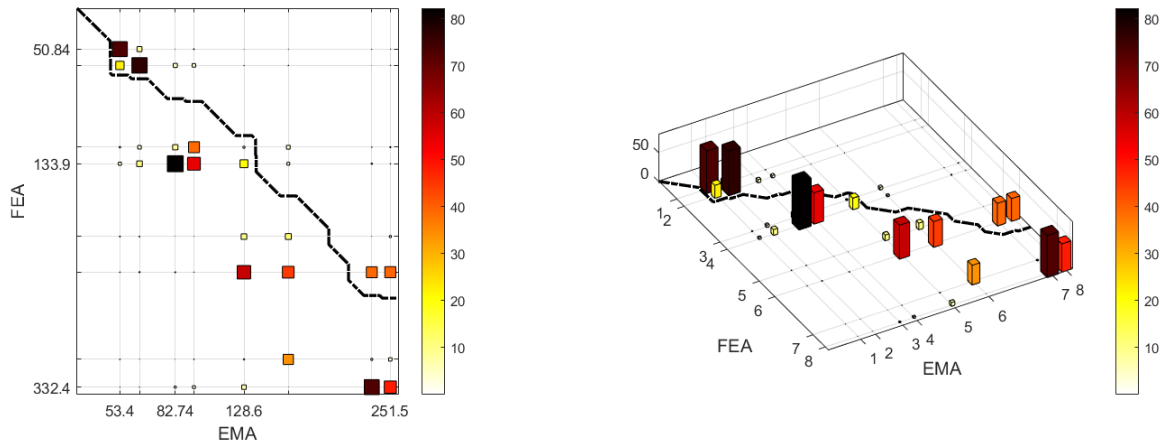


Figure 2.6.10 – MAC of yz axes at 0.005 mm, top view (left) 3D view (right).

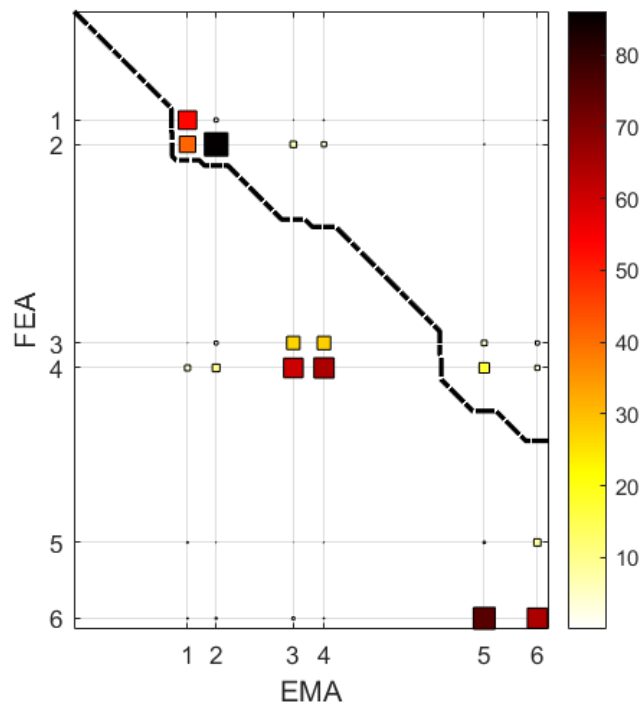


Figure 2.6.11 – MAC of yz axes at 0.010 mm.

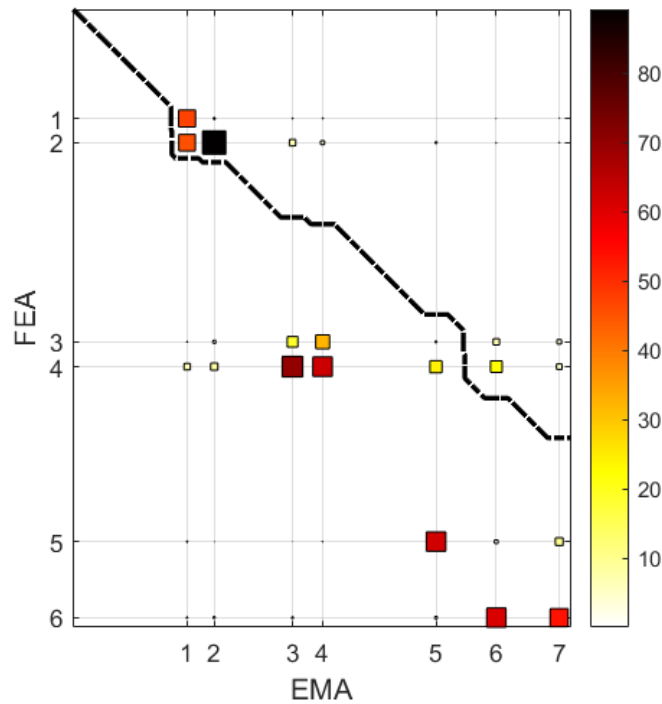


Figure 2.6.12 – MAC of yz axes at 0.012 mm.

In MAC analysis using combination of direction yz it is possible to obtain the best results from experimental data. In this case, correlations with high percentage are observed for the first four modes. In Table 2.6.2 are resumed these modes and the relative frequency with numerical and experimental simulation.

It is worth notice that mode n°1 and 2 in both tests are very close. This is also appreciable from MAC analysis (correlation of 80%) where the coloured square on Figure 2.6.13 are on the main diagonal, while the frequency of mode n°3 and 4 have different values, this behaviour influences the MAC graph, where the coloured columns are out of main diagonal (lower left position) with values of 50-85%.

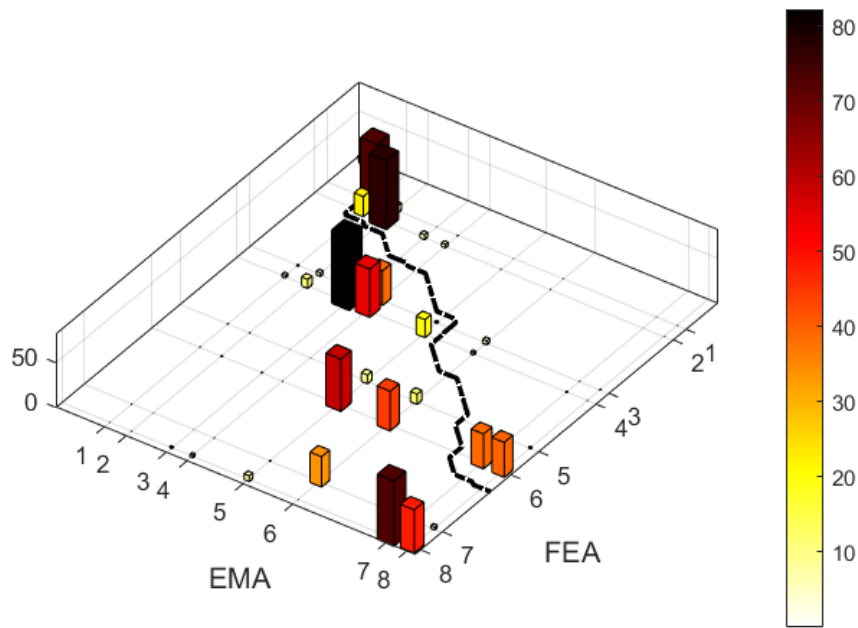


Figure 2.6.13 – MAC of yz axis at 0.005 mm with mode shapes for the comparison.

Table 2.6.2 – Firsts four mode in numerical and experimental analysis.

Numerical frequency [Hz]	Experimental frequency [Hz] yz at 0.005 mm	Description
60.77	53.40	Coupled pads out of phase
61.29	58.01	Coupled pads in phase
159.2	82.74	Torsional out of phase
160.1	86.17	Torsional in phase

MAC on xyz axes

All analysis conducted, which involve x axis, are quite poor of information, since acquiring the experimental data on this axis was difficult. As consequence, the combination of information with other axis decreases the quantity of data stopping at around 150 Hz the results and decrease the quality of information of the third and fourth mode shapes.

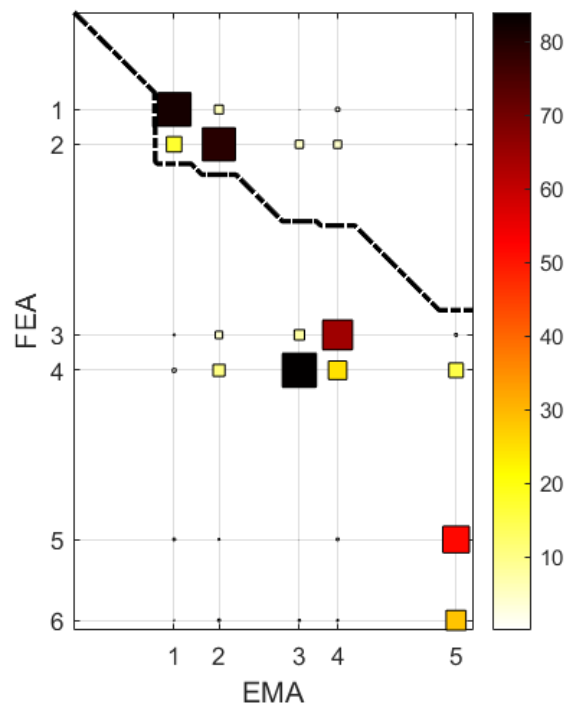


Figure 2.6.14 – MAC of *xyz* axes at 0.005 mm.

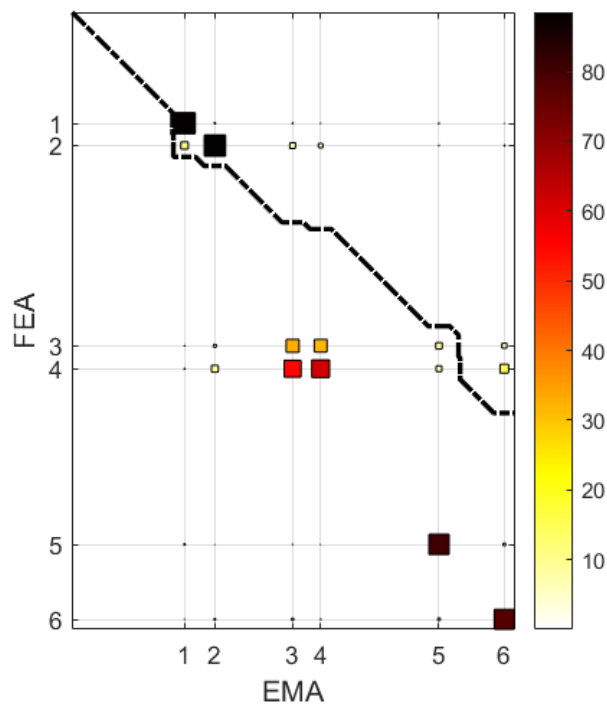


Figure 2.6.15 – MAC of *xyz* axes at 0.010 mm with mode shapes.

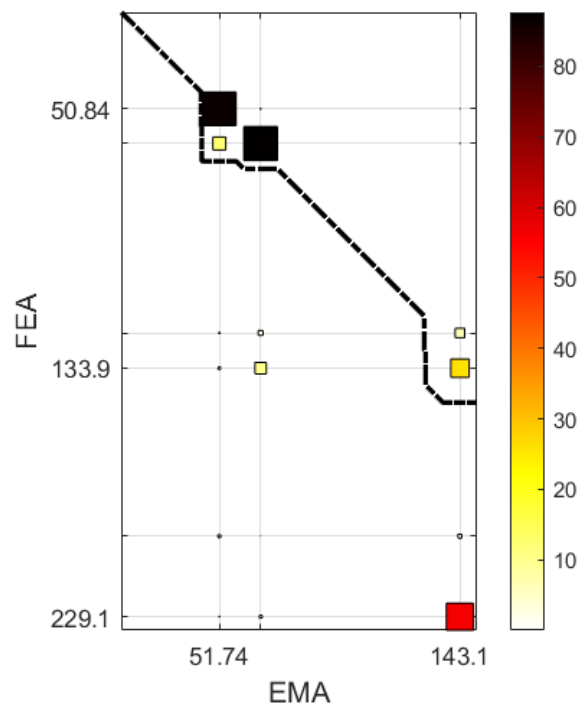


Figure 2.6.16 – MAC of *xyz* axes at 0.012 mm.

2.7 Conclusions on first experiment

In general, the frequencies identified in TestLab are lower than the ones found in numerical test on Lupos. This behaviour is probably due to a different setup between the numerical and the experimental models.

It is possible notice that there are incoherencies in the frequencies of torsional behaviour. During the experiments we observed values close to 80 Hz, while in numerical simulation this behaviour occurred at doubled frequencies, around 160 Hz. Another difference is present in the mode shapes on numerical and experimental model.

The most interesting result is obtained in the test with imposed displacement of 0.005 mm. These post processing results come from the analysis of y and z axes with 0.005 mm. Notice that the frequencies found on yz and in y cases are very close. Thus, for future comparison and analysis the data from y axis are used.

Increasing the value of displacement results in losing data quality and diminishing of the number of natural frequencies found during identification.

The first four experimental frequencies are reported in Table 2.7.1 together with the correspondent numerical ones. The experimental frequencies are identified along y axis at 0.005 mm (numerical reference system). From this table, it is clear that some updates must be done on the numerical model.

Table 2.7.1 – Numerical and experimental frequencies

Numerical frequency [Hz]	Experimental frequency [Hz] y at 0.005 mm	Description
60.77	53.25	Coupled pads out of phase
61.29	57.97	Coupled pads in phase
159.2	82.64	Torsional out of phase
160.1	85.95	Torsional in phase

About MAC correlation, a maximum index 80-85% is obtained on the first/second mode shape. In fact, the firsts two mode shapes are similar since frequency in both experimental and numerical result. For the torsional mode shapes (3rd and 4th) the correlation between numerical and experimental results decreases. In fact, in some graphs there are four columns with similar height, instead of two singular columns on main diagonal, as it happens for the first two mode shapes.

Moreover, at frequency higher than 200 Hz it was difficult to associate relative modes, and consequently the correlation between numerical and experimental data is influenced.

3. Roving hammer test

The second experiment on Levit device took place at Valeo on 2021-07-19. Two types of tests have been done. The one faced on this chapter is the roving hammer test.

The objective of this test is to look further into the study of vibrational transmissibility and the research of the natural frequencies, in accordance with mode shapes.

During this test is used a dynamometric hammer to excite several points of the Levit, while accelerometers handled the response due to excitation. The accelerometers convey the measurements to the acquisition system.

3.1 Experiment description

First, the setup condition of the device is controlled. It is checked the presence of possible damage and if the symmetry between pads is respected. The springs did not seem perfectly equal calibrated, thus the distance and then the stiffness is modified respect to the sweep experiment. After this correction, the symmetry is restored. However, this modification of the setup will affect the test and the results. Comparing these results with the ones from sweep tests must be taken into consideration the symmetry aspect.

This type of test, also known as modal testing, allows us to calculate the natural frequencies and mode shapes of the device. For the test a (roving) dynamometric hammer is used and the accelerometers are set as are reported in Figure 3.1.1. The hammer generates impulse that excites four points, where the accelerometers are positioned. On the other hand, the accelerometers measure the response generated from the impact.

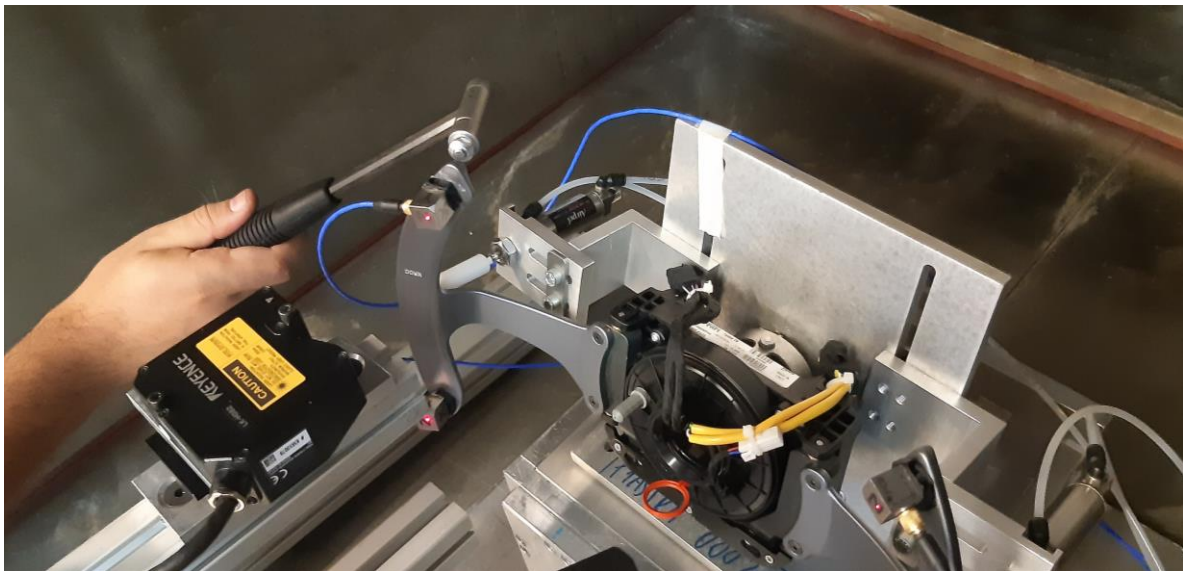


Figure 3.1.1 – Example of roving hammer test.

In theory, the points under test should be impact with a perfect impulse, with perpendicular direction with respect to the surface. The impact should be very quick and precise. The designated part of Levit which undergoes to the impact is on the back pad of device and the impact is imposed in direction $-y$ respect to device reference frame. Figure 3.1.2 shows how the hammer impacts the

device during the excitation of point 3. In the front part of Levit there is the accelerometer to measure the response of the part.

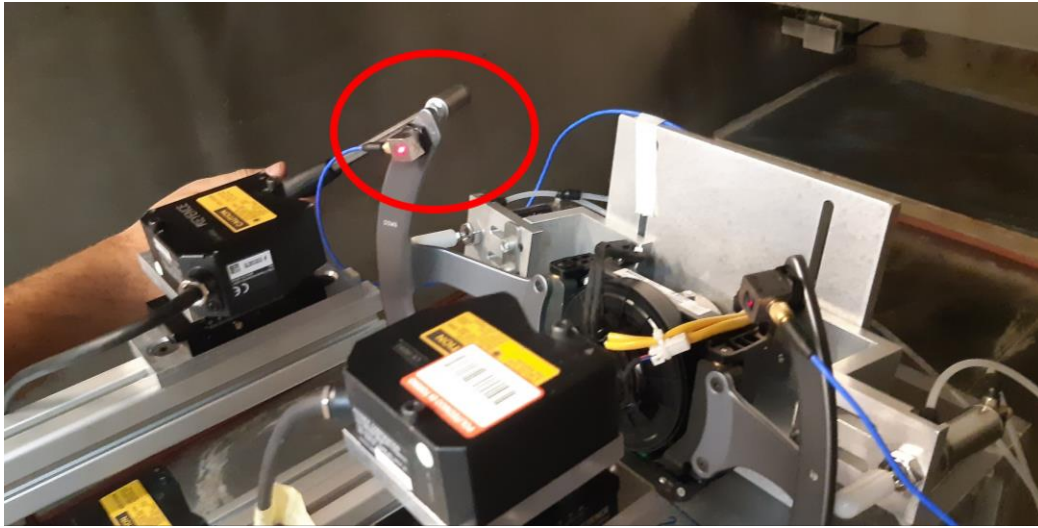


Figure 3.1.2 – Contact between hammer and device during the test on point 3.

The test is repeated for each of the four points in the same way. Accelerometers record the response of each excitation, which are reported in next paragraph.

The results of these test can be compared with the results from sweep test and should help in the improvement of numerical model.

3.2 Frequency response function

It is possible to give a first look to frequency response function on Testlab interface. However, it is convenient export all data acquired in Matlab due to the simplest management of information. For this experiment it is possible to talk about frequency response function FRF. This function is defined as acceleration (from accelerometer) on the force imposed by hammer.

Figure 3.2.1 shows the excitation and response on y axis of all points when the first accelerometer undergoes to impact test.

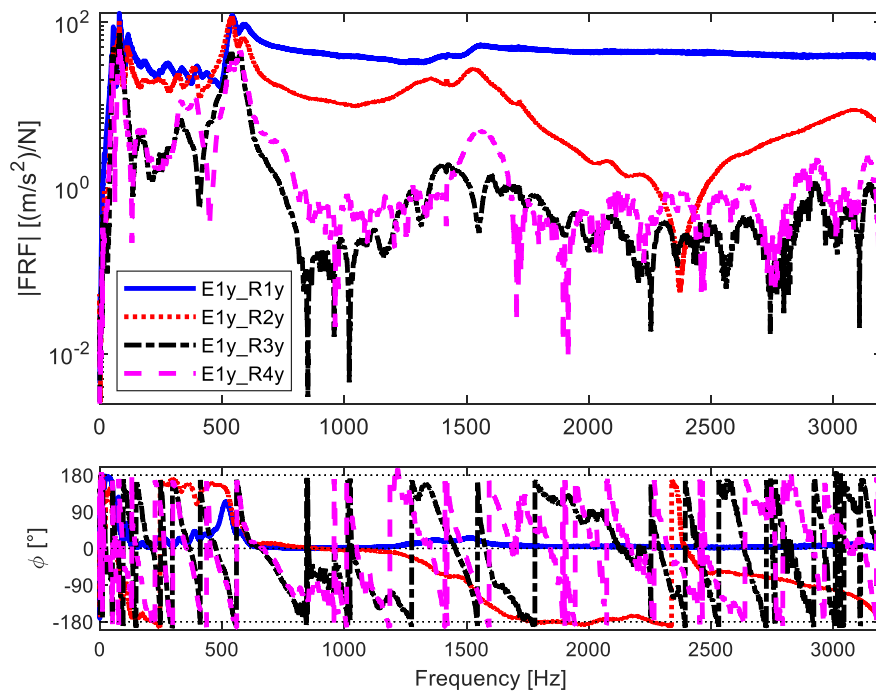


Figure 3.2.1 – Excitation on 1st accelerometer and response on y axis of all accelerometers.

Figure 3.2.2 and Figure 3.2.3 give information about the frequency during the excitation of second point and the response of all accelerometers on y and x axis.

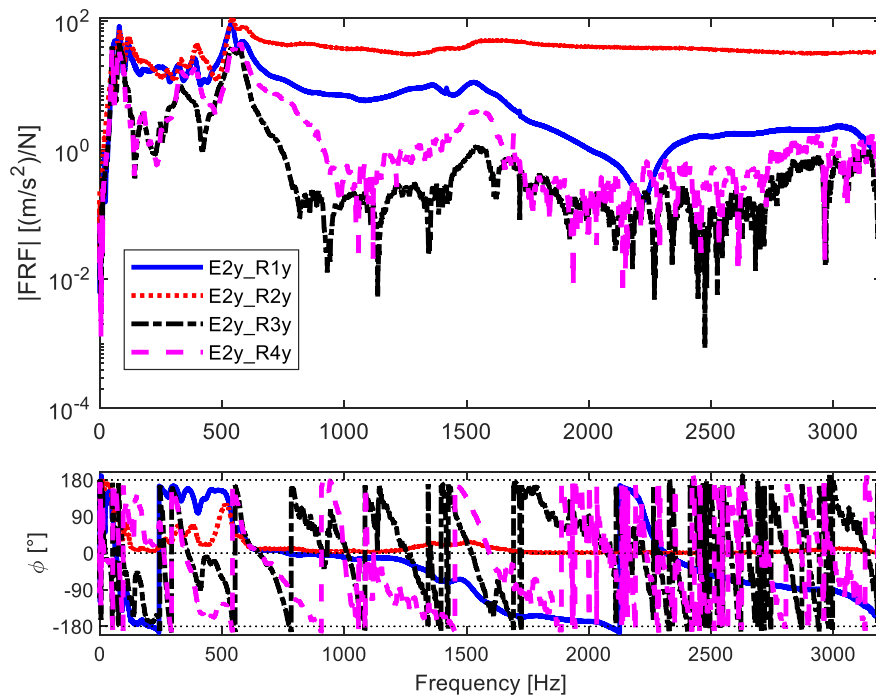


Figure 3.2.2 – Excitation on 2nd accelerometer and response on y axis of all accelerometers.

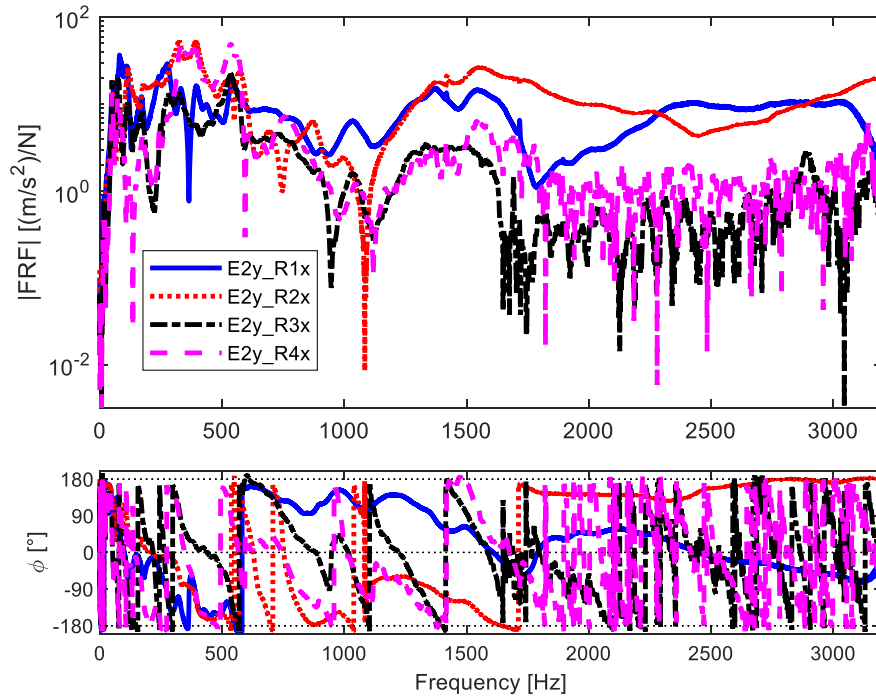


Figure 3.2.3 – Excitation on 2nd accelerometer and response on *x* axis of all accelerometers.

Figure 3.2.4 presents the FRF of the third accelerometer, excitation, and response on *y* axis.

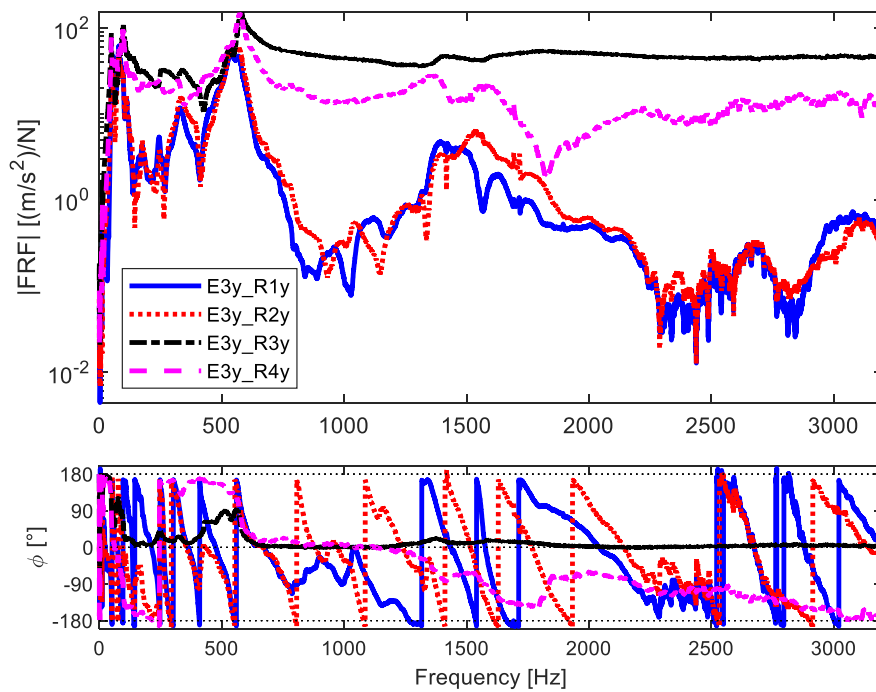


Figure 3.2.4 – Excitation on 3rd accelerometer and response on *y* axis of all accelerometers.

Figure 3.2.5 presents the excitation on *y* axis of the fourth accelerometer and the response of the others.

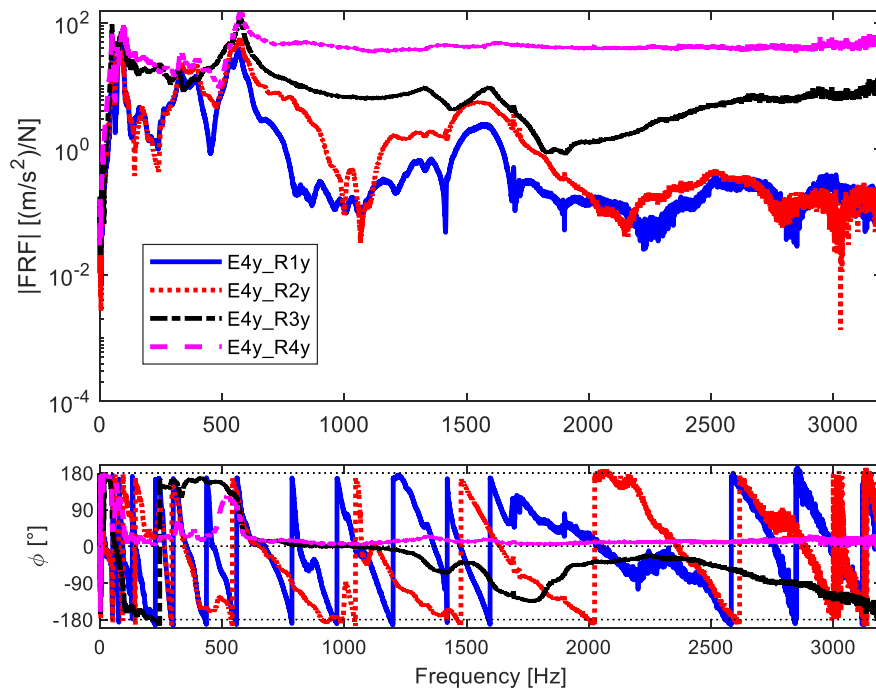


Figure 3.2.5 – Excitation on 4th accelerometer and response on y axis of all accelerometers.

3.3 Natural frequencies

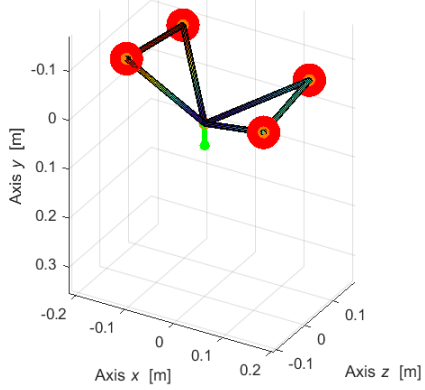
For the post process it is used TestLab software and for the research of natural frequency is used the same technique already take for the sweep experiment. Once selected the stable point from experimental curve, the frequency and the mode shapes are identified and exported from Testlab. The frequency found are resumed in Table 3.3.1. The description part wants to give an idea of the behaviour of movement, it is not the final ones. Consider that these descriptions are made on experimental simulation which take into account just 5 points for movements of the Levit.

Table 3.3.1 – Mode shapes and natural frequency of hammer test from ‘EMA Actuation 2’.

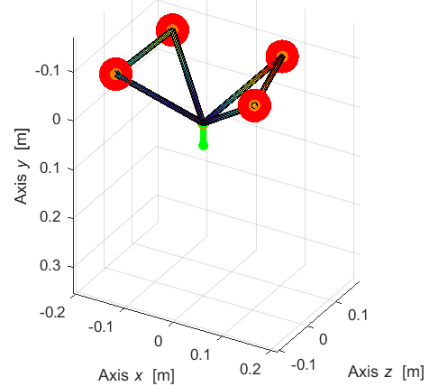
Mode shape	Frequency [Hz]	Description
1	49.50	Coupled pads out of phase
2	56.68	Coupled pads in phase
3	73.02	Torsional in phase
4	81.10	Torsional out of phase
5	96.30	Motion of left pad
6	113.80	Motion of right pad
7	239.30	Bending of pads out of phase xz plane
8	250.50	Bending of pads in of phase xz plane

The results from frequency analysis are used to start a simulation on a Lupos simplified model of the Levit. The model simply reproduces a basic shape of pad, with the four accelerometers in red. Figure 3.3.1 reports the mode shapes with Lupos simulation.

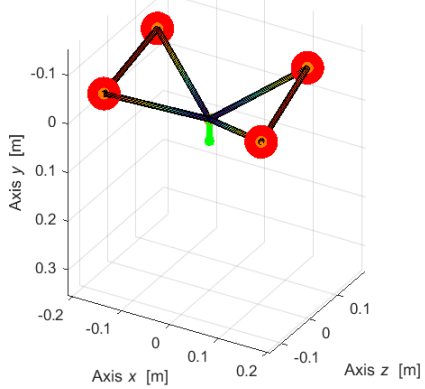
Mode 1 - 49.5 Hz



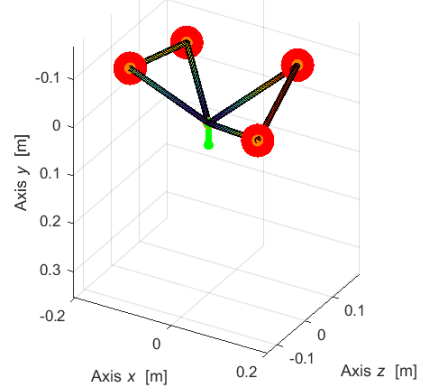
Mode 2 - 56.68 Hz



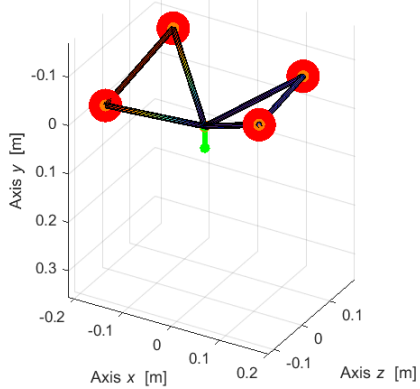
Mode 3 - 73.02 Hz



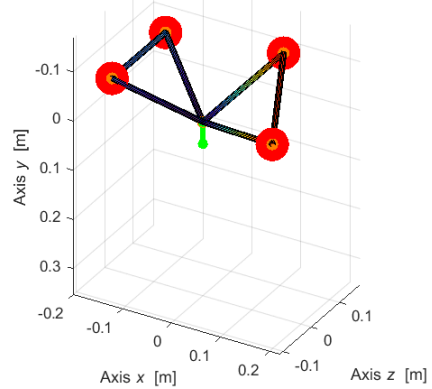
Mode 4 - 81.1 Hz



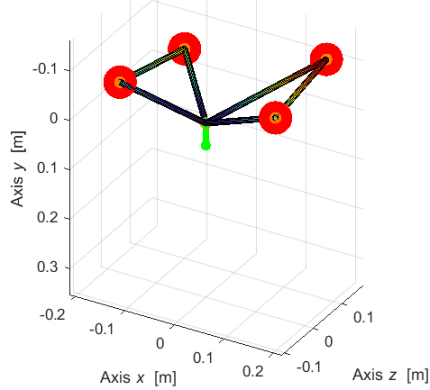
Mode 5 - 96.3 Hz



Mode 6 - 113.8 Hz



Mode 7 - 239.7 Hz



Mode 8 - 250.2 Hz

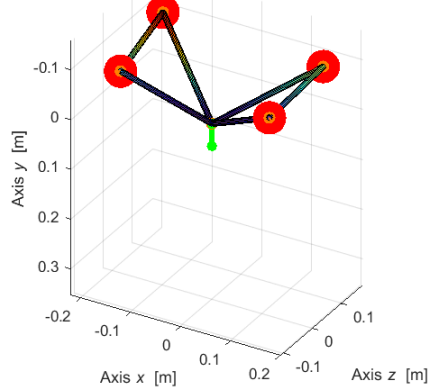


Figure 3.3.1 – Mode shapes and frequencies of hammer test.

3.4 Frequency response function and natural frequencies

Figure 3.4.1 shows the FRF of the first accelerometer with the natural frequencies identified in TestLab. The following figures present the FRF with information from other accelerometers. Notice that the vertical line representing the natural frequency coincide with peaks of FRF. In these cases, it is quite sure that the natural frequency is correct. This can help finding the right mode shapes and natural frequency.

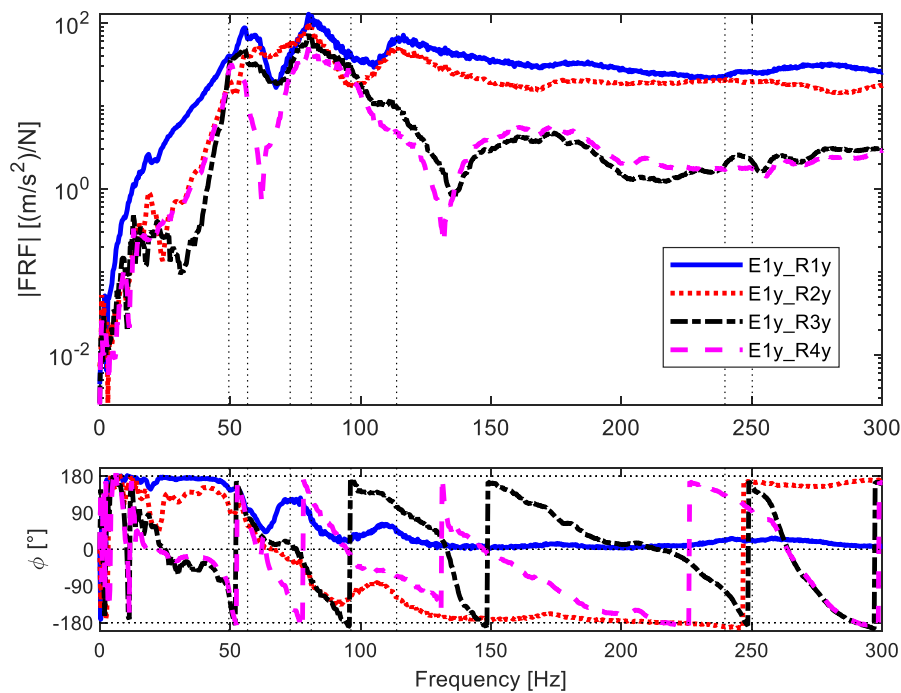


Figure 3.4.1 – FRF with frequency first accelerometer.

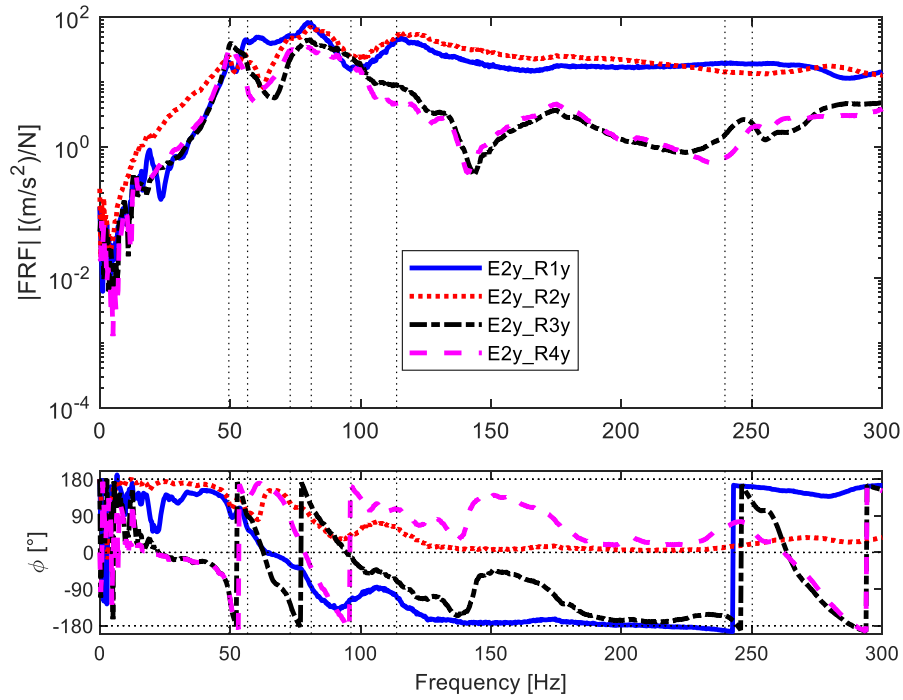


Figure 3.4.2 – FRF with frequency second accelerometer.

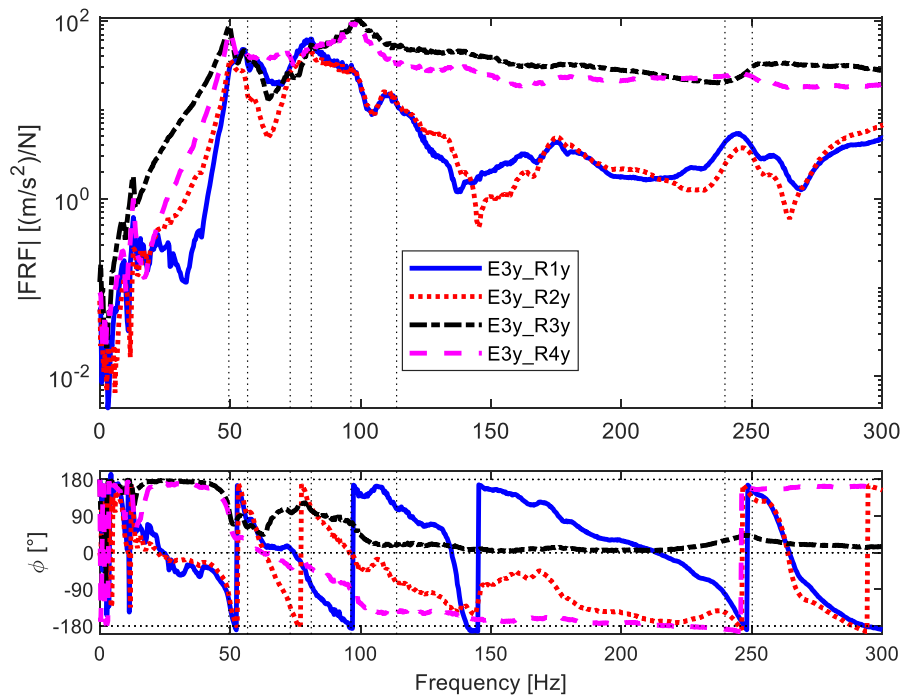


Figure 3.4.3 – FRF with frequency third accelerometer.

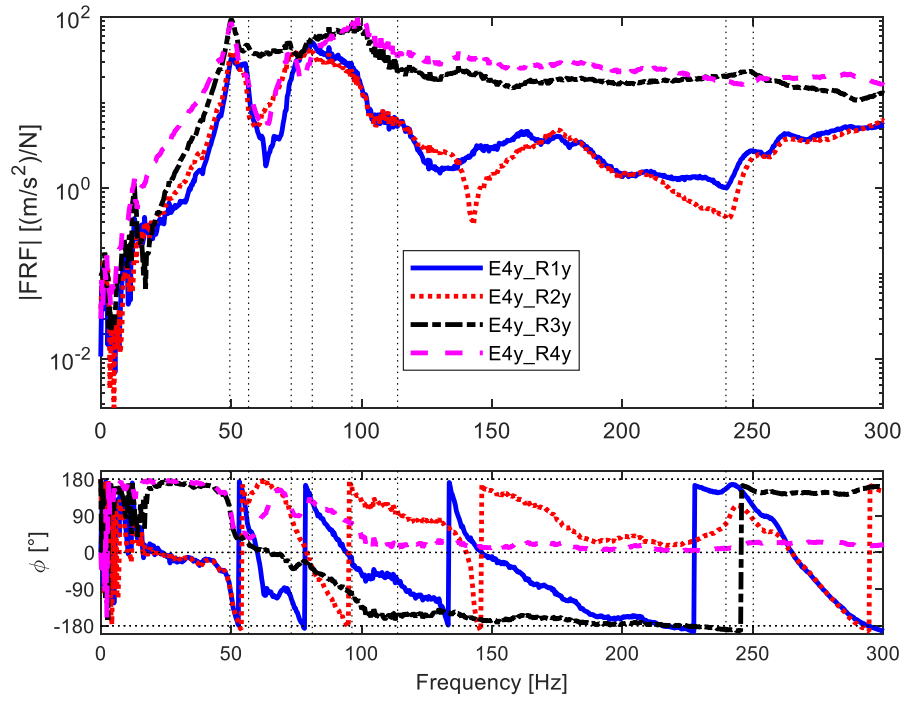


Figure 3.4.4 – FRF with frequency fourth accelerometer.

3.5 Parametric analysis

Parametric analysis is used to increase the knowledge about the numerical model with Lupos and to improve the model itself. It is important to consider both the experimental and numerical data in order to bring the Lupos model closer to the real one.

Using Lupos is possible to set up the parametric analysis, in particular this technique is used once to change the mass of the accelerometer and then concentrating the study on the stiffness. This type of analysis is useful to evidence phenomena of crossing or veering which influence the whole structure.

On graphs of parametric analysis crossing phenomena appears when two lines, representing two different mode shapes, cross each other and switch their behaviour. The veering effect happens when two lines approach each other, influence their trend, and then take different paths.

Several parametric analyses are built to develop the model. One parameter at time is changed while the others are kept constant. The choice of parameter depends on the results obtained during simulation. The aim is to choose the parameter which allows to obtain results of frequencies closer to the experimental ones. Once the parameter value is found, there is an update of code in Matlab and of the results, that will be used for the next simulation.

In the following Table 3.5.1 the parameters of model defined in the previous project are resumed. These parameters will be considered and updated in the next chapters.

Table 3.5.1 – Initial model parameters.

Parameter	Value
K_{bar} [N/m]	$1 \cdot 10^8$ [1 2 1]
K_{mag} [N/m]	$4.5 \cdot 10^5$
K_{hinge} [N/m]	Infinite

3.5.1 Accelerometer mass

In both experiments, sweep and hammer test, the Levit is enriched by the mass of four accelerometers. These can influence the behaviour and so the mode shapes of the device.

So, it is interesting to see what happens when changing the value of the mass accelerometers. It is decided to build the vector for mass variation from a zero value to a 200% of the mass of accelerometer. Taking account that 14.2 g is the mass of whole accelerometer body, the values under test go from 0 to 28.4 g.

This parametric analysis is conducted without any changes with stiffness parameter but changing the accelerometer mass. This parameter is put in red in Table 3.5.1.1.

Table 3.5.1.1 – Model parameters for parametric analysis on accelerometer mass.

Parameter	Value
Nominal accelerometer mass	config
K_{bar} [N/m]	$1 \cdot 10^8$ [1 2 1]
K_{mag} [N/m]	$4.5 \cdot 10^5$
K_{hinge} [N/m]	Infinite

We have focused our attention on the first six modes, but to have a better overview on the behaviour of single mode it is interesting to keep under analysis a bigger number of modes, such as 12, as shown in Figure 3.5.1.1.

Figure 3.5.1.1 shows the behaviour of frequency when the accelerometers mass change. It is possible to see that the first two modes are superimposed, and they are little affected by the variation in mass. On the other hand, modes from 3 to 8 are more influenced by mass. Especially for modes 3-4 the lines have a decrease in frequency of 50 Hz adding the accelerometer mass. Similar differences are present for other modes from 5 on.

The vertical black line on Figure 3.5.1.1 is used to evidence correct added mass for experiments, such as 14.2 g per point.

In general, the accelerometer mass does not have a big influence in frequency values for the first two modes, while they can influence more the following mode shapes.

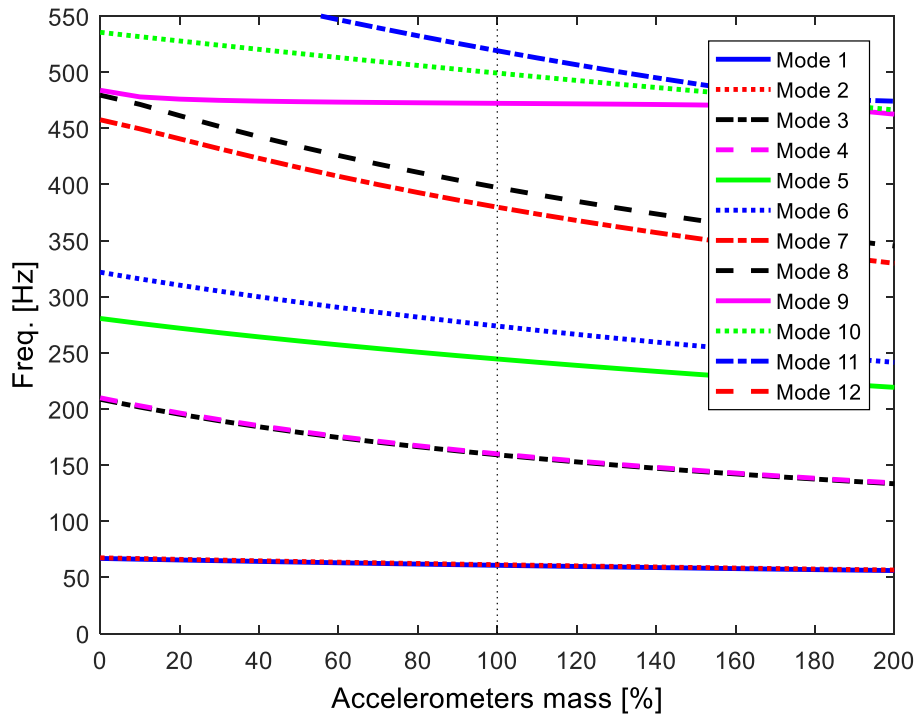


Figure 3.5.1.1 – Effect of accelerometer mass on the device model.

In Table 3.5.1.2 are resumed the frequency at mass 100%, such as a mass of 14.2 g.

Table 3.5.1.2 – Natural frequencies and descriptions.

Mode	Frequency [Hz]	Description
1	60.77	Coupled pads out of phase
2	61.29	Coupled pads in phase
3	159.2	Torsional out of phase
4	160.1	Torsional in phase
5	244.5	Bending of pads out of phase on <i>xz</i> plane
6	273.9	Bending of pads in phase on <i>xz</i> plane

Figure 3.5.1.2 shows the first 6 mode shapes, calculated with the presence of four accelerometers.

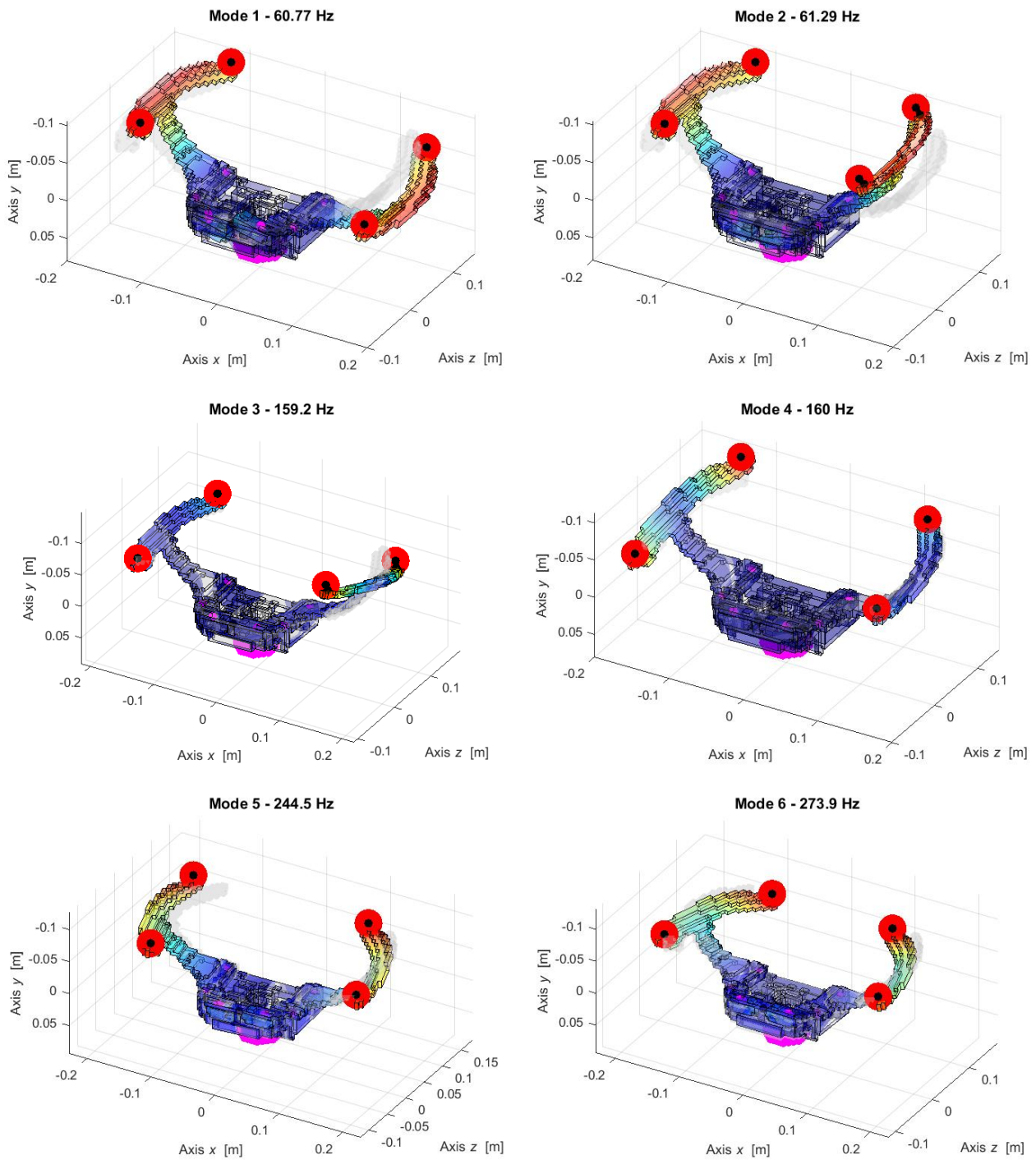


Figure 3.5.1.2 – Numerical real modal analysis of the first 6 mode shapes with update1.

3.5.2 Steering bar stiffness

The parametric analysis on steering stiffness gives more interesting results. The goal of this analysis is about make closer the numerical data to the experimental.

In this analysis the steering bar stiffness is the parameter which change in the range from 10^3 N/m to 10^8 N/m.

The steering bar is represented on Lupos as many elastic-damped elements. In this section is analysed the stiffness of the elements, which are placed on the steering column. Table 3.5.2.1 resumes the stiffness parameter, in red the one under analysis (steering bar).

Table 3.5.2.1 – Model parameters for parametric analysis on steering bar.

Parameter	Value
Accelerometer mass [g]	14.2
K_{bar} [N/m]	config [1 2 1]
K_{mag} [N/m]	$4.5 \cdot 10^5$
K_{hinge} [N/m]	Infinite

Figure 3.5.2.1 shows the results of the parametric variation. Are represented 14 mode shapes in order to see possible veering and crossing effects which could influence the mode at lower frequency. The values on vertical axis are limited between 0 and 550 Hz.

All modes are influenced by the values of steering bar, especially the firsts two.

At $k_{bar} = 10^4$ N/m there are a first effect of veering between mode 2-3. At values of 10^5 N/m the firsts 4 mode reach a stable position. Other veering phenomena are visible between mode 5-7 at $4 \cdot 10^4$ N/m. Crossing phenomena are clearly visible for mode 7 (red dashed line) which cross mode n.º6 at 150 Hz. At $k_{bar} > 10^6$ N/m the lines are more horizontal since the frequency is less influenced by steering bar stiffness.

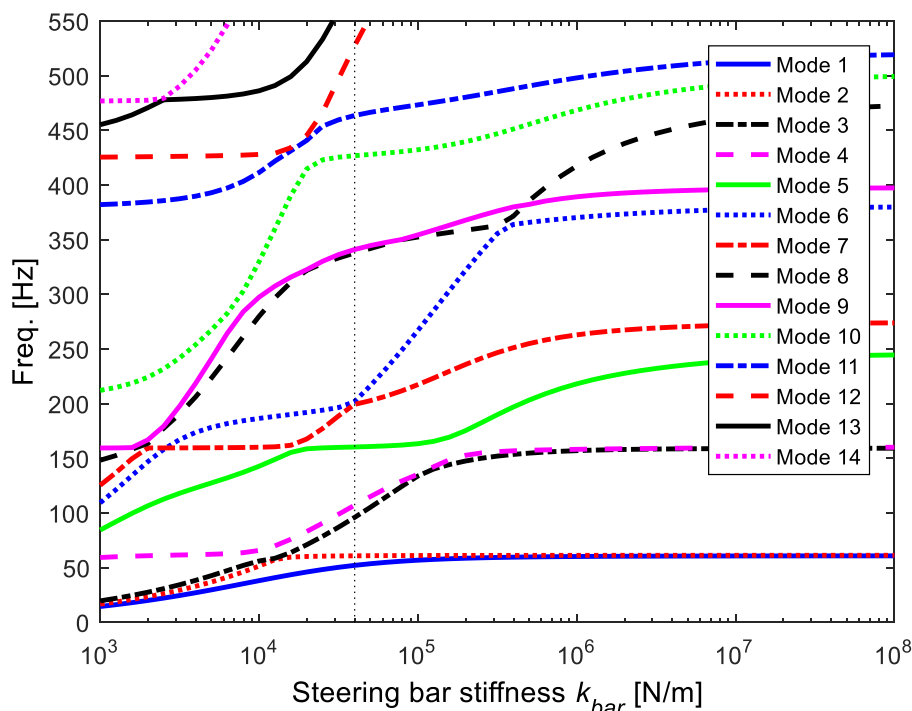


Figure 3.5.2.1 – Effect of steering bar stiffness on the model with accelerometer.

In order to approach the experimental natural frequency with the numerical model is chosen to change the stiffness steering bar. The value of $4 \cdot 10^4$ N/m can give the best result, in particular for the firsts 2 modes. In Figure 3.5.2.1 is put a vertical line in correspondence to the designated value.

Figure 3.5.2.2 shows parametric analysis and two experimental frequencies from hammer test. Experimental frequency n.º1 and 2 are reported as horizontal lines.

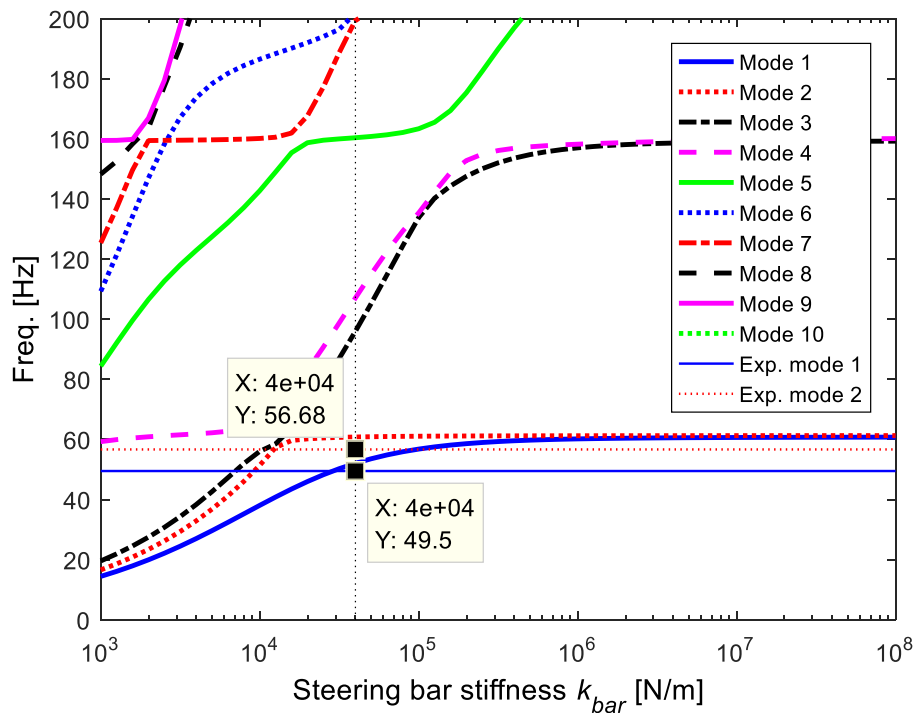


Figure 3.5.2.2 – Effect of steering bar stiffness on the model with first 2 experimental frequencies.

Introducing the value of $k_{bar} = 4 \cdot 10^4$ N/m in Table 3.5.2.1 and in the model on Lupos, there is the first update of the model. Table 3.5.2.2 shows the updated parameter.

Table 3.5.2.2 – Model parameters for parametric analysis on steering bar.

Parameter	Value
Accelerometer mass [g]	14.2
K_{bar} [N/m]	$4 \cdot 10^4$ [1 2 1]
K_{mag} [N/m]	$4.5 \cdot 10^5$
K_{hinge} [N/m]	Infinite

The frequency result of the simulation with file updated are resumed in Table 3.5.2.3. In Figure 3.5.2.3 are represented the relative mode shapes.

It is important to state that the descriptions of all modes are not perfectly assigned. So, in some case the description is quite easy and simple to be identified, while in other case in the resume table can be found ‘to be defined’ in grey. All mode shapes will have a correct description at the end of the update part, in the latest version.

Table 3.5.2.3 – Model parameters for parametric analysis on steering bar.

Mode	Frequency [Hz]	Description
1	52.08	Coupled pads out of phase
2	60.82	Coupled pads in phase

3	95.98	Torsional
4	107.1	Torsional in phase
5	160.4	Torsional out of phase
6	199.3	To be defined

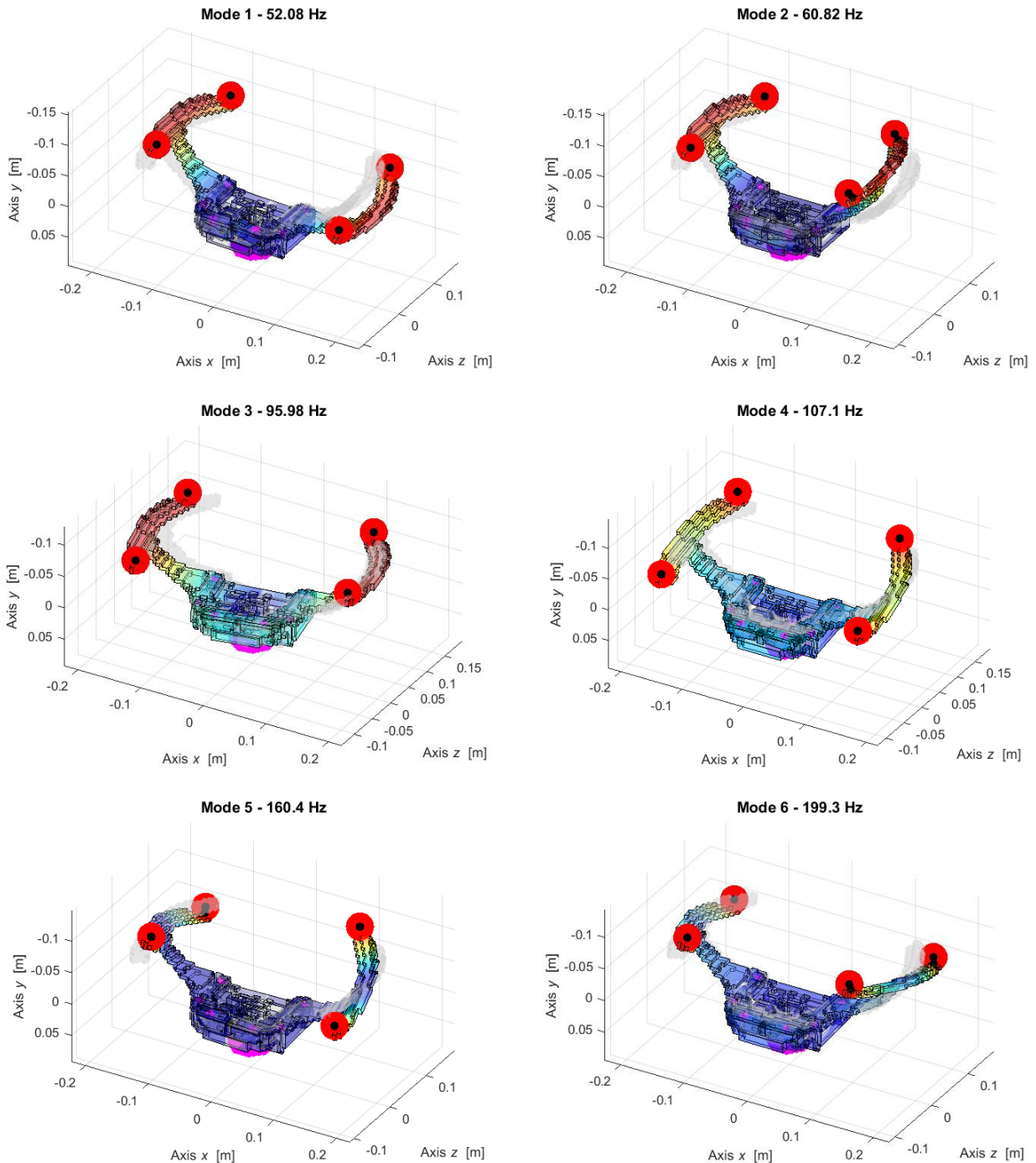


Figure 3.5.2.3 – Numerical real modal analysis of the first 6 mode shapes with update2.

It is worth notice that the third mode shape is new respect to the previous case with only the accelerometer added. This mode is a pure torsional mode, and it takes the third position in the list of modes. It takes the place of the torsional out of phase mode presented in Table 3.5.1.3.

It follows another important difference about the torsional mode shapes. With the update 2 there is the inversion of in phase and out of phase mode. The corrected and updated list is in Table 3.5.2.3. So, it is possible summarize the changes happened from update1 to update 2 in Table 3.5.2.4.

Table 3.5.2.4 – Difference between update1 and update2.

Mode	Update1 (accelerometer mass)		Update2 (steering bar)	
	Frequency [Hz]	Description	Frequency [Hz]	Description
3	159.2	Torsional out of phase	95.98	Torsional
4	160.1	Torsional in phase	107.1	Torsional in phase
5	-	-	160.4	Torsional out of phase

3.5.3 Magnets stiffness

The second parametric analysis done involves the magnets stiffness. These parameters are magnetic spring and are reported in the numerical model as elastic elements. They are placed on the device between the case and the element named bracket. As elastic elements they have a stiffness, which the first attempt value was $4.5 \cdot 10^5$ N/m.

In this analysis the magnets stiffness is the parameter which change in a range from 10^3 N/m to 10^8 N/m.

Table 3.5.3.1 resumes the stiffness parameter, in red the one under analysis (magnets stiffness).

Table 3.5.3.1 – Model parameters for parametric analysis on magnetic spring.

Parameter	Value
Accelerometer mass [g]	14.2
K_{bar} [N/m]	$4 \cdot 10^4$ [1 2 1]
K_{mag} [N/m]	config
K_{hinge} [N/m]	Infinite

Figure 3.5.3.1 presents how 12 modes change in frequency when the magnets stiffness value moves from 10^3 N/m (weak stiffness) to 10^8 N/m (very rigid spring).

Two are the most important observation. The first one is about the influence of this parameter on the mode shapes. Only the mode 1-2 and 6 are influenced a lot by the different values. The other modes are represented by almost flat lines. The second involve the crossing effect of mode 6-7 at around $k_{mag} = 4 \cdot 10^5$ N/m. This could affect the mode shapes and frequency of these two modes.

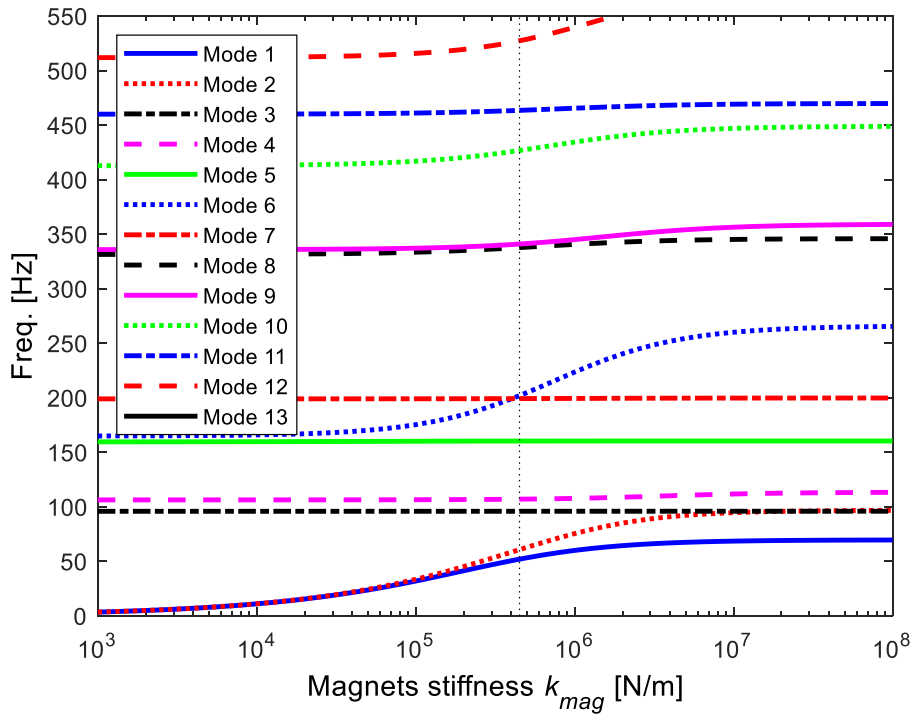


Figure 3.5.3.1 – Effect of magnets stiffness on the device model.

Again, the target of this analysis is to make closer the numerical model to the experimental one. So, to approach numerically the experimental frequency it is necessary change also the magnets stiffness.

The best value to do so, is evidence with a vertical dot line in Figure 3.5.3.1, at $k_{mag} = 4.5 \cdot 10^5$ N/m. The new updated parameters are resumed in Table 3.5.3.2

Table 3.5.3.2 – Model parameters for parametric analysis on magnetic spring.

Parameter	Value
Accelerometer mass [g]	14.2
K_{bar} [N/m]	$4 \cdot 10^4$ [1 2 1]
K_{mag} [N/m]	$4.5 \cdot 10^5$
K_{hinge} [N/m]	Infinite

Figure 3.5.3.2 shows parametric analysis and four experimental frequencies from hammer test. Experimental frequency n.º1÷2 is reported as horizontal line.

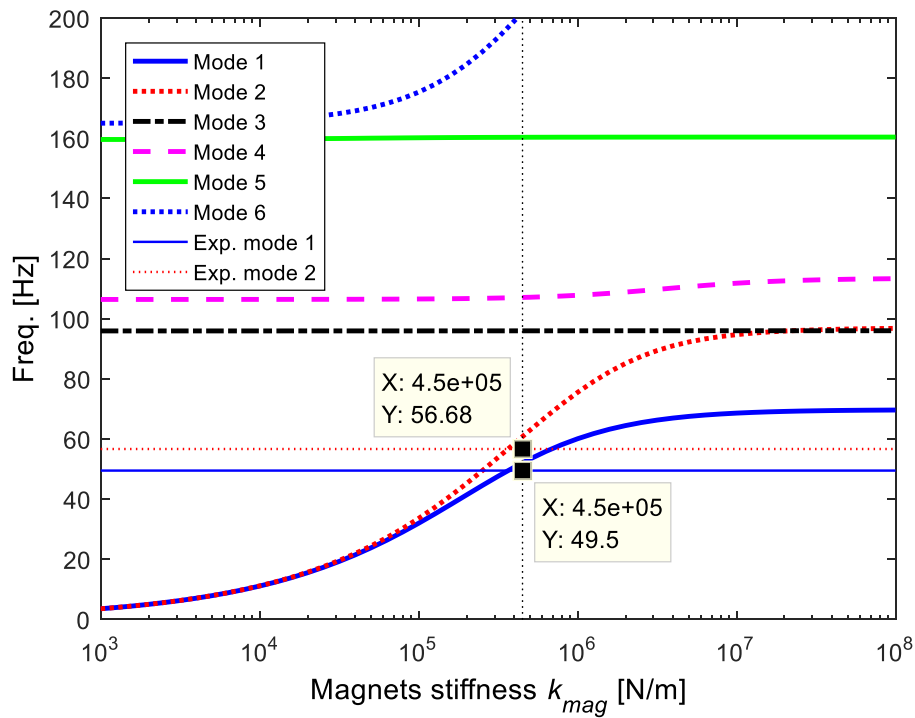


Figure 3.5.3.2 – Effect of magnets stiffness on the model with first 2 experimental frequencies.

From this update it is possible to have numerical model natural frequencies closer than before to the experimental model.

The frequency results of the simulation with file updated (update3) are resumed in Table 3.5.3.3. In Figure 3.5.3.3 are represented the relative mode shapes.

Table 3.5.3.3 – Model parameters for parametric analysis on magnetic spring.

Mode	Frequency [Hz]	Description
1	52.08	Coupled pads out of phase
2	60.82	Coupled pads in phase
3	95.98	Torsional
4	107.1	Torsional in phase
5	160.4	Torsional out of phase
6	199.3	To be defined

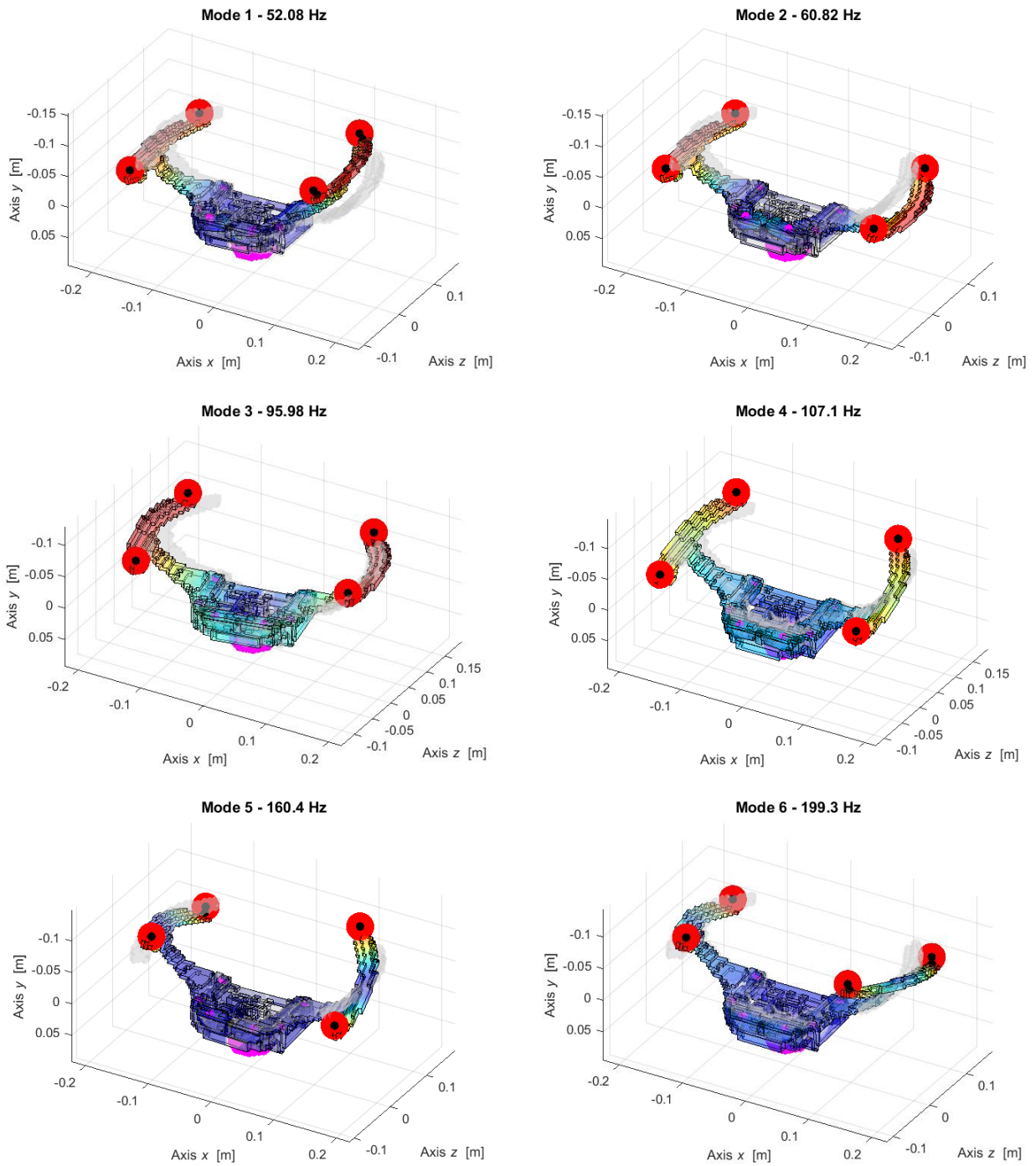


Figure 3.5.3.3 – Numerical real modal analysis of the first 6 mode shapes with update3.

Notice that Table 3.5.3.4 has equals values for update2 and update3 because it was confirmed the K_{mag} value already used in update2.

Table 3.5.3.4 – Comparison between frequency from update 1, 2, 3.

Mode	Update1 Accelerometer		Update2 Steering bar		Update3 Magnetic spring	
	Frequency [Hz]	Description	Frequency [Hz]	Description	Frequency [Hz]	Description
1	60.77	Coupled pads out of phase	52.08	Coupled pads out of phase	52.08	Coupled pads out of phase
2	61.29	Coupled pads in phase	60.82	Coupled pads in phase	60.82	Coupled pads in phase
3	159.2	Torsional out of phase	95.98	Torsional	95.98	Torsional
4	160.1	Torsional in phase	107.1	Torsional in phase	107.1	Torsional in phase
5	244.5	Bending of pads out of phase on <i>xz</i> plane	160.4	Torsional out of phase	160.4	Torsional out of phase
6	273.9	Bending of pads in phase on <i>xz</i> plane	199.3	To be defined	199.3	To be defined

3.5.4 Hinges stiffness

The following analysis involves the parametric variation of hinges stiffness. These elements are represented on Lupos as rigid joints with RBE elements. They are the junction between the pads and the case. There are two elements for each pad.

Making this analysis, the pin constraints (modeled by the rigid joints) become elastic elements. The pin constraints are RBE elements on *x*, *y*, *z* direction. It is changed the pin constraints elements into elastic elements for *x* and *z* direction, while pin constraints on *y* direction remains very rigid as RBE elements.

To find the correct stiffness K_{hinge} for hinges/pins in done the parametric analysis.

Following this strategy can be reach great results for the first 2 mode between numerical and experimental.

Table 3.5.4.1 resumes the stiffness parameter, in red the one under analysis (hinge stiffness).

Table 3.5.4.1 – Model parameters for parametric analysis on pin constrains.

Parameter	Value
Accelerometer mass [g]	14.2
K_{bar} [N/m]	$4 \cdot 10^4$ [1 2 1]
K_{mag} [N/m]	$4.5 \cdot 10^5$
K_{hinge} [N/m]	config

Figure 3.5.4.1 presents how 16 modes change in frequency when the magnets stiffness value moves from 10^3 N/m (weak stiffness) to 10^8 N/m. This last value should give results in frequency like the previous case (magnets stiffness) because it represents a very rigid joint.

In Figure 3.5.4.1 there is a vertical black line which indicate the hinges stiffness value that can give better results for firsts mode. The chosen value is $K_{hinge} = 2 \cdot 10^5$ N/m.

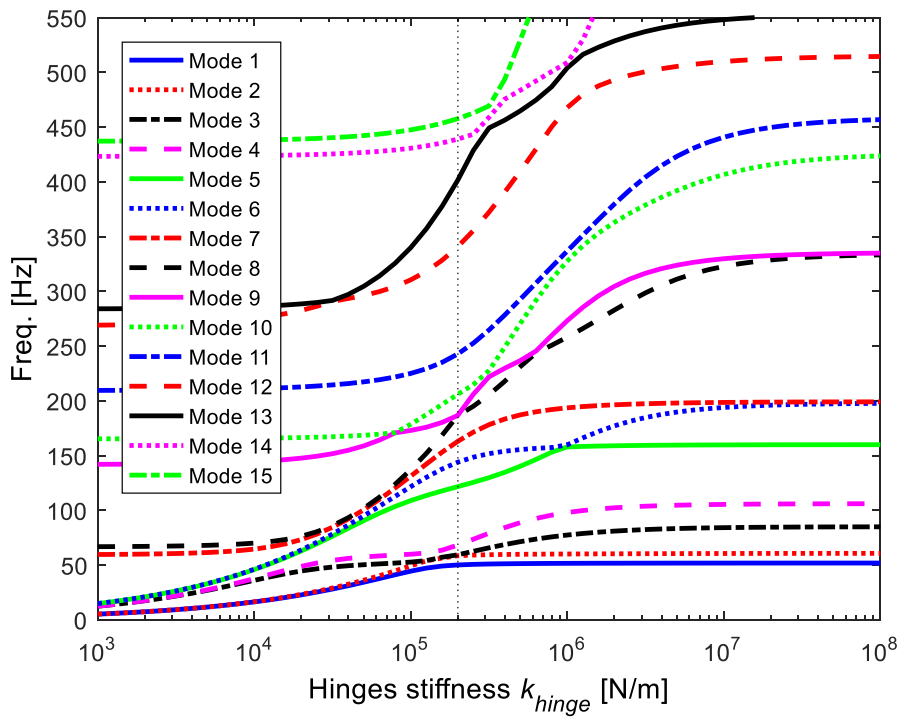


Figure 3.5.4.1 – Effect of hinges stiffness on the device model.

The analysis on hinges gives good results on frequency for the mode 1, 2 and for mode 4 but the subsequent mode shapes are not clearly identifiable as before.

Figure 3.5.4.2 shows parametric analysis and four experimental frequencies from hammer test. Experimental frequency n.º1÷7 is reported as horizontal line.

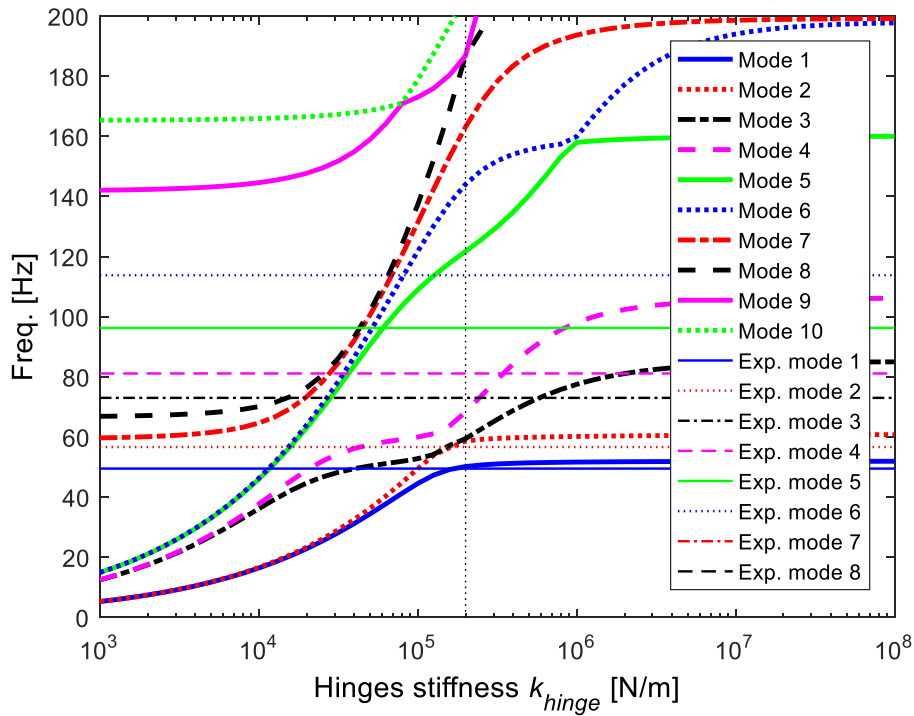


Figure 3.5.4.2 – Effect of hinge stiffness on the model with 4 experimental frequencies.

From this update it is possible to have some natural frequencies from numerical model almost equal to the experimental. Table 3.5.4.2 shows the update parameters.

Table 3.5.4.2 – Model parameters for parametric analysis on pin constrains.

Parameter	Value
Accelerometer mass [g]	14.2
K_{bar} [N/m]	$4 \cdot 10^4$ [1 2 1]
K_{mag} [N/m]	$4.5 \cdot 10^5$
K_{hinge} (on x, z) [N/m]	$2 \cdot 10^5$
K_{hinge} (on y) [N/m]	Infinite

The frequency result of the simulation with file updated (update4) are resumed in Table 3.5.4.3. In Figure 3.5.4.3 are represented the relative mode shapes.

Table 3.5.4.3 – Model parameters for parametric analysis on magnetic spring.

Mode	Frequency [Hz]	Description
1	50.55	Coupled pads out of phase
2	58.65	Coupled pads in phase
3	62.1	Torsional
4	68.5	Torsional in phase
5	122.2	To be defined
6	145.4	To be defined

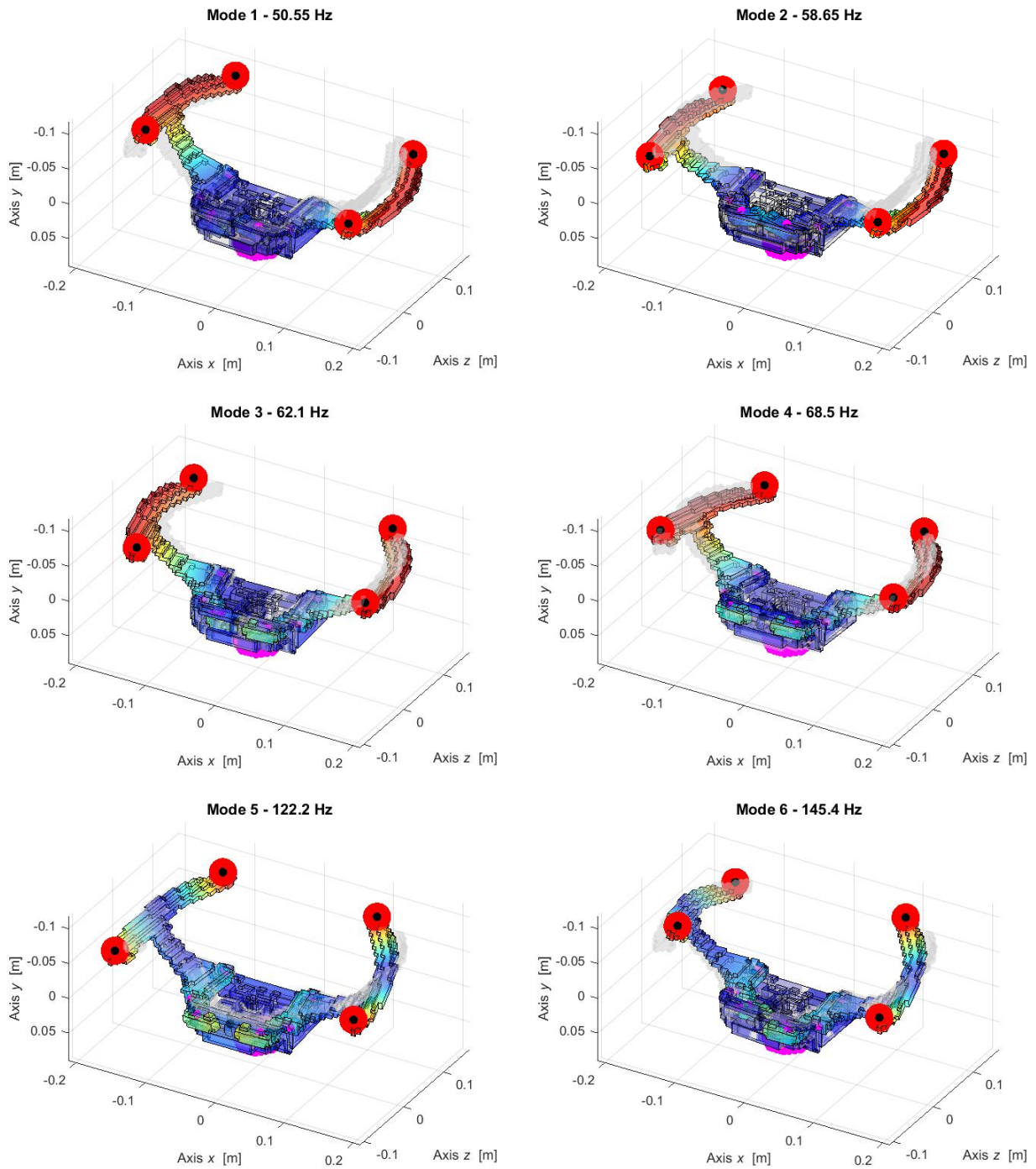


Figure 3.5.4.3 – Numerical real modal analysis of the first 6 mode shapes with update4.

In Table 3.5.4.4 are resumed all frequency found from numerical simulation. With parameters from Table 3.5.4.2 it is possible have a similitude on frequency and mode shapes for the firsts four which are evidenced in red in Table 3.5.4.4.

Table 3.5.4.4 – Comparison between updates and experimental results.

	Update1 Accelerometer	Update2 Steering bar	Update3 Magnetic spring	Update4 Pin constraints	Experimental
Mode	Frequency [Hz]	Frequency [Hz]	Frequency [Hz]	Frequency [Hz]	Frequency [Hz]
1	60.77	52.08	52.08	50.55	49.50
2	61.29	60.82	60.82	58.65	56.68
3	159.2	95.98	95.98	62.1	73.02
4	160.1	107.1	107.1	68.5	81.14
5	244.5	160.4	160.4	122.2	96.30
6	273.9	199.3	199.3	145.4	113.80

3.5.5 Density and Young modulus modification

With the previous updates it is difficult reach the values of experimental frequency. The mode that are less comparable depends on the motion of pads. So, it is important understand how the pad behave and their characteristics.

First, it is important to define the main structural parameter, like volume, mass and consequently density, these data are reported in Table 3.5.5.1 and Table 3.5.5.2 for both the real and numerical model. It is considered real model the one with data coming from SolidWorks/CAD model or from the real device. For the numerical model the data come from the Lupos model.

In order to compare the results, we must consider as a single whole body the pad and the arm for left and right side.

Table 3.5.5.1 – Structural data of elements of green pad.

	Volume [mm³]	Mass [g]	Density ρ [kg/m³]
Pad SX	38911.91	104.3	2680.41
Pad DX	38929.72	104.2	2676.62
Braccio SX	17675.80	46.3	2619
Braccio DX	17671.89	46.3	2619
Total	113189.32	301.1	2749.48

Table 3.5.5.2 – Structural data of two pads + two arms.

	Real/CAD model	Numerical model
Volume [m³]	$1.1319 \cdot 10^{-4}$	$2.1737 \cdot 10^{-4}$
Mass [kg]	0.3011	0.5869
Density ρ [kg/m³]	2660.14	2700.00
Young modulus E [GPa]	69	69

Analysing data of Table 3.5.5.2 it is visible the difference in volume and mass between the two models. In general, the model on Lupos results bigger than the real object. Probably, this is due to the brick simplification done for the Lupos model. The volume of all bricks together is higher than the volume of single pads and arms.

It can be noticed that the ratio numerical mass on real mass is about 194%, similar results are obtained for the volume which is 190%. Therefore, the numerical model is about two times the mass and volume of real/CAD model.

In that way, if density is calculated as in Table 3.5.5.2, the results for both model is close.

So, the main problem became the Young modulus property. Assuming the value of $E = 69$ GPa as reference value for aluminium, it is used this value for the two model which have different structural properties. In numerical model is overestimated the Young modulus properties, giving to all numerical mass an E equal to 69 GPa. But consider that the numerical mass is higher that the real mass.

Another parameter to take under control is the ratio E/ρ . This ratio on the real model is very close to the numerical one, and it is equal to 0.025 GPa/(kg/m³).

Now, one way to proceed can be re-do the mesh for the model brick simplification. Since the results from the model simulation are not so bad, it is tried to modify the structural parameter.

Keeping the numerical volume as in Table 3.5.5.2, it is possible to change the density in order to have the experimental/real mass also on the numerical model.

$$m_{\text{exp}} = m_{\text{numerical}} = 0.3011 \text{ kg.}$$

Imposing the mass and having the numerical volume from Lupos, it is possible to calculate the desired density.

$$\rho = m_{\text{exp}}/V_{\text{num}} = 1385.2 \text{ kg/m}^3$$

With this value of density, it is possible to guarantee the same real mass of pads + arms on numerical model.

Then, it is done a parametric analysis on the density and make an update to the model.

It is chosen the value of 1385.2 kg/m³ for the density.

Figure 3.5.5.1 shows the parametric analysis when the density change. The vertical black line evidenced the chosen value.

Table 3.5.5.3 resumes the frequency value with this parameter, then Figure 3.5.5.2 reports the mode shapes.

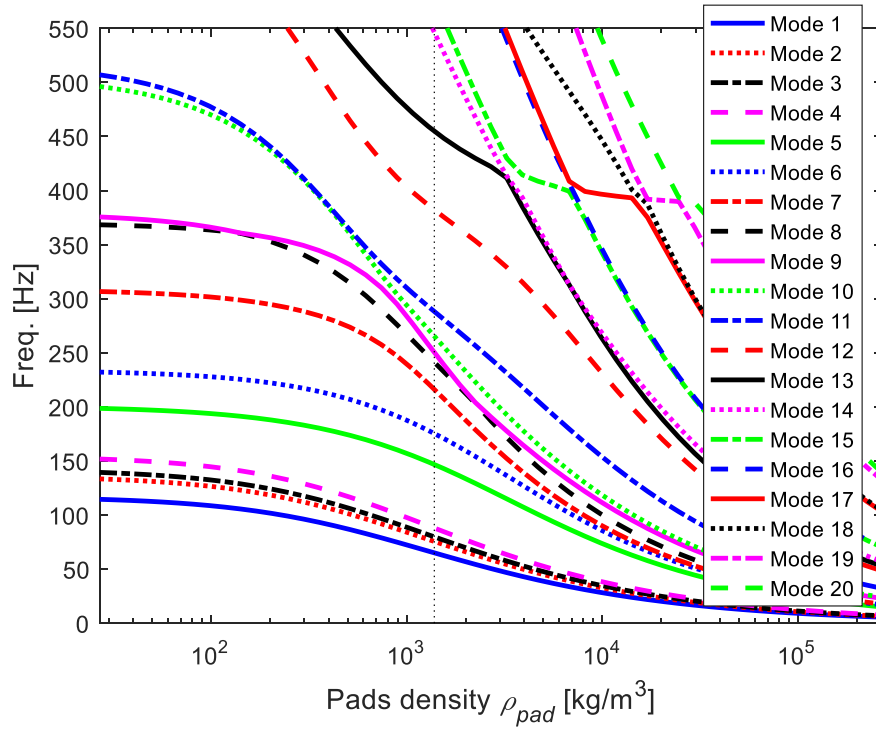
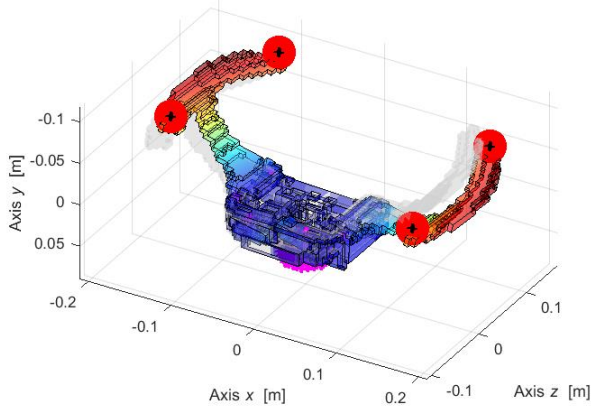


Figure 3.5.5.1 – Parametric analysis for pads density ρ .

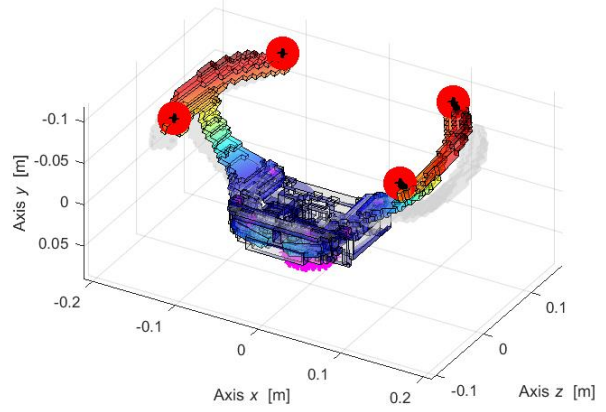
Table 3.5.5.3 – Natural frequency with density pads 1385.2 kg/m^3 .

Mode	Frequency [Hz]	Description
1	65.09	Coupled pads out of phase
2	75.61	Coupled pads in phase
3	79.86	To be defined
4	88	To be defined
5	146.8	To be defined
6	175.4	To be defined
7	216.2	Bending in phase on xy plane
8	241.3	Bending out of phase on xy plane

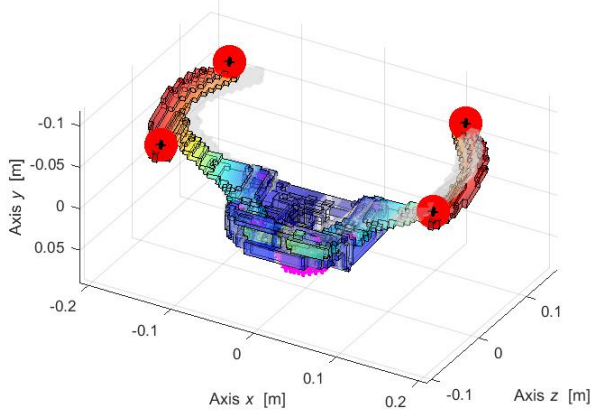
Mode 1 - 65.09 Hz



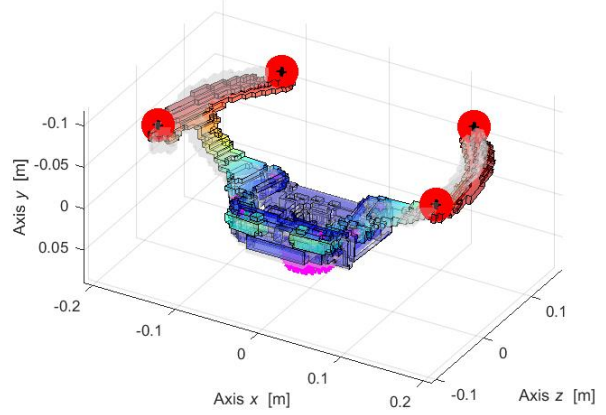
Mode 2 - 75.61 Hz



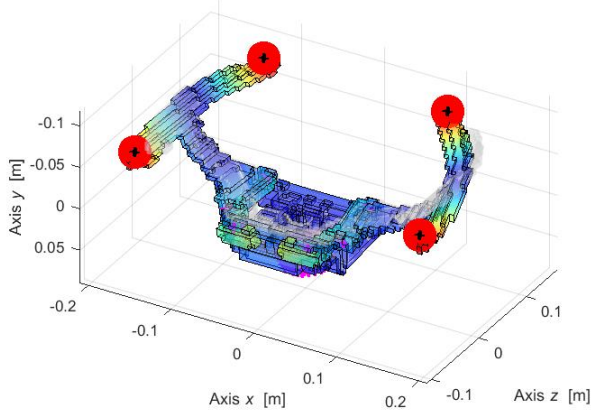
Mode 3 - 79.86 Hz



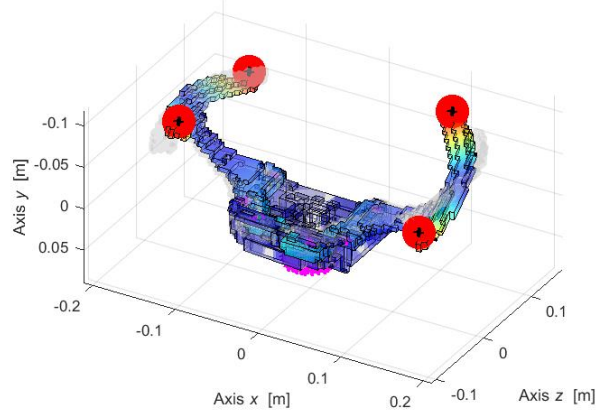
Mode 4 - 88 Hz



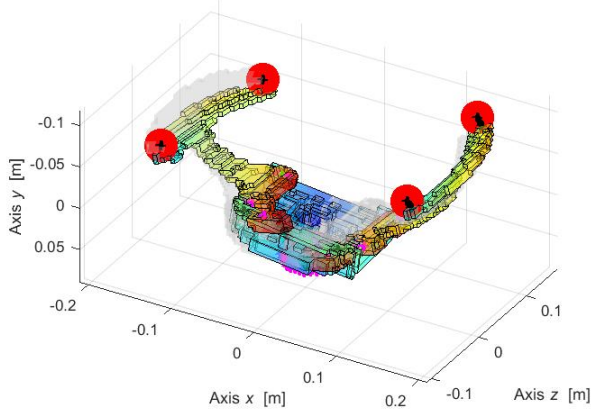
Mode 5 - 146.8 Hz



Mode 6 - 175.4 Hz



Mode 7 - 216.2 Hz



Mode 8 - 241.3 Hz

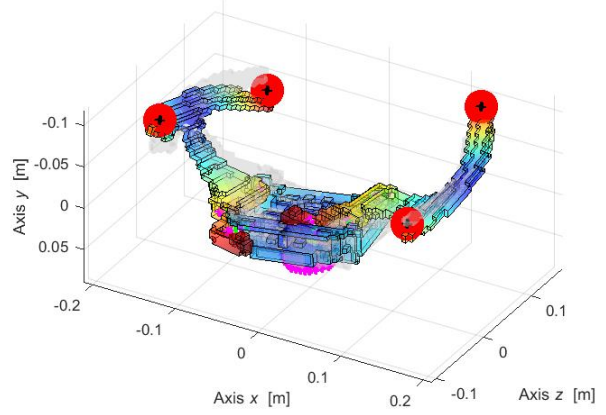


Figure 3.5.5.2 – Numerical real modal analysis of the first 8 mode shapes with update7.

If we want to keep constant the ratio E/ρ with the new density, we will have a Young modulus of 35.9 GPa. The material properties in this case are unchanged.

Table 3.5.5.4 – Natural frequency for Young modulus 35.9 GPa.

Mode	Frequency [Hz]	Description
1	61.66	Coupled pads out of phase
2	70.12	Coupled pads in phase
3	78.84	Torsional
4	86.27	Torsional in phase
5	126.4	Torsional out of phase
6	137.73	To be defined
7	211.5	To be defined
8	226.8	To be defined

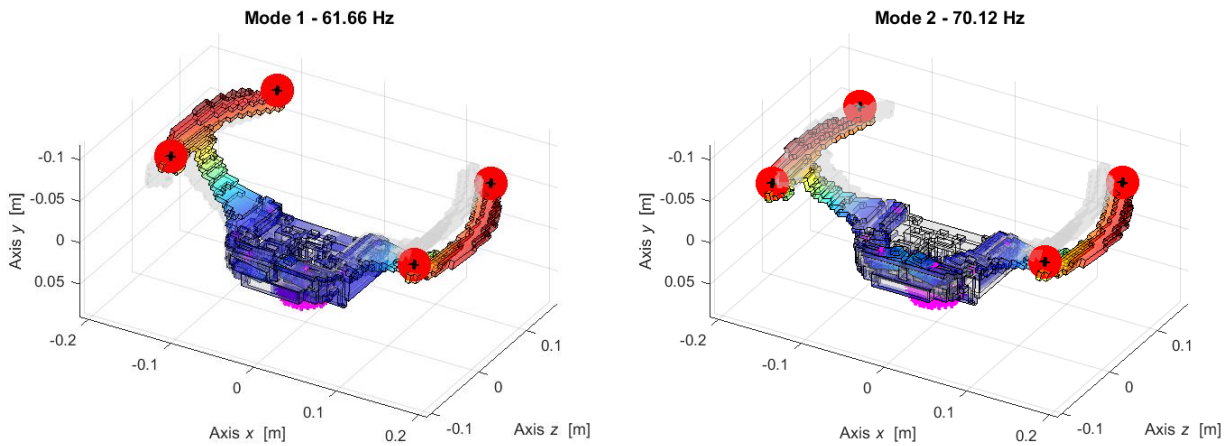


Figure 3.5.5.3 – Results of numerical real modal analysis of the first 2 mode shapes with E_{pad} 35.9 GPa.

After that, it is done a parametric analysis on the Young modulus. In Figure 3.5.5.4 is reported the results and with a black vertical line is evidenced the value 35.9 GPa. If the value of E decrease, it is possible to have better results in term of frequency on the firsts 6 modes.

In particular choosing the value of 10.94 GPa as Young modulus for the pad the results are close to experimental ones (red line in Figure 3.5.5.4).

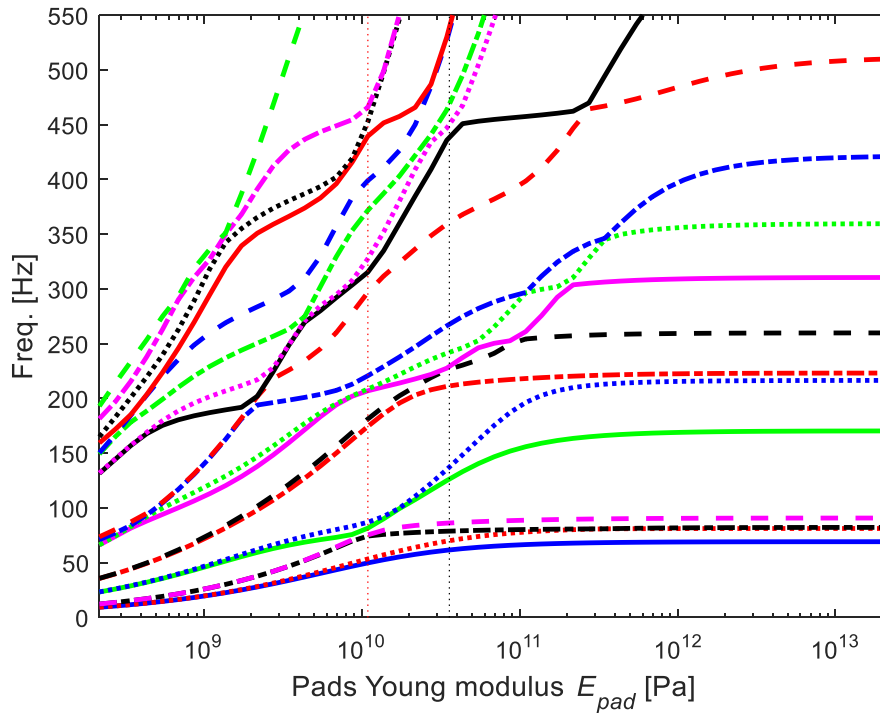


Figure 3.5.5.4 – Parametric analysis for Young modulus E_{pad} .

Table 3.5.5.5 resumes the results with $E_{pad} = 10.94$ GPa. Using this value, the ratio E/ρ is not constant, but it allows to have good results. From this table it is possible to have an accurate description, which is not the last one.

Notice that mode 3 and 4 are switched respect to the previous experimental results (i.e., update4).

Table 3.5.5.5 – Natural frequency for Young modulus 10.94 GPa (update8).

Mode	Frequency [Hz]	Description
1	49.82	Coupled pads out of phase
2	53.45	Coupled pads in phase
3	74.35	Torsional out of phase
4	75.42	Torsional in phase
5	81.57	Bending of pads out of phase on xz and yz planes
6	86.96	Bending of pads in phase on xz and yz planes
7	174.5	Bending of pads out of phase on xy plane
8	181.2	Bending of pads in phase on xy plane

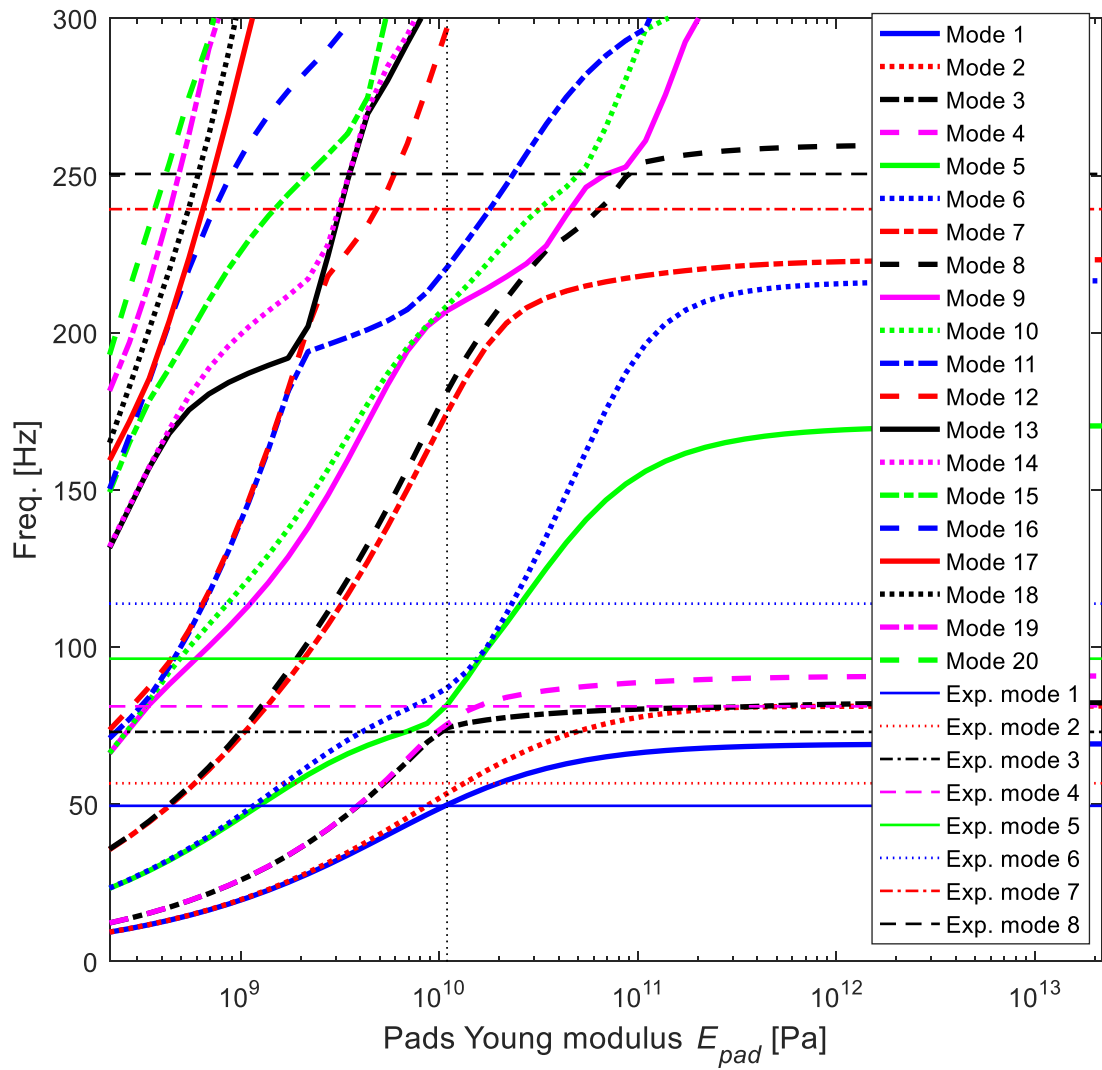
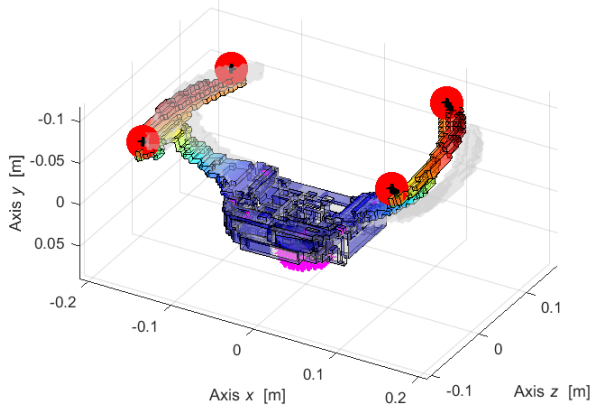
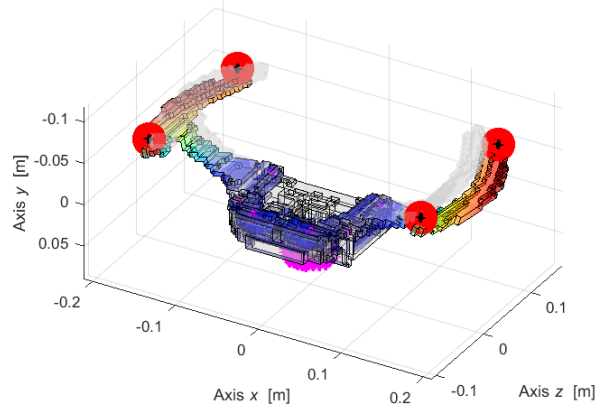


Figure 3.5.5.5 – Parametric analysis for Young modulus E_{pad} 10.94 GPa with experimental frequency.

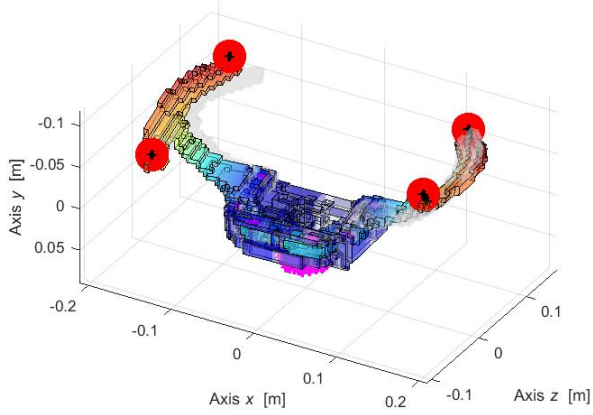
Mode 1 - 49.82 Hz



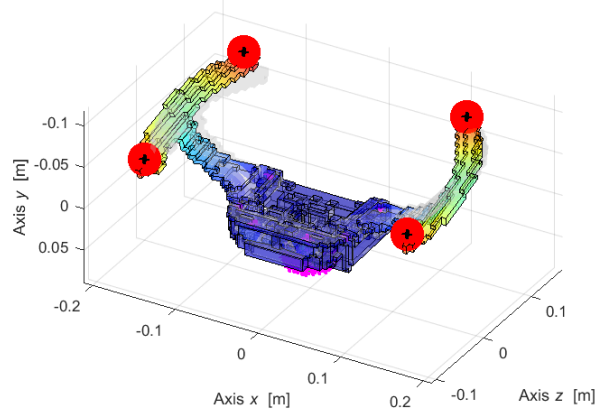
Mode 2 - 53.45 Hz



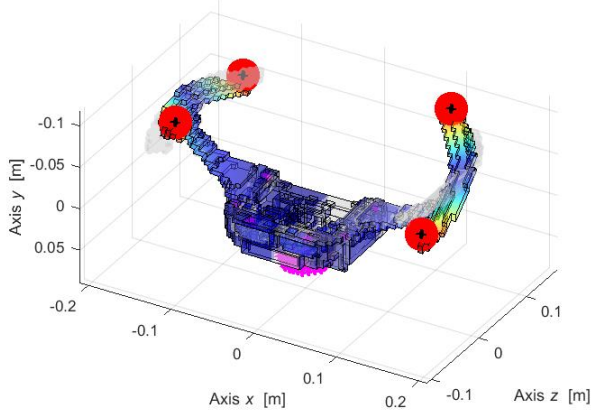
Mode 3 - 74.35 Hz



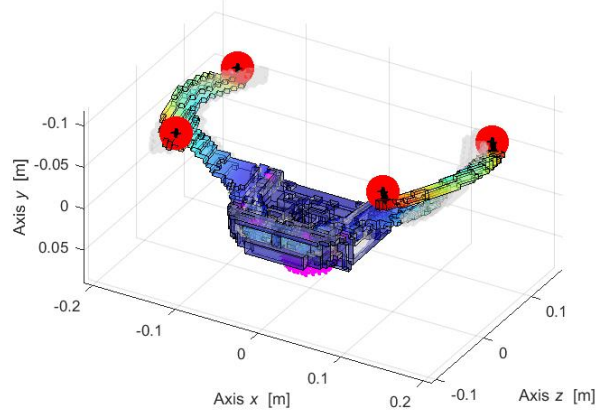
Mode 4 - 75.42 Hz



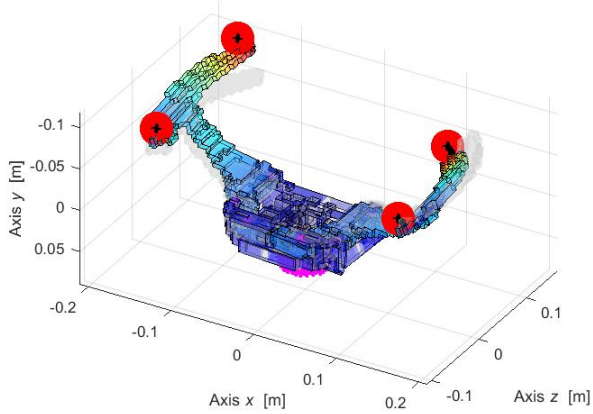
Mode 5 - 81.57 Hz



Mode 6 - 86.96 Hz



Mode 7 - 174.5 Hz



Mode 8 - 181.2 Hz

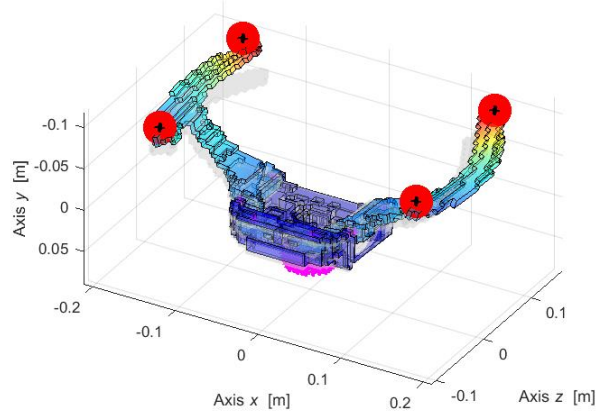


Figure 3.5.5.6 – Results of numerical real modal analysis 8 mode shapes with E_{pad} 10.94 GPa in update8.

Table 3.5.5.6 – Structural data of two pads + two arms in the numerical model.

	Real/CAD model	Numerical model
Volume [m ³]	$1.1319 \cdot 10^{-4}$	$2.1737 \cdot 10^{-4}$
Mass [kg]	0.3011	0.3011
Density ρ [kg/m ³]	2660.14	1385.2
Young modulus E [GPa]	69	10.94

3.5.6 Pin constraints modification

With this new update it is possible to have results very close to the experimental. The mode 3 and 4 respect the sequence of mode of the experimental results. The frequencies are very similar at low frequency in both cases.

To improve the model, from the previous model of paragraph 3.5.5, it is done a parametric analysis on the stiffness of hinges. Parametric analysis is showed in Figure 3.5.6.1.

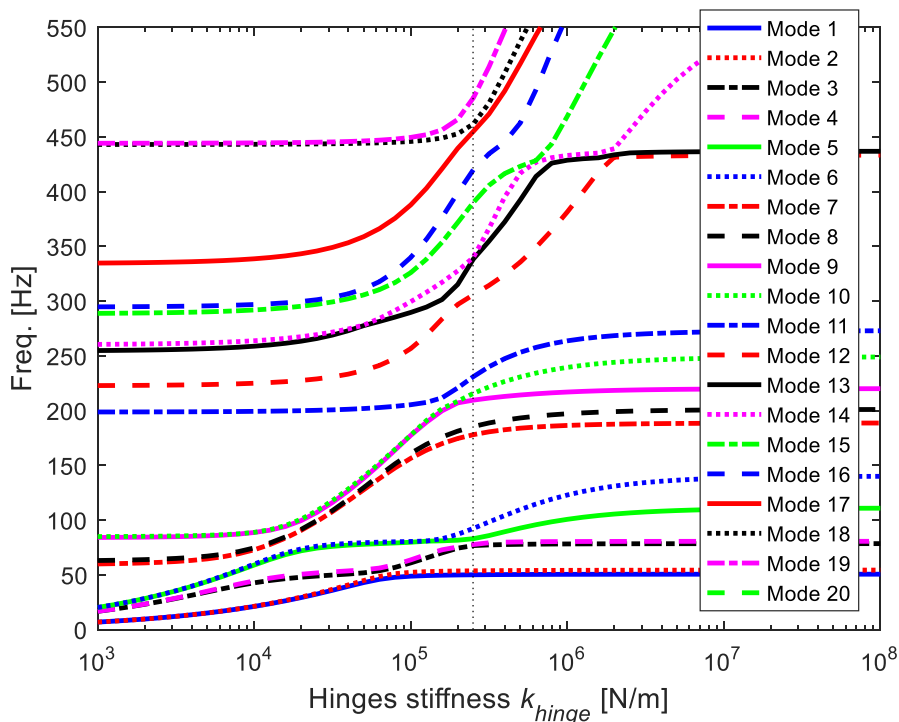


Figure 3.5.6.1 – Parametric analysis on hinges stiffness.

From this analysis it is chosen a new value for K_{hinge} , which is $2.5 \cdot 10^5$ N/m.

Figure 3.5.6.2 reports the parametric analysis of hinges stiffness with the experimental frequencies 1÷6.

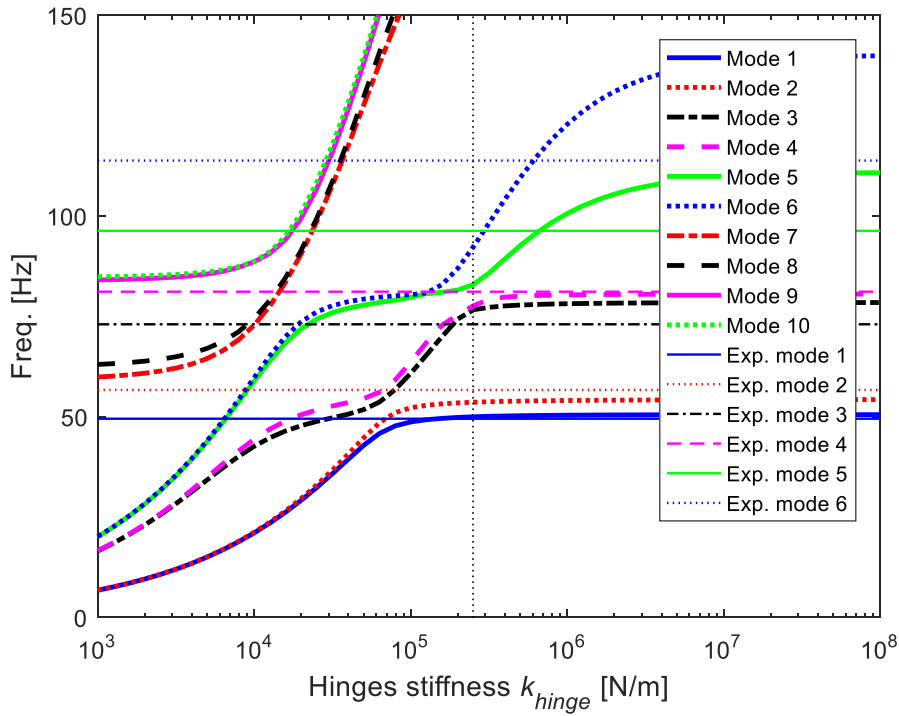


Figure 3.5.6.2 – Parametric analysis on hinges stiffness with 6 experimental frequencies.

Figure 3.5.6.3 shows a zoom of parametric analysis. It is important describe the red circle that involves mode 3-4. The two lines are very close, especially near the new designed value of K_{hinge} . The choice of this value probably will cause the switch of mode 3-4 and the re-establishment of similitude between experimental and numerical results.

In fact, with the update8 the mode 3-4 are inverted respect to experimental results, while after the update10 the mode shapes are again equal to the experimental.

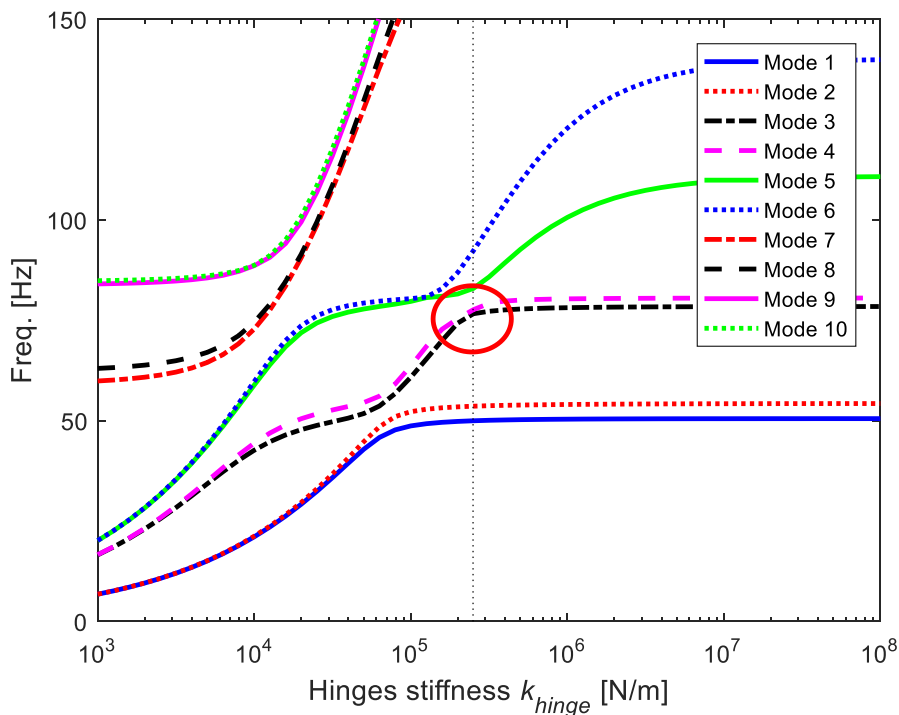


Figure 3.5.6.3 – Zoom on parametric analysis of hinges stiffness.

From this analysis it is chosen a new value for K_{hinge} , which is $2.5 \cdot 10^5$ N/m. Adding this parameter to the other found previous (Table 3.5.6.1) it is possible to find new optimal results.

Table 3.5.6.1 – Parameter for the final update model.

Parameter	Numerical model
Volume [m ³]	$2.1737 \cdot 10^{-4}$
Mass [kg]	0.3011
Density ρ [kg/m ³]	1385.2
Young modulus E [GPa]	10.94
Accelerometer mass [g]	14.2
K_{bar} [N/m]	$4 \cdot 10^4$ [1 2 1]
K_{mag} [N/m]	$4.5 \cdot 10^5$
K_{hinge} (on x, z) [N/m]	$2.5 \cdot 10^5$
K_{hinge} (on y) [N/m]	Infinite

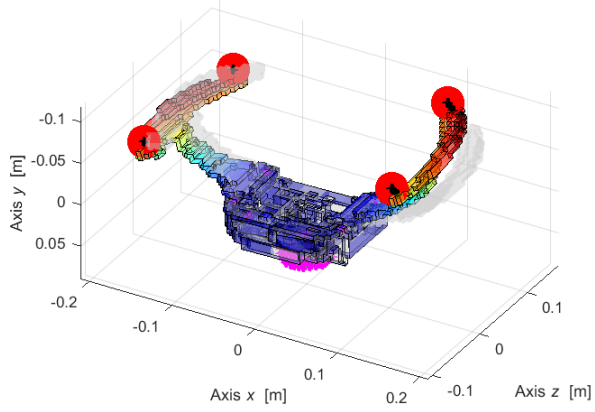
The results are resumed in Table 3.5.6.2. Mode 3 and 4 in this case are reverse respect the update8, this is a good result. In Table 3.5.6.2 are presented the experimental results for a direct comparison. The frequencies values are very similar, especially in the first four mode, but the behaviour of excitation is the same for all eight modes. This is a very important result.

Table 3.5.6.2 – Natural frequencies for final update10.

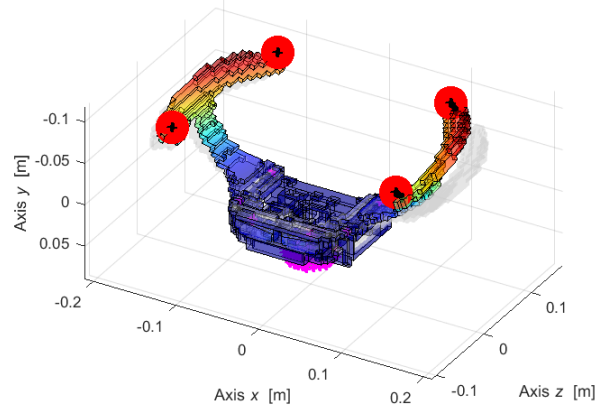
Mode	Frequency [Hz]	Description	Experimental frequency [Hz]
1	49.98	Coupled pads out of phase	49.50
2	53.61	Coupled pads in phase	56.68
3	76.62	Torsional in phase	73.02
4	77.59	Torsional out of phase	81.14
5	82.9	Bending of pads out of phase on xz and yz planes	96.30
6	92.21	Bending of pads in phase on xz and yz planes	113.80
7	177.9	Bending of pads out of phase on xy plane	239.30
8	185.3	Bending of pads in phase on xy plane	250.50

The mode shapes are the same for all experimental and numerical results.

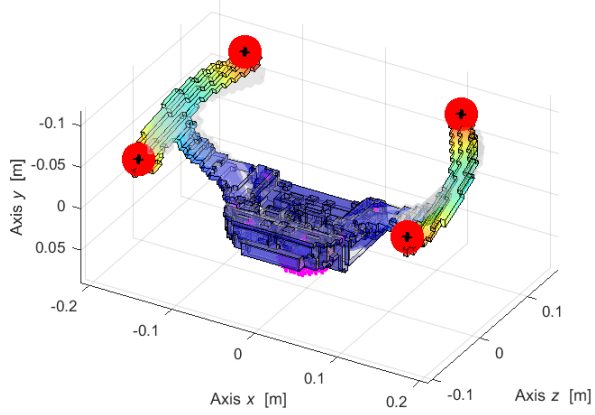
Mode 1 - 49.98 Hz



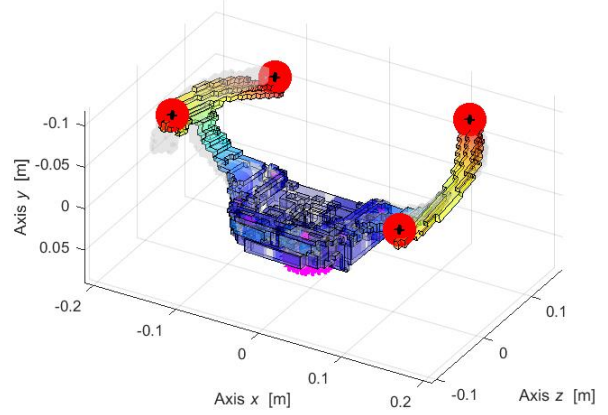
Mode 2 - 53.61 Hz



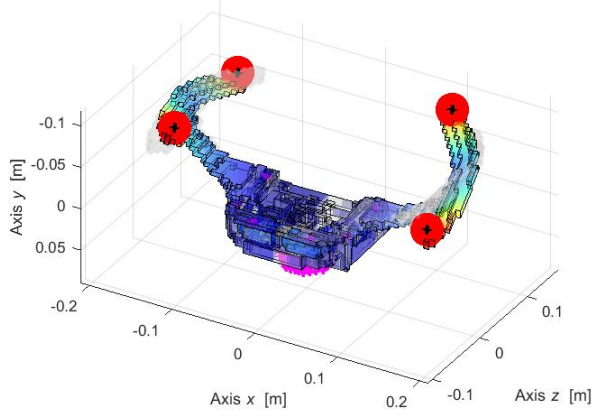
Mode 3 - 76.62 Hz



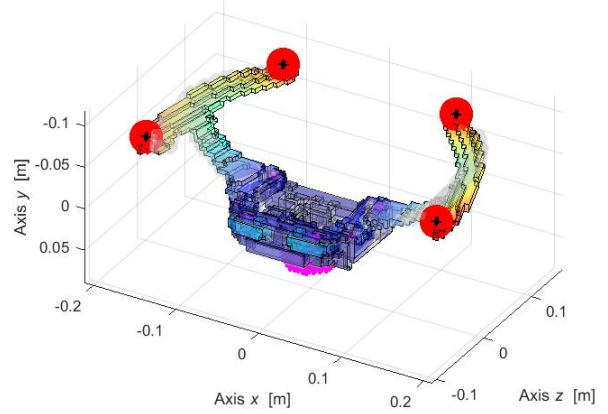
Mode 4 - 77.59 Hz



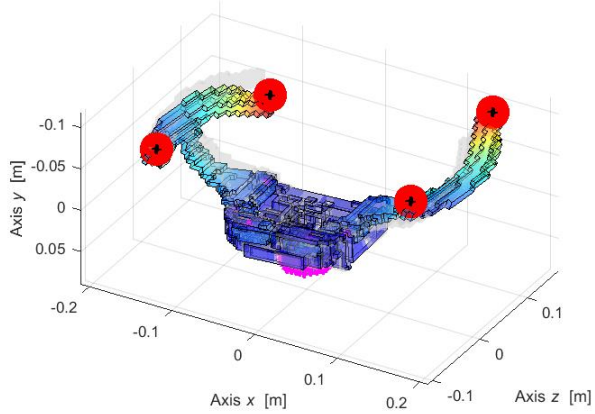
Mode 5 - 82.9 Hz



Mode 6 - 92.21 Hz



Mode 7 - 177.9 Hz



Mode 8 - 185.3 Hz

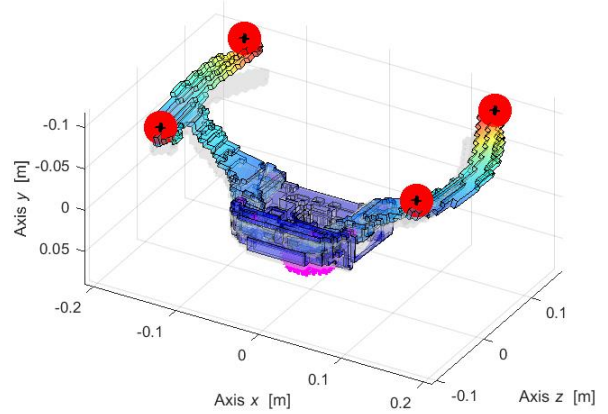


Figure 3.5.6.4 – Real numerical results with update10.

Table 3.5.6.3 – Comparison between updates 7, 8, 10 and experimental results.

	Update7 Density pads	Update8 Young modulus pads	Update10 K_{hinge}	Experimental
Mode	Frequency [Hz]	Frequency [Hz]	Frequency [Hz]	Frequency [Hz]
1	65.09	49.82	49.98	49.50
2	75.61	53.45	53.61	56.68
3	79.86	74.35	76.62	73.02
4	88	75.42	77.59	81.14
5	146.8	81.57	82.9	96.30
6	175.4	86.96	92.21	113.80
7	216.2	174.5	177.9	239.30
8	241.3	181.2	185.3	250.50

The important differences between update8 and update10 are about the mode shapes, while the values of frequencies have not big changes. Both updates give numerical results close to experimental ones.

Table 3.5.6.4 – Comparison between frequency from update 7, 8, 10.

	Update7 Density pads		Update8 Young modulus pads		Update10 K_{hinge}	
Mode	Frequency [Hz]	Description	Frequency [Hz]	Description	Frequency [Hz]	Description
1	65.09	Coupled pads out of phase	49.82	Coupled pads out of phase	49.98	Coupled pads out of phase
2	75.61	Coupled pads in phase	53.45	Coupled pads in phase	53.61	Coupled pads in phase
3	79.86	-	74.35	Torsional out of phase	76.62	Torsional in phase
4	88	-	75.42	Torsional in phase	77.59	Torsional out of phase
5	146.8	-	81.57	Bending of pads out of phase on <i>xz</i> and <i>yz</i> planes	82.9	Bending of pads out of phase on <i>xz</i> and on <i>yz</i> planes
6	175.4	-	86.96	Bending of pads in phase on <i>xz</i> and <i>yz</i> planes	92.21	Bending of pads in phase on <i>xz</i> and <i>yz</i> planes
7	216.2	Bending of pads out of phase on <i>xy</i> plane	174.5	Bending of pads out of phase on <i>xy</i> plane	177.9	Bending of pads out of phase on <i>xy</i> plane

8	241.3	Bending of pads in phase on <i>xy</i> plane	181.2	Bending of pads in phase on <i>xy</i> plane	185.3	Bending of pads in phase on <i>xy</i> plane
---	-------	---------------------------------------------	-------	---------------------------------------------	-------	---------------------------------------------

3.5.7 Pads asymmetry

To study better the numerical model, it is important seeing how the magnets stiffness influenced the behaviour of the device.

For this reason, it is done another parametric analysis on the magnet's stiffness. This time one magnet it is kept constant (on the right side of device) while the other is the parameter which varies. In Table 3.5.7.1 are reported the parameters used for analysis.

Table 3.5.7.1 – Parameter analysis on asymmetry.

Parameter	Numerical model
Volume [m ³]	$2.1737 \cdot 10^{-4}$
Mass [kg]	0.3011
Density ρ [kg/m ³]	1385.2
Young modulus E [GPa]	10.94
Accelerometer mass	14.2 g
K_{bar} [N/m]	$4 \cdot 10^4$ [1 2 1]
K_{mag} [N/m] (right)	$4.5 \cdot 10^5$
K_{mag} [N/m] (left)	config
K_{hinge} (on <i>x</i> , <i>z</i>) [N/m]	$2.5 \cdot 10^5$
K_{hinge} (on <i>y</i>) [N/m]	Infinite

Figure 3.5.7.1 resumes trend of 19 mode shapes when the variable parameter is the left magnets.

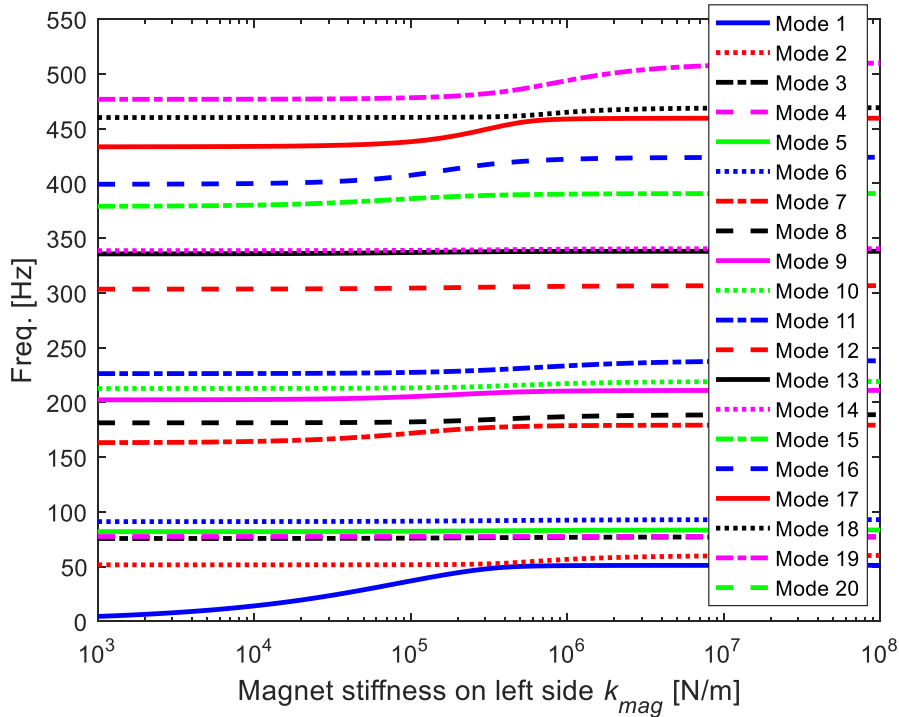


Figure 3.5.7.1 – Parametric analysis for just one magnet stiffness.

Figure 3.5.7.2 shows 8 modes when change the stiffness of magnets. The mode 1, 2, and 7 are the most affected. It is worth noticing that at $k_{mag} = 4.5 \cdot 10^5$ the blue curve is very close to the red one. Moreover, that value is the one fixed for previous update (black vertical line) and it is the same value assigned to right magnetic spring. From Figure 3.5.7.2 could be interesting find a different value for left magnet stiffness.

It is chosen value $1 \cdot 10^5$, represented on graph as red vertical line.

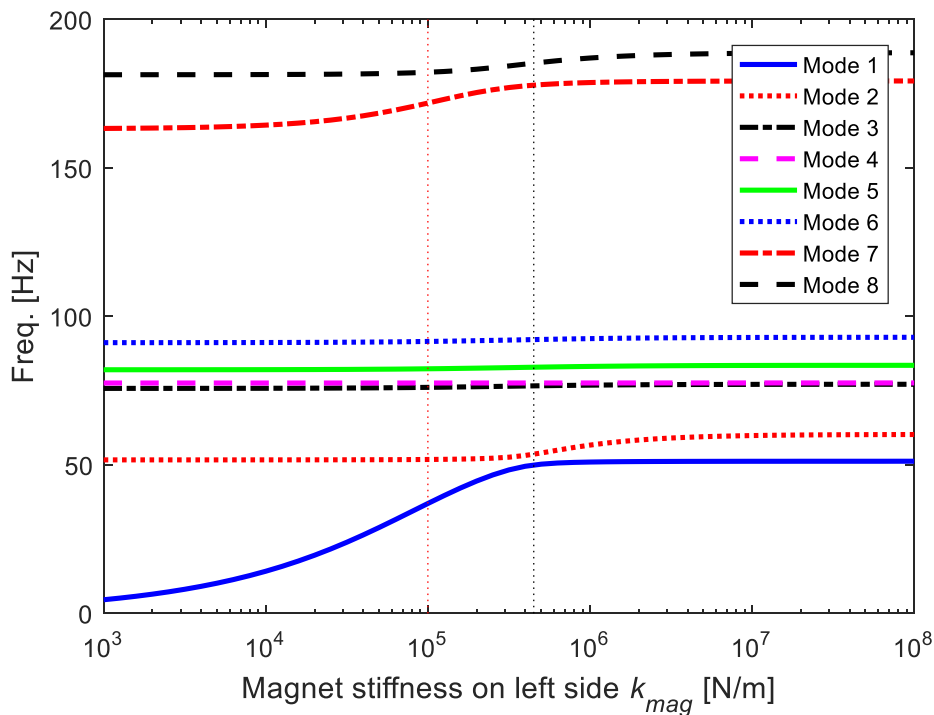


Figure 3.5.7.2 – Zoom of parametric analysis of one magnet stiffness.

It is done the analysis on frequency and mode shapes with the following parameters.

Table 3.5.7.2 – Parameter chosen for asymmetric behaviour.

Parameter	Numerical model
Volume [m ³]	$2.1737 \cdot 10^{-4}$
Mass [kg]	0.3011
Density ρ [kg/m ³]	1385.2
Young modulus E [GPa]	10.94
Accelerometer mass	14.2 g
K_{bar} [N/m]	$4 \cdot 10^4$ [1 2 1]
K_{mag} [N/m] (right)	$4.5 \cdot 10^5$
K_{mag} [N/m] (left)	$1 \cdot 10^5$
K_{hinge} (on x, z) [N/m]	$2.5 \cdot 10^5$
K_{hinge} (on y) [N/m]	Infinite

Figure 3.5.7.3 and Figure 3.5.7.4 report the results of first two mode shapes with the modification proposed above. From the animation of figures is visible the uncoupled behaviour of pads left and right. In this configuration the frequencies change, especially the first one decrease by 12 Hz. In Figure 3.5.7.3 there is the motion of left pad, while the right pad stands still. For Figure 3.5.7.4 the behaviour is the opposite, the right pad moves up and down.

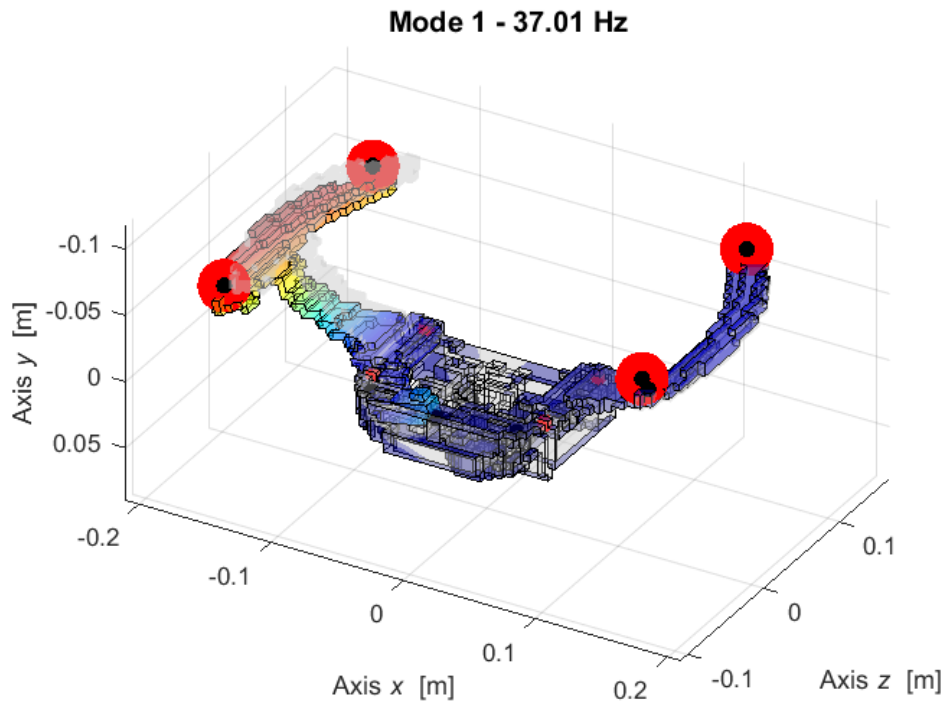


Figure 3.5.7.3 – First mode shape with one magnet stiffness modification.

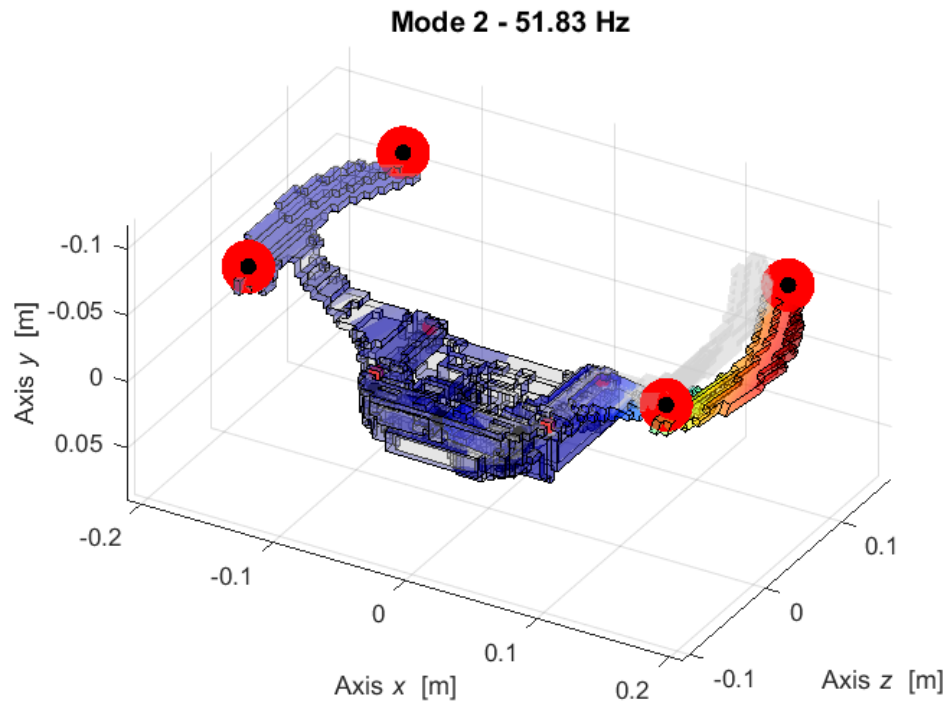


Figure 3.5.7.4 – Second mode shape with one magnet stiffness modification.

The differentiation choosing the magnets stiffness can support the procedure to uncouple the first modes. In this way the two pads have not connected one another in the first two mode shapes.

3.6 Hammer experimental MAC

Once chosen the update and defined the numerical model, it is useful know which is the correlation between experimental and numerical model. So, the MAC (Modal Assurance Criterion) analysis should be done.

This analysis allows to compare two eigenvector and set a percentage of similitude between two eigenvectors.

In this section are proposed some MAC of few updates, just to demonstrate how the numerical model develops and improves.

- **EMA Hammer - FEA Upd4**

Figure 3.6.1 shows the modal assurance criterion between the numerical model at update4 (setting of k_{hinges} or pin constraints) and the experimental hammer data.

The maximum percentage of correlation is on the MAC_{1-1} about 67%, then this value decrease. Moreover, mode 3-4 numerical are not well correlated with the experimental ones. In that area there are more squares/columns. Similar considerations are valid for mode 5-6 and their surroundings. In few words this means that the numerical model can be improved.

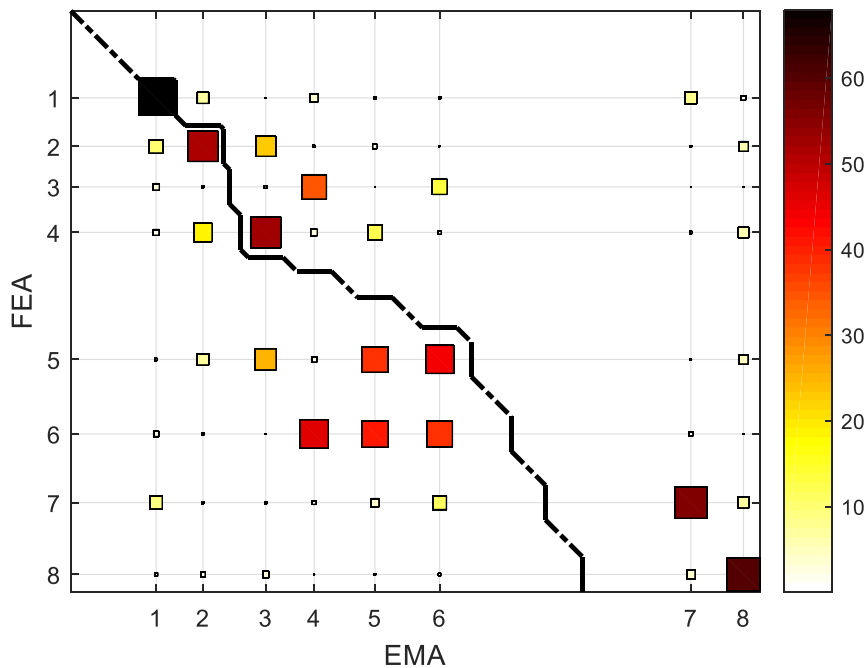


Figure 3.6.1 – MAC results between experimental and numerical model (Upd4).

- **EMA Hammer - FEA Upd8**

With update8 the mechanical properties of Levit are recovered. From Figure 3.6.2 it is visible that the mode shapes are well coupled, also the percentage of correlation is increased respect Figure 3.6.1 with update4.

Modes 1-2 are again well identified. The eigenvectors of modes 3-4 have like 80% of correlation. Notice that these two modes are exchanged one with the other, they differ from previous update and also to the next one. Modes 5-6 have already low percentage value, and the squares/columns are out of main diagonal. For last two modes the similitude between numerical and experimental is high but the frequency numbers are different.

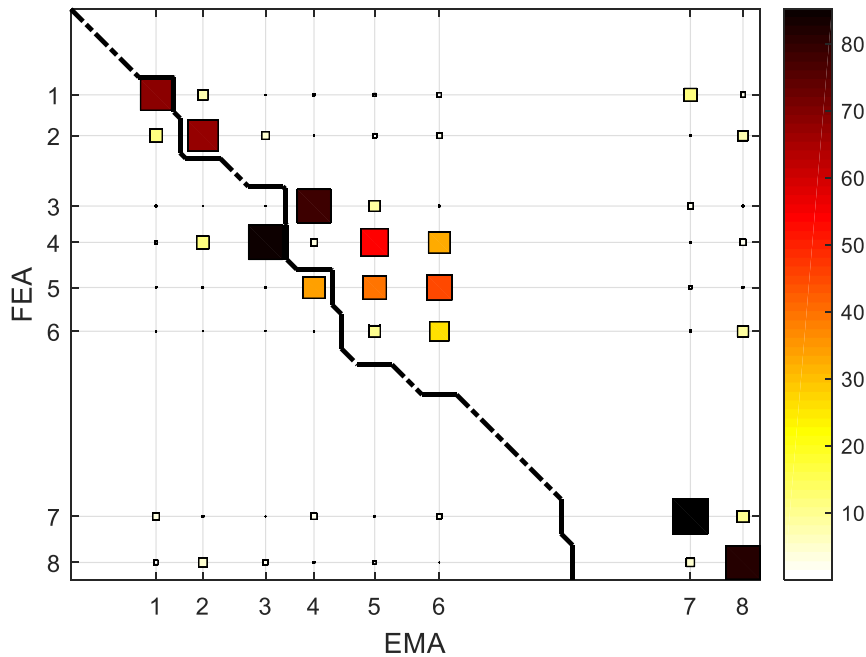


Figure 3.6.2 – MAC results between experimental and numerical model (Upd8).

- **EMA Hammer - FEA Upd10**

Here are exposed the data which refers to last update. With this one the mode shaped are very similar with each other.

Figure 3.6.1 shows the correlation between experimental (EMA) and numerical (FEA) model.

The correlation is acceptable for the first 2 mode, very good for mode 3-4, which come back in the same order from experimental and numerical. Then the percentage decreases at mode 5-6. Mode 7-8 have correlation of 85-80%, even if the representative columns are out of main diagonal. Which evidences that those frequency values are far away one another.

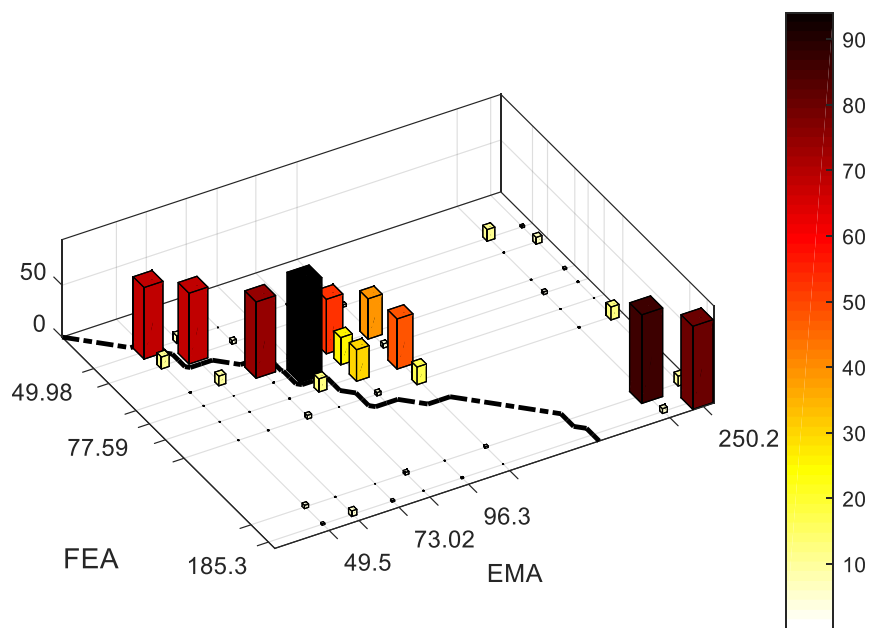
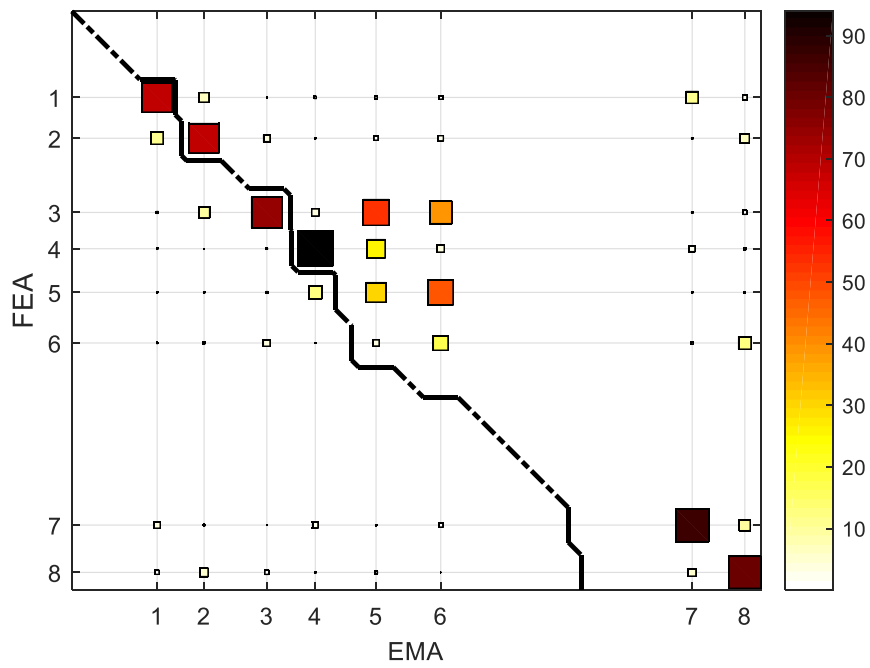


Figure 3.6.3 – MAC results between experimental and numerical model (Upd10).

In Table 3.6.1 are resumed the value of correlation of Figure 3.6.3, just to clarify graph descriptions.

Table 3.6.1 – Correlation percentage of experimental and numerical model (Upd10).

MAC _{i-j}	Correlation value %
MAC ₁₋₁	69
MAC ₂₋₂	68

MAC ₃₋₃	73
MAC ₄₋₄	94
MAC ₅₋₅	30
MAC ₆₋₆	16
MAC ₇₋₇	85
MAC ₈₋₈	80

It is important spend some words about values of MAC₅₋₅ and MAC₆₋₆. It is clear from Table 3.6.1 that correlation is low but seeing the simulation on Lupos of both experimental and numerical case there is a similar behaviour. Probably the experimental information recorded from accelerometer for these two cases are too poor, so the MAC function cannot give sufficient results.

3.7 Conclusions on second experiment

The impact hammer test is implemented during the second experimental day. The aim of this test is to excite the device and observe the reaction from experimental data. Another important point is to compare this experiment and the sweep test, which will be done in next chapter.

Conducting an impact, it is possible to observe the reaction of pad due to a semi-instantaneous excitation. Since this is very quick and few data are collected, implementing the numerical model based on the observed results becomes easier.

First of all, the natural frequencies are found, leading to results similar to the one of first experiment. Then, the post processing of frequency response function is carried out, which is readable in both amplitude and phase despite the complex type of experiment. The peaks and depression are visible on FRF graphs, and these are also highlighted by the lines of natural frequencies.

The most important progress taken forward from this test is the development of the numerical model through several parametric analysis. Once a time only one parameter is modified and the value which gives the better simulation results is selected. The main important changes are obtained with the modification of stiffness of steering bar, then with hinges stiffness of pads, in the end with attentions on mechanical properties.

In fact, the goal of this phase is to bring the numerical model results closer to the ones obtained through experimental tests. This objective is reached for the first 5 frequencies. As far as the mode shapes are concerned, the similarities between two model are reached for the all 8-mode compared and considered.

In the following Table are resumed the experimental and numerical frequencies (at update10).

Table 3.7.1 – Experimental and numerical natural frequencies.

Mode	Experimental frequency [Hz]	Numerical frequency [Hz]	Description
1	49.50	49.98	Coupled pads out of phase
2	56.68	53.61	Coupled pads in phase
3	73.02	76.62	Torsional in phase
4	81.14	77.59	Torsional out of phase
5	96.30	82.9	Bending of pads out of phase on xz and yz planes
6	113.80	92.21	Bending of pads in phase on xz and yz planes
7	239.30	177.9	Bending of pads out of phase on xy plane
8	250.50	185.3	Bending of pads in phase on xy plane

Another very important result is observed with the analysis of asymmetry of pads. An aspect relevant for Valeo is to decouple the motion of pads breaking the energy path between them. It is possible to obtain this result at the first two natural frequencies modifying the symmetry of pads with different magnets stiffness.

About the MAC analysis, the correlation between the two models is good (like 70%) for the firsts two modes, then decreases for the following. Considering that the experimental model takes information about modes shapes just from 4 points the results are quite satisfactory. It is important to compare the two model with active simulation on Lupos to observe and understand better the similarities.

4. Comparison between sweep and impact tests

The two experiments compared are the sine sweep vibration and the impact hammer test. Both have as objective to give information about the natural frequency and mode shapes.

Regarding the sweep are carried out a lot of tests along all three axes (x, y, z), while for the hammer test are excited only the y axis.

In Table 4.1 are resumed the most significant frequencies for the sweep test and the cumulative results from the other. Recall that the sweep frequencies come from the excitation on y axis at 0.005 mm (numerical reference system). In both cases are experimentally found 8 natural frequencies.

Table 4.1 – Comparison of experimental frequencies.

Mode	Sweep test Frequency [Hz]	Hammer test Frequency [Hz]
1	53.25	49.50
2	57.97	56.68
3	82.64	73.02
4	85.95	81.14
5	163.9	96.30
6	238.7	113.80
7	251.2	239.30
8	262.4	250.50

Probably, the difference between the first and second experimentation is due to the change of magnets stiffness during the experimental setup. For the hammer test the real device has been modified, the spring assets was re-established, and the screws were tightened better. Finally, the symmetry of device was guarantee in second experiment.

Figure 4.1 is used to give an idea of the effect on modes trend when the magnets stiffness change. It is done during the second experimental setup. From graph are to be considered just the behaviour of first four mode shapes and in particular the modes 3-4.

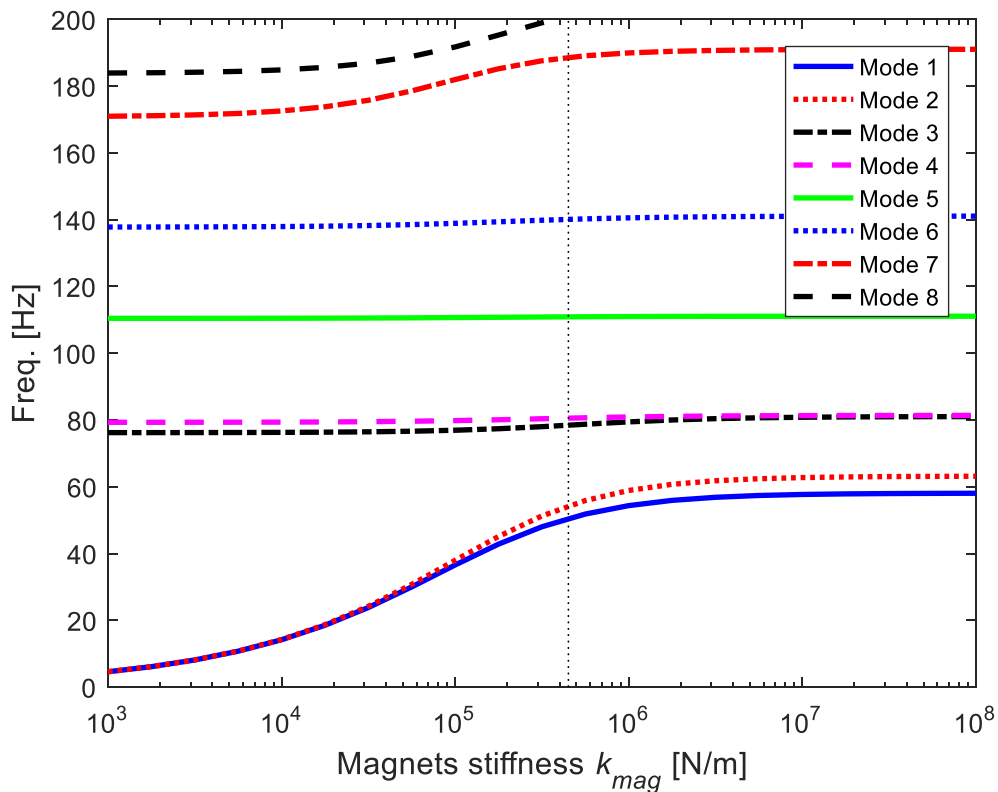


Figure 4.1 – Example of possible effect on magnets stiffness change.

The experimental data are recorded by Testlab in points where the accelerometers are placed. To correctly analyse data, it is necessary to create a reference scheme on Testlab and set the coordinates of accelerometer. The same sketch is built on Lupos in Matlab in order to compare the elaborated experimental data and the numerical ones. The final shape of the scheme is like two triangles with a single tip in common.

In following figures are reported the Lupos simulation of mode shapes for both the sweep and hammer test. On the left part there are the simulation of sweep experiment, on right there are the ones from roving hammer.

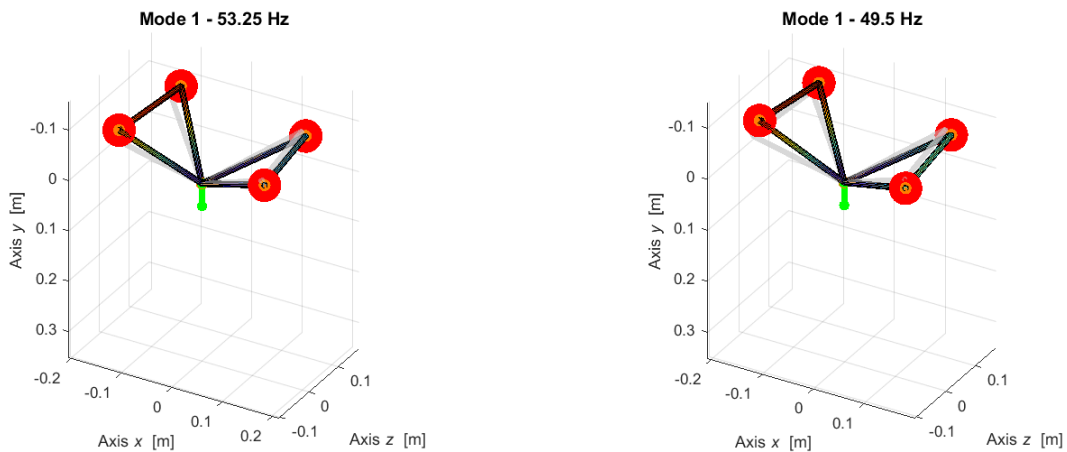


Figure 4.2 – 1st mode shape, with coupled pads out of phase.

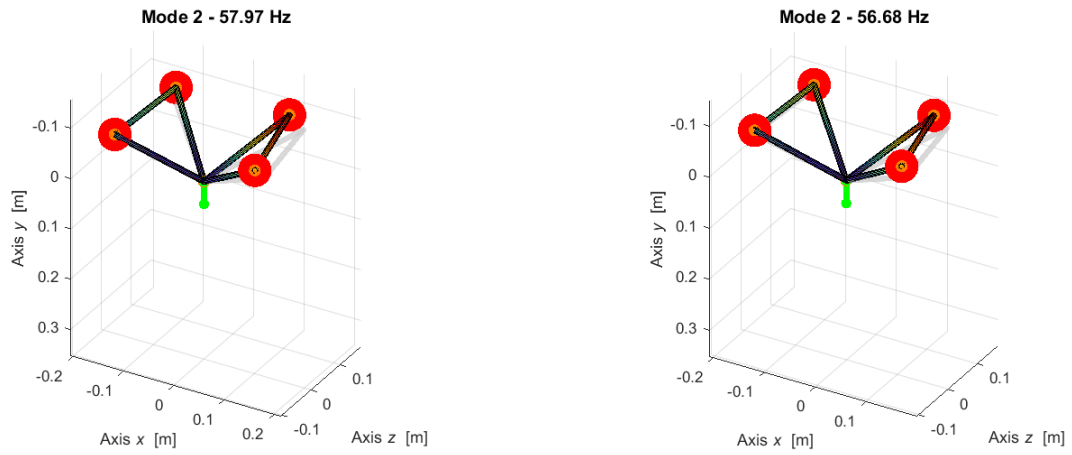


Figure 4.3 – 2nd mode shape, coupled pads in phase.

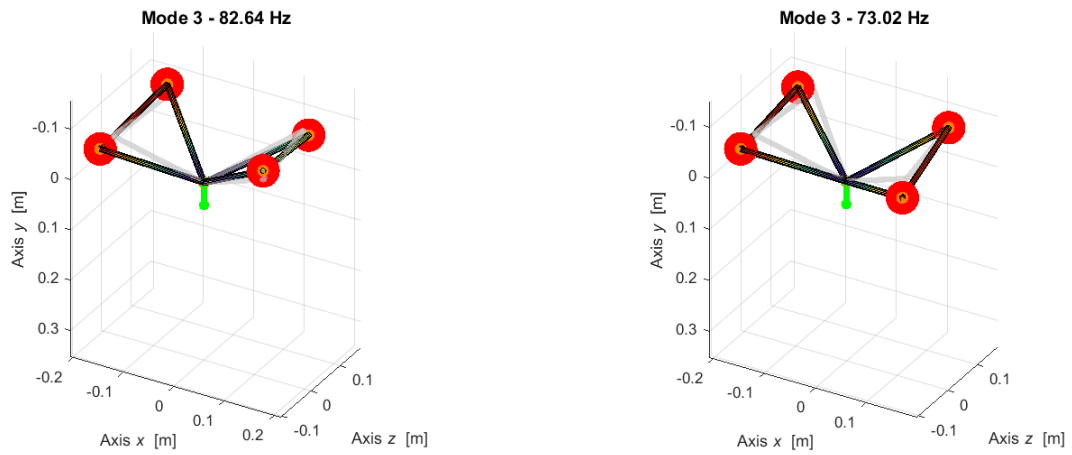


Figure 4.4 – 3rd mode shape, on left for sweep torsional out of phase, on right for roving hammer torsional in phase.

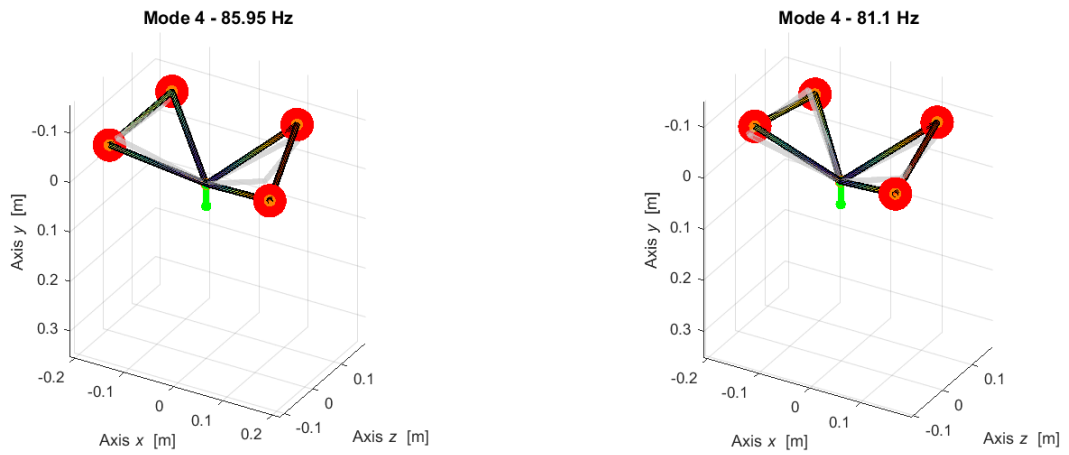


Figure 4.5 – 4th mode shape, on left for sweep torsional in phase, on right for roving hammer torsional out of phase.

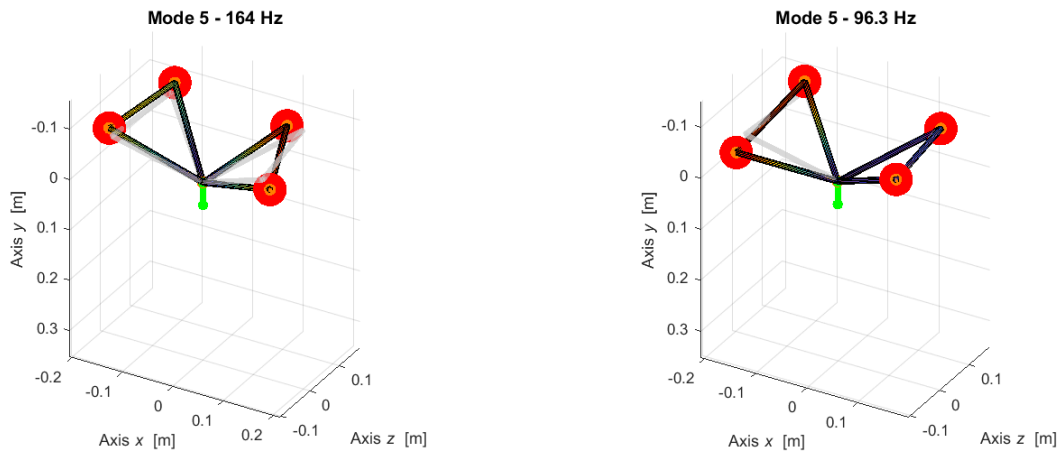


Figure 4.6 – 5th mode shape, bending of pads on xz and yz planes, for left/sweep in phase, for right/hammer out of phase.

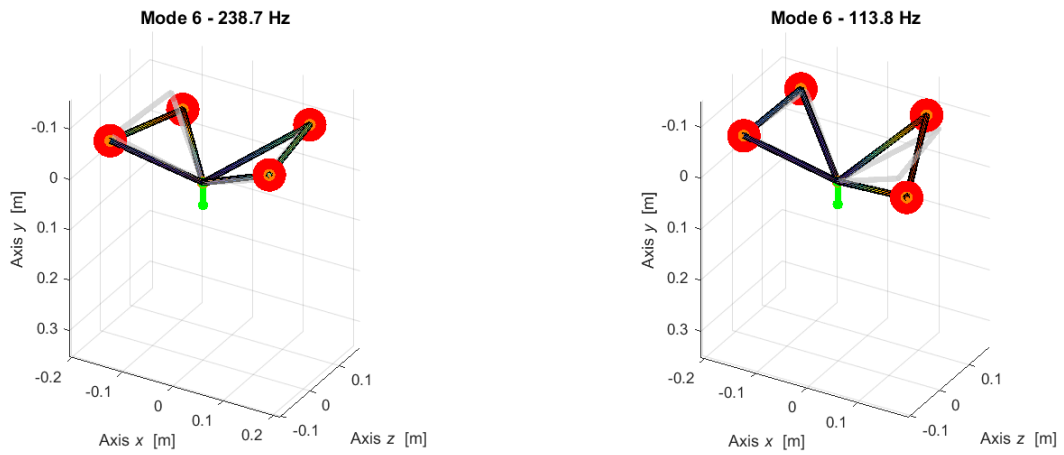


Figure 4.7 – 6th mode shape, bending of pads on xz and yz planes, for left/sweep out of phase, for right/hammer in phase.

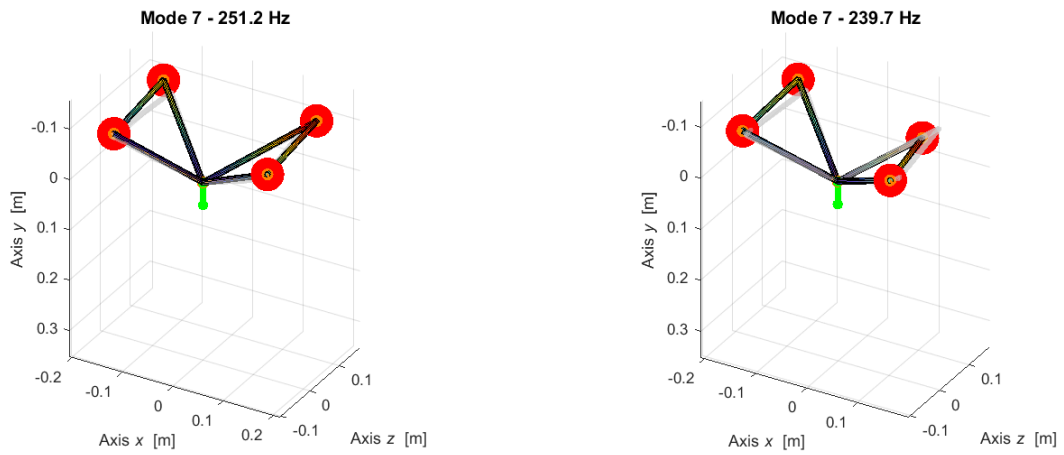


Figure 4.8 - 7th mode shape, bending of pads in phase on xy plane for sweep, bending of pads out of phase on xy plane for hammer.

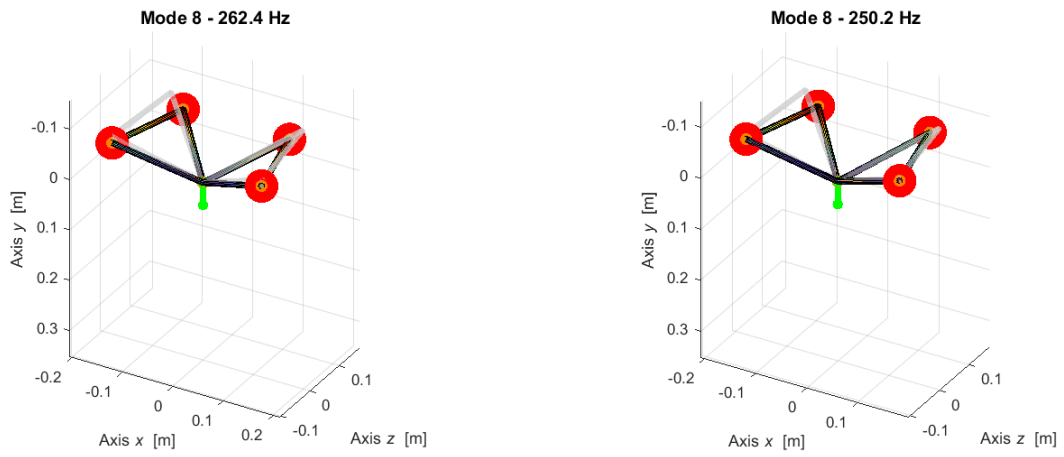
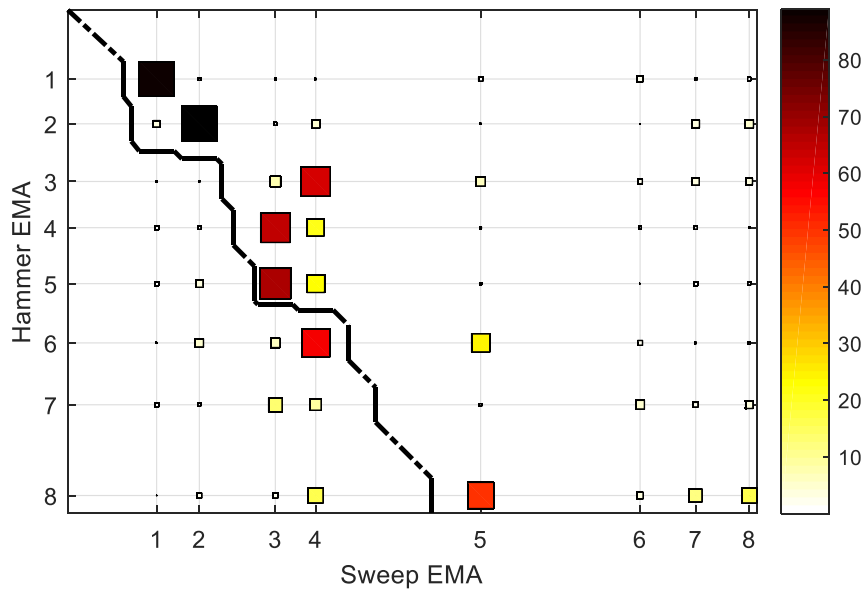


Figure 4.9 - 8th mode shape, bending of pads in phase on xy plane.

Figure 4.10 shows the MAC correlation between the two experimental tests.



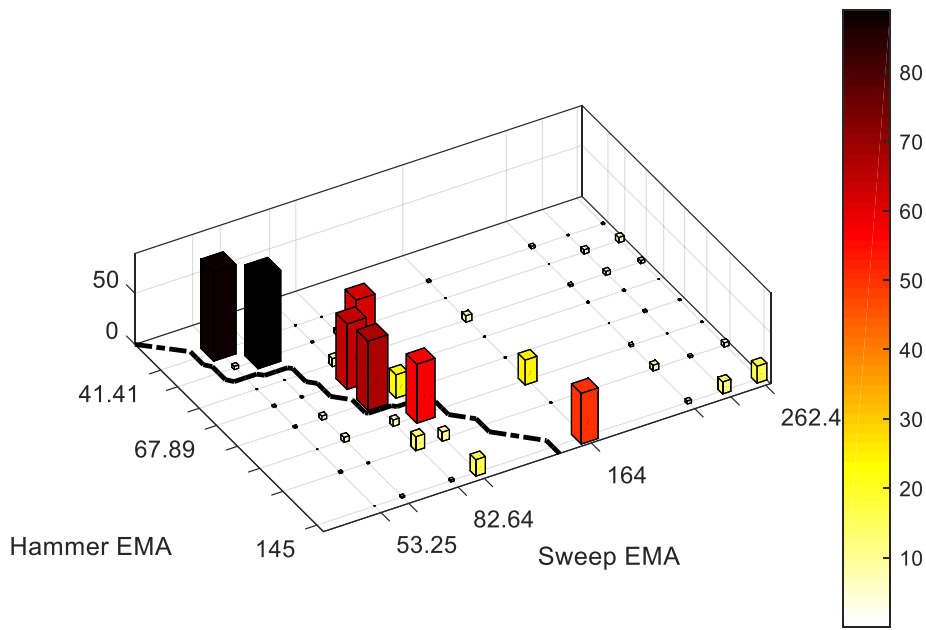


Figure 4.10 – MAC results between experimental model hammer and sweep.

The comparison with MAC is interesting just for the first six modes. The frequencies of modes 7-8 have very different values, thus they are out of main black diagonal and are not considered in MAC correlation.

Modes 1-2 have a very high percentage of correlation. Moreover, from Figure 4.9 it is visible that modes 3-4 are switched between two experiments. Mode 3 of hammer has correspondence with mode 4 of sweep. On the contrary, for 4th mode of hammer experiment, it is evident the correspondence with 3rd mode of sweep.

The correlation at MAC₅₋₅ and MAC₆₋₆ has low percentage, probably due to quality of information of hammer results. The eigenvectors information of these two modes of hammer results gives not complete overview about the real motion of the device. Consider that these data come from excitation on one single test axis.

Table 4.2 – Resume of most significant MAC correlation of two experiments.

	Hammer-Sweep [%]
MAC ₁₋₁	87
MAC ₂₋₂	89
MAC ₃₋₄	62
MAC ₄₋₃	64

From the presentation of mode shapes on figure above and the MAC results there are different kind of information. As state before, due to the different type of experiments (sweep vibration and roving hammer) the results can differ, especially considering only the mathematical point of view.

Observing the experiment simulation of Levit model on Lupos can be defined description exposed in Table 4.3. These definitions take into account the results from numerical model.

Table 4.3 – Description of two experimental tests.

Mode	Sweep test		Hammer test	
	Frequency [Hz]	Description	Frequency [Hz]	Description
1	53.25	Coupled pads out of phase	49.50	Coupled pads out of phase
2	57.97	Coupled pads in phase	56.68	Coupled pads in phase
3	82.64	Torsional out of phase	73.02	Torsional in phase
4	85.95	Torsional in phase	81.14	Torsional out of phase
5	163.9	Bending of pads in phase on <i>xz</i> and <i>yz</i> planes	96.30	Bending of pads out of phase on <i>xz</i> and <i>yz</i> planes
6	238.7	Bending of pads out of phase on <i>xz</i> and <i>yz</i> planes	113.80	Bending of pads in phase on <i>xz</i> and <i>yz</i> planes
7	251.2	Bending of pads in phase on <i>xy</i> plane	239.30	Bending of pads out of phase on <i>xy</i> plane
8	262.4	Bending of pads in phase on <i>xy</i> plane	250.50	Bending of pads in phase on <i>xy</i> plane

As last comparison it is showed the MAC correlation between the sweep experiment and the updated numerical model.

From Figure 4.11 is visible the similitude between mode 1 and 2, the inversion of modes 3-4 respect to numerical model which is already discussed and the loss of quality information for other modes.

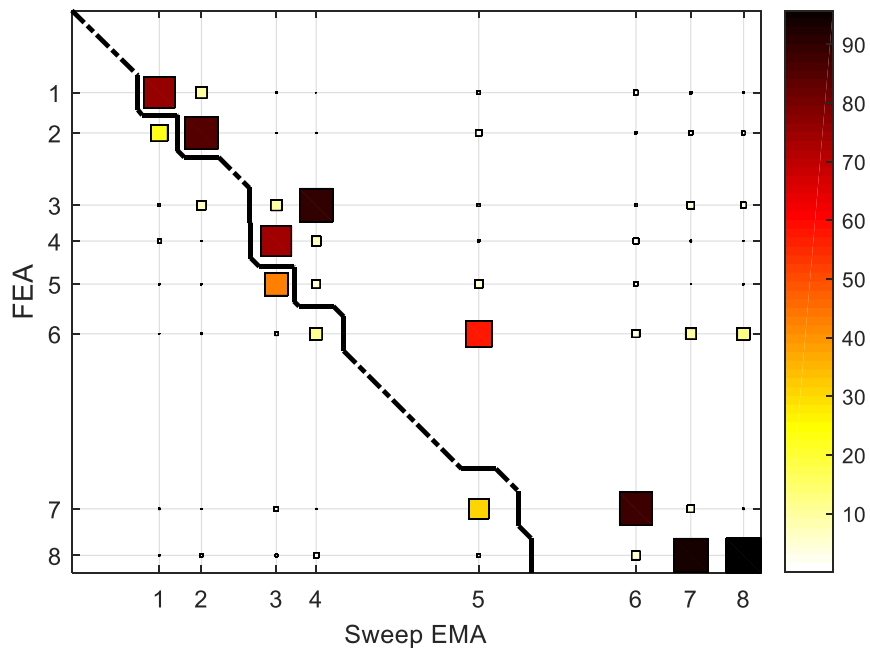


Figure 4.11 – MAC results between experimental sweep test and updated numerical model.

5. Actuation and release test

The second part of experimental on Levit device took place at Valeo in 2021-07-19, it involves two tests, the roving hammer test already described and the actuation and release test.

This last experiment regards the actuation and release of the pads. This analysis is conducted through the instrumentation present in Valeo. The acquisition of data is done thanks to the accelerometers, the lasers and by a Siemens Scadas Mobile provided by Politecnico, which allows the user to have a direct interface with acquired data.

During these tests, the lasers are used for the acquisition of displacements, which is the most important measurement. Accelerometers add information, however the test is carried on with and without them, to observe their influence on performance.

5.1 Setup

As for the hammer experiments, it is important to control the condition of the device. In particular, it is checked the symmetry between pads. The springs close to magnets and below the bracket are equally calibrated, thus, the distance and hence the stiffness is modified respect to the sweep experiment. After this correction, the symmetry is restored. It is worth noticing that this setup modification will affect the test and the results.

To perform the test, the device is fixed on a support structure which carry the actuation and release punches, these last ones will produce the motion of the pads. This support is presented in Figure 5.1.1 on left and it is composed by the proper support for Levit and by an aluminium cube. The first support, marked as A simulates the position of the Levit on the vehicle, in fact the device has an inclination respect to the vertical axis of 22° .

Figure 5.1.1 shows on right the command panel for the actuation/release of pistons.



Figure 5.1.1 – Support for the Levit (left), command panel for the pistons (right).

In Figure 5.1.2 the inclination axis of device is shown. The support A is placed on a cube (B), they are fixed together and screwed on the shaker plate. With label C is identified the support for lasers, this structure was built in order to make the lighting lasers perpendicular to the face of pads.

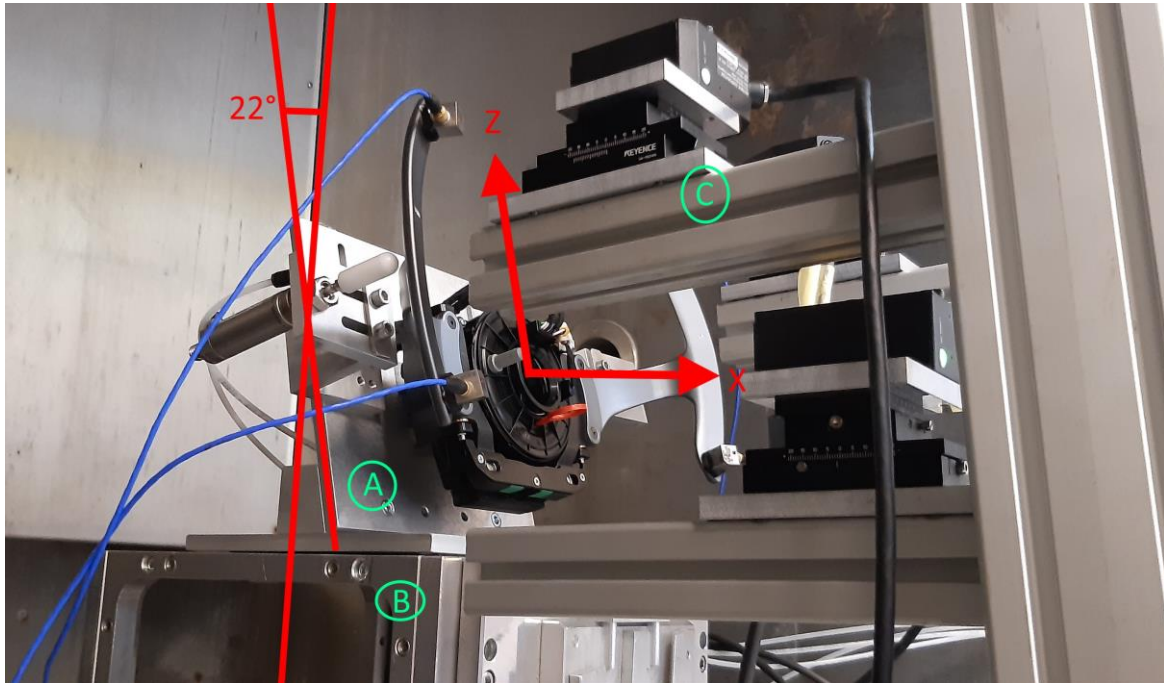


Figure 5.1.2 – Inclination of the device respect to cube reference system.

In Figure 5.1.3 is shown the laser structure, which is inclined of α angle, equal to 22° respect of the normal to the ground plane. On the structure are placed four lasers for measurement, one for each accelerometer placed at the four extremities of two pads. The lasers are numbered from one to four according to the nomenclature of accelerometers in the first experimental part with sweep test.

In the background of Figure 5.1.3 it is possible to see the Levit in its correct final position, ready for the test.

In Figure 5.1.4 there is another point of view of the structure and the nomenclature of the accelerometers.

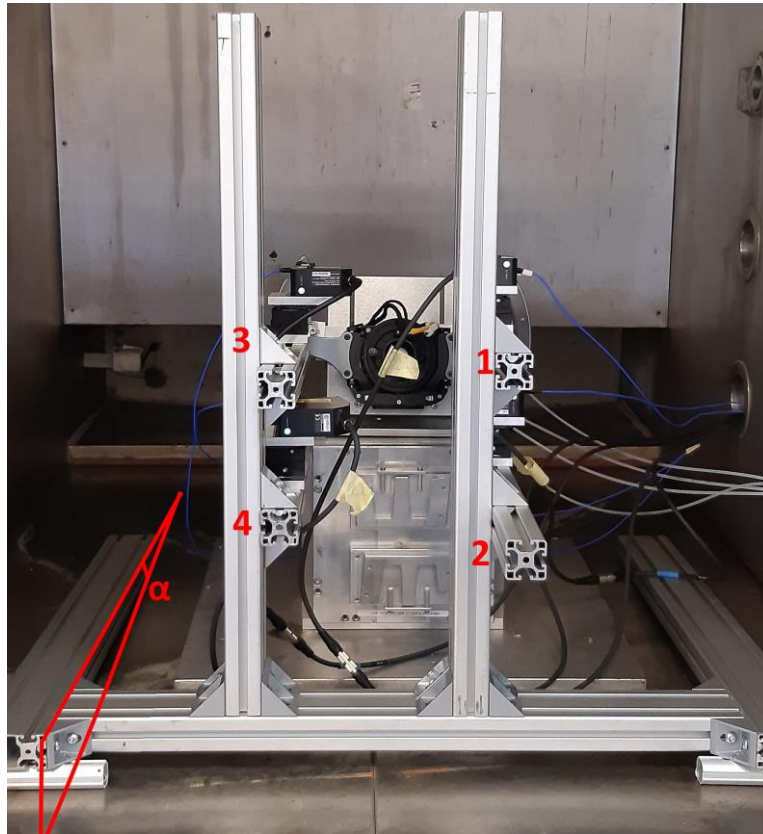


Figure 5.1.3 – Laser structure and nomenclature in the final setup.



Figure 5.1.4 – Accelerometer position and nomenclature.

In Figure 5.1.5 the two pistons that manage the actuation and release of the pads are put in evidence in red box. The piston with box A moves the left pads (the one with the inscription ‘DOWN’), while the B piston provides the motion for the right pad (‘UP’).

At last, in the Figure 5.1.5 can be noticed the four lasers in black, which direct their light on the surface of accelerometers.

Figure 5.1.6 shows the Levit under analysis putting in evidence the UP and DOWN pads.

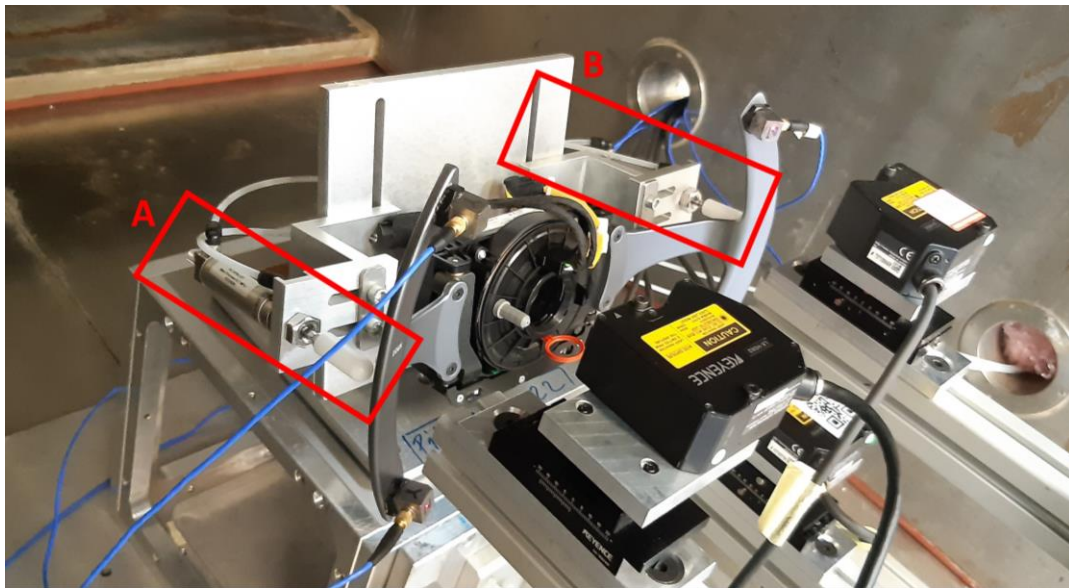


Figure 5.1.5 – Pistons for actuation and release.



Figure 5.1.6 – Levit device with difference on pads.

5.2 Experiment description

An automatic cycle is built to conduct the experiment. A profile motion of 10 seconds is imposed, divided in the phase of actuation and of release. This profile is repeated ten times, moving the DOWN pad (on left of the device), and then other ten times moving the UP pad (on the right part). Another setup condition involves the presence/absence of accelerometers.

In general, the actuators are released after 0.5 sec, then the actuation phase start. After that, the pads are hold for a period, then the release phase starts, and the pads come back to their original configuration.

After the release phase, it is visible the transient oscillation period between 4 and 5 seconds.

On y axis is presented the displacements due to motion of pads in millimetres, x axis presents the time. Data from one test are shown in Figure 5.2.1.

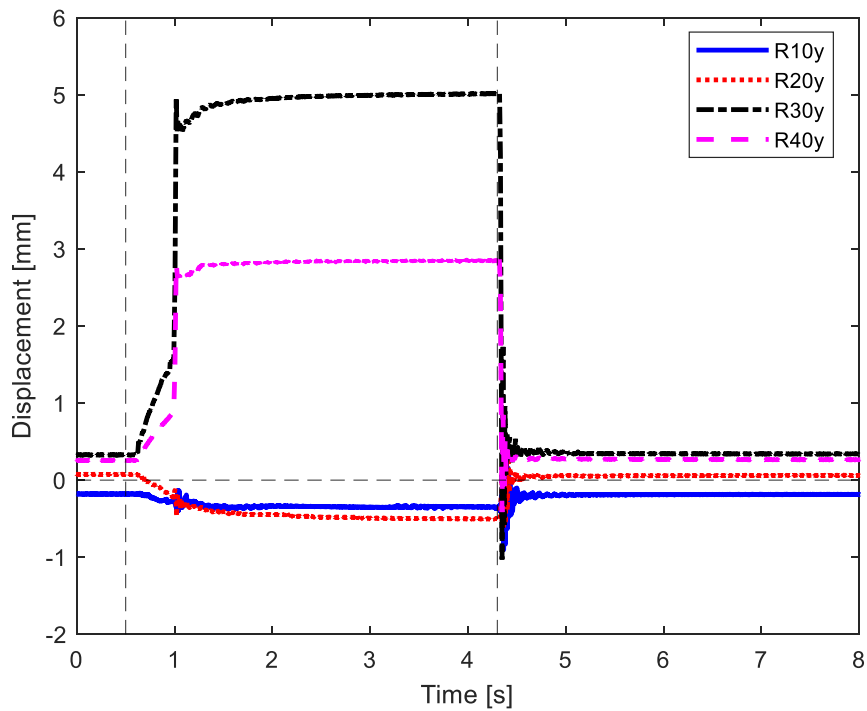


Figure 5.2.1 – Test to show time history, at 0.5 sec actuation phase, hold phase and release phase.

The acquisition of data during experiment is done through 14 channels on the SCADAS. Four of them are used for information coming from laser, the remaining ten are reserved for the accelerometers. In particular, the time history of accelerometer 1, 3 are registered on all three directions (x , y , z), while for accelerometer 2 and 4 the acquired directions are only x , y .

To have an easier reading of legend of following figure Table 5.2.1 is used, where the acronyms are resumed.

Table 5.2.1 – General meaning of legend.

Legend elements	Meaning
R10y, R20y, R30y, R40y	Identification of measure acquired from laser in the four points.
R1x, R1y, R1z	Identification of measure taken from accelerometer n. ^o 1 in all three directions
R2x, R2y	Identification of measure taken from accelerometer n. ^o 2 in two directions
R3x, R3y, R3z	Identification of measure taken from accelerometer n. ^o 3 in all three directions
R4x, R4y	Identification of measure taken from accelerometer n. ^o 4 in two directions

The same procedure is repeated with and without the accelerometers acquisition signal. To do the test without the accelerometer the laser must be resettled and calibrated again. Figure 5.2.2 and Figure 5.2.3 illustrate the two final setups.

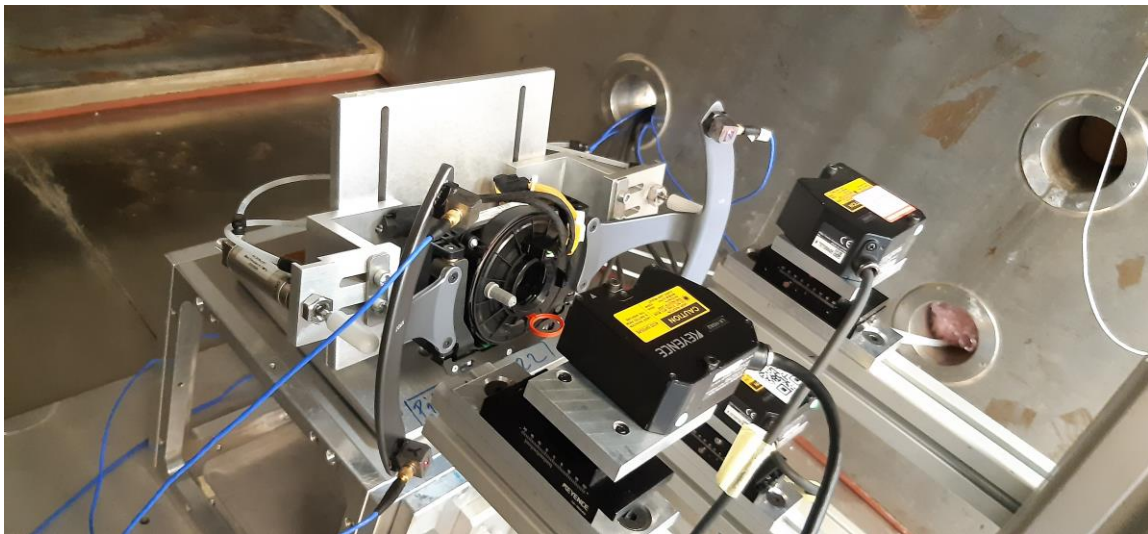


Figure 5.2.2 – Setup with laser and accelerometers.

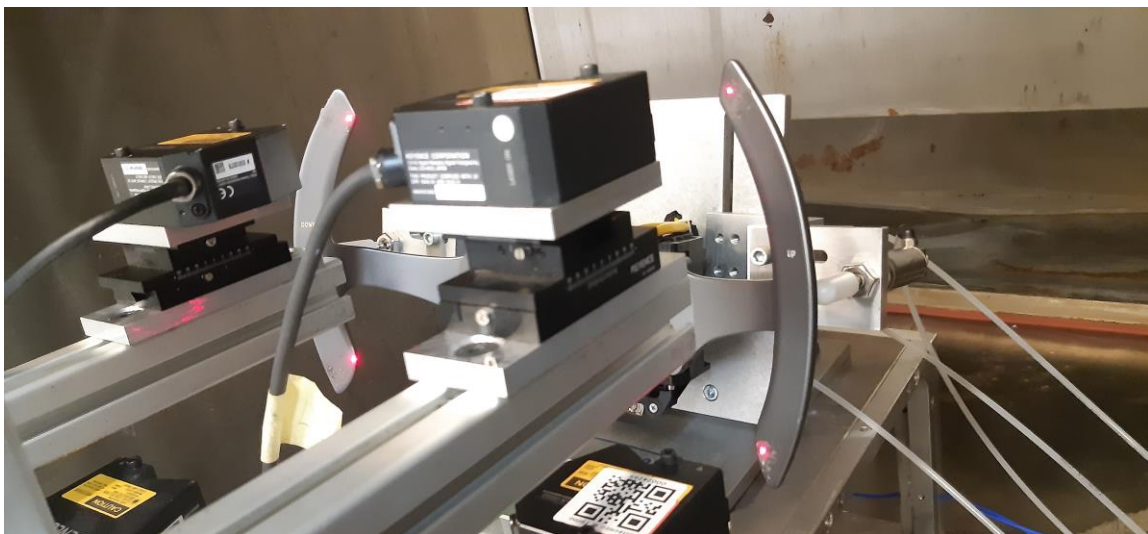


Figure 5.2.3 – Setup with laser only.

5.3 Results of pad DOWN

As mentioned above, two type of data acquisition were recorded on the left pad (Levit DOWN command): the one measured by accelerometers and the other coming from laser.

The accelerometers data are not complete on all available axes. Figure 5.3.1 represents all these data in one graph. It is possible to notice that in three point we have oscillation peaks which correspond to the time of actuation, hold, and release of the piston.

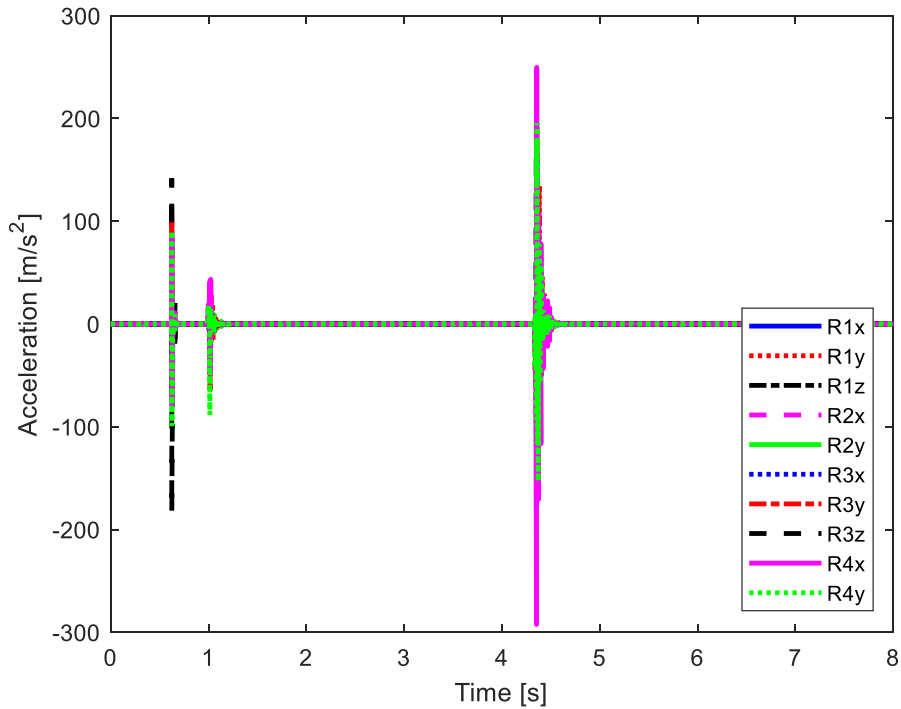


Figure 5.3.1 – Test n.º2 accelerometers acquisition.

In Figure 5.3.2 are presented the data acquired by four accelerometers on *y* axis. The shape and the time position of the peaks up/down are similar for all the ten tests but changes their magnitude. For *y* axis we have the first peak at 0.6 second with displacement at around +100 m/s² and -100 m/s² in the correspondence to the actuation of piston, the second peak has lower displacements, then the third peaks when the release phase start, around 4.4 seconds with amplitude between +200 and -170 m/s².

The excited pad is the down pad. It is visible from the coloured lines in the legend of graph below which have major displacements: the accelerometers on up pad (1 and 2) move as reaction to the external force applied on down pad.

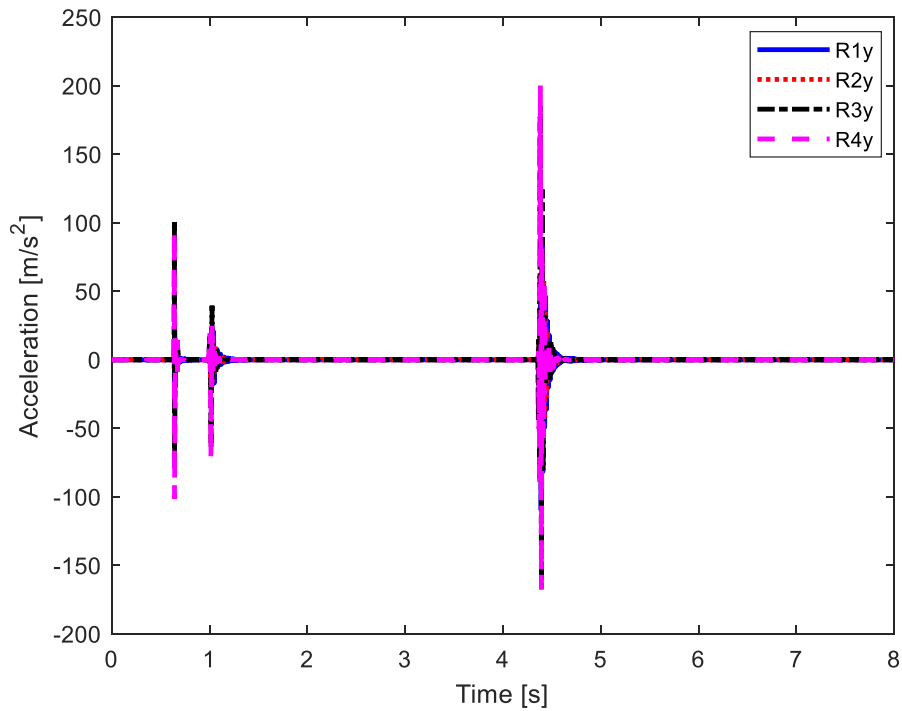


Figure 5.3.2 – Test n.º5 accelerometers acquisition on y axis.

Figure 5.3.3 represent the details of test n.º5 during the release phase. The major reaction at 4.35÷4.4 sec involve the accelerometers 3 and 4 on down pads (black and magenta lines), then these oscillations reduce more respect to the blue and red line (accelerometers 1, 2). At 4.6 seconds the oscillations diminish and stop.

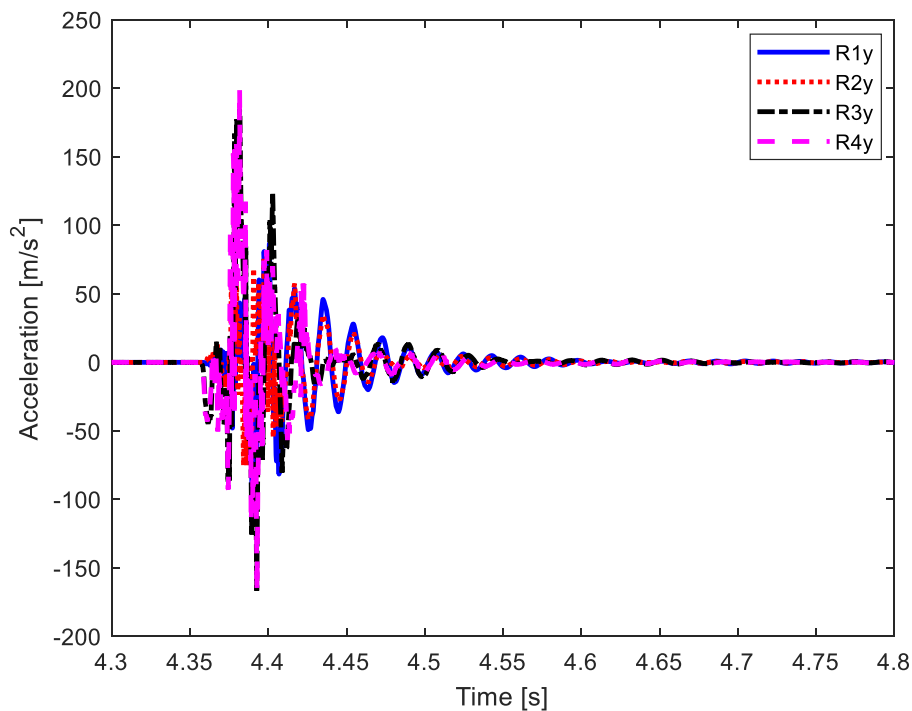


Figure 5.3.3 – Details on test n.º5 accelerometers acquisition on y axis.

In order to appreciate the similitude between tests, in Figure 5.3.4 are superposed result of test n.º2 and n.º3. Notice that the two curves have same behaviours, but they are translated of about 0.006 s. Figure 5.3.4 shows the releasing phase.

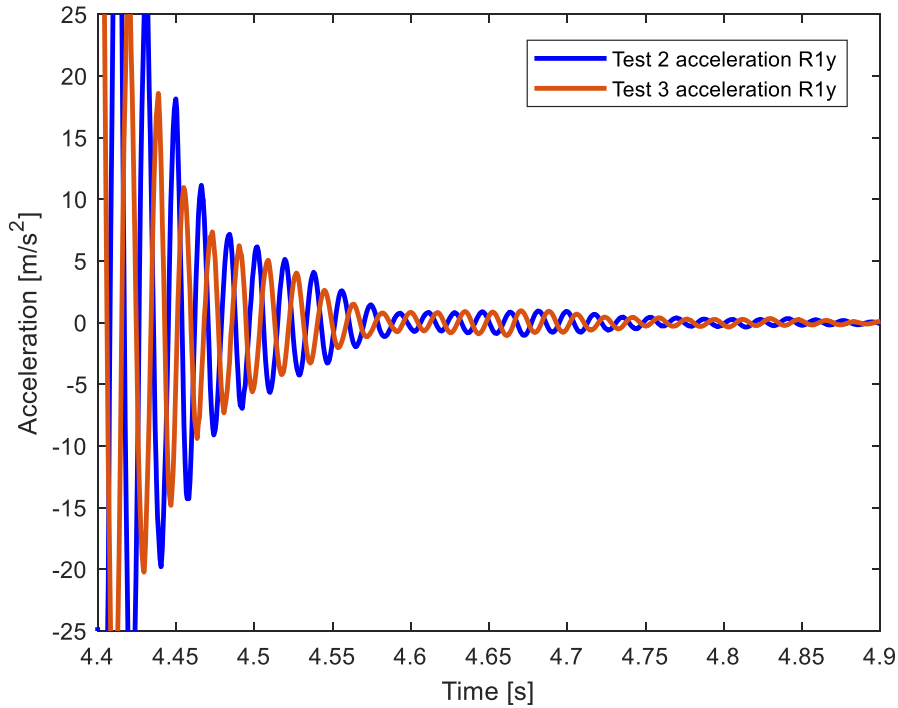


Figure 5.3.4 – Details of superposition on test n.º2 and n.º3 of the signal on y axis from accelerometer 1.

Figure 5.3.5 presents curves of test n.º4 and n.º5, these data come from the third accelerometer on y axis. Two details are reported to visualize both the actuation and release phase. It can be noticed how the blue and orange curves are close each other, especially between 1 and 1.1 s.

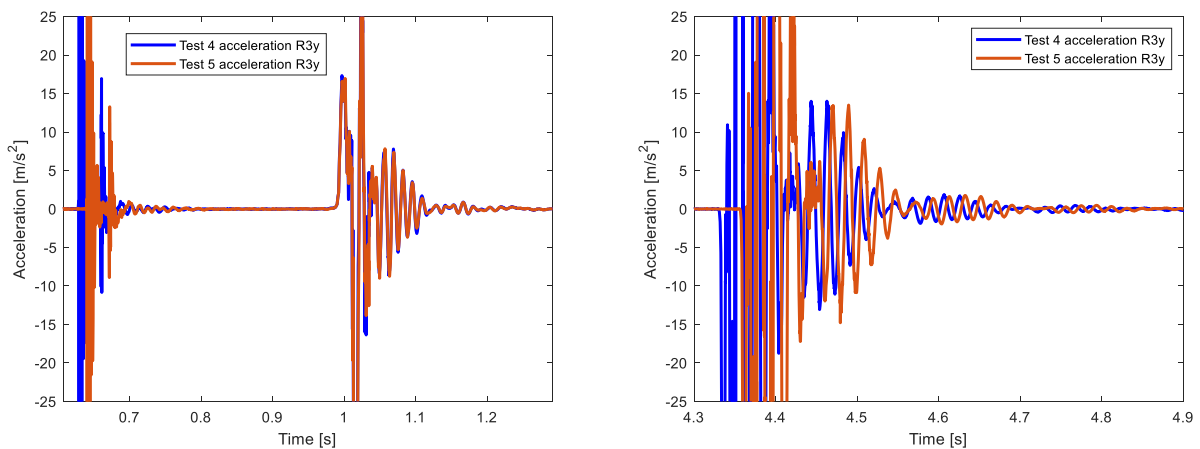


Figure 5.3.5 – Details of superposition on test n.º4 and n.º5 of the signal on y axis from accelerometer 3: actuation phase on left, release phase on right.

In Figure 5.3.6 there is a representation of position acquired by laser. This kind of information is numerically derived twice to obtain velocity and acceleration. They could be affected by uncertainties due to numerical derivation.

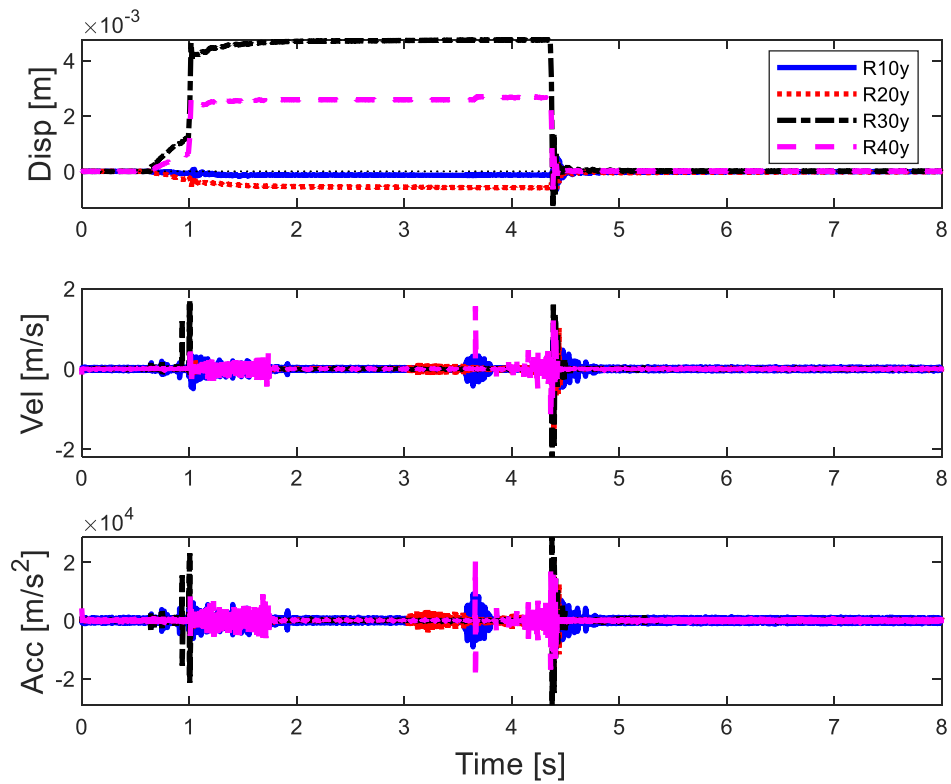


Figure 5.3.6 – Test n.º5 with position, velocity, and acceleration.

In next figures are shown the acquisition data of the four lasers, they report the trend of displacements between the laser and the surface of the accelerometer. Each laser is set up manually and then it is stabilized with the acquisition software (TestLab).

Figure 5.3.7 presents the test n.º2 as it is, the data are reported without any modification on ordinates axis.

From figure on left it is possible to see that after the release the pads do not come back to zero line.

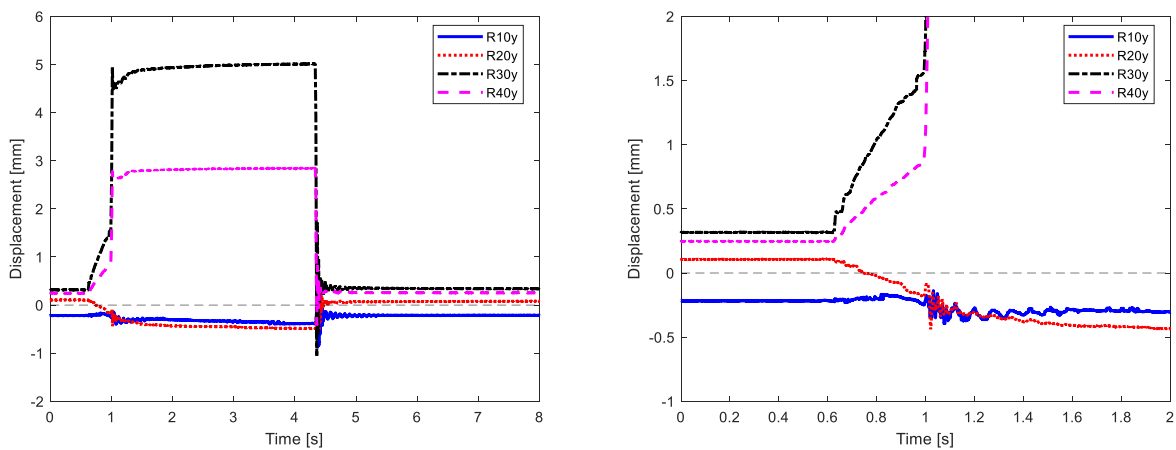


Figure 5.3.7 - Test n.º2 laser acquisition without any correction on initial displacements (left), details of initial displacements (right).

To have a better comparison of data, it is more interesting set all curves to zero at their initial condition, in order to see the displacement independently. All the following figures are corrected at their initial conditions. To achieve this behaviour, the position of the four points under test is decreased during Matlab post processing by the value they have at the beginning of the test.

Figure 5.3.8 presents the first test. This one is used to provide a settlement for the system. In these figures is analysed the first test for actuation/release of down pad, the following tests are more similar each other's, but differ from the first one. Probably with first test the system Levit and support find a correct position which it is maintained for the following tests.

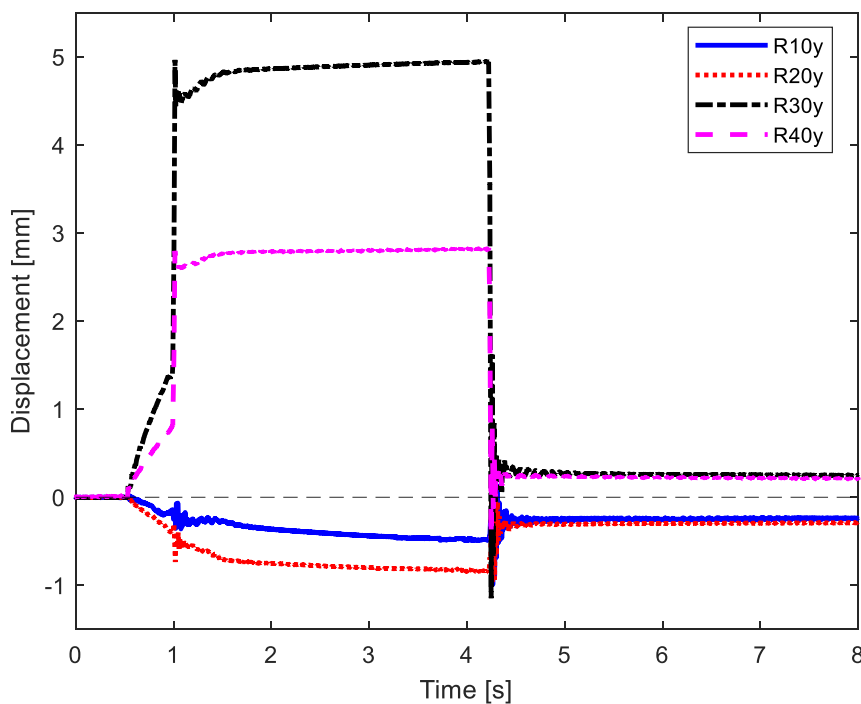


Figure 5.3.8 - Test n.º1 laser acquisition.

Analysing Figure 5.3.9 the graph from the time zero, it is possible to see that the four points under analysis start from line zero due to the modification of initial values.

When the actuation phase starts the point 3, 4 on pad down (left) move, the pad is push up, in the direction of the laser. Between 0.5 and 1 second the piston slowly moves the down pad, the motion is instantaneous on 1 sec. At the same time on up pad there is a little oscillation, the oscillation is simultaneous on both point 1 and 2 belonging to same pad.

In the phase of hold is reached the maximum displacement in point 3, placed on the top part of pad, at around 4.7 mm, on the other hand is present on point 4 half displacements, in the bottom part of left pad. In the meantime, the right pad (up) has a little negative displacement, reacting to the motion of the other pad. Thus, it is important to notice that the excitation of one pad influence the other one. That is visible on graph from the displacements of all curves when one pad is actuated.

In the phase of release at 4.2 sec, there are consistent oscillations of both pads until 5 seconds. After that, the motion of pads stops and the pad assume their relaxed position, all forces are released. Anyway, it is possible to see how the pad get close to zero when the transient finishes.

It is worth notice that at the end the displacements have values around zero, this means that the pads came back in the same position/configuration as the initial one.

Figure 5.3.10 presents a zoom of the release phase. Black and magenta come down from high displacements, oscillate from 4.35 to 4.9 sec and get close to zero line. Also, the blue and red line return to zero line, oscillates and stabilize.

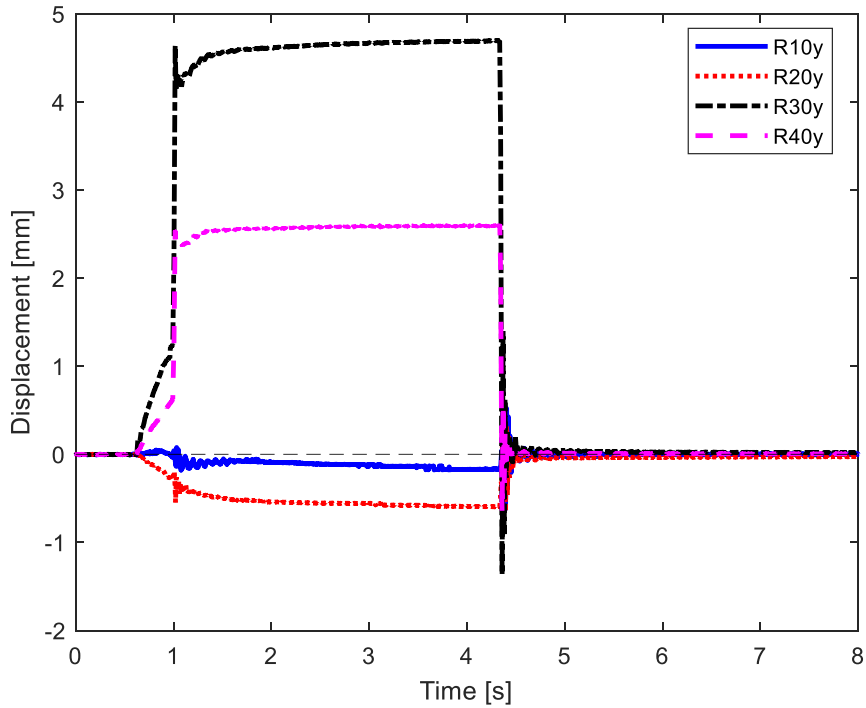


Figure 5.3.9 – Test n.º2 laser acquisition.

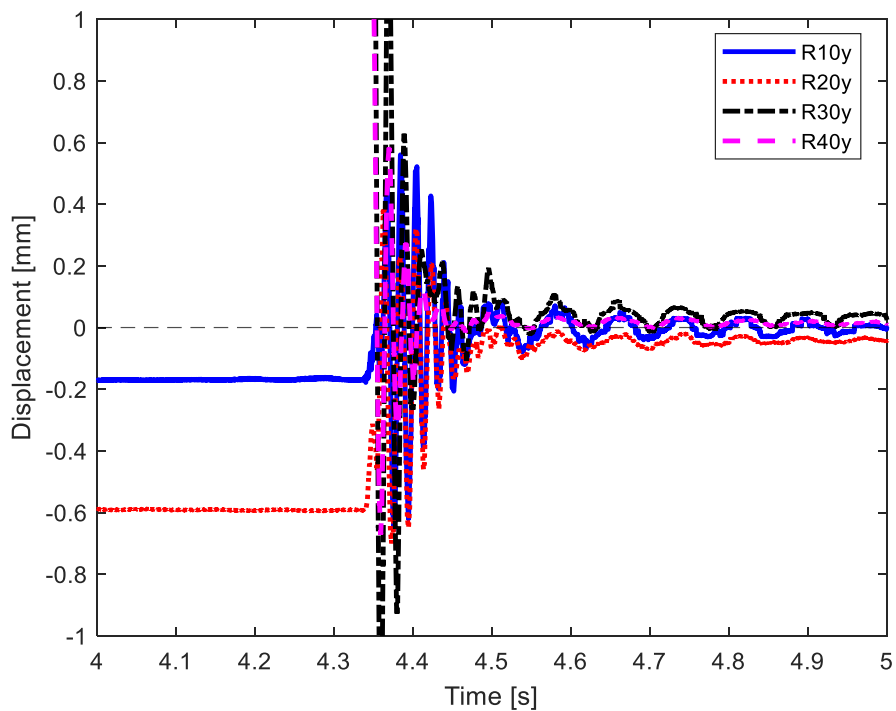


Figure 5.3.10 – Details of test n.º2 laser acquisition on release phase.

Figure 5.3.11 shows the test n.º7. In general, the behaviour is very similar, at 0.5 sec the actuation phase start, then it is hold and followed by the release of piston, the displacements reach the same values.

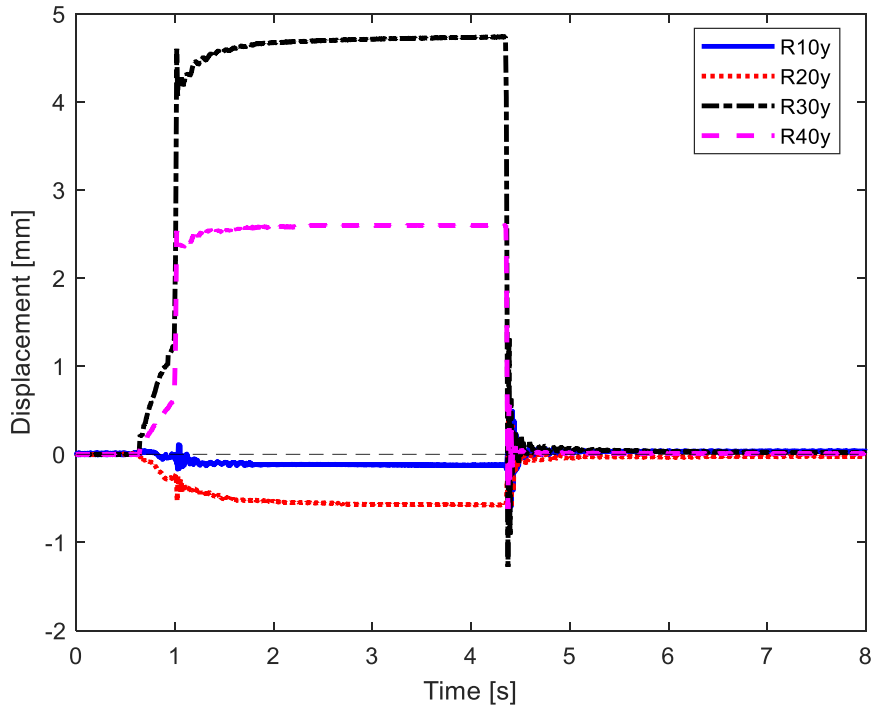


Figure 5.3.11 – Test n.º7 laser acquisition.

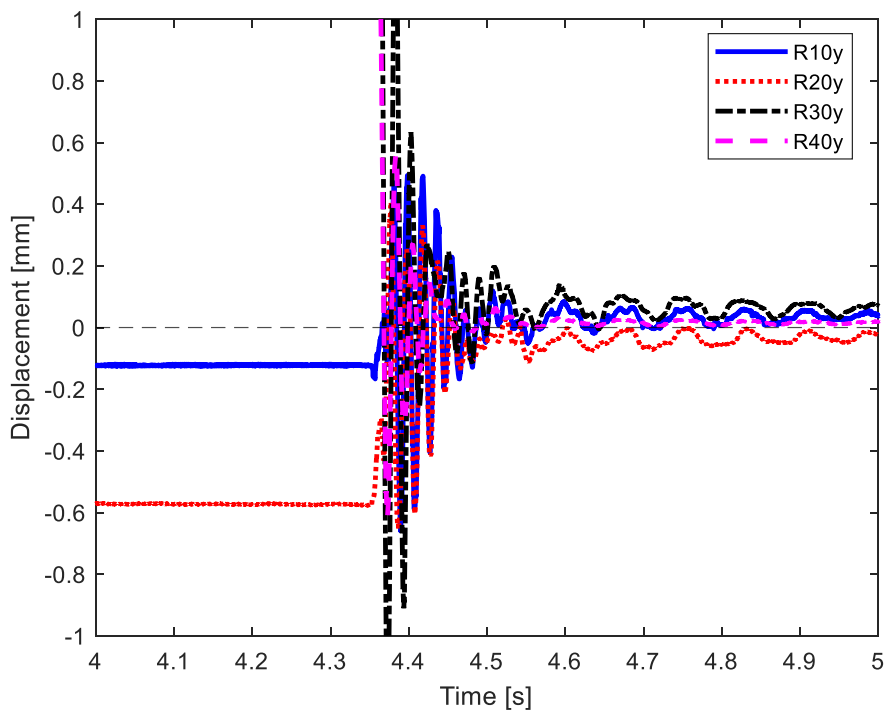


Figure 5.3.12 – Details of test n.º7 laser acquisition on release phase.

Thanks to the automatic build of this cycle, the test is very repeatable, in fact tests from the second to the last one are very similar.

In Figure 5.3.13 some of these tests are resumed to get visual proof of previous statement.

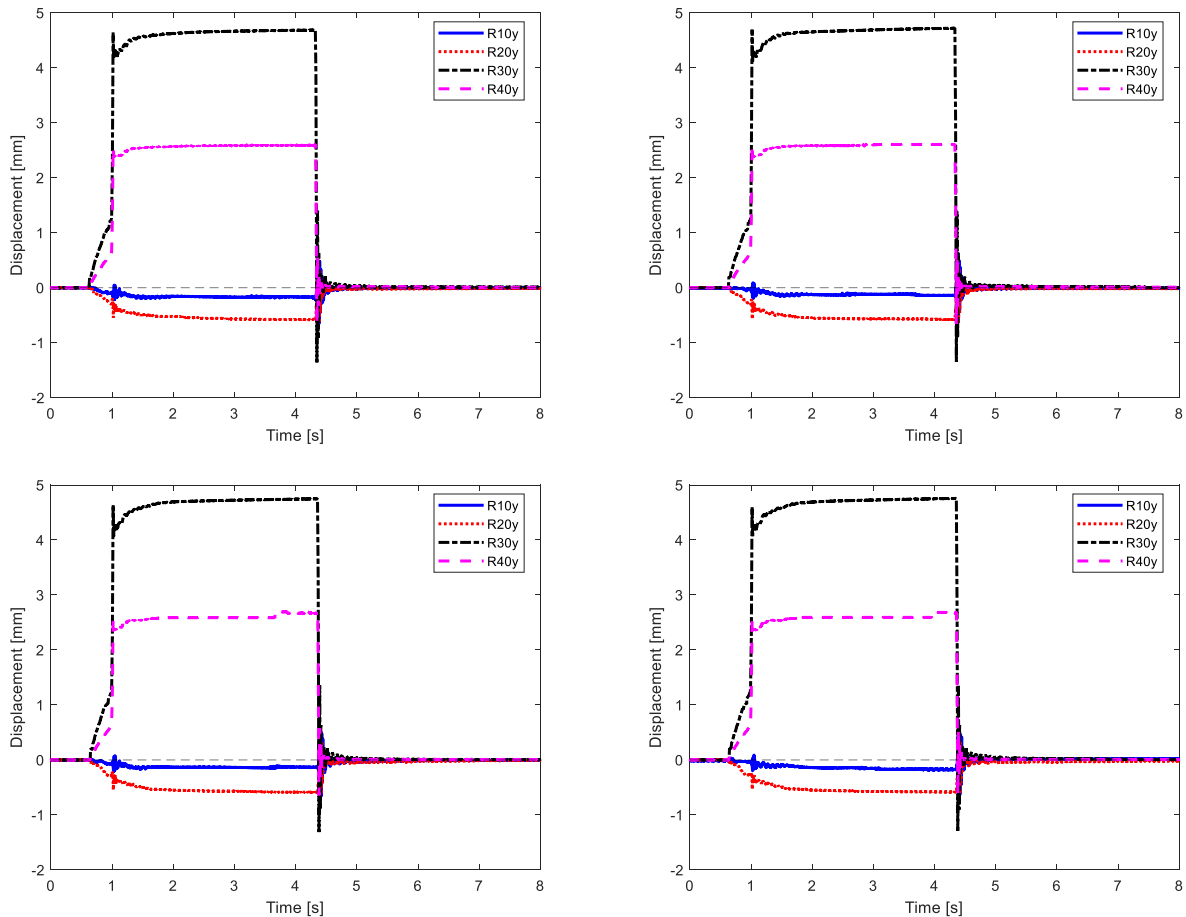


Figure 5.3.13 – Test: n.º3 (top left), n.º4 (top right), n.º5 (bottom left), n.º6 (bottom right) with laser acquisition.

In Figure 5.3.14 is reported the second test in the case without the accelerometer. As for previous test, the first is used just for the settle of configuration and it is not considered later.

The general behaviour of these tests is similar to the experiment with the accelerometer, however, there are significant differences about the maximum displacement and the oscillations in the release phase.

From figure it is possible identify the maximum displacements at 4 mm with the point 3, then see that the point 2 (red line) oscillate between 3 and 4 seconds, probably influenced by the actuation of piston on the other pad.

Respect to the previous graphs, during the unforced position the lines belonging to same pad remain more close each other.

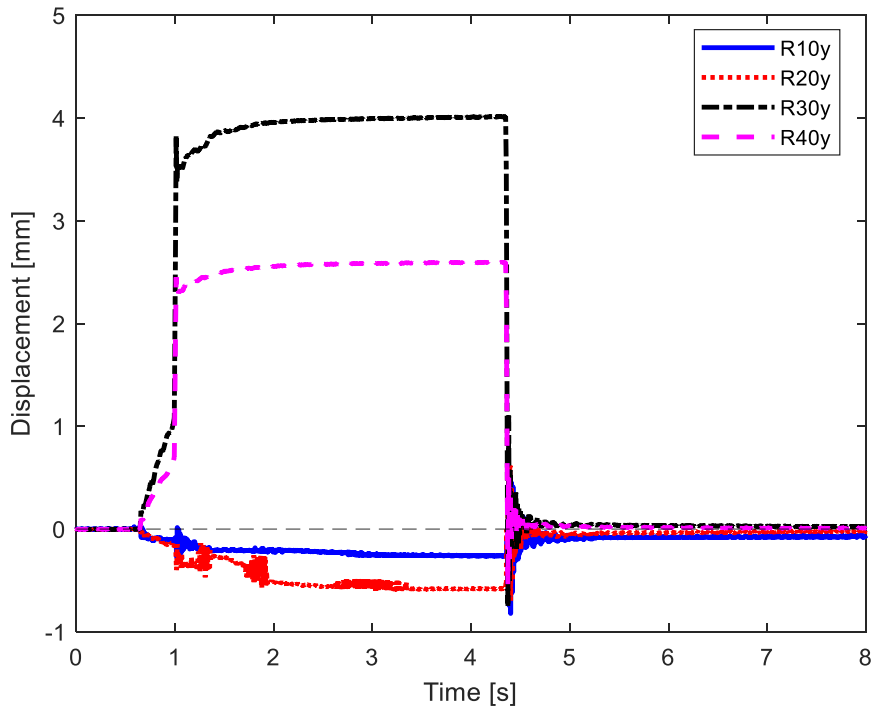


Figure 5.3.14 – Test n.º2 of laser acquisition without accelerometers.

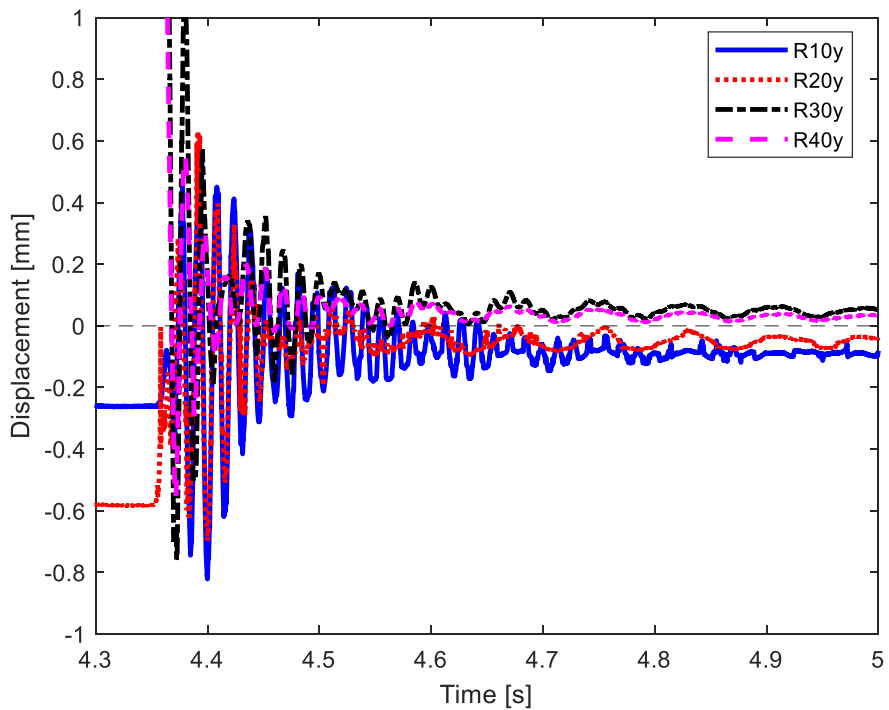


Figure 5.3.15 – Details on test n.º2 of laser acquisition without accelerometers.

Figure 5.3.16 shows test number 9, it is similar to the first one, so the repeatability of the experiment is confirmed, and this give confidence in the test results.

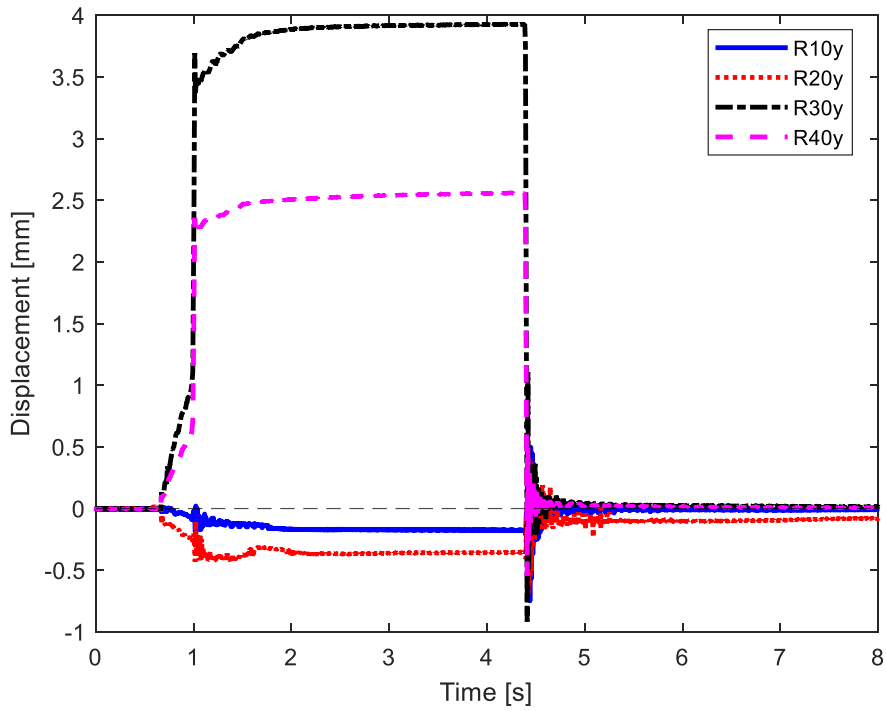


Figure 5.3.16 – Test n.º9 of laser acquisition without accelerometers.

In Figure 5.3.17 is proposed an overlap of test 3 and 4 for put under evidence the similitude and repeatability of the test. It is reported the motion of second and fourth accelerometer.

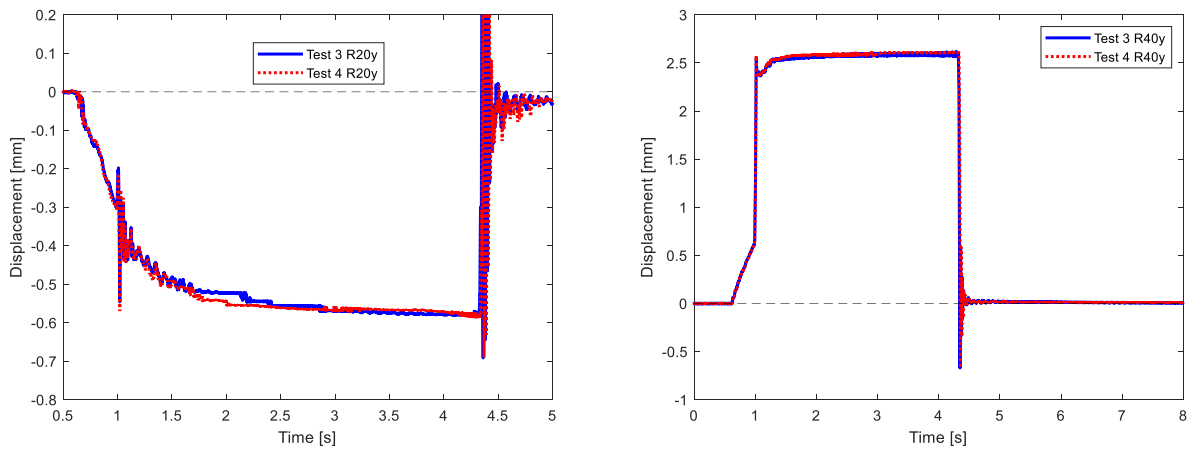


Figure 5.3.17 – Overlap of position of test n.º3 and 4 on the second and fourth accelerometer.

5.4 Results of pad UP

As in the previous section, also with UP pad are done two types of experiments, with and without accelerometers.

In this case is activated the right pad, responsible of the upshift, on which are present the accelerometers/points 1 and 2.

First of all, are reported the general accelerometers data in Figure 5.4.1.

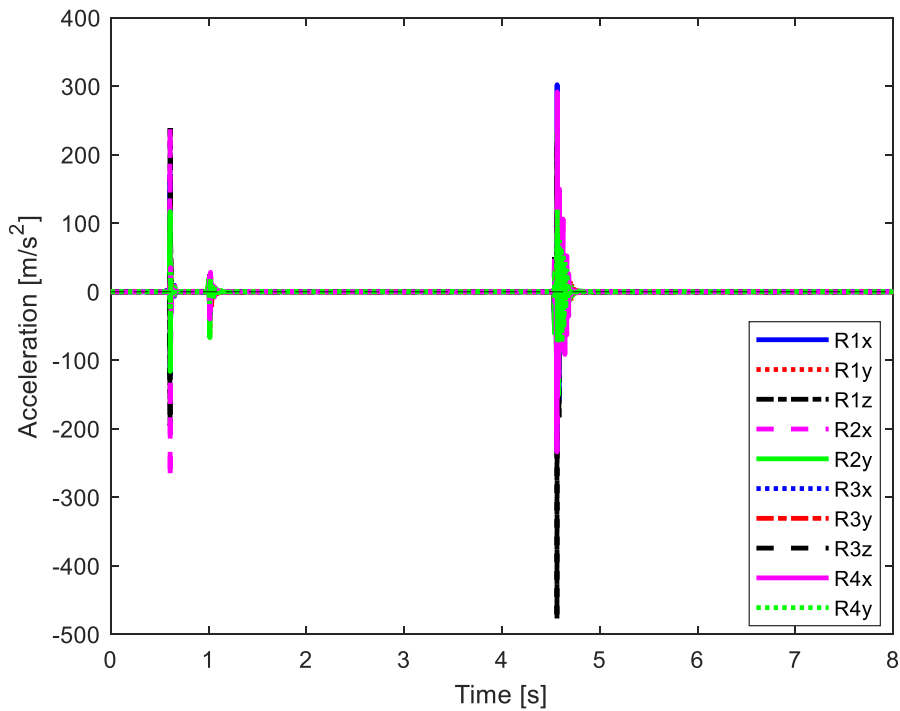


Figure 5.4.1 – Test n.º4 accelerometers acquisition.

In Figure 5.4.2 is reported the acceleration during the actuation, hold, and release of the up pad. It is visible that the blue and red line undergo to high oscillation in presence of the external force.

The use of accelerometer data is useful to understand when there is the contact or not between the pad and the piston.

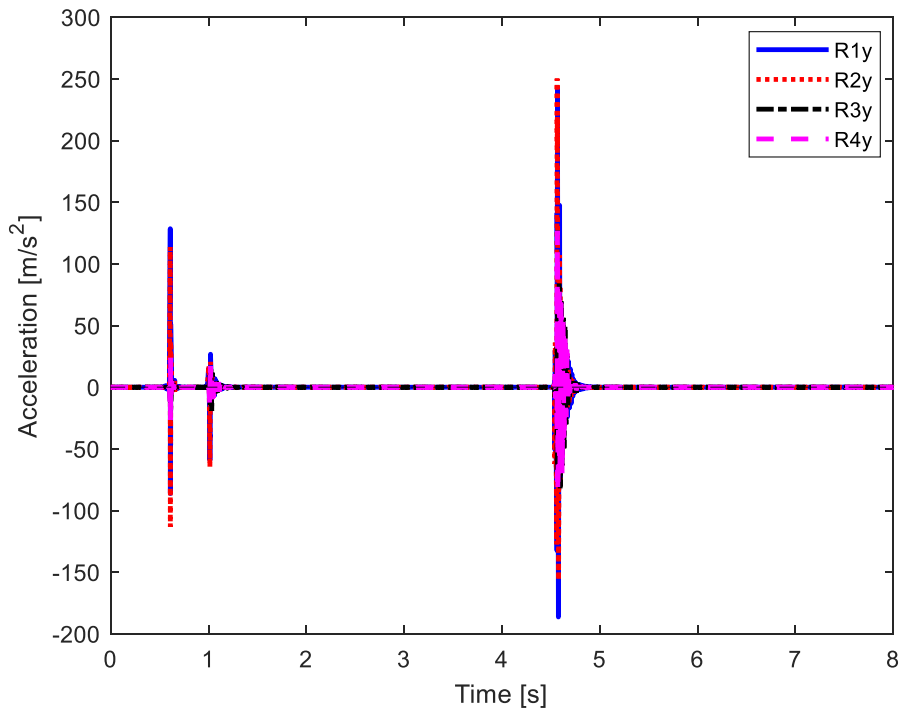


Figure 5.4.2 – Test n.º5 accelerometers acquisition on y axis.

Figure 5.4.3 on left shows a zoom on the actuation phase, at time 0.55 happen the first contact between the up pad and the piston. It is worth notice that the actuation phase was very slow respect to the release. At 1 second the oscillation of accelerometers gives information about the end of the actuation and the start of hold phase.

In Figure 5.4.3 on right is presented the release phase on the same test, which is more instantaneous, and it is done in one single moment.

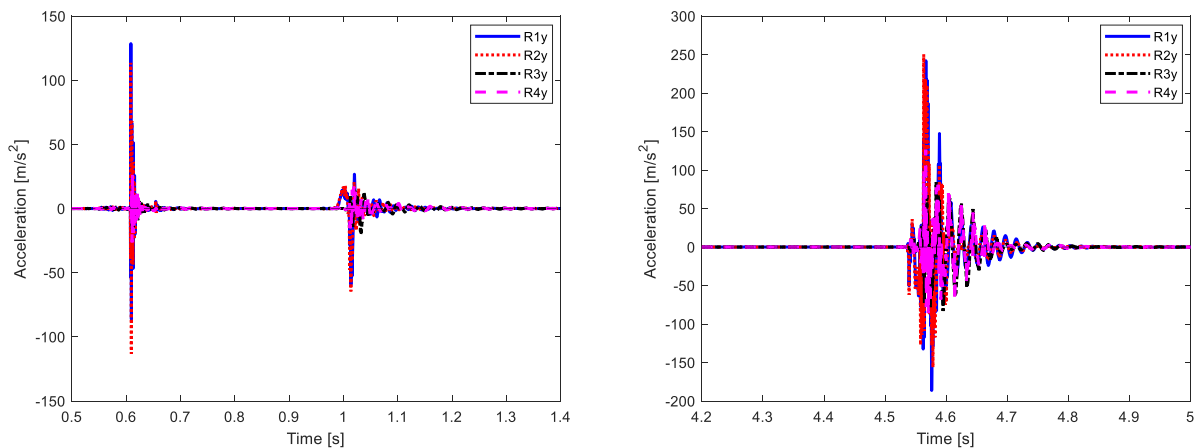


Figure 5.4.3 – Details of test n.º5 accelerometers acquisition on y axis actuation (left) and release (right).

Figure 5.4.4 shows the overlap of curves from test n.º 3 and 4, considering accelerometer on point 1 and only the y acquisition. The curves are identical but translated of about 0.004 seconds.

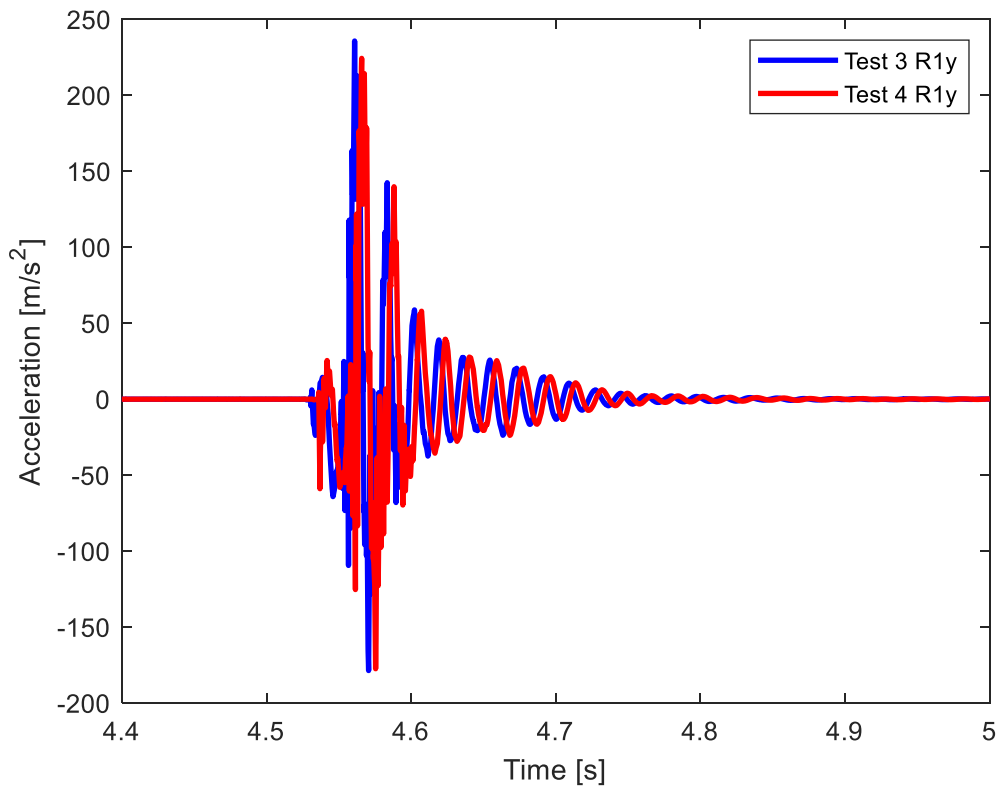


Figure 5.4.4 – Test n.º3 and 4 with accelerometers acquisition.

After the acceleration are reported the data acquired from laser.

Figure 5.4.5 reports the displacements record from laser during the first test with the actuation of up pad. The point 1 and 2 and relative accelerometers move from the rest position at around 0.55 second. As in the experiment with down pad, the initial position in test one is unique, after the first release the pads keep a new distance from zero line and maintain the new arrangement for the next tests.

When the actuation of pad starts, the blue and red lines begin to rise, at 1 sec the growth is instantaneous, reaching 4 and 5 mm of displacements, continue slowly to grow until the maximum distance at 6 and 7 mm. This is followed by the release of piston, as seen from graph that action is quicker than the actuation. At the end of the release there is a transient part that after 1 second disappear and the device come back to stationary position.

At the same time the black and magenta line decrease under zero, this mean that the down pad is moving away from the laser, the distance increase again and oscillates during the release phase of up pad. In Figure 5.4.6 is shown a zoom on the transient of the release, keep attention on the distance between coloured lines and zero line, which maintains constant until the end (8 seconds).

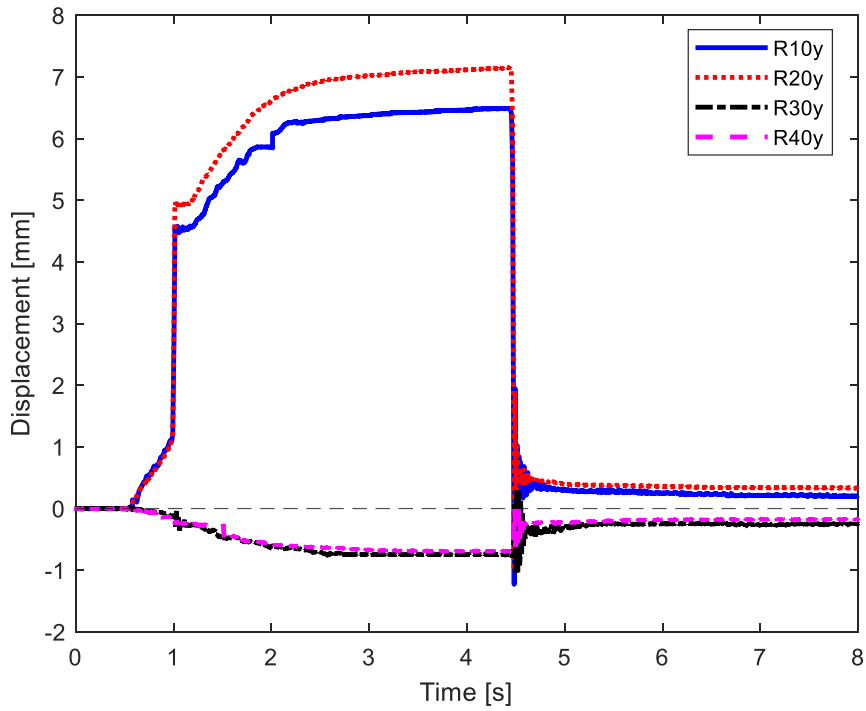


Figure 5.4.5 – Test n.º1 laser acquisition.

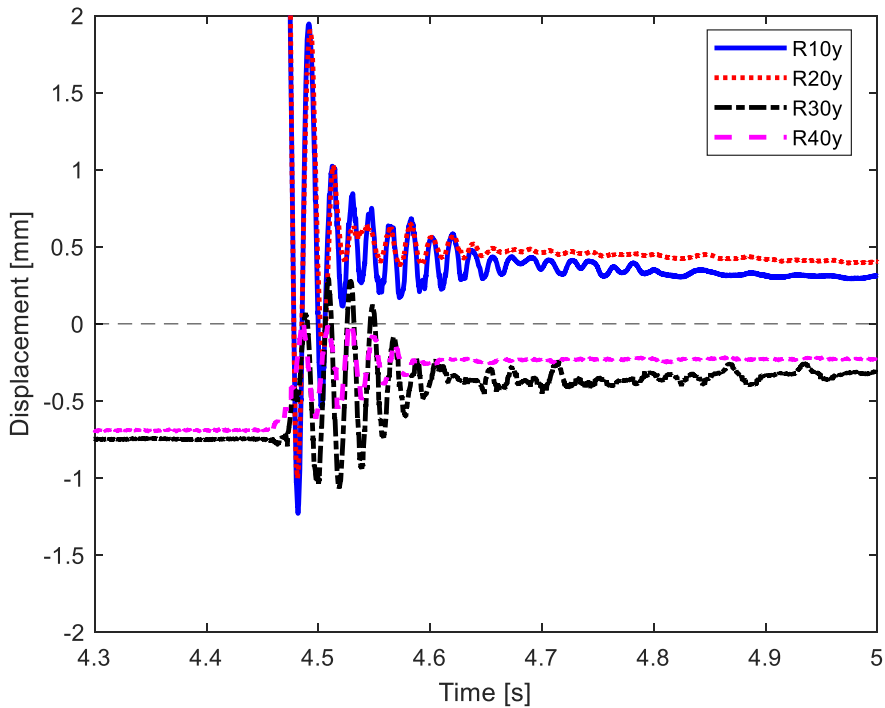


Figure 5.4.6 – Details of test n.º1 laser acquisition on release phase.

In Figure 5.4.7 is reported the test n.º3, 6, 7, 8 to evidence the similarities of tests and their repeatability.

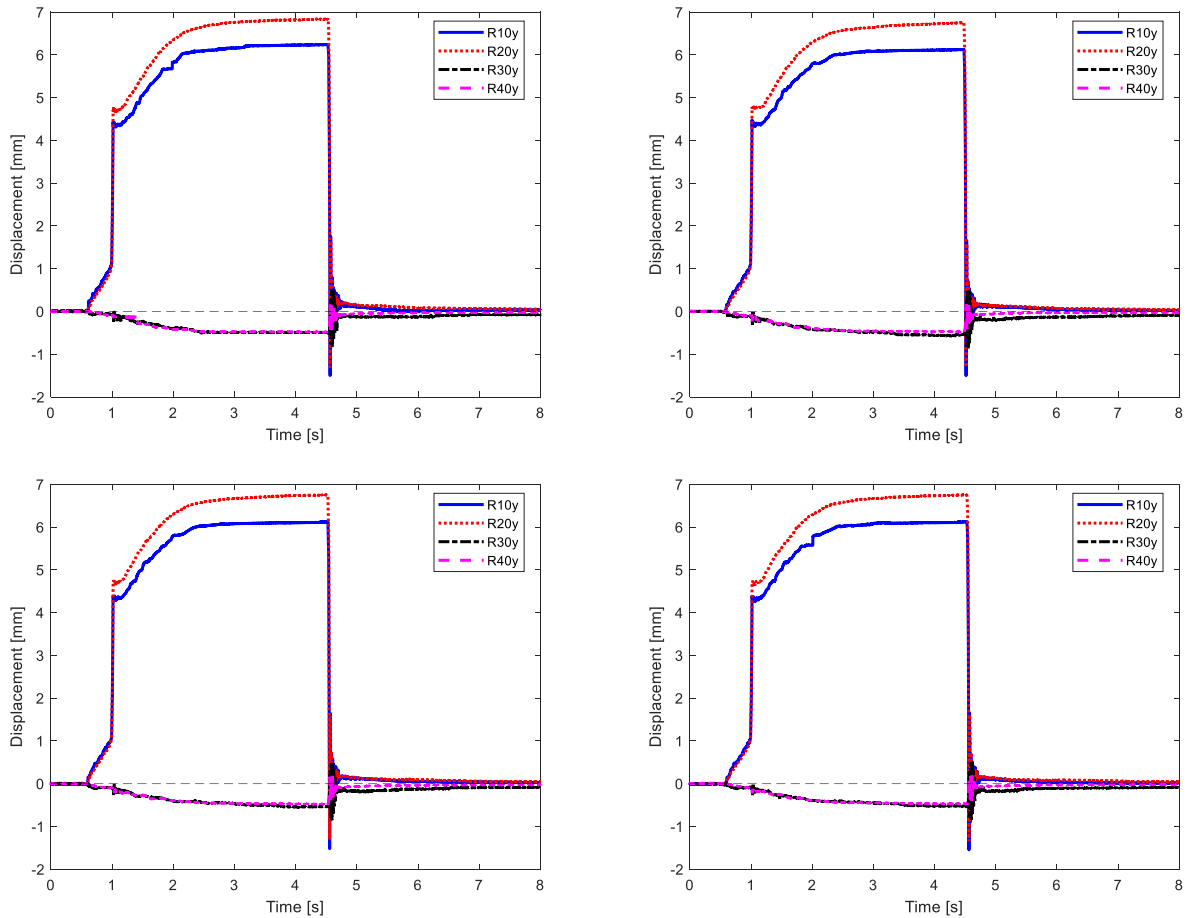


Figure 5.4.7 – Test n.º3 (top left), 6 (top right), 7 (bottom left), 8 (bottom right) laser acquisition.

Figure 5.4.8 and Figure 5.4.9 show the displacements of the device without the accelerometers during second and the last test. It can be noticed the similitude in the shape and trend, in the graph all curves are close to zero at the beginning of the test and the end, while in the middle the points assume different direction of motion respect to the excitation that they undergo.

The main difference between experiments with and without accelerometers are:

- The maximum displacement which decreases in the case without accelerometers from 7 to 6 mm.
- The step-up during actuation, which is smoother with the accelerometers, and it seems divided in two steps in the other case.
- The measure distance of pads when any excitation is applied.
- The amplitude of oscillation in the transient release phase.

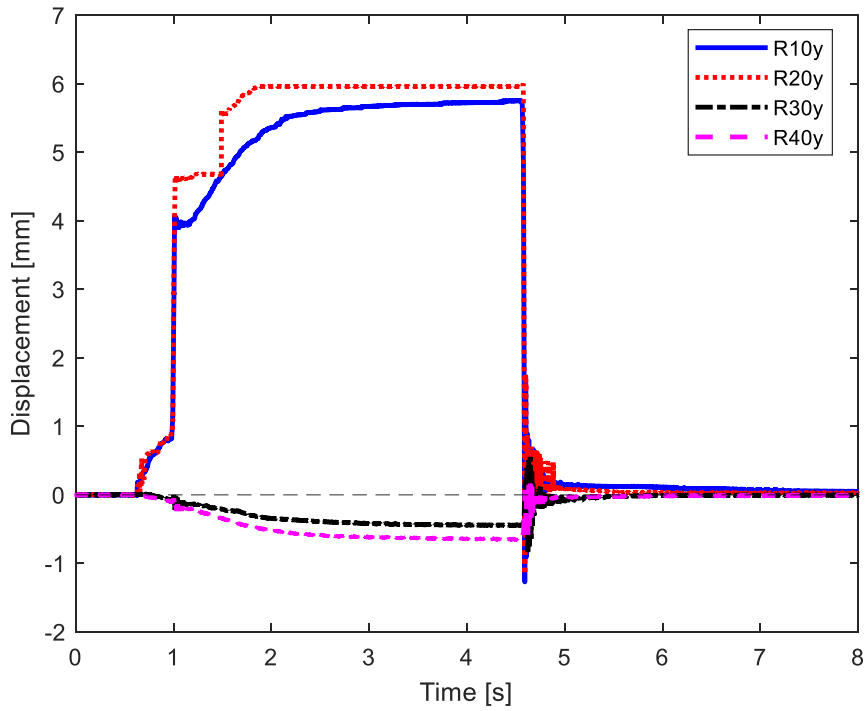


Figure 5.4.8 – Test n.º2 laser acquisition without accelerometers.

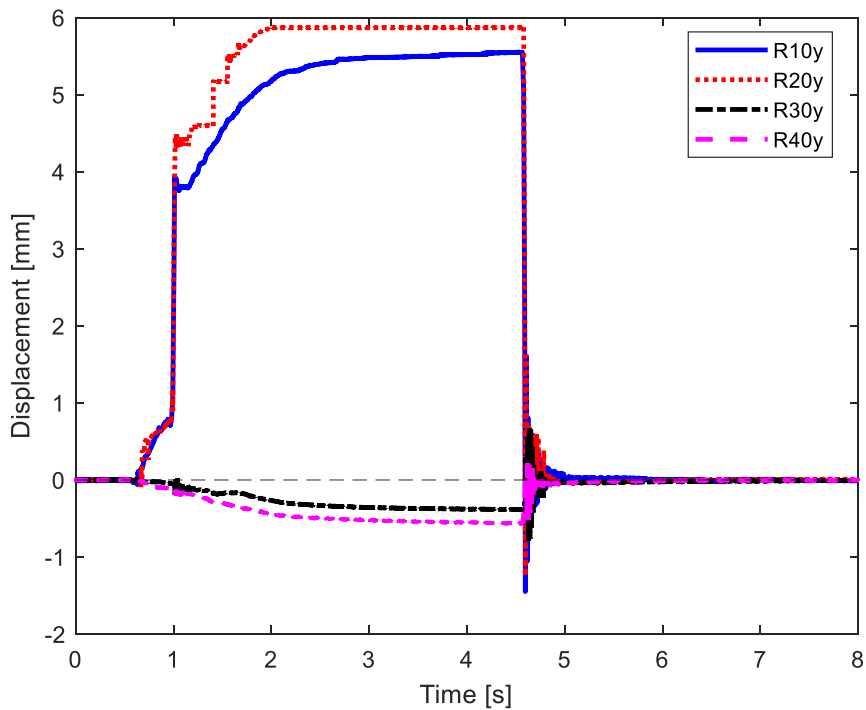


Figure 5.4.9 – Test n.º10 laser acquisition without accelerometers.

The following figures are used to evidence the similarities between two different tests, in particular test n.º3 and 4. Figure 5.4.10 shows position in time of the first accelerometer on the left, while the fourth accelerometer is on the right.

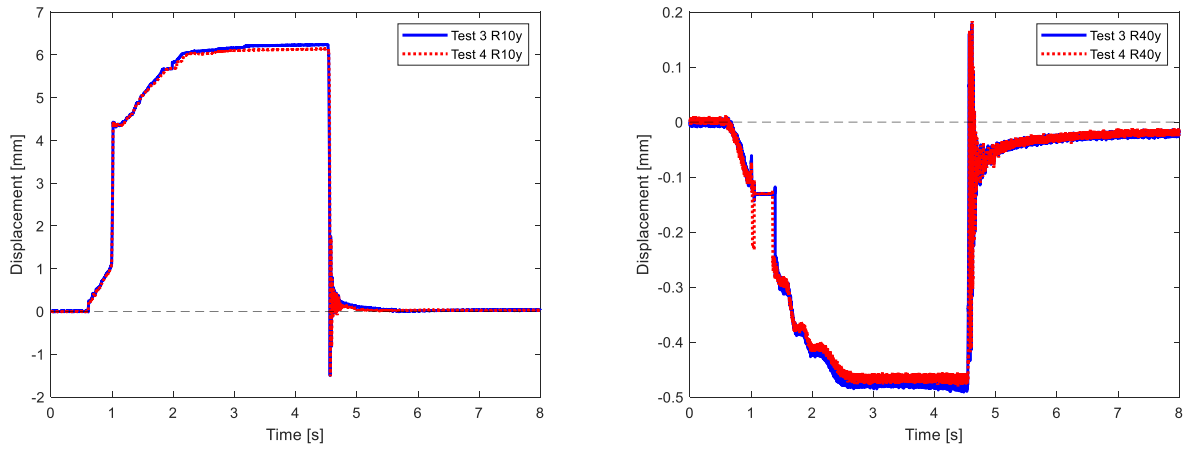


Figure 5.4.10 – Overlap of test n.º3 and 4 of laser acquisition with accelerometers 1 (on the left) and 4 (on the right).

5.5 Results comparison

One way to compare results is shown in Figure 5.5.1. For each figure is compared each single point 1, 2, 3 and 4 with actuation of the down pad in the case with and without accelerometers. It is considered just the laser measurement. The graphs in Figure 5.5.1 are disposed as on Levit arrangement, such as, point 1 at the top right, point 2 at the bottom right, point 3 at top left, point 4 at bottom left.

It is visible the difference between the two cases, especially in point 3, which belongs to the actuated pad. Probably this gap is related to the distance between the accelerometer n.º3 and the point of contact during actuation.

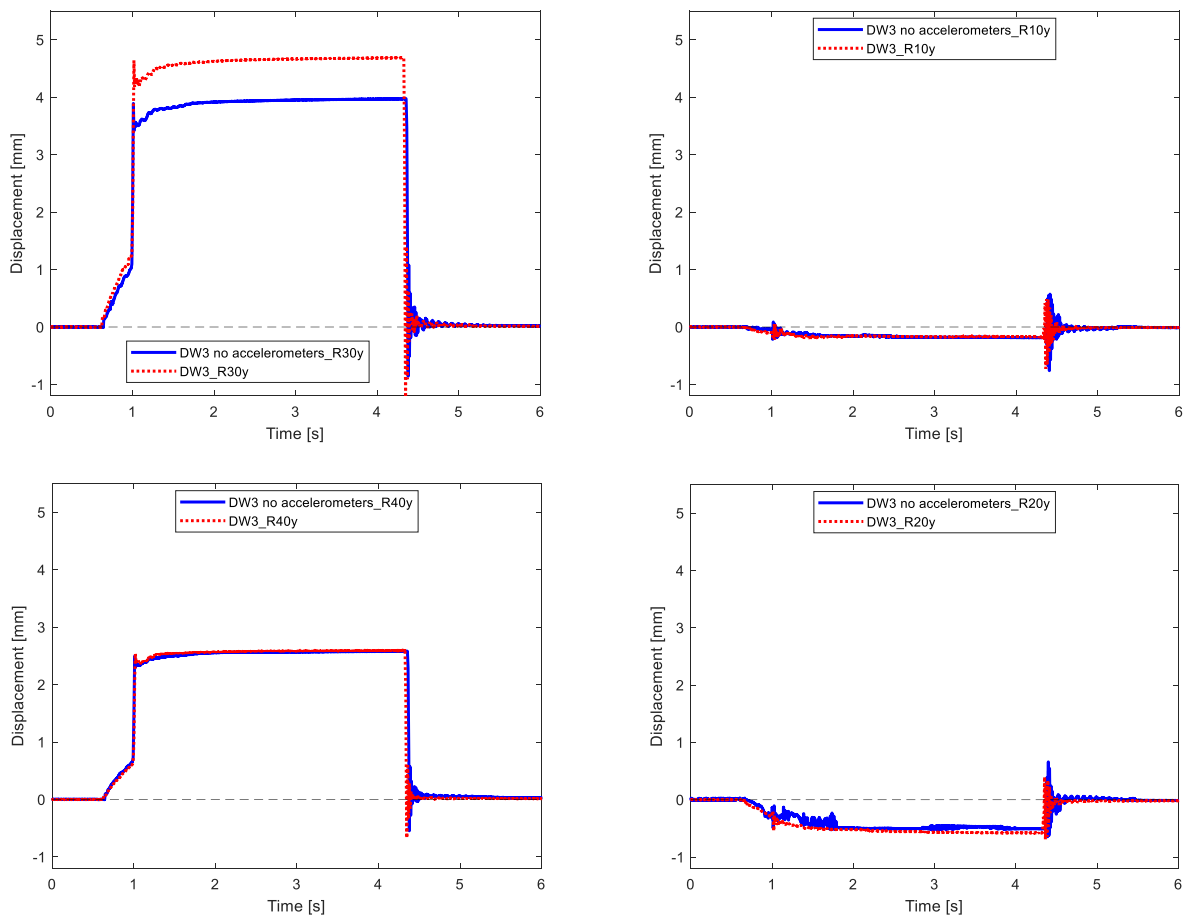


Figure 5.5.1 – Comparison with and without accelerometers when DOWN pad is excited in test n.º3.

A similar consideration can be done with the excitation on up pad. In Figure 5.5.2 is present the measurement from laser when the up pad is actuated and released.

The same configuration of graphs is reported in figure, the position of each graph respects the analogous order on the real device during experiment.

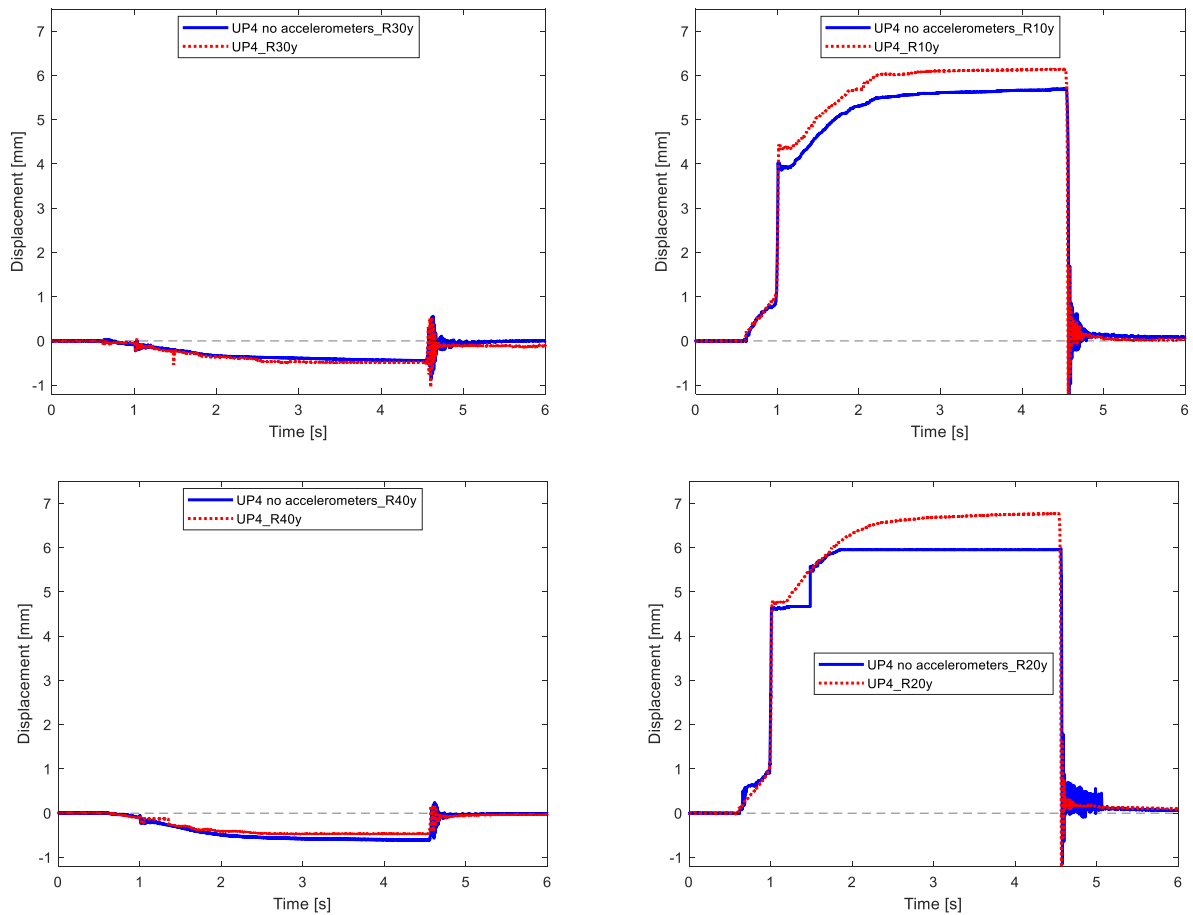


Figure 5.5.2 – Comparison with and without accelerometers when UP pad is excited in test n.º4.

In Figure 5.5.3 are shown the displacements when both down and up pad are excited. For each figure are reported the down and up motion for point 1 at top right, 2 at bottom right, 3 at top left, 4 at bottom left.

In each graph it is possible to see how the point under analysis react to the different excitations, actuation, or release.

Notice that the curve blue and red are translated of a certain time, so the two phase of actuation and release do not coincide.

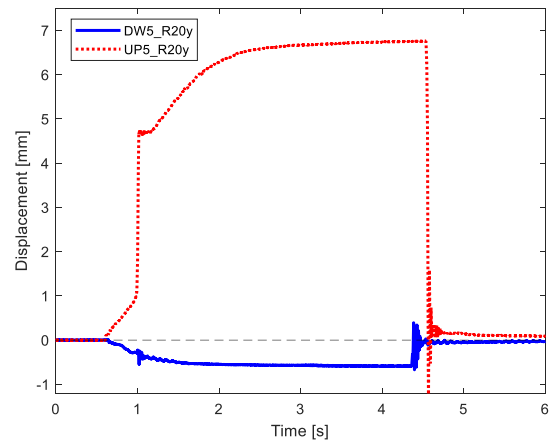
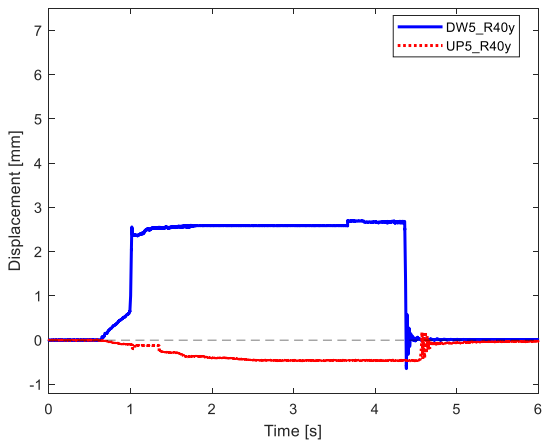
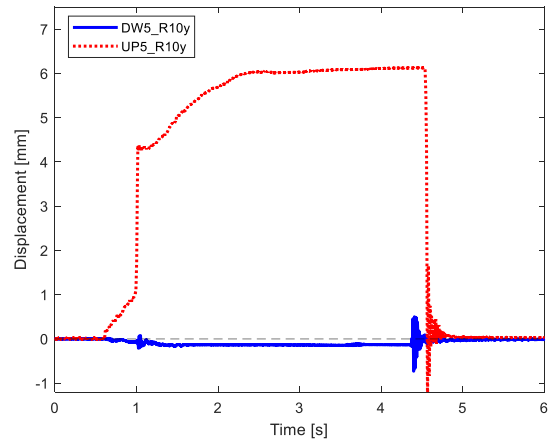
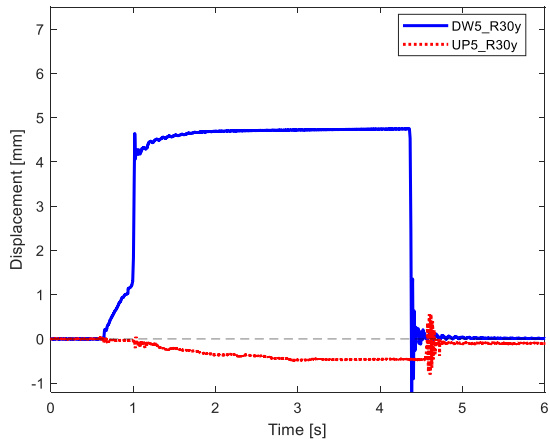


Figure 5.5.3 – Comparison with accelerometers is excited in test n.º5.

5.6 Conclusions on third experiment

In this experiment the performance of pads is tested when they are used for the upshift or downshift. To study it, the Levit is located as in vehicle with the same inclination, in order to reproduce the assets vehicle as accurately as possible.

An automatic cycle is built to test the response capacity of the Levit device and to guarantee repeatability of actions. It is interesting to see how the pads react to these excitations. The measures are recorded by accelerometers and lasers.

Both the test of actuation and of release are repeated ten times. The obtained performances are very similar within the different test experiments. In this way it is possible to be confident about the behaviour of Levit during excitation. Particular attention is kept in the post processing of displacements from laser and in the construction of meaningful graphs.

In general, the behaviour during actuation is quite linear and to reach its maximum displacement it takes some milliseconds. This phase seems to be slower than the release phase. After that the pads is hold activated for a time frame about 4-5 seconds. Then, it follows the release phase, which are very fast. In contrast with the first phase, this last one shows a non-linear behaviour, oscillations of almost 0.7 seconds are observed on both pads.

These oscillations are visible in all type of test. They are more evident on the excited pad but are also present in the other pad. This behaviour is a consequence of the energy that the two pads can exchange the one with the other. Moreover, the symmetry body of the device enhance this connection between pads.

Conclusions

The first test, sine sweep experiment, focused on the excitation of the Levit to increase the knowledge about its natural frequencies. Moreover, the device mode shapes are studied based on the test results.

The most interesting results comes from the post processing of the excitation on y axis respect to device reference system. The performance on this axis is important due to the vehicle asset. The y axis will be the one most excited during the usage of device.

The results of the three axes can be combined during post processing to give more accurate results. Anyway, it is observed that the achieved results are close to the ones which consider just the y axis. For this reason, the observation of y axis becomes relevant.

Analysing the natural frequencies and the mode shapes, it is also important to consider the numerical model. A comparison between the experimental and numerical results is pursued. In this way, the discrepancies between them become clearer. Although mode shapes from 1 to 8 find correspondence between two tests, nevertheless some differences are found (i.e., switched modes or different frequencies values).

In order to reduce the distance between results it is conducted another study in the transmissibility and for the research of natural frequencies. This represents the second experiments presented, the roving hammer test.

For this test only the y axis is considered for two reasons: the importance of this direction in the analysis and the nature of performed test, which should excite just one direction.

The post processing of results takes to natural frequencies similar to the ones of first sweep test. Moreover, the first two mode shapes of coupled pads are present, the third and fourth modes (torsional modes) are inverted in the two experiments due to different setup before the relative tests. The following mode 5-6 and 7-8 have similarities but are not completely equals.

The similitude obtained between the two tests is very interesting, it means that the two experiments are well set and leads to reliable results.

The Lupos numerical model brings to mode shapes very similar to the ones of experiments, leading to satisfactory results. However, the numerical model could be improved. To achieve this, a parametric analysis is adopted. Several simulations are proposed and for each only one parameter of the numerical model is changed. Once chosen the parameter's value which gives better results a new analysis is computed, until the results are satisfactory. To decide whenever the achieved results are satisfactory the natural frequencies values and mode shapes similarities between experimental and numerical results are considered. In particular, the results from roving hammer test are considered in the comparison for this analysis. Another important aspect to consider is that the numerical model can be still improved, because the high frequency values do not coincide with the experimental ones.

Once the numerical model is updated and the relative simulations on Lupos produce results close to the experimental ones, it is possible to setup another test for the Levit device.

The last experiment is the actuation and release test. The Levit is settle (position and inclination) as in real vehicle and the pads are moved by a piston as to perform the gear shifting.

These tests are repeatable and produce accurate results. It is interesting to observe how the energy is transmitted from one pad to another. In fact, when the up pad is moved, a motion is visible also on the down pad and vice versa. However, consider that the non-excited pad has smaller displacement, with a maximum of 2 mm from lasers recording.

Then, during the release phase is evident an oscillation which takes about 0.7 ± 1 second to become stable again. It evidences a non-linear behaviour, which will be investigated in a future work.

Appendix

Example of Matlab code for transmissibility graphs

It is reported the code used for post processing the FRF/transmissibility of different experiments from the universal file of Testlab.

```
clc
clear all
close all

plot_color = strvcat('b','r','k','m','g');
plot_line = strvcat('-',':','-','--');
% plot_color = strvcat('r','g','b','m','k');
% plot_line = strvcat('-', '-', '-', '-');
plot_symbol = ' ';
plot_markersize = [6 7 6 7];

title = ['TF_a4_Ely_R1x.dat'
         'TF_a4_Ely_R1y.dat'
         'TF_a4_Ely_R1z.dat'
         'TF_a3_Ely_R2x.dat'
         'TF_a3_Ely_R2y.dat'
         'TF_a3_Ely_R2z.dat'
         'TF_a2_Ely_R3x.dat'
         'TF_a2_Ely_R3y.dat'
         'TF_a2_Ely_R3z.dat'
         'TF_a1_Ely_R4x.dat'
         'TF_a1_Ely_R4y.dat'
         'TF_a1_Ely_R4z.dat'];
titleleg = ['Ely_R1x'
            'Ely_R1y'
            'Ely_R1z'
            'Ely_R2x'
            'Ely_R2y'
            'Ely_R2z'
            'Ely_R3x'
            'Ely_R3y'
            'Ely_R3z'
            'Ely_R4x'
            'Ely_R4y'
            'Ely_R4z'];

only_x = 1:3:12;
only_y = 2:3:12;
only_z = 3:3:12;

% elaboration of only x axis
figure()
set(gcf,'Color',[1 1 1]);
set(gcf,'Name','only x');

for count = 1:size(only_x,2)

    index= only_x(count);
    TF = load(title(index));
```

```

    TF_ph = UnwrapThres_deg(TF,15,1,0); % use of dataunwrap code, and save new
data with new phase

    subplot(3,1,[1 2])
    semilogy(TF_ph(:,1),TF_ph(:,2), [plot_color(1+rem(count-
1,size(plot_color,1)),:)] ...
        plot_line(1+rem(count-1,size(plot_line,1)),:)] ...
        plot_symbol(1+rem(count-
1,size(plot_symbol,1)),:)], 'Linewidth',2,'Displayname','|FRF|')
    hold on
    ylabel('|FRF| [(m/s^2)/N]')
    xlim([0,3200])
    subplot(3,1,[3])
    plot(TF_ph(:,1),TF_ph(:,3), [plot_color(1+rem(count-1,size(plot_color,1)),:)]
...
        plot_line(1+rem(count-1,size(plot_line,1)),:)] ...
        plot_symbol(1+rem(count-
1,size(plot_symbol,1)),:)], 'Linewidth',2,'Displayname','\angle FRF')
    hold on
    ylabel('\phi [°]')
    xlabel('Frequency [Hz]')
    xlim([0,3200])
    plot(xlim,0*[1 1],':k','Handlevisibility','off')
    plot(xlim,-180*[1 1],':k','Handlevisibility','off')
    plot(xlim,+180*[1 1],':k','Handlevisibility','off')
    set(gca,'ytick',[-180:90:+180])
end
linkaxes([subplot(3,1,[1 2]) subplot(3,1,[3])], 'x')
subplot(3,1,1:2)
legend(titleleg(only_x,1), 'Location', 'best', 'Interpreter', 'none')

% elaboration of only y axis
figure()
set(gcf,'Color',[1 1 1]);
set(gcf,'Name','only y');

for count = 1:size(only_y,2)

    index= only_y(count);
    TF = load(title(index));
    TF_ph = UnwrapThres_deg(TF,15,1,0); % use of dataunwrap code, and save new
data with new phase

    subplot(3,1,[1 2])
    semilogy(TF_ph(:,1),TF_ph(:,2), [plot_color(1+rem(count-
1,size(plot_color,1)),:)] ...
        plot_line(1+rem(count-1,size(plot_line,1)),:)] ...
        plot_symbol(1+rem(count-
1,size(plot_symbol,1)),:)], 'Linewidth',2,'Displayname','|FRF|')
    hold on
    ylabel('|FRF| [(m/s^2)/N]')
    xlim([0,3200])
    subplot(3,1,[3])
    plot(TF_ph(:,1),TF_ph(:,3), [plot_color(1+rem(count-1,size(plot_color,1)),:)]
...
        plot_line(1+rem(count-1,size(plot_line,1)),:)] ...
        plot_symbol(1+rem(count-
1,size(plot_symbol,1)),:)], 'Linewidth',2,'Displayname','\angle FRF')
    hold on
    ylabel('\phi [°]')
    xlabel('Frequency [Hz]')
    xlim([0,3200])
    plot(xlim,0*[1 1],':k','Handlevisibility','off')

```

```

    plot(xlim,-180*[1 1],':k','Handlevisibility','off')
    plot(xlim,+180*[1 1],':k','Handlevisibility','off')
    set(gca,'ytick',[-180:90:+180])

end
linkaxes([subplot(3,1,[1 2]) subplot(3,1,3)],'x')
subplot(3,1,1:2)
legend(titleleg(only_y,1),'Location','best','Interpreter','none')

% elaboration of only z axis
figure()
set(gcf,'Color',[1 1 1]);
set(gcf,'Name','only z');

for count = 1:size(only_z,2)

    index= only_z(count);
    TF = load(title(index));
    TF_ph = UnwrapThres_deg(TF,15,1,0); % use of dataunwrap code, and save new
data with new phase

    subplot(3,1,[1 2])
    semilogy(TF_ph(:,1),TF_ph(:,2), [plot_color(1+rem(count-
1,size(plot_color,1)),:)] ...
        plot_line(1+rem(count-1,size(plot_line,1)),:)] ...
        plot_symbol(1+rem(count-
1,size(plot_symbol,1)),:)], 'Linewidth',2,'Displayname','|FRF|')
    hold on
    ylabel('|FRF| [(m/s^2)/N]')
    xlim([0,3200])
    subplot(3,1,[3])
    plot(TF_ph(:,1),TF_ph(:,3), [plot_color(1+rem(count-1,size(plot_color,1)),:)]
...
        plot_line(1+rem(count-1,size(plot_line,1)),:)] ...
        plot_symbol(1+rem(count-
1,size(plot_symbol,1)),:)], 'Linewidth',2,'Displayname','\angle FRF')
    hold on
    ylabel('\phi [°]')
    xlabel('Frequency [Hz]')
    xlim([0,3200])
    plot(xlim,0*[1 1],':k','Handlevisibility','off')
    plot(xlim,-180*[1 1],':k','Handlevisibility','off')
    plot(xlim,+180*[1 1],':k','Handlevisibility','off')
    set(gca,'ytick',[-180:90:+180])

end
linkaxes([subplot(3,1,[1 2]) subplot(3,1,3)],'x')
subplot(3,1,1:2)
legend(titleleg(only_z,1),'Location','best','Interpreter','none')

```

Matlab code: Phi_correction.m

Here below is reported the code Phi_correction, used for the correction of some parameter of sweep test, such as

```

clear all;
close all;
clc;

% Correction for TestLab data, change the reference system of SweepExperiment

```

```

% to have compliance with the numerical system. Prepare data for the MAC
% correlation.
% Use saving data (experimental EMA data) to build MAC in Test_Mac.m

Model.Geo = load('geo_Ema.dat', '-ascii');
Simul.Phi = load('Phi_Ema.dat', '-ascii');
Simul.NodesPhi = load('NodesPhi_Ema.dat', '-ascii');
Simul.W2 = load('W2_Ema.dat', '-ascii');
Simul.Zeta = load('Zeta_Ema.dat', '-ascii');
Simul.Freq = load('Freq_Ema.dat', '-ascii');

%Correction for reference systems
% x->-x
% y->-z
% z->-y
Model.Geo(:, [2 3 4]) = -Model.Geo(:, [2 4 3]);

%Correction for modal data
for count = 1 : size(Simul.NodesPhi,1)
    switch Simul.NodesPhi(count,2)
        case 1
        case 2
            Simul.NodesPhi(count,2) = 3;
        case 3
            Simul.NodesPhi(count,2) = 2;
    end
end
clear count
Simul.Phi = -Simul.Phi;
%Reordering
[~,pos] = sort(Simul.NodesPhi(:,1)+0.1*Simul.NodesPhi(:,2));
Simul.NodesPhi = Simul.NodesPhi(pos,:);
Simul.Phi = Simul.Phi(pos,:);
clear pos

%Saving
SaveData('GeoExp.geo', Model.Geo, 'deee')
temp = Simul.Phi;
save('PhiExp.dat', 'temp', '-ascii')
SaveData('NodesPhiExp.dat', Simul.NodesPhi, 'dd')
temp = Simul.W2;
save('W2Exp.dat', 'temp', '-ascii')
temp = Simul.Zeta;
save('ZetaExp.dat', 'temp', '-ascii')
temp = Simul.Freq;
save('FreqExp.dat', 'temp', '-ascii')
clear temp

```

Example of Matlab code for parametric analysis

It is reported an example of the code used for the parametric analysis. In particular reports the parametric analysis of mass accelerometers. The parameter **config** will change.

```

%Load data
%Model.Geo = matrix of geometric position of nodes [NodeId x y z] (G x 4)
%Model.Sh4 = matrix of quad shell [NodeId1 NodeId2 NodeId3 NodeId4 col t ro E v
c_alpha c_beta] (Q x 11)
%Model.Hex = matrix of hexa solid [NodeId1 NodeId2 NodeId3 NodeId4 NodeId5
NodeId6 NodeId7 NodeId8 col ro E v c_alpha c_beta] (H x 14)
%Model.Mss = matrix of lumped masses [NodeId m Jxx Jyy Jzz Jxy Jxz Jyz] (M x 8)

```

```

%           or [NodeId mx my mz Jxx Jxy Jxz Jyx Jyy Jyz Jzx Jzy Jzz] (M x 13)
%Model.Dmp = matrix of lumped dampers [NodeId1 dof1 NodeId2 dof2 c] (C x 5)
%Model.ab = vector of the viscous damping coefficients [c_alpha; c_beta] (2 x
1)
%Model.Els = matrix of lumped springs [NodeId1 dof1 NodeId2 dof2 k] (K x 5)
%Model.RJs = matrix with rigid joints [NodeId1 NodeId2] (J x 2)
%Model.BCs = matrix with dofs to be deleted [NodeId dof] (V x 2)
%Model.FMs = matrix with generalised forces [NodeId dof Amp] (F x 3)

Geo1 = dlmread('StructureRef_Freq2_comp1.geo');
Hex1 = dlmread('StructureRef_Freq2_comp1.hex');
Geo2 = dlmread('StructureRef_Freq2_comp2.geo');
Hex2 = dlmread('StructureRef_Freq2_comp2.hex');
Geo3 = dlmread('StructureRef_Freq2_comp3.geo');
Hex3 = dlmread('StructureRef_Freq2_comp3.hex');
GeoExp = dlmread('GeoExp.geo');
Model.Geo = [
    GeoExp
    100 0 0.045 0
    Geo1
    Geo2
    Geo3
];
Model.Hex = [Hex1; Hex2; Hex3];
Model.Mss = [
    1 0.0142 0.46386e-6 0.46386e-6 0.46386e-6 0 0 0
    2 0.0142 0.46386e-6 0.46386e-6 0.46386e-6 0 0 0
    3 0.0142 0.46386e-6 0.46386e-6 0.46386e-6 0 0 0
    4 0.0142 0.46386e-6 0.46386e-6 0.46386e-6 0 0 0
];
Model.Mss(:,2:end) = config/100*Model.Mss(:,2:end);
Model.Dmp = [
    110520 2 310520 2 1.0e1 %Magnetic eddy currents
    110534 2 310534 2 1.0e1
    221099 6 321099 6 0 %Pins
    221125 6 321125 6 0
    250737 6 350737 6 0
    250763 6 350763 6 0
];
Model.Els = [
    110520 2 310520 2 4.5e5 %Magnetic spring
    110534 2 310534 2 4.5e5
];
%Elastic and dissipative steering bar
pos = find(Geo2(:,3)>=0.040);
Model.Dmp = MultiElem_ElsDmp(Model.Dmp,100*ones(size(pos,1),1),Geo2(pos,1),[1 2
3].',1e4*[1 2 1].');
Model.Els = MultiElem_ElsDmp(Model.Els,100*ones(size(pos,1),1),Geo2(pos,1),[1 2
3].',1e8*[1 2 1].');
%Contact between support and steel bar
Model.RJs = [
    1 383699
    1 383700
    1 385816
    1 385817
    2 311798
    2 311799
    2 313915
    2 313916
    3 383646
    3 383647
    3 385763
    3 385764
];

```

```

        4  311737
        4  311738
        4  313854
        4  313855
    208410 108410
    212633 112633
    212655 112655
    ];
%Pin constraints
Model.RBE = [
    221099 1 321099 1
    221099 2 321099 2
    221099 3 321099 3
    221125 1 321125 1
    221125 2 321125 2
    221125 3 321125 3
    250737 1 350737 1
    250737 2 350737 2
    250737 3 350737 3
    250763 1 350763 1
    250763 2 350763 2
    250763 3 350763 3
    ];
Model.BCs = [
    100 1
    100 2
    100 3
    100 4
    100 5
    100 6
    ];
clear GeoExp Geo1 Geo2 Geo3 Hex1 Hex2 Hex3 pos

Simul.RefSys = 'xyz';
Simul.axis_par = [-0.2 +0.2 -0.1 +0.08 -0.1 +0.15];
Simul.view_par = [30 30];
Simul.Par_name = 'Accelerometers mass [%]';

```

Matlab code for update 10

In the following there the code used for update10 the last one, which leads to the final model.

```

%Load data
%Model.Geo = matrix of geometric position of nodes [NodeId x y z] (G x 4)
%Model.Sh4 = matrix of quad shell [NodeId1 NodeId2 NodeId3 NodeId4 col t ro E v
c_alpha c_beta] (Q x 11)
%Model.Hex = matrix of hexa solid [NodeId1 NodeId2 NodeId3 NodeId4 NodeId5
NodeId6 NodeId7 NodeId8 col ro E v c_alpha c_beta] (H x 14)
%Model.Mss = matrix of lumped masses [NodeId m Jxx Jyy Jzz Jxy Jxz Jyz] (M x 8)
%Model.Dmp = matrix of lumped dampers [NodeId1 dof1 NodeId2 dof2 c] (C x 5)
%Model.ab = vector of the viscous damping coefficients [c_alpha; c_beta] (2 x 1)
%Model.Els = matrix of lumped springs [NodeId1 dof1 NodeId2 dof2 k] (K x 5)
%Model.RJs = matrix with rigid joints [NodeId1 NodeId2] (J x 2)
%Model.BCs = matrix with dofs to be deleted [NodeId dof] (V x 2)
%Model.FMs = matrix with generalised forces [NodeId dof Amp] (F x 3)

Geo1 = dlmread('StructureRef_Freq2_comp1.geo');
Hex1 = dlmread('StructureRef_Freq2_comp1.hex');
Geo2 = dlmread('StructureRef_Freq2_comp2.geo');
Hex2 = dlmread('StructureRef_Freq2_comp2.hex');

```

```

Geo3 = dlmread('StructureRef_Freq2_comp3.geo');
Hex3 = dlmread('StructureRef_Freq2_comp3.hex');
Hex3(:,10) = 1385.2; % calculated equivalent density [kg/m^3]
Hex3(:,11) = 10.94e9; %case A
% Hex3(:,11) = 35.9e9; %case B with proportionality E/rho

GeoExp = dlmread('GeoExp.geo');
Model.Geo = [
    GeoExp
    100 0 0.045 0
    Geo1
    Geo2
    Geo3
];
Model.Hex = [Hex1; Hex2; Hex3];
Model.Mss = [
    1 0.0142 0.46386e-6 0.46386e-6 0.46386e-6 0 0 0
    2 0.0142 0.46386e-6 0.46386e-6 0.46386e-6 0 0 0
    3 0.0142 0.46386e-6 0.46386e-6 0.46386e-6 0 0 0
    4 0.0142 0.46386e-6 0.46386e-6 0.46386e-6 0 0 0
];
Model.Dmp = [
    110520 2 310520 2 1.0e1 %Magnetic eddy currents
    110534 2 310534 2 1.0e1
    221099 6 321099 6 0 %Pins
    221125 6 321125 6 0
    250737 6 350737 6 0
    250763 6 350763 6 0
];
Model.Els = [
    110520 2 310520 2 4.5e5 %Magnetic spring
    110534 2 310534 2 4.5e5
    221099 1 321099 1 2.5e5 %Pin constraints
    221099 3 321099 3 2.5e5
    221125 1 321125 1 2.5e5
    221125 3 321125 3 2.5e5
    250737 1 350737 1 2.5e5
    250737 3 350737 3 2.5e5
    250763 1 350763 1 2.5e5
    250763 3 350763 3 2.5e5
];
%Elastic and dissipative steering bar
pos = find(Geo2(:,3)>=0.040);
Model.Dmp = MultiElem_ElsDmp(Model.Dmp,100*ones(size(pos,1),1),Geo2(pos,1),[1 2
3].',1e4*[1 2 1].');
%Model.Els = MultiElem_ElsDmp(Model.Els,100*ones(size(pos,1),1),Geo2(pos,1),[1 2
3].',1e8*[1 2 1].');
Model.Els = MultiElem_ElsDmp(Model.Els,100*ones(size(pos,1),1),Geo2(pos,1),[1 2
3].',4e4*[1 2 1].');
%Contact between support and steel bar
Model.RJs = [
    1 383699
    1 383700
    1 385816
    1 385817
    2 311798
    2 311799
    2 313915
    2 313916
    3 383646
    3 383647
    3 385763
    3 385764
];

```

```

        4  311737
        4  311738
        4  313854
        4  313855
208410 108410
212633 112633
212655 112655
    ];
%Pin constraints
Model.RBE = [
%   221099  1  321099  1
    221099  2  321099  2
%   221099  3  321099  3
%   221125  1  321125  1
    221125  2  321125  2
%   221125  3  321125  3
%   250737  1  350737  1
    250737  2  350737  2
%   250737  3  350737  3
%   250763  1  350763  1
    250763  2  350763  2
%   250763  3  350763  3
    ];
Model.BCs = [
    100  1
    100  2
    100  3
    100  4
    100  5
    100  6
    ];
clear GeoExp Geo1 Geo2 Geo3 Hex1 Hex2 Hex3 pos

Simul.RefSys = 'xzy';
Simul.axis_par = [-0.2 +0.2 -0.1 +0.08 -0.1 +0.15];
Simul.view_par = [30 30];
%Simul.Par_name = '\Delta\ith\rm [%]';

```

Reference

- [1] Bonisoli E., *LUPOS – Lumped Parameters Open Source FEM Code*, release 2021-09-16, Politecnico di Torino, 2021.
- [2] Bonisoli E., Lisitano D., Technical evaluation through numerical time and/or modal approaches on LEVIT devices, 2020.
- [3] <https://www.plm.automation.siemens.com/global/it/products/simcenter/testlab.htm> available in 2021-08-22.
- [4] <https://www.dataphysics.com/applications/structural-testing/impact-testing.html> available in 2021-09-12.
- [5] Allemang, R. J., Brown, D. L, Rost R. W., “Experimental Modal Analysis and Dynamic Component Synthesis. Volume 2. Measurement Techniques for Experimental Modal Analysis”, 1987.

